Characterisation of the mode of action of chelating agents against Gram-negative and Gram-positive bacteria

JOY RUTH PATERSON

Characterisation of the mode of action of chelating agents against Gram-negative and Gram-positive bacteria

Joy Paterson

A thesis presented for the degree of
Doctor of Philosophy

Durham University

Department of Biosciences

September 2021

Characterisation of the mode of action of chelating agents against Gram-negative and Gram-positive bacteria

Joy Paterson

Limiting the availability of metals in an environment is known to restrict bacterial growth and proliferation. For example, humans sequester iron, manganese and zinc to help prevent infection by pathogens, a system termed nutritional immunity. Chelators are small ligands that bind tightly to metals and thus have antibacterial properties that mimic these innate immune processes. However, the modes of action of many of these chelating agents in bacterial growth inhibition and their selectivity in metal deprivation *in cellulo* remain ill-defined. In this thesis, we expand upon previous work in which the effect of eleven chelators on the cellular metal concentrations of *Escherichia coli* was examined. Building upon these insights, the antibacterial activity of a group of seven chelants was studied in two Gram-negative species, *E. coli* and *Pseudomonas aeruginosa*, and two Gram-positive species, *Bacillus subtilis* and *Staphylococcus aureus*. Selected chelant-chelant and chelant-antibiotic combinations were evaluated for efficacy in antibacterial hostility. The influence of these chelating agents on cellular metal concentrations in *P. aeruginosa* was also determined. An experimental evolution approach was employed with *E. coli* and *S. aureus* to obtain mutants which have acquired some level of resistance to EDTA and DTPMP. Changes affecting iron and zinc uptake pathways in *E. coli* were identified, while alterations in cell wall metabolism and surface charge were found in *S. aureus*. Our results reveal significant insights into the mechanism of growth inhibition by chelants, highlighting their potential as antibacterial agents and as tools to probe the ways in which bacteria tolerate selective metal deprivation.

Table of Contents

List of figures

List of tables

Additional publications

Additional experimental data was collected over the course of this PhD which was not included in this thesis as the topics were unrelated. This additional work was incorporated in the following publications:

Chakraborti, S., Balakrishnan, D., Trotter, A.J., Gittens, W.H., Yang, A.W.H., Jolma, A., **Paterson, J.R.**, Świątek, S., Plewka, J., Curtis, F.A., Bowers, L.Y., Pålsson, L.O., Hughes, T.R., Taube, M., Kozak, M., Heddle, J.G., Sharples, G.J. (2020) A bacteriophage mimic of the bacterial nucleoid-associated protein Fis. Biochem J. 477: 1345-1362

Cox, H.J., Lia, J., Sainia, P., **Paterson, J.R.**, Sharples, G.J. and Badyal, J.P.S. (2021) Bioinspired and eco-friendly high efficacy cinnamaldehyde antibacterial surfaces. J. Mat. Chem. B 9: 2918-2930

Declaration

I hereby declare that except where specific reference is made to the work of others, the contents of this dissertation are original and have not been submitted in whole or in part for consideration for any other degree or qualification in this, or any other university. This dissertation is my own work and contains nothing which is the outcome of work done in collaboration with others, except as specified in the text and acknowledgements. This work was supported by a BBSRC NLD DTP CASE studentship with Procter & Gamble.

Statement of Copyright

'*It seems to me that when confronted with the marvels of life and the universe, one must ask why and not just how.*' - Arthur L. Schawlow

'*The more I study nature, the more I stand amazed at the work of the Creator.*' - Louis Pasteur

Acknowledgements

First and foremost, I am deeply indebted to Dr Gary Sharples, without whom, undoubtedly, this thesis wouldn't exist. I honestly couldn't have asked for a better supervisor and I'm so grateful to count you not only as my mentor, but now also as a friend. Thank you for your endless patience, your compassion and understanding, and for the countless hours you've spent editing this thesis. Choosing to do this PhD with you was one of the best decisions I've ever made. I'm looking forward to continuing to work with you, and am excited for all the discoveries yet to come.

Thanks also to my secondary supervisor Professor Nigel Robinson for his boundless enthusiasm and pertinent insights, and to Dr Akis Karakesisoglou and Professor Carrie Ambler for their support and guidance along the way.

I am deeply grateful to those who have contributed their knowledge and data to this thesis. Thanks to Dr Marikka Beecroft, for laying the groundwork for this project, and for helping me find my feet in the lab. Special thanks to Dr Andrew Foster and Dr Deenah Osman for running ICP-MS samples on my behalf. Thanks also to Lydia Newton and Rebecca Lee for helping with further mutant characterisation, to Dr Beth Bromley for cell surface charge experiments, to Professor Waldemar Vollmer for his assistance in peptidoglycan analysis, and to Dr Kevin Waldron for providing mutants from the Nebraska Transposon Mutant Library. I would also like to extend my sincere gratitude to Nancy Reeder, Justin Casserta, Ping Hu, and the whole team at P&G, Cincinnati for their suggestions and support over the course of this project. I'm sorry that Covid disrupted my plans to meet you all in person, but hope that I might have the chance to do so some time in the future. Thanks also to Gareth Davies for liaising between us, and arranging opportunities for us to share our data.

I'm also immensely grateful for those who made the day-to-day science such a joy. To members of CG229/CG234/CG209 past and present who have shared their expertise, lab equipment, and cake with me.

Thanks also to those who have cheered me on from afar. To my grandparents for always showing an interest in what I'm doing, and for your ceaseless prayers. To Ruth and Julie for never letting me get away with anything less than my best. And to my parents and siblings who have encouraged, loved, and prayed for me every step of the way.

And finally to my husband Mark, my biggest distraction, my strongest supporter, and my best friend. Thank you for sharing all the joys and sorrows of these past few years with me, and being my chief reminder that life is about so much more than this. I am eternally grateful for you.

1 Introduction

1.1 The significance of metals in biology

The importance of metal homeostasis is exemplified by the availability of multiple mechanisms for metal import and export found throughout the three domains of life (Yannone et al., 2012). All organisms must ensure that they can obtain and maintain sufficient levels of essential metal ions as cofactors for metalloenzymes which allow them to carry out the core functions necessary for life, including respiration, energy generation and growth (Waldron & Robinson, 2009). Recent technological advances have allowed the importance of various metals to be more clearly defined in bacterial and mammalian model systems and have revealed significant new insights into the mechanisms of metal acquisition and homeostasis.

Metal ions are required by about one-third of proteins and half of all enzymes (Waldron et al., 2009), and both humans and prokaryotes possess a broad range of metal acquisition and storage molecules. Metals are essential for several classes of metalloproteins including metalloenzymes, storage proteins, and transcription factors (Hood & Skaar, 2012), and the electrostatic properties of transition metals allow them to stabilize substrates or reaction intermediates by facilitating redox reactions (Hood & Skaar, 2012). However, the factors that make metals so useful in catalysing reactions also make them potentially dangerous. Mismetallation can induce structural abnormalities in metalloenzymes, rendering them inactive (Imlay, 2014). In addition to this, iron, in its soluble ferrous form, interacts with peroxide *via* a process known as the Fenton reaction in which toxic hydroxyl radicals are formed (Sánchez et al., 2005). These radicals are extremely potent oxidising agents which have the potential to cause extensive damage within the cell. It is therefore essential that metals are present in appropriate quantities and that metalloproteins can obtain the correct metal from a limited and tightly restricted pool. Organisms must be able to regulate their

intracellular metal levels to fulfil physiological needs without coming to harm through toxic metal overload. In the case of infection, hosts are able to harness both the essential and toxic nature of transition metals to defend against bacterial pathogens (Hood & Skaar, 2012).

1.1.1 Nutritional immunity and the prevention of metal deficiency or excess

The metal status of a given host is known to dramatically impact on their susceptibility to different bacterial infections; impaired metal homeostasis increases metal availability for opportunistic pathogens with limited metal acquisition capabilities (Weiss & Carver, 2018). Conditions affecting iron homeostasis such as haemochromatosis or β-thalassaemia, which result in iron overload, are often associated with increased levels of bacterial infection (Cassat & Skaar, 2013; Ricerca et al., 2009), and can leave patients susceptible to infection with pathogens that would normally be non-invasive (Palmer & Skaar, 2016). High levels of iron can also be caused by environmental exposure; workers exposed to high levels of iron-containing dust have higher rates of respiratory tract infection and are more prone to pneumonia (Palmer & Skaar, 2016). Metal deficiencies have also been linked to bacterial infection, for example, copper deficiency is associated with neutropenia and can also increase susceptibility to *Salmonella enterica* infection (Djoko et al., 2015).

The term ‘nutritional immunity’ refers to the mechanisms through which a mammalian host alters its metal homeostasis in response to infection. This involves increased production of proteins which sequester essential metals such as iron, manganese and zinc, while simultaneously directing metal toxicity in such a way as to eliminate a bacterial pathogen, flooding sites of infection with toxic metals such as copper (Hood & Skaar, 2012). In response to host nutritional immunity, pathogenic bacteria have coevolved the ability to sense decreased levels of metals and produce high affinity siderophores. Some bacteria are also capable of using metal-sparing pathways which allow metabolism to continue under conditions of metal depletion

(Chandrangsu et al., 2017). Intracellular pathogens are particularly damaging because they are able to access more readily accessible nutrient pools of metal in the host cytosol (Leon-Sicairos et al., 2015).

Most bacterial species are able to obtain metals through three different acquisition pathways: elemental metal import, extracellular metal capture through siderophores and metal acquisition from host proteins, also known as 'metal piracy' (Palmer & Skaar, 2016). As our knowledge and understanding of the mechanisms underlying bacterial metal homeostasis increases, this opens up new potential targets for therapeutics. Greater understanding of these essential cellular processes gives us increased scope for manipulation of these natural homeostatic systems.

1.1.2 Requirement for metals in pathogen and host

As previously mentioned, half of all enzymes require at least one metal cofactor in order to function, and the essential nature of metal acquisition and homeostasis is reflected in the presence of multiple mechanisms for the import, homeostasis and export of metals in both prokaryotic and eukaryotic organisms. The uses for these metals in both host and pathogen are wide-ranging. In the following section, some of the essential metals used by both host and bacterial pathogen are summarised, including known mechanisms for acquisition and homeostasis.

1.1.2.1 Iron

Iron is the most abundant element on Earth, and is also the most widely used transition metal in biological systems, with extensive roles in essential processes such as deoxyribonucleic acid (DNA) replication, transcription, and cofactor biosynthesis (Cassat & Skaar, 2013). In its soluble form (Fe^{2+}) iron is often physiologically unavailable to bacteria due to host restriction, and many bacteria therefore possess multiple import systems for insoluble, ferric iron (Fe^{3+}). Human hosts sequester two-thirds of their iron through binding to haemoglobin (Cassat & Skaar, 2013), and insoluble ferric iron is bound by transferrin in serum, ferritin in cells, or lactoferrin in

milk, saliva, tears, mucus, and within neutrophils (Cronin et al., 2019). In order to colonise the human host, therefore, bacteria must evolve mechanisms of iron acquisition which allow them to survive within the iron-restricted environment of the human host. The main mechanisms of iron acquisition in both Gram-negative and Gram-positive bacteria are outlined in Figure 1.1.

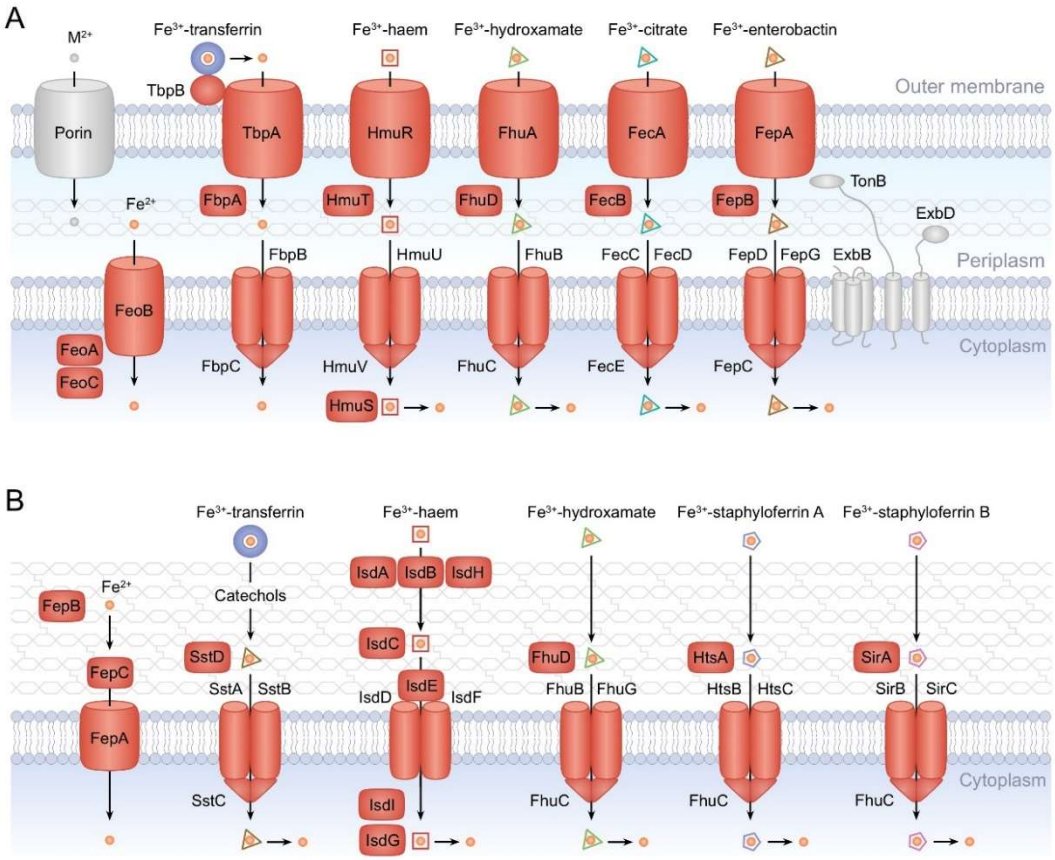

Figure 1.1 Bacterial iron acquisition pathways. (A) Iron import in Gram-negative bacteria. Fe^{2+} and other metals (M^{2+}) can gain entry to the periplasm *via* outer membrane porins before entering the cytoplasm by means of the FeoB channel. Fe^{3+} is imported in complexed form, mediated by a variety of specific outer membrane receptors, mediated by the TonB/ExbBD complex in most cases. The iron complexes are transported into the cytoplasm using ABC transporters. Fe^{3+} is solubilised through reduction in the cytoplasm to form Fe^{2+}. (B) Iron import in Gram-positive bacteria. Fe^{2+} can be taken up *via* FepABC. Iron uptake from haem is mediated by the iron-regulated surface determinant (Isd) system, while uptake from hydroxamate siderophores is mediated by the Fhu system. Iron uptake from carboxylate-type siderophores, staphyloferrin A and staphyloferrin B is carried out by the Hts and Sir systems, respectively. Note that not all systems are illustrated and even those that are can vary

in nomenclature between species and not all systems will necessarily be present in a single species. Peptidoglycan is depicted as chains of hexose sugars with peptide crosslinks indicated. See text for further details and references. This figure was assembled by Dr Gary Sharples using EazyDraw.

Ferrous iron (Fe^{2+}) can enter the periplasm through outer membrane porins, and is then taken up into the cytoplasm *via* the FeoB membrane transporter. FeoA and FeoB work at the inner membrane of Gram-negatives to help import this ferrous iron, which is more readily available under anaerobic or microaerophilic conditions (Fig. 1.1A, Lau et al., 2016). As stated previously, levels of soluble ferrous iron are often very low within a human host, and many bacteria therefore deploy siderophores to bind ferric iron within the host to facilitate uptake. Some iron siderophores have a sufficiently high affinity to facilitate 'iron piracy' in which iron is stolen from host proteins with lower affinity for this element (Miethke & Marahiel, 2007). Many bacterial pathogens encode several different siderophores which can be expressed under different physiological conditions, including pH, in response to host siderophore production and competition from other commensals or pathogens (Wilson et al., 2016). Some pathogenic species, such as *P. aeruginosa*, are able to avoid the metabolic cost of siderophore production by scavenging siderophores produced by others in a process known as 'cheating' (Palmer & Skaar, 2016).

Several pathogens are able to use iron from non-haem proteins such as transferrin, lactoferrin and ferritin. For example *Neisseria gonorrhoeae* can acquire ferric iron from lactoferrin and transferrin using the receptors LbpAB and TpbAB, respectively (Caza & Kronstad, 2013). Binding of transferrin to TpbAB results in a conformational change in which iron is released from transferrin and transiently docks within the β-barrel of TpbA. This ferric iron is then transferred to the periplasmic binding protein FbpA which mediates transfer to the cytosol *via* the FpbB ATP-binding cassette (ABC) transporter (Fig. 1.1A, Noinaj et al., 2012). Iron must then be released from these siderophores and solubilised through reduction before use. In response to

this, vertebrate hosts produce lipocalin 2 which binds siderophores to prevent their uptake (Cassat & Skaar, 2013). As a consequence, some bacteria have evolved stealth siderophores which are capable of evading lipocalin 2 binding (Cassat & Skaar, 2013). One such stealth siderophore, salmochelin, is produced chiefly by *Salmonella* species (Müller et al., 2009), but has also been shown to confer virulence in a non-pathogenic strain of *E. coli* (Wilson et al., 2016).

Since a large portion of iron within the human body is inaccessible within erythrocytes, many bacterial pathogens have developed haem acquisition strategies involving initial lysis of the erythrocyte, sequestration of haem proteins and subsequent degradation to release the bound iron (Cassat & Skaar, 2013). In response to erythrocyte lysis, mammalian hosts release haemopexin and haptoglobin which sequester haem and haemoglobin respectively (Cassat & Skaar, 2013). In response, bacteria possess haem acquisition systems with surface-associated receptors which bind to haem or haem-associated proteins to facilitate their transport into the cell (Cassat & Skaar, 2013). For Gram-negative species, this requires outer membrane receptors such as HmuR and TonB-ExbB-ExbD transporting systems to promote transport across the outer membrane. The haem is then transported into the cytoplasm *via* the HmuU ABC transporter (Fig. 1.1A, Simpson et al., 2000).

E. coli also possesses transport systems for other Fe^{3+}-binding ligands such as hydroxamate, citrate and enterobactin (Fig. 1.1A, Parrow et al., 2013). The *E. coli* FhuABCDE system can import the hydroxamate-type siderophore ferrichrome-Fe^{3+} complexes made by other microbes, while the FecABCDE system takes up ferric iron, Fe^{3+}, in complex with citrate (Fig. 1.1A, Miethke, 2013). Production of enterobactin from chorismate, a precursor of aromatic amino acid biosynthesis, is mediated by the EntABCDEF multienzyme pathway (Raymond et al., 2003) and exported *via* EntS and TolC (Garénaux et al., 2011). Fe^{3+}-siderophore complexes are recovered by association with an outer membrane receptor FepA. The TonB/ExbBD complex provides energy from the proton motive force to mediate release of the Fe^{3+}-

enterobactin complex from FepA, facilitated by FepB, and delivery to the FepCDG ABC-family, ATP-dependent inner membrane permease (Fig. 1.1A, Raymond et al., 2003). Complexed iron is finally released by the esterase Fes which breaks apart the enterobactin organic backbone (Brickman & Mcintosh, 1992).

Systems for iron acquisition in Gram-positive bacteria are broadly similar to those of Gram-negatives in that they are comprised of cell surface receptors, cell wall proteins for internalisation, ABC transporters for membrane translocation and proteases and esterases which facilitate iron release from ferric iron complexes (Fig. 1.1B, Caza & Kronstad, 2013). Gram-positives are also capable of importing ferrous iron *via* the FepA lipoprotein in conjunction with the FepB iron-dependent peroxidase, and the FepC iron permease (Fig. 1.1B, Shahmirzadi et al., 2016). The Sst iron acquisition system relies on the affinity of SstD for ferrated catecholamines and catechol siderophores (Beasley et al., 2011), which are then imported *via* the SstABC transporter (Fig. 1.1B). *S. aureus* utilises the iron-regulated surface determinant system (Isd) to acquire free or complex-bound haem (Cassat & Skaar, 2013; Caza & Kronstad, 2013). Isd proteins, which in *S. aureus* include IsdB, IsdH and IsdA, bind to haem at the cell surface before using specific transporters to shuttle it to IsdC. Once bound, IsdC then transfers the haem to the membrane-associated transporter IsdDEF for transport across the cell membrane (Choby & Skaar, 2016). Upon entering the cytosol, haem is incorporated into staphylococcal proteins or degraded by the IsdG and IsdI haem oxygenases (Fig. 1.1B, Choby & Skaar, 2016).

While staphylococci are unable to synthesise their own hydroxamate-type siderophores such as aerobactin and ferrichrome, some species such as *Bacillus subtilis* and *S. aureus* possess cell surface receptors which allow them to use these ferric siderophores as iron sources (Sheldon & Heinrichs, 2012). Ferric uptake from hydroxamate siderophores is mediated through the substrate-binding lipoprotein FhuC, the FhuBG heterodimeric permease and the FhuC ATPase (Sheldon & Heinrichs, 2012). *S. aureus* can also extract iron from two carboxylate-type

siderophores, staphyloferrin A and staphyloferrin B, *via* the transporters Hts and Sir, respectively (Fig. 1.1B, Beasley et al., 2011). Deletion of either of these iron import systems has little impact on bacterial growth under iron limited conditions, however when these deletions are combined with each other, or with inactivation of the *sst* system, significantly reduced growth is apparent (Beasley et al., 2011).

1.1.2.2 Manganese

Manganese serves as a cofactor for enzymes involved in DNA replication, central metabolism and management of oxidative stress, including manganese superoxide dismutase (MnSOD) (Juttukonda & Skaar, 2015; Kehl-Fie & Skaar, 2010; Kehres & Maguire, 2003). Bacterial manganese import is mediated by two main transport pathways, ABC permeases and natural resistance-associated macrophage protein (NRAMP) transporters (Eijkelkamp et al., 2015), and is very similar between Gram-negative and Gram-positive species (Fig. 1.2A-B). Many organisms possess both types of transporter, for example, *S. aureus* has a Mn^{2+}-ABC permease (*mntABC*) alongside an NRAMP transporter (*mntH*), and the loss of either or both of these transporters detrimentally affects pathogen virulence (Kehl-Fie et al., 2013). Expression of *mntH* is regulated by both MntR and Fur in *E. coli*, supporting close links between iron and manganese homeostasis (Lisher & Giedroc, 2013; Patzer & Hantke, 2001).

Some Gram-negative species, such as *Bradyrhizobium japonicum,* also produce the outer membrane protein MnoP under conditions of manganese starvation: inactivation of *mnoP* causes a significant growth reduction under manganese limited conditions (Fig. 1.2A, Hohle et al., 2011). In response to iron or manganese starvation, *E. coli* imports Mn^{2+} using the MntH NRAMP-family transporter (Kehl-Fie et al., 2013) and ZupT which is primarily a zinc uptake protein but can also import Mn^{2+} when manganese availability is constrained (Fig. 2.1A, Cerasi et al., 2014). Although *E. coli* Δ*mntH* Δ*zupT* double mutants lacking both known manganese uptake

systems remain capable of colonising mice (Kupz et al., 2013), *mntH* mutants are more susceptible to killing by hydrogen peroxide, indicating their increased vulnerability to oxidative stress (Kehres et al., 2000). Gram-positive species may have other mechanisms through which they can tolerate manganese stress. For example, the Gram-positive species *Streptococcus pyogenes* possesses an ABC transporter MtsABC in which MtsA is plays an important role in iron uptake (Sun et al., 2008). However, MtsA has also been shown to bind Mn^{2+} and it has been suggested that it plays a role in manganese uptake (Janulczyk et al., 2003), although its affinity for Mn^{2+} is considerably lower than Fe^{2+} (Sun et al., 2008).

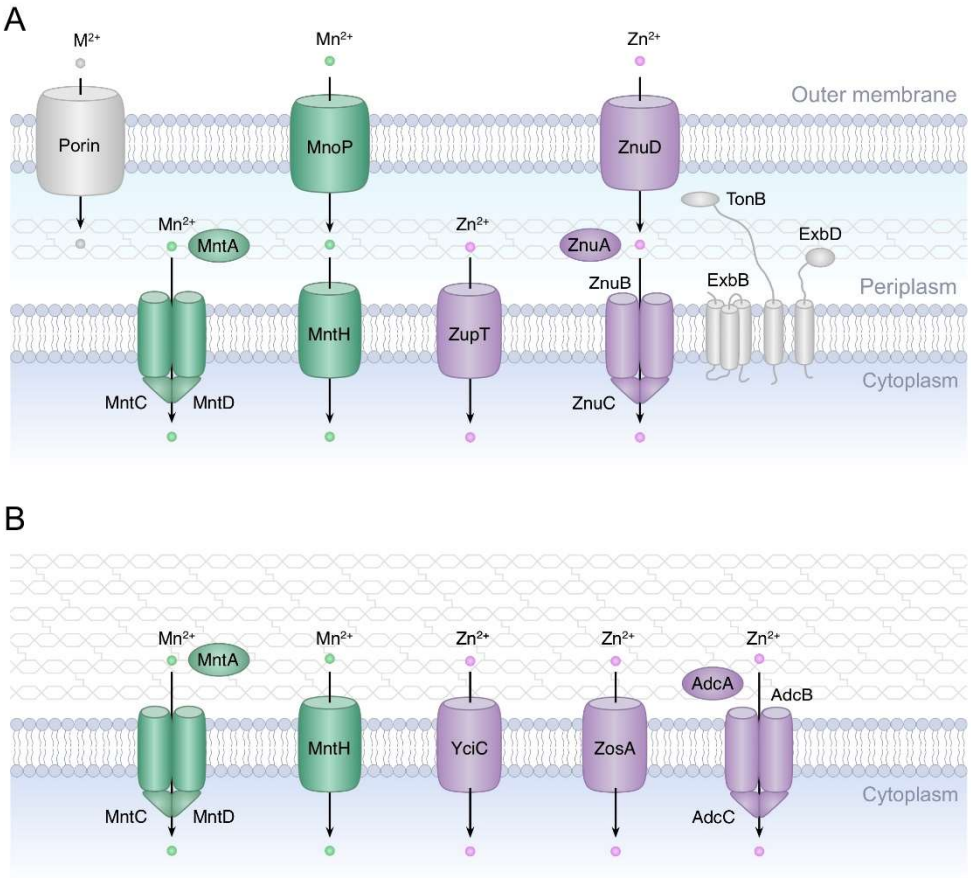

Figure 1.2 Bacterial manganese and zinc acquisition pathways. (A) Manganese and zinc import in Gram-negative bacteria. In addition to the MntH NRAMP-family transporter, some Gram-negative species also have MnoP, an outer membrane protein which is expressed under conditions of manganese starvation. ZupT serves as the main pathway for zinc uptake in Gram-negatives in zinc replete conditions. (B)

Manganese and zinc import in Gram-positive bacteria. Some Gram-positives additionally possess the low affinity YciC importer and/or the oxidative stress-induced ZosA importer. Not all systems are illustrated and not all systems will necessarily be present in a single bacterial species. Peptidoglycan is depicted as chains of hexose sugars with peptide crosslinks indicated. See text for further details and references. This figure was assembled by Dr Gary Sharples using EazyDraw.

Under conditions of manganese excess, some species such as *Streptococcus pneumoniae* can export manganese using the *mntE* efflux pump (Rosch et al., 2009). Deletion of *mntE* confers increased resistance to oxidative stress, but reduces pathogenicity in the host (Rosch et al., 2009), suggesting that maintenance of manganese homeostasis is essential for both survival and virulence.

The host innate immune system has evolved both intra- and extracellular manganese restriction mechanisms (Palmer & Skaar, 2016). Calprotectin is capable of binding Mn^{2+} extracellularly to prevent bacterial uptake. Bacterial infection triggers the expression of NRAMP1 in both macrophages and neutrophils which depletes the phagosome of manganese (Juttukonda & Skaar, 2015; Kehl-Fie & Skaar, 2010). Polymorphisms in the gene encoding NRAMP1 in humans (*SLCA11*) have been found to alter susceptibility to tuberculosis, meningococcal diseases and leprosy (Palmer & Skaar, 2016). Interestingly, expression of *SLCA11* in macrophages induces expression of lipocalin 2, suggesting a link between different mechanisms of host nutritional immunity (Fritsche et al., 2012).

1.1.2.3 Zinc

Zinc is the next most abundant metal cofactor after iron and is required for many metalloproteases (McCall et al., 2000). Zinc homeostasis in bacteria is maintained by balancing zinc import and export in response to zinc sensing by zinc-responsive transcription factors. These include Zur and AdcR, in Gram-negatives and Gram-positives, respectively, to up-regulate zinc import, and ZntR, SmtB, ZiaR and CzrA to increase export or intracellular sequestration of zinc (Mikhaylina et al., 2018).

In Gram-negative bacteria, zinc uptake is primarily carried out by ZupT, a constitutively expressed low-affinity transporter which is capable of managing zinc import under metal replete conditions (Fig. 1.2A, Cerasi et al., 2013, 2014; Quan et al., 2020). The ZnuABC transporter is a member of the ABC transporter family which has a high affinity for zinc. This system comprises three proteins: a transmembrane-spanning permease (ZnuB), a cytoplasmic ATPase (ZnuC) and a periplasmic solute binding protein (ZnuA) which captures Zn^{2+} within the periplasm and delivers it to ZnuB (Cerasi et al., 2013; Quan et al., 2020). Some bacteria also possess ZinT which forms a complex with ZnuA in the presence of zinc and is thought to increase the capacity of ZnuA to recruit zinc (Cerasi et al., 2013). Recently, a TonB-dependent outer membrane receptor (ZnuD) was identified in the Gram-negative species *Neisseria meningitidis*, which mediates both haem and zinc uptake, and is regulated by both the ferric uptake regulator Fur (Seo et al., 2014) and the zinc uptake regulator Zur (Fig. 2.1A, Kumar et al., 2012), highlighting the importance of this pathway to maintain appropriate levels of both iron and zinc.

Gram-positive bacteria possess a similar zinc uptake system, AdcABC. The AdcA component incorporates two structural domains which share sequence and structural homology with ZnuA and ZinT, respectively (Cerasi et al., 2013). In addition to this, some Gram-positives, such as *B. subtilis,* express the membrane protein YciC, which functions as part of a lower affinity zinc uptake pathway and is transcriptionally regulated by Zur (Fig. 2.1B, Gaballa & Helmann, 1998). *B. subtilis* also expresses the metal-transporting ATPase ZosA, which serves as a major zinc uptake pathway under conditions of oxidative stress and is not under Zur control, nor is it repressed by excess Zn^{2+} (Fig. 1.2B, Gaballa & Helmann, 2002).

During the acute response to inflammation, zinc uptake and sequestration by metallothionein in liver cells increases, causing a drop in serum zinc levels (Gammoh & Rink, 2017). Mammalian host cells also produce calprotectin, an abundant protein which binds to Zn^{2+} and Mn^{2+} in order to sequester these metals during infection

(Gammoh & Rink, 2017). Some bacterial species have evolved outer membrane receptors, such as CbpA, to bind calprotectin and extract the zinc in a TonB-dependent manner (Gammoh & Rink, 2017).

Since zinc, like manganese, does not participate in Fenton chemistry, it is likely that it exerts its toxicity exclusively through mismetallation (Imlay, 2014). In *Streptococcus pyogenes*, zinc competitively inhibits manganese binding, while zinc efflux by the *S. pyogenes* cadmium-zinc-cobalt exporter was found to be essential in a mouse model of infection (Palmer & Skaar, 2016). Human neutrophils respond to *S. pyogenes* infection by increasing free cytosolic zinc, however it is unclear whether this is exclusively a response to the pathogen, or whether this is necessary for mobilisation of the wider immune system (Djoko et al., 2015).

1.1.2.4 Copper

Copper is an important cofactor of cytochrome *c* oxidase and copper-zinc superoxide dismutase (Horn & Barrientos, 2008), yet it remains uncertain whether copper is restricted during nutritional immunity, and the mechanisms of copper uptake remain unclear. There have been some suggestions that the siderophore yersiniabactin is able to bind Cu^{2+}, and can be imported by uropathogenic *E. coli* using the TonB-dependent siderophore importer FyuA (Koh et al., 2015).

Copper is particularly important in toxicity; it has long been recognised for its roles as an antimicrobial agent (Djoko et al., 2017; Djoko & McEwan, 2013). The primary targets of copper in *E. coli* are the iron-sulphur cluster proteins in branched chain amino acid synthesis (Macomber & Imlay, 2009). During bacterial infection, host interferon-γ induces expression of Copper Transport protein 1 (CTR1) which causes a cascade resulting in copper accumulation within the phagolysosome (Samanovic et al., 2012). In order to persist within a phagolysosome therefore, bacteria must develop resistance mechanisms to overcome this metal overload. Uropathogenic *E. coli* for example is able to use Cu^{2+}-yersiniabactin to protect against copper toxicity; binding

to the free metal prevents uncontrolled Fenton chemistry and therefore reduces oxidative damage (Koh et al., 2015). Excess copper has also been shown to inhibit haem biosynthesis (Djoko & McEwan, 2013).

1.1.2.5 Other transition metals

Less is known concerning the roles of cobalt and nickel acquisition in bacterial pathogenesis. Nickel and cobalt are both known to be essential cofactors for various virulence factors and although no specific cobalt transporters have been identified, many bacterial pathogens encode nickel-cobalt transporters (Rodionov et al., 2006). In *S. aureus*, the cobalt and nickel transporter Cnt is required for infection in systemic infections in mice (Remy et al., 2013), and recent work has demonstrated that Cnt is able to transport metals complexed with staphylopine, a metallophore capable of binding nickel, cobalt, zinc, copper, and iron (Grim et al., 2017). Staphylopine is the first characterised broad-spectrum metallophore, and may play roles in acquisition of transition metals lacking specific importers. Further examination of these transition metals at the host-pathogen interface may reveal more about their roles in bacterial virulence and host nutritional immunity. There are no described mechanisms of host-induced toxicity regarding the remaining transition metals, but all are known to be toxic at high concentrations (Palmer & Skaar, 2016).

Although all of these metals are essential for life, they can also prove toxic through production of reactive oxygen species (ROS) which cause damage to DNA, proteins, and lipids, and can inactivate metalloenzymes through mismetallation. Mass mismetallation within a cell will result in the interruption of essential pathways, leading to cell death (Foster et al., 2014). The metals that a pathogen may be exposed to will depend greatly upon its niche within the human host, and therefore different metal efflux pumps will be required by different species. The presence of exogenous agents such as chelating agents which are capable of disrupting metal homeostasis must also be considered.

1.2 Chelating agents

Chelating agents, also known as chelants, are organic or inorganic compounds which bind with high affinity to positively charged metal ions. They form complex ring-like structures called ‘chelates’ through the formation of coordinate bonds with metal cations, and can form bidentate or multidentate complexes which are highly stable (Flora & Pachauri, 2010). Chelants are therefore useful as metal storage molecules, which can hold essential metals in close proximity to their appropriate metalloenzymes until these ions are required. They dissociate from these metals to provide sufficient levels of free metal ions to act as cofactors for many essential metalloenzymes. The presence of excessive levels of chelating agents can therefore adversely affect metal homeostasis.

More recently, chelating agents have been employed as antimicrobial agents and have been shown to inhibit microbial growth, although little is known about how they mediate these effects (Corbin et al., 2008; Paterson et al., 2022). Although not currently prescribed for infections, their widespread use in medicine suggests they can be safely administered to patients. If their use as antimicrobial agents can be conclusively proven, it may therefore be possible that chelants can be adopted in hospitals and clinics as both a preventative measure and in the treatment of various microbial infections such as intractable wound infections. They can be even considered in combination with antibiotics as potentiators of antimicrobial efficacy (Brown & Richards, 1965; Umerska et al., 2018). The main group of chelants examined for effects on bacterial growth within this thesis are outlined in Section 1.2.1 below.

1.2.1 Chelating agents relevant to this study

In the following section, a brief introduction is given to seven of the chelating agents examined within this thesis, including any current known uses. The chemical structures of all of these chelants are illustrated in Chapters 3 and 4 (Fig. 3.1 and

4.1). The other seven chelants examined (BCS, CAT, DTPA GLDA, HBED, MGDA and TPEN) are described more fully by Beecroft (2019).

1.2.1.1 EDTA

Ethylenediaminetetraacetic acid (EDTA) is a well-known metal chelating agent which has a wide range of applications, from use as a preservative in consumer products, such as soaps and shampoos, to the treatment of patients with heavy metal poisoning (Finnegan & Percival, 2015). EDTA is one of the very few chelating agents which has been used in a medical context, both in treatment of heavy metal poisoning (Flora & Pachauri, 2010; Porru & Alessio, 1996) and in commercially available wound dressings to help manage infection (Finnegan & Percival, 2015). EDTA has been used in product formulations by the cosmetic industry for many years due to its high efficacy as a preservative and its relative safety (Lanigan et al., 2002), although more recent studies have highlighted problems with its persistence in the environment (Oviedo & Rodríguez, 2003). EDTA is one of the highest-level organic pollutants found in surface waters in Europe and cannot be degraded by the conventional biological and physicochemical methods used in treating waste water or purifying drinking water (Nörtemann, 1999).

The mechanism through which EDTA exerts its antimicrobial effects has yet to be defined. Early studies into the effects of EDTA on *E. coli* suggested that this chelant is capable of increasing the permeability of the Gram-negative cell membrane (Alakomi et al., 2006; Leive, 1965b; Voss, 1967). It was proposed that membrane destabilisation due to the removal of divalent cations Mg^{2+} and Ca^{2+} leaves the cells more vulnerable to osmotic stress and thus more susceptible to lysis. Early studies into the use of EDTA in conjunction with antibiotics demonstrated that pre-treatment of *P. aeruginosa* with EDTA results in increased susceptibility to β-lactams such as ampicillin (Haque & Russell, 1974). More recent studies have indicated that co-treatment of *P. aeruginosa* biofilms with EDTA alongside ciprofloxacin and ampicillin

can reduce the minimum inhibitory concentration (MIC) of these antibiotics 30-fold (Liu et al., 2017). Some research even suggests that EDTA treatment can reverse the resistant phenotype of methicillin-resistant *S. aureus*, causing biofilms to become unstable and disperse, thereby increasing antibiotic access (Jain et al., 2016). Most recently, it has been demonstrated that EDTA causes 5- to 15-fold reduction in cellular manganese concentrations in *E. coli,* coupled with lesser reductions in zinc and iron (Paterson et al., 2022). Further applications of EDTA, including its use in a therapeutic context, are discussed further in Section 1.2.2.

1.2.1.2 DTPMP

Diethylenetriamine pentamethylene phosphonic acid (DTPMP) is an organophosphonate which binds tightly to di- and trivalent metal ions including iron, copper and zinc (Cardiano et al., 2017). DTPMP is often used in the production of detergents and in treatment of waste water and water softening, as it binds to metals within the water, preventing them from forming insoluble aggregates (Rott et al., 2018). Along with EDTA, DTPMP has been widely used in the bleaching of pulp in paper manufacture. Transition metals are known to have high catalase activity, and uncomplexed transition metals are capable of catalysing the degradation of hydrogen peroxide, thereby reducing the efficiency of the bleaching process, and lowering the quality of the final product. The addition of chelating agents means any transition metals are complexed, preventing them from exercising their catalase activities and restoring the efficiency of the bleaching process (Pirkanniemi et al., 2003).

Few studies have investigated the effect of DTPMP on bacterial growth, however preliminary data indicates that it causes a reduction in cellular iron coupled with an increase in cellular manganese in *E. coli* (Paterson et al., 2022). Use in humans is currently limited, though early studies have indicated that oral and dermal absorption of DTPMP are extremely low (MAK Value Documentation, 2015). However, prolonged exposure to DTPMP has been shown to affect iron metabolism, eventually

resulting in anaemia. Effects on magnesium, calcium, and phosphate metabolism have also been observed after long-term exposure of rats to high doses of DTPMP (MAK Value Documentation, 2015).

1.2.1.3 CHA

Octanohydroxamic acid (also known as caprylohydroxamic acid, CHA) has very few cited applications. An extensive literature search revealed that its only known uses are in mineral purification, manufacture of supercapacitor electrodes and as a preservative in consumer products. Cassiterite is an economically important tin mineral in the earth's crust that is difficult to extract. The most effective method used in its separation is froth flotation in which metals are separated according to their surface hydrophobicity differences. CHA is used as a chelator in this process to bind metal cations and aid purification of the tin ore (Ren et al., 2018). Another primary use of CHA is in the production of supercapacitor electrodes (Milne & Zhitomirsky, 2018). Here, CHA forms insoluble complexes with MnO_2 and Mn_3O_4 to aid their extraction in this process. In consumer products such as shampoos and moisturisers, CHA has been used as a preservative, but has recently been linked to allergic contact dermatitis and therefore caution is advised when using this chelant for topical applications (Ackermann et al., 2017). Treatment with CHA does not alter the concentration of key transition metals in *E. coli* (Paterson et al., 2022) and therefore the mechanisms through which it exerts its antibacterial effects remain unclear.

1.2.1.4 PO

Piroctone olamine (PO) is commonly used as an antifungal in product formulations, most notably in shampoos to prevent dandruff (Schmidt-Rose et al., 2011). Its mechanism of action is complex and poorly understood, but it is known that this chelant has the ability to penetrate cells and form complexes with Fe^{2+} and Fe^{3+} ions to inhibit the metabolism of pathogenic fungi (Kim et al., 2011). More recently, PO has been used to treat intra-abdominal fungal infections in mice (do Couto et al., 2016),

suggesting that its range of applications has not yet been fully realised. PO results in a decrease in cellular iron and an increase in cellular manganese in *E. coli* (Paterson et al., 2022).

1.2.1.5 Tropolone

Tropolones are non-benzenoid seven-membered aromatic compounds with a carbonyl group (Liu et al., 2014). Tropolone has been known for many years to be bactericidal for a wide range of bacterial species (Trust, 1975). Treatment with tropolone results in cell lysis of both Gram-positive and Gram-negative species, (Trust, 1975). A more recent study focusing on *S. aureus* highlighted the importance of the action of tropolone against the bifunctional metalloenzyme CapF, involved in the production of capsular polysaccharide in this pathogenic species. Tropolone binds tightly to the Zn^{2+} ion needed by this enzyme, and thereby destabilises the enzyme and halts production of this essential polysaccharide, leaving the cells vulnerable to lysis (Nakano et al., 2015).

1.2.1.6 Hinokitiol

Hinokitiol (β-thujaplicin) is a tropolone derivative which has demonstrated strong antibacterial activities against both *E. coli* and *S. aureus* (Morita et al., 2007). It has been suggested that its bactericidal activity may be due in part to its metabolic inhibition of the cell membrane and repression of cellular respiration (Morita et al., 2007). More recent studies have even suggested that hinokitiol may be used in the treatment of cancer through inhibition of proliferation and colony formation of lung adenocarcinoma cells, suggesting DNA damage, autophagy and cell cycle inhibition as the three modes of action (Li et al., 2014). Hinokitiol is capable of binding to Fe^{2+} or Fe^{3+} with high affinity, and the resultant cellular iron deprivation has been shown to inhibit DNA synthesis (Ido et al., 1999). Hinokitiol derivatives which do not possess iron binding capabilities show no ability to cause DNA fragmentation (Ido et al., 1999).

1.2.1.7 Fusaric acid

Fusaric acid (FA) is a mycotoxin which is able to chelate copper ions at a ratio of two FA molecules to one Cu^{2+} ion (Yin et al., 2015). A study which investigated the ability of bacteria and fungi to detoxify FA demonstrated that none of the bacterial strains were capable of chemically modifying FA, suggesting that it may prove to be a potent antimicrobial (Crutcher et al., 2017). Indeed, it was seen that highly resistant strains were found only in Gram-negative bacteria, mainly in the *Pseudomonas* genus, and appeared to be dependent upon the number of efflux pumps available (Crutcher et al., 2017). The fact that Gram-positive strains are more susceptible to FA may indicate that it is able to penetrate the single cell membrane, but the outer cell wall provides some protection. Interestingly, FA has also demonstrated hypotensive properties due to its ability to inhibit dopamine-β-hydroxylase, an enzyme involved in biosynthesis of norepinephrine (Hidaka et al., 1969). FA has also been shown to potentially reduce symptoms of mania in a patient with Wilson's disease; a disorder characterised by excess copper accumulating within the body (Pandey et al., 1981), though this has not been confirmed.

1.2.1.8 Summary

While all of these chelants show preferential binding to specific metal ions, they are also capable of binding to other metal ions depending on the metal bioavailability in their environment. Just as metalloenzymes are capable of mismetallation, chelating agents can also bind to other metals if they are found in much greater abundance than their metal of preference. The chelators listed above were selected for analysis based on their predicted metal affinities and chemical properties (Appendix, Table 9.1). Industrial considerations such as regulatory frameworks and cost were also considered in partnership with Proctor and Gamble. EDTA is known to increase the efficacy of preservatives (Ghelardi et al., 2013), CHA is currently used in beauty care (Ackermann et al., 2017) and PO has been used in commercial products to inhibit

fungal growth (Schmidt-Rose et al., 2011). Use of each of these chelating agents as antimicrobial agents in their own right has received little attention, however, and the precise mechanisms of action through which they mediate their antimicrobial properties remains a fascinating area of research.

1.2.2 Therapeutic applications of EDTA

EDTA has been extensively used to treat patients with heavy metal poisoning; chelating toxic metal ions to allow them to be safely excreted from the body (Flora & Pachauri, 2010; Porru & Alessio, 1996; Sears, 2013). It has also been used to treat vascular disease and may improve endothelial function through removal of calcium found in atherosclerotic plaques (Flora & Pachauri, 2010; Lamas et al., 2013; Lamas & Ergui, 2016), however the data is not yet sufficiently convincing to suggest this as the main method of treatment for patients with vascular or heart disease. Of chief interest in this thesis, however, are uses of EDTA in the management of microbial infections, as outlined in greater detail below.

1.2.2.1 Wound care

There is an expanding body of evidence suggesting that EDTA could be employed as an antimicrobial and anti-biofilm agent in skin and wound care treatments (Finnegan & Percival, 2015). Antimicrobial effects of EDTA have been documented against both Gram-negative and Gram-positive organisms, as well as yeasts, amoeba and fungi (Alakomi et al., 2006; Finnegan & Percival, 2015; Leive, 1965a; Weiser et al., 1968). In Gram-negative bacteria, magnesium and calcium ions are known to be essential for the stabilisation of the negative charges in the lipopolysaccharides found in the outer leaflet of the outer membrane (Leive, 1965b). EDTA appears to remove these, or other, essential cations, thereby releasing up to 50% of the LPS molecules and exposing the inner membrane (Walsh et al., 2003).

Not only would this lower the integrity of the cell wall against turgor pressure, but it should also increase access for other antimicrobials.

Biofilms present a significant problem in the treatment of wounds, creating a barrier against phagocytic cells from the host and protecting against antimicrobials. Biofilms are composed of a heterogeneous matrix of polymers including polysaccharides, proteins, nucleic acids, glycoproteins, metal ions and phospholipids (Finnegan & Percival, 2015). EDTA can be used to decrease the cation concentration of biofilms to help increase permeability to allow penetration of antimicrobials by reducing the extent of crosslinking within the biofilm (Robertson et al., 2012). Wound dressings can be used to deliver both therapeutics and antimicrobials to the site of the wound to help prevent and treat wound infections. Recently, EDTA has been used in combination with other substances in wound dressings to prevent and manage the formation of biofilms (Finnegan & Percival, 2015). EDTA may also be capable of chelating iron which is vital for microbial virulence and pathogenicity (Griffiths, 1991).

One of the best studied model organisms for biofilm formation is the Gram-negative *Pseudomonas aeruginosa* which is implicated in many types of infections, often as an opportunistic pathogen in immunocompromised individuals or burn victims. Exposure of *P. aeruginosa* biofilms to EDTA results in 1,000-fold greater killing than treatment with gentamicin, an antibiotic commonly used to treat *Pseudomonas* infections (Banin et al., 2006). This study additionally showed that using EDTA in combination with gentamicin could completely eradicate *P. aeruginosa* from model biofilms. EDTA treatment facilitates two processes; cell detachment and cell killing. Addition of magnesium resulted in a prevention of cell killing, although some detachment was still apparent. When calcium or iron ions were added, both detachment and killing were completely blocked, suggesting that these metal cations have essential roles in the impact of EDTA (Banin et al., 2006).

1.2.2.2 Combination therapies

Despite its other therapeutic applications, EDTA has not yet been recognised as a significant antimicrobial in its own right, instead being seen as a potentiator of the effects of other antimicrobial substances from as early as the 1960s (Brown & Richards, 1965; Umerska et al., 2018). The ability of EDTA to disrupt the outer membrane of Gram-negative bacteria through removal of calcium and magnesium ions means that it is often used in combination with other antimicrobials to increase their efficacy by facilitating access to the inner cell membrane. EDTA was initially seen to work well in combination with polymyxin B sulphate, benzalkonium chloride and chlorhexidine diacetate against *Pseudomonas* cultures (Brown & Richards, 1965) and with carbamyl phosphate, o-nitrophenlygalactoside and actinomycin D against *E. coli* (Leive, 1965a). Interestingly, *E. coli* is completely resistant to actinomycin D before EDTA treatment, suggesting that inclusion of EDTA in therapeutic contexts could allow a greater arsenal of antibiotics to be deployed in combatting antibiotic-resistant pathogens.

More recently, EDTA has been shown to exhibit synergistic interactions with multiple antimicrobial peptides including ARVA and AA230 (Umerska et al., 2018). When used in combination with EDTA, the concentration of AA230 can be reduced up to 4-fold, even in multidrug resistant clinical isolates. EDTA treatment alone has proven bacteriostatic against multiple Gram-negative species including *P. aeruginosa* and *E. coli*, but was not toxic to these species at concentrations as high as 16 mg/ml (Umerska et al., 2018).

Antibiotic resistance can be caused by a permeability barrier which prevents the antibiotic from reaching its target in the bacterial cell; such is the case with chloramphenicol, actinomycin, benzyl penicillin and vancomycin (Weiser et al., 1968). In the case of the Gram-negative species *E. coil, P. mirabilis* and *P. aeruginosa*, sub-inhibitory concentrations of EDTA resulted in a reduction in the MIC of each strain

against ampicillin, penicillin G, chloramphenicol and tetracycline (Weiser et al., 1968). Complete reversal of antibiotic resistance was noted with all tetracycline-resistant organisms and with penicillin and ampicillin-resistant strains of *P. aeruginosa* (Weiser et al., 1968). Interestingly, further experiments demonstrated that the EDTA-induced reversal of antibiotic resistance could be completely prevented through the addition of magnesium sulphate or calcium chloride; suggesting that magnesium and calcium chelation could play important roles in the mechanism of action of EDTA. It should be noted however, that increasing the permeability of the cell membrane may not be the only mechanism by which EDTA enhances the efficacy of other antibiotics. Addition of Mg^{2+} and Fe^{2+} has been seen to reduce the antimicrobial efficacy of tetracycline against Gram-negative bacteria (Weinberg, 1957). This would be consistent with EDTA sequestering these ions out of the nutrient broth, rather than exerting its effects at the cell wall in order to enhance antibiotic activity.

1.3 Aims of this thesis

Despite the widespread use of chelating agents in industry, commercial products and healthcare, there is limited published work examining the mode of action of chelating agents as antimicrobials, especially in terms of their effects on metal deprivation. Further exploration of this area could provide an alternative approach in combatting the emerging crisis in antibiotic resistance. It may also allow the selection of more biodegradable and environmentally-friendly options in consumer goods, especially, soaps, shampoos and disinfectants. The evidence to date suggests that metal deprivation and outer membrane damage are important in chelant-mediated growth inhibition. In this project, I aim to build upon and enhance our understanding of the mechanisms by which chelating agents retard or prevent the growth of Gram-positive and Gram-negative bacteria.

Using a novel selection of chelants, I will investigate the differences in response of Gram-negative and Gram-positive species to chelant-mediated growth inhibition; both

singly and using pairs of chelants to determine synergistic or antagonistic combinations against either *E. coli* or *P. aeruginosa*. Chelants will also be paired with commonly used antibiotics with known mechanisms of action to determine whether chelants assist in inhibiting the growth of bacteria in the presence of conventional antimicrobials. Using ICP-MS, the effects of chelating agents on cellular metal concentrations in *P. aeruginosa* will be examined and compared, where available, with previously generated data on *E. coli* to examine species-specific effects.

I will further examine the resistance or susceptibility of single gene deletion mutants from the Keio collection in an effort to highlight genes responsible for tolerance of chelating agents. In addition to this, *E. coli* and *S. aureus,* as model Gram-negative and Gram-positive species, will be grown in low levels of either of two chelants to select for mutants with increased resistance with the aim of identifying targets of chelant action. Genome sequencing of any chelant-resistant mutants obtained will provide further insight into genes of significance in the development of resistance to chelant-mediated growth inhibition.

In summary, this project aims to expand our understanding of the antibacterial mechanism of action of chelating agents with an emphasis on how bacteria are restricted in their ability to acquire metals. A more complete understanding of how chelants function as antibacterials should allow improvements in efficacy of microbial hostility in products and potentially contribute to tackling the increasing threat of antimicrobial resistance.

2 Materials and methods

2.1 Bacteria, plasmids, chelants and antibiotics

2.1.1 Bacterial strains and plasmids

Bacterial strains and plasmids used in this study are listed in Table 2.1 and Table 2.2, respectively.

Table 2.1 Bacterial strains used in this study. Genotype shown where available.

Species	Strain	Source and genotype
Bacillus subtilis	Strain 186, ATCC6051	Ehrenberg, Cohn, *ind⁻ tyr⁺*. From Elizabeth Sockett, University of Nottingham.
Escherichia coli	BL21-AI	*B F⁻ ompT gal dcm lon hsdSB(rB⁻ mB⁻) [malB⁺]K-12(λS) araB::T7RNAP-tetA*. Purchased from ThermoFisher Scientific.
	BW25113, CGSC7636	*lacI⁺ rrnBT14 ΔlacZWJ16 hsdR514 ΔaraBADAH33 ΔrhaBADLD78 rph-1 Δ(araB–D)567 Δ(rhaD–B)568 ΔlacZ4787(::rrnB-3) hsdR514 rph-1*. Wild-type strain from the Keio collection (Baba et al., 2006). All 'JW' strains below are from this collection obtained *via* David Weinkove, Durham University.
	JW1111	As BW25113, but Δ*acrB*::*kan*
	JW0891	As BW25113, but Δ*aroA*::*kan*
	JW4094	As BW25113, but Δ*cadC*::*kan*
	JW3582	As BW25113, but Δ*cysE*::*kan*
	JW5646	As BW25113, but Δ*envC*::*kan*
	JW4251	As BW25113, but Δ*fecA*::*kan*
	JW4250	As BW25113, but Δ*fecB*::*kan*
	JW4248	As BW25113, but Δ*fecD*::*kan*
	JW4247	As BW25113, but Δ*fecE*::*kan*
	JW5086	As BW25113, but Δ*fepA*::*kan*
	JW0584	As BW25113, but Δ*fepB*::*kan*
	JW0580	As BW25113, but Δ*fepC*::*kan*
	JW0582	As BW25113, but Δ*fepD*::*kan*
	JW0576	As BW25113, but Δ*fes*::*kan*
	JW4331	As BW25113, but Δ*fhuF*::*kan*
	JW2008	As BW25113, but Δ*hisI*::*kan*

	JW1667	As BW25113, but Δ*lpp*::*kan*
	JW2388	As BW25113, but Δ*mntH*::*kan*
	JW5503	As BW25113, but Δ*tolC*::*kan*
	JW1848	As BW25113, but Δ*znuB*::*kan*
	JW1847	As BW25113, but Δ*znuC*::*kan*
Pseudomonas aeruginosa	NCTC10662, ATCC25668	Schroeter, Migula; originally a clinical isolate. Obtained from Public Health England.
Staphylococcus aureus	FDA209P, ATCC6538P	Reference methicillin-sensitive *S. aureus* (MSSA) strain (Singh et al., 2015).
	SAUSA300	JE2, USA300 LAC. Wild-type community-associated methicillin-resistant (CA-MRSA) parental strain for the NARSA collection (Fey et al., 2013). Obtained from the University of Nebraska *via* Kevin Waldron, Newcastle University.
	SAUSA300_2441	As SAUSA300, but *fnbA*::*erm*
	SAUSA300_0959	As SAUSA300, but *fmtA*::*erm*
	SAUSA300_0647	As SAUSA300, but *vraF*::*erm*
	SAUSA300_2568	As SAUSA300, but *arcD*::*erm*
	SAUSA300_1807	As SAUSA300, but *tcyC*::*erm*
	SAUSA300_1607	As SAUSA300, but *1546*::*erm*

Table 2.2 Plasmids used in this study. All plasmids were supplied by Genscript.

Plasmid name	Details	Gene length (bp)
pCadC	*E. coli* K12 *cadC* gene inserted in pET22b using NdeI and BamHI sites at 5' and 3' ends, respectively.	1548
pCadC-Thr236Ala	As pCadC, but with Thr236Ala substitution.	1548
pCadC-Met448Ala	As pCadC, but with Met448Ala substitution.	1548
pCadC-Tyr453His	As pCadC, but with Tyr453His substitution.	1548
pEntD	*E. coli* K12 *entD* gene inserted in pET22b using NdeI and BamHI sites at 5' and 3' ends, respectively.	630
pFepA	*E. coli* K12 *fepA* gene inserted in pET22b using NdeI and BamHI sites at 5' and 3' ends, respectively.	2250
pFruB	*E. coli* K12 *fruB* gene inserted in pET22b using NdeI and BamHI sites at 5' and 3' ends, respectively.	1140
pNanM	*E. coli* K12 *nanM* gene inserted in pET22b using NdeI and BamHI sites at 5' and 3' ends, respectively.	1116
pQuuQ	*E. coli* K12 *quuQ* gene inserted in pET22b using NdeI and BamHI sites at 5' and 3' ends, respectively.	762

pThiD	*E. coli* K12 *thiD* gene inserted in pET22b using NdeI and BamHI sites at 5' and 3' ends, respectively.	810
pYahJ	*E. coli* K12 *yahJ* gene inserted in pET22b using NdeI and BamHI sites at 5' and 3' ends, respectively.	1392

2.1.2 Media

Luria Bertani (LB Lennox) medium was used for bacterial cultivation on agar plates (Sigma Aldrich, L7533) and broth (Sigma Aldrich, L3022). Mueller-Hinton broth (Sigma Aldrich, 70192) or Iso-Sensitest broth (Oxoid, CM0473) were also used for bacterial cultivation in liquid culture. All media and agar was sterilised at 121˚C for 15 min at 15 psi in a Dixons Vario 1528 autoclave. Media and other water-soluble reagents were made up in distilled water obtained from a Milli-Q® Integral 15, Merck Millipore water filtration system, and sterilised by autoclaving.

2.1.3 Chelants and antibiotics

Chelants and antibiotics used are listed in Tables 2.3 and 2.4, respectively, and were sterilised by filtration through a 0.2 µM filter (Fisher Scientific, 15206869).

Table 2.3 Chelating agents used in this study. For chelants provided in liquid form, no solvent was required prior to testing.

Synonym	Formal Name (s)	CAS Number	Source	Solvent
BCS	*Bathocuproine disulphonic acid (disodium salt)*	52698-84-7	Sigma-Aldrich	Water
CAT	*Catechol, 1,2-dihydroxybenzene*	120-80-9	Sigma-Aldrich	Water
CHA	*Caprylhydroxamic acid, octanohydroxamic acid*	7377-03-9	Fluorochem	DMSO
CHL	*Chloroxine, dichlorchinolinolum,*	773-76-2	Sigma-Aldrich	DMSO
DTPA	*Diethylenetriaminepentaacetic acid*	67-43-6	Sigma-Aldrich	Water
DTPMP	*Diethylenetriaminepentakis(methylphosphonic acid)*	15827-60-8	Sigma-Aldrich	N/A
EDTA	*Ethylenediaminetetraacetic acid*	60-00-4	Melford	Water
FA	*Fusaric acid, 5-butylpyridine-2-carboxylic acid, fusarinic acid*	536-69-6	Sigma-Aldrich	DMSO

GLDA	*N,N-bis(carboxymethyl)-L-glutamic acid (tetrasodium salt)*	51981-21-6	Biosynth Carbosynth	Water
HBED	*N,N'-di(2-hydroxybenzyl)ethylene diamine-N,N'-diacetic acid (monohydrochloride hydrate)*	35369-53-0	Strem Chemicals	DMSO
HNK	*2-Hydroxy-6-(propan-2-yl)cyclohepta-2,4,6-trien-1-one, β-Thujaplicin, hinokitiol*	499-44-5	Sigma-Aldrich	DMSO
MGDA	*Methylglycinediacetic acid, N-(1-carboxylatoethyl)iminodiacetate (trisodium hydrate)*	164462-16-2	TCI	Water
PO	*Piroctone olamine, 1-hydroxy-4-methyl-6-(2,4,4-trimethylpentyl)-2(1H)-pyridone ethanolammonium salt*	68890-66-4	Combi-Blocks	DMSO
TPEN	*N,N,N',N'-tetrakis(2-pyridinylmethyl)-1,2-ethanediamine*	16858-02-9	Cayman Chemical	Ethanol
TRO	*Tropolone, 2-Hydroxy-2,4,6-cycloheptatrien-1-one,*	533-75-5	Sigma-Aldrich	DMSO

DTPA and EDTA were solubilised by addition of NaOH to pH8.

Table 2.4 Antibiotics used in this study. Discs were used according to the manufacturer's instructions, as outlined in section 2.4.4.

Antibiotic	Supplier	Catalogue number	Solvent
Ampicillin	Melford	A0104	Water
Cefotaxime	ThermoFisher Scientific Oxoid discs	15219946 11903042	Water N/A
Cefoxitin	Sigma-Aldrich Oxoid discs	C4686 11944022	Water N/A
Cefsulodin	Sigma-Aldrich	C8145	Water
Chloramphenicol	Melford	C0113	Ethanol
Kanamycin	Sigma-Aldrich Oxoid discs	K1876 CT0026B	Water N/A
Moenomycin	Santa Cruz Biotechnology	362031	DMSO
Penicillin G	Sigma-Aldrich Oxoid discs	13752 10340953	Water N/A
Spectinomycin	Sigma-Aldrich	S4014	Water

Streptomycin	Sigma-Aldrich	S6501	Water
Tetracycline	Sigma-Aldrich Oxoid discs	87128 CT0054B	Ethanol N/A
Vancomycin	Oxoid discs	CT0058B	N/A

2.1.4 Bacterial culture preparation

Overnight cultures were prepared by picking a single colony from a Luria Bertani (LB) agar plate using a sterile plastic loop (Sarstedt, 86.1562.010) and inoculating 5 ml of LB broth in a sterile 15 ml screw-capped Falcon tube (Sarstedt, 62.554.502). Cultures were incubated at 37°C in a shaking incubator at 150 rpm (Stuart Orbital Incubator SI500) for 16-20 h. Both plates and overnight cultures were stored at 4˚C for 1-3 weeks. Longer term storage of strains was achieved through mixing an overnight culture with sterile 80% glycerol in a 1.6:1 ratio in 1.5 ml screw-capped microtubes (Sarstedt, 72.692.005) which were frozen at -80˚C.

2.1.5 Plasmid transformation

Plasmid constructs are listed in Table 2.2 and all codon-optimised genes were synthesised and inserted into appropriate vectors by Genscript. 0.5 ml of overnight culture was added to 7.5 ml of LB in 15 ml Falcon tubes. Cultures were incubated at 37°C with shaking at 150 rpm until an $A_{600\,nm}$ of ~0.5 using a spectrophotometer (Cole-Parmer, Jenway 6300, 630501). Cells were pelleted by centrifugation at 5,000 x *g* for 5 min at 4°C and the supernatant discarded. Cell pellets were resuspended in 0.5 ml of ice-cold 100 mM $CaCl_2$ (ThermoFisher Scientific, 10171800) for 10-20 min. The resulting competent cells (100 µl) were transferred to a 1.5 ml microtube (Sarstedt, 72.690.001) and 1 µl of plasmid DNA added. Mixtures were incubated on ice for 20 min before transfer to 37°C for 2 min. These samples were returned to ice for 5 min before addition of 0.3 ml of LB broth and further incubation at 37°C for 30 min. The transformed cells were spread onto LB agar plates containing an appropriate antibiotic. Plates were incubated at 30°C overnight in a sealed plastic container.

2.2 Isolation and genome sequencing of chelant-resistant mutants

Mutants resistant to chelants were isolated by repeated subculture of *E. coli* (BW25113) and *S. aureus* (FDA209P) in sub-MIC concentrations of EDTA or DTPMP. Bacteria were initially cultivated in LB broth in 1 ml volumes in 1.5 ml Eppendorf tubes (Sarstedt, 72.690.001) in the presence or absence of each chelant and repeatedly subcultured daily for 15 days at 37°C. Cultures were streaked on LB agar plates to obtain single colonies and frozen stocks retained for subsequent analysis. Day 15 cultures were then transferred to sterile, lidded 96-well microtitre plates (Sarstedt, 82.1582.001) to allow additional (higher) chelant concentrations to be used. 25 µl of overnight culture in 225 µl LB were each divided into three separate cultures and daily subculture performed for a total of 29 days. Microcentrifuge tubes and sealed microtitre plates were incubated at 4°C over weekends during this period. After the final cycle on Day 29, 50 µl of the highest growing of each triplicate was used to inoculate 5 ml of LB and a frozen stock created from the resulting overnight culture. Single colonies from these stocks were selected alongside Day 15 strains to determine whether any had developed resistance to DTPMP or EDTA. The genome sequence of these mutants, alongside the parental wild-type *E. coli* and *S. aureus* strains, was determined using an Illumina MiSeq platform with 30 times coverage by Microbes NG with further analysis and interpretation carried out by Ping Hu, (P&G, Cincinnati). An annotation pipeline was devised and differences between the parental strains and mutants identified.

2.3 Bacterial mutant characterisation

2.3.1 *E. coli* and *S. aureus* growth curves

1 ml of LB broth was inoculated with 50 µl of a bacterial overnight culture in a sterile semi-micro cuvette (Sarstedt, 67.742) which was sealed with parafilm (Sigma Aldrich, P7668). Sealed cuvettes were incubated at 37°C with shaking at 150 rpm until

reaching an $A_{650\,nm}$ of ~0.07, equivalent to a 0.5 MacFarland standard (240 µM $BaCl_2$ in 0.18 M H_2SO_4 aq.), as measured using a spectrophotometer (Cole-Parmer, Jenway 6300, 630501). Cultures were diluted 1:10 in LB and 100 µl applied to the wells of a microtitre plate, giving a final cell concentration of approximately 4.5 x 10^6 cfu/ml for *E. coli* and 1 x 10^6 cfu/ml for *S. aureus*. This plate was incubated at 37°C with shaking at 300 rpm for 16 h in a plate reader (Spectrostar Nano, BMG Labtech), taking readings at $A_{650\,nm}$ every 10 min. The mean and standard deviation was calculated for each strain in triplicate after subtracting negative controls containing media alone.

2.3.2 Minimum inhibitory concentration (MIC) assays

50 µl of bacterial overnight culture was inoculated into 1 ml of LB (Sigma Aldrich, L3022), Iso-sensitest (Oxoid, CM0473), or Mueller-Hinton (Sigma Aldrich, 70192) broth in a sterile semi-micro cuvette sealed with parafilm. Sealed cuvettes were incubated at 37°C with shaking at 150 rpm until reaching an $A_{650\,nm}$ of ~0.07 and then diluted 1:10 in the appropriate media. Two-fold serial dilutions of the chelant or antibiotic to be tested were performed in the appropriate media and 50 µl of each dilution series transferred to the wells of a microtitre plate to give a gradient of compound concentration. The diluted bacterial culture (50 µl) was then applied to the appropriate wells of the plate alongside the relevant positive and negative controls. Plates were incubated at 37°C with shaking at 150 rpm for 16 h in a sealed plastic container. Absorbance at 600 nm was then measured using a Spectrostar Nano plate reader. The mean and standard deviation was calculated for each mutant after subtracting the negative controls. Minimum inhibitory concentrations were defined as the minimum concentration of chelant needed to inhibit growth by ≥90%. Where required in BL21-AI plasmid-carrying strains, the LB into which the bacterial cultures were grown was supplemented with 1 mM IPTG (Melford, 156000 MB1008) and 0.2% arabinose (Melford, A3256) to induce gene expression. For media comparison experiments, the original cultures were grown in LB media in a cuvette as described

above, but after reaching an $A_{650\ nm}$ of 0.07, the 1:10 dilution of culture was carried out in Iso-sensitest broth, Mueller-Hinton broth, supplemented Mueller-Hinton broth (containing 25 mg/L $CaCl_2$ and 12.5 mg/L $MgCl_2$), and standard LB media, ensuring that the final concentration of LB in the resultant assays was no more than 0.5% for Iso-sensitest and Mueller Hinton experiments but allowing use of the same inoculum in each case.

2.3.3 Viability assays

1 ml of LB broth was inoculated with 50 µl of a bacterial overnight culture in a cuvette, grown to an $A_{600\ nm}$ of ~0.4. Cultures were used to create 10-fold serial dilutions in 1 ml volumes in chilled LB broth. 60 ml of sterile LB agar was poured into a square plate (Sarstedt, 82.9923.422) to which chelant was added to give final concentrations of 0, 250, 375, or 500 µM EDTA, or 0, 100, 200, or 300 µM DTPMP. Similar assays were performed with high salt concentrations (0.5 or 1 M NaCl) to evaluate susceptibility to osmotic stress, and again with moenomycin (0.0025 or 0.01 µg/ml) to determine susceptibility to this antibiotic. These plates were allowed to cool and set, and were then dried in a 30°C incubator for a minimum of 20 min. 10 µl of each of the serial dilutions was applied to the surface of each agar plate and allowed to soak in. Plates were incubated at 30°C overnight and imaged at various points over the following days.

2.4 Further *S. aureus* mutant characterisation

2.4.1 Susceptibility of *S. aureus* to Triton X-100

0.5 ml of an overnight culture was inoculated into 4.5 ml of LB broth and incubated with shaking at 150 rpm at 37°C until an $A_{650\ nm}$ of 0.6. Cells were pelleted by centrifugation at 5,000 x *g* for 7 min and supernatant discarded. Cell pellets were resuspended in 1 ml of PBS (Melford, P32080 P3203) and transferred to 1.5 ml micro-tubes, before centrifugation at 20,000 x *g* for 1 min. This process was repeated until

cells had been washed three times. 90 µl of washed cells were then transferred to a microtitre plate. 10 µl of 1% Triton X-100 (Sigma Aldrich, T8787) was added to the relevant wells of the plate (giving a final concentration of 0.1% Triton X-100), while 10 µl of sterile distilled water was added to controls. Absorbance at 650 nm was monitored at 5 min intervals for 3 h using a plate reader. The mean and standard deviation were calculated for each strain at each time point.

2.4.2 Susceptibility of *S. aureus* to lysostaphin

0.5 ml of an overnight culture was inoculated into 4.5 ml of LB broth and incubated with shaking at 150 rpm at 37°C until an $A_{650\ nm}$ of 0.6. Cells were pelleted by centrifugation at 5,000 x *g* for 7 min and supernatant discarded. Cell pellets were resuspended in 1 ml of PBS and transferred to 1.5 ml micro-tubes, before centrifugation at 20,000 x *g* for 1 min. This process was repeated until cells had been washed three times. 90 µl of washed cells were then transferred to a microtitre plate. 10 µl of 25 µg/ml lysostaphin (Sigma Aldrich, L7386) was added to the relevant wells of the plate (giving a final concentration of 2.5 µg/ml lysostaphin). Absorbance at 650 nm was monitored at 5 min intervals for 3 h (first 30 min shown) using a plate reader. The mean and standard deviation were calculated for each strain at each time point.

2.4.3 Susceptibility of *S. aureus* to lysozyme

60 ml of sterile LB agar was poured into a square plate (Sarstedt, 82.9923.422). Plates were allowed to cool and set and were then dried in a 30°C incubator for a minimum of 20 min with lids open and the agar surface facing downwards. Bacterial overlays were made by inoculating 7.5 ml of cooled molten 0.6% LB agar (10 g/L tryptone (Melford, T60065), 5 g/L yeast extract (Melford, Y1333.0100), 10 g/L NaCl (ThermoFisher Scientific 10735921), 2 ml/L 1 M NaOH (Sigma Aldrich, S5881), 6 g/L agar (Sigma Aldrich, A4550)) with 0.5 ml of a bacterial overnight culture in a 15 ml Falcon tube (kept at 60°C in a water bath) which was mixed briefly by inversion. Poured plates were allowed to cool and dry as described above. Serial dilutions of

lysozyme (Melford, L38100) at 50, 25, and 12.5 mg/ml were prepared in sterile distilled water. 20 µl volumes of each dilution were applied to the overlay surface and three repeats were performed. Plates were allowed to dry at room temperature and incubated at 30°C overnight in a sealed plastic container.

2.4.4 Susceptibility to antibiotics using discs

Bacterial overlays were made as described above and plates allowed to cool and dry before applying antibiotic discs containing defined amounts of cefotaxime, cefoxitin, penicillin G (Oxoid, 11903042, 11944022, and 10340953 respectively). Plates were incubated at 30°C overnight in a sealed plastic container. Photographs were taken in a Bio-Rad Gel Doc system and analysed using ImageJ (Fuji) to permit measurement of the zones of inhibition surrounding each antibiotic disc. At least three measurements were taken per zone in different orientations, and the mean and standard deviation from three disc measurements calculated.

2.4.5 *S. aureus* cytochrome *c* binding assay

The following method was adapted from the protocol outlined by T.W. Cullen (Cullen et al., 2015). 3 ml of bacterial overnight was inoculated into 5 ml of LB broth and incubated with shaking at 150 rpm at 37°C until an $A_{650\ nm}$ of 1. Cells were pelleted at 5,000 x *g* for 10 min and supernatant discarded. Cell pellets were resuspended in 1 ml of 20 mM MOPS (Sigma Aldrich, M1254) and transferred to 1.5 ml microtubes before centrifugation at 20,000 x *g* for 1 min. This was repeated until cells were washed three times. Final resuspension was carried out in 0.5 ml 20 mM MOPS. Cells were normalised to an $A_{600\ nm}$ of approximately 2-2.5 using 100 µl samples in a microtitre plate. 450 µl of the normalised culture was transferred to a fresh 1.5 ml microtube. 50 µl of 5 mg/ml cytochrome *c* (Merck, C2506) was added to each culture to give a final concentration of 0.5 mg/ml cytochrome *c*. A negative control was prepared using 450 µl 20 mM MOPS and 50 µl of 5 mg/ml cytochrome *c*. Samples were incubated at room temperature for 15 min before centrifugation at 20,000 x *g* for

2 min to pellet the cells. Three 100 µl aliquots of the supernatant from each sample were transferred to a microtitre plate and the absorbance at 440 nm was read immediately using a SPECTROstar Nano plate reader. The mean and standard deviation were recorded for each sample.

2.4.6 *S. aureus* zeta potential

The following method was adapted from the protocol outlined by L.B. Rawlinson (Rawlinson et al., 2011). 1 ml of overnight culture was inoculated into 7 ml of LB broth and incubated with shaking at 150 rpm at 37°C for 16 h. The 8 ml cultures were pelleted at 5,000 x *g* for 10 min, and the supernatant was discarded. Cell pellets were resuspended in 1 ml of 0.5 mM sodium phosphate (Sigma Aldrich, S3139 with Sigma Aldrich, S0876) and transferred to 1.5 ml microtubes which were pelleted at 20,000 x *g* for 1 min. This was repeated until cells were washed three times. Cell pellets were resuspended in 7 ml of 0.5 mM sodium phosphate to give $A_{600\ nm}$ of 0.4. The samples were placed into disposable cuvettes (DTS1070) that were conditioned using deionized water and then buffer matching the cell suspension. Samples were analysed by Dr Elizabeth Bromley (Department of Physics, Durham University) using a Zetasizer instrument (Malvern Panalytical). Instrument settings were optimized by the instrument software, with repeat measurements made over time to check for sedimentation.

2.4.7 *S. aureus* peptidoglycan cross-linking analysis

25 ml of bacterial overnight culture was prepared in a 50 ml screw-capped tube (Sarstedt, 62.547.254) using a 5 ml inoculum in 20 ml of LB broth. This resultant culture was then incubated at 37°C, shaking at 150 rpm for 16 h. 2 ml from this overnight culture was added to 20 x 38 ml LB broth in 50 ml screw-capped tubes, giving a final culture volume of 800 ml. Cultures were incubated at 37°C, shaking at 150 rpm until reaching $A_{600\ nm}$ of 0.4-0.6. Cells were then pelleted through centrifugation at 5,000 x *g* for 10 min. Cell pellets were resuspended in 2 ml of ice-

cold 50 mM Tris-HCl (Melford, T60050), pH 7. All resuspended pellets for each strain were then pooled into one 50 ml screw-capped tube which was placed on ice. The cell suspension was then added drop-wise to 120 ml of 5% SDS (Melford, L22010) at 95°C in a conical flask using a Pasteur pipette. Stirring was maintained at approximately 100 rpm using a stirrer bar on a hot plate. The temperature and stirring was maintained for 15 min after the final cell addition. The samples were then allowed to cool to room temperature before transferring to four 50 ml screw-capped tubes. The resultant samples were frozen at -20°C prior to transfer to Newcastle University. Muropeptides were purified and analysed by high performance liquid chromatography (HPLC) according to protocols described by J. A. F. Sutton (Sutton et al., 2021). Cells were sheared using a homogeniser, and the sacculi separated for analysis by centrifugation. Wall teichoic acids and other cell wall polymers were removed using hydrofluoric acid, and purified sacculi washed in Tris-HCl to adjust the pH before a final wash was carried out in distilled water. HPLC analysis of purified muropeptides was carried out by Professor Waldemar Vollmer (Centre for Bacterial Cell Biology, Newcastle University).

2.4.8 *S. aureus* susceptibility to osmotic stress

100 µl of a normalised overnight culture of *S. aureus* was added to 2 ml of LB broth in a sterile semi-micro cuvette and sealed with parafilm. Parallel cultures were prepared in LB broth containing 0.5 M NaCl according to the following recipe: 10g/L tryptone (Melford, T60065), 5g/L yeast extract (Melford, Y1333.0100), and 24.22 g/L NaCl (ThermoFisher Scientific 10735921). The sealed cuvettes were incubated for 6 h at 37°C with shaking at 150 rpm. Absorbance at 600 nm was measured at 45 min intervals using a spectrophotometer, inverting the cuvettes to mix before each reading.

2.5 Checkerboard assays

1 ml of LB broth was inoculated with 50 µl of a bacterial overnight culture in a cuvette, grown to an $A_{650\ nm}$ of ~0.07 and diluted 1:10 in fresh LB broth as described above. Two-fold serial dilutions of chelants or antibiotics were prepared in LB, and 25 µl of each dilution series was transferred to a microtitre plate, with 25 µl of the alternative chelant or antibiotic making a serial dilution in a perpendicular manner in a checkerboard pattern. The diluted bacterial inoculum (50 µl) was then applied to the appropriate wells in the plate. Both positive and negative controls were employed, along with appropriate DMSO and/or ethanol controls where required. Microtitre plates were incubated at 37°C with shaking at 150 rpm for 16 h and growth monitored at an $A_{650\ nm}$ in a plate reader. The mean and standard deviation was calculated for each bacterial strain after subtracting the negative controls. A similar protocol was used to perform the EDTA-$MnCl_2$ supplementation assay. Minimum inhibitory concentrations were defined as the minimum concentration of chelant needed to inhibit growth by ≥90%. A Fractional Inhibitory Concentration index (FICI) was defined as the minimum concentration of chelant needed to inhibit growth by >90% individually and in combination and FIC index values were interpreted as synergistic (≤0.5), indifferent (>0.5-4.0) or antagonistic (>4) based on published methods (Bonapace et al., 2002; Leber, 2016). To highlight any biases based on method of interpretation, both a mean and individual FICI were calculated for each checkerboard pairing based on methods 1 and 3 presented by Bonapace et al. (Bonapace et al., 2002). The formula for defining interactions is shown in Equation 2.1.

Equation 2.1 Fractional Inhibitory Concentration Index (FICI)

$$\text{FIC index} = \frac{\text{MIC of chelant A in combination}}{\text{MIC of chelant A alone}} + \frac{\text{MIC of chelant B in combination}}{\text{MIC of chelant B alone}}$$

2.6 *P. aeruginosa* cellular metal content analysis

Glassware was prepared by submersion in 4% nitric acid for a minimum of 16 h to remove any contaminants and rinsed thoroughly with MilliQ water. 48 ml of LB broth in 250 ml acid-washed conical flasks were sealed with a foam bung and foil top and sterilised by autoclaving. Concentrations of each chelant were used which would inhibit bacterial growth by 10-15%, alongside a control flask without chelant and a DMSO (ThermoFisher Scientific, 10127403) control containing the highest concentration used where applicable. After addition of chelant, 2 ml of a bacterial overnight culture was added to each flask and incubated with shaking at 150 rpm at 37°C until mid-late-log phase ($A_{600\ nm}$ of 0.6-0.7). Cells were transferred to 50 ml Falcon tubes and pelleted by centrifugation at 5,000 x *g* for 50 min. Cell pellets were resuspended in 10 ml of 0.5 M D-sorbitol (Sigma Aldrich, S1876), 10 mM HEPES (ThermoFisher Scientific, 10081113) at pH7.8 using pipette tips that had not been autoclaved (to eliminate the risk of metal contamination) and centrifuged for a further 10 min at 5,000 x *g* until cells had been washed three times. The resultant cell pellets were digested in 0.5-1 ml of 65% Supra-pur nitric acid (VWR, 1.00441.1000) for a minimum of 16 h. Calibration samples were prepared using known quantities of metals in nitric acid (ICP multi-element standards, CertiPUR®, Sigma Aldrich & Merck) diluted in matrix-matched solutions. Dilutions and a calibration curve were analysed using inductively coupled plasma mass spectrometry (ICP-MS, Thermo XSERIES 2). Instrument control, analysis and quantification was obtained using software interface PlasmaLab (ThermoScientific) and further analysis was conducted in Microsoft Excel. Mean and standard deviation values were determined from quadruplicate biological analyses.

2.7 Bacterial permeability assays

Method adapted from protocol by I.M. Helander (Helander & Mattila-Sandholm, 2000). 2 ml of LB broth was inoculated with 150 µl of a bacterial overnight culture in

a cuvette and grown to an $A_{600\ nm}$ of ~0.5. 2 ml of culture was then centrifuged at 20,000 x *g* for 2 min and the supernatant discarded. Cell pellets were resuspended in 1 ml of 5 mM HEPES (ThermoFisher Scientific, 10081113) pH 7.2 at room temperature. Chelants at a range of concentrations in 5 mM HEPES were mixed with the bacterial cells in a microtitre plate (OptiPlate-96 Black Microplate, PerkinElmer, 6005270). The plate was incubated at room temperature for 10 min to allow an interaction between the chelant and bacteria. 50 µl of 40 µM N-Phenyl-1-naphthylamine (NPN, Merck Life Science UK, 104043) in 5 mM HEPES was then added to relevant wells using a multichannel pipette to give a final NPN concentration of 10 µM. The plate was immediately transferred to a BioTek™ Synergy™ H4 Hybrid Microplate Reader (ThermoFisherScientific) programmed to excite at 355 nm and monitor emission at 405 nm. Experiments were performed in triplicate for each chelant at two chelant concentrations.

3 Susceptibility of *E. coli* to chelating agents

3.1 Introduction

Chelating agents offer considerable potential as antibacterial agents since they bind tightly to metals and thereby impose a micronutrient restriction similar to that found in host nutritional immunity (Flora & Pachauri, 2010). This chapter builds upon previous work by Beecroft (2019) on the antibacterial properties of eleven chelating agents against *E. coli*. The compounds were evaluated as inhibitors of bacterial growth both individually and in combination to generate a more robust data set. A revised analysis of chelant impact as antibacterials in relation to metal homeostasis is provided. These initial experiments were then extended to examine *E. coli* mutants from the Keio collection defective in key metal import pathways to assess their contribution to the selective metal deprivation as a result of chelant exposure. A screen of the Keio collection with PO was performed by Nancy Reeder and Justin Caserta at P&G, Cincinnati.

3.2 Chelating agents

Eleven chelators were selected based on their known or predicted metal ion affinities (Hancock, 1992; Hancock & Martell, 1989; Pettit, 2009) and differing chemical structures that might elicit a variety of complementary cellular effects (Fig. 3.1). The selection includes EDTA (hexadentate), its octadentate analogue DTPA, and the closely-related biodegradable aminocarboxylates, GLDA and MGDA, all of which are expected to bind strongly to a broad range of metal ions, especially Fe^{3+}. The metal ion affinities of GLDA and MGDA (Pinto et al., 2014) are lower than those of DTPA and EDTA, indicating that higher concentrations may be required to chelate biologically relevant metal ions. DTPMP has a similar nitrogenous backbone to DTPA but possesses five pendant phosphonates instead of carboxylates. HBED is another aminocarboxylate, but it also incorporates phenolic units that favour binding to Fe(III)

(Hancock & Martell, 1989). Catechol (CAT; a unit that occurs in enterobactin) has very high selectivity for Fe^{3+} *in vitro* (Sánchez et al., 2005), although its effective binding strength at pH 7 is attenuated due to competitive protonation. CHA is a simple hydroxamate that resembles the constituent binding units of the siderophore desferrioxamine, which binds Fe^{3+} extraordinarily strongly (Sidarovich et al., 2015). Piroctone (the metal binding unit of piroctone ethanolamine, PO) is a related cyclic hydroxamate. TPEN and BCS are “softer” ligands that favour binding to late transition metals such as Zn^{2+} (Haase et al., 2013) and Cu^{+} (Rapisarda et al., 2002), respectively.

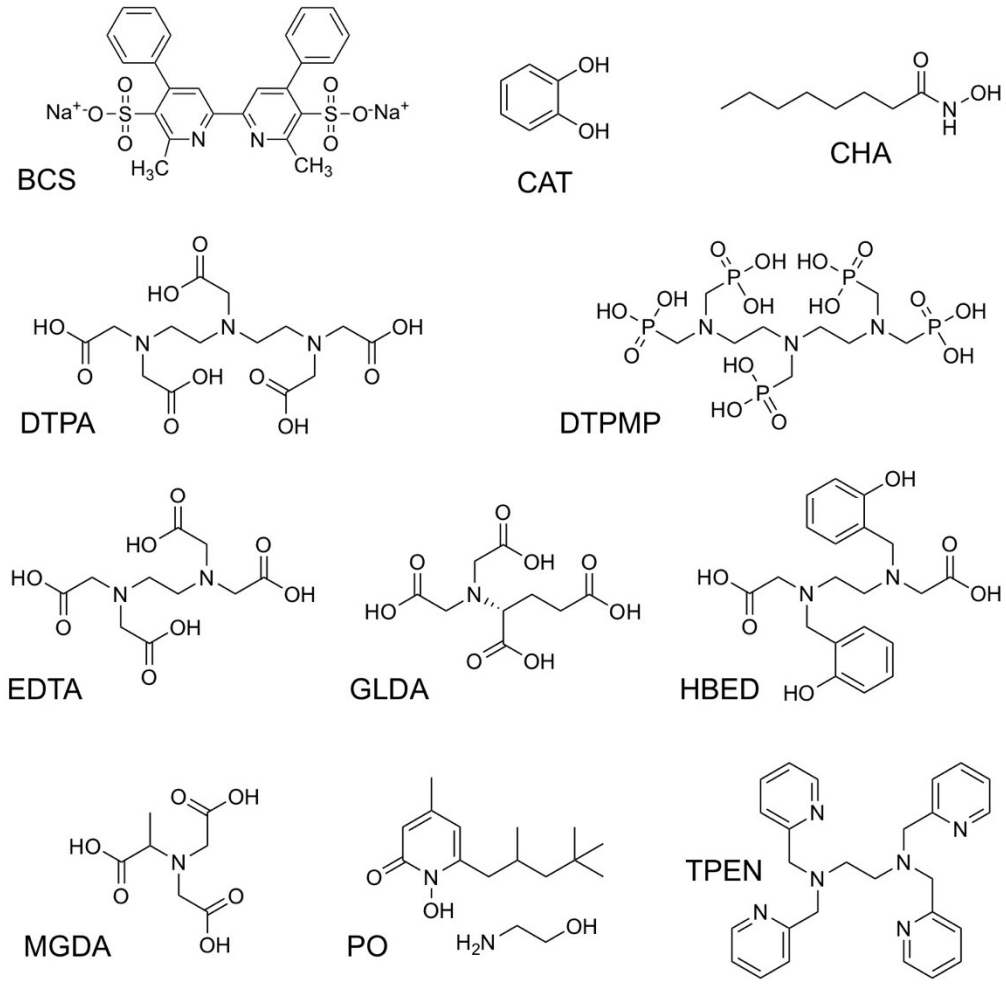

Figure 3.1 Chemical structure of chelants selected for analysis. BCS (bathocuproine disulphonic acid), CAT (catechol), CHA (caprylhydroxamic acid), DTPA (diethylenetriaminepentaacetic acid), DTPMP

(diethylenetriaminepentamethylene phosphonic acid), EDTA (ethylenediaminetetraacetic acid), GLDA (glutamic acid-N,N-diacetic acid), HBED (N,N-bis (2-hydroxybenzyl) ethylenediamine-N,N-diacetic acid), MGDA (methylglycinediacetic acid), PO (piroctone olamine) and TPEN (N,N,N',N'-tetrakis (2-pyridylmethyl) ethylenediamine). The most biodegradable isomer of GLDA (L-GLDA) is shown.

3.3 Assessing antimicrobial efficacy

There are multiple approaches that can be used to evaluate the efficacy of potential antibacterial agents, as reviewed by Balouiri *et al*. (2016). Soluble compounds can be soaked into disc filters or applied in wells on agar plates seeded with bacteria and their growth monitored visually. Alternative methods include TLC (thin layer chromatography)-direct bioautography, which enables isolation of antimicrobial substances in more complex mixtures, such as plant extracts (Jesionek et al., 2015). Although these methods can be performed relatively quickly and easily for compound screening, they tend to provide qualitative data (Balouiri et al., 2016). A more quantitative methodology commonly used to determine antibacterial activity is the broth-dilution method (Andrews, 2001; Wiegand et al., 2008). In these assays, the compound of interest is serially diluted in liquid media in which a standardised number of bacterial cells is added, typically in tubes or in the wells of a microtitre plate. Samples are then incubated for a pre-determined period of time (16-24 h), after which bacterial growth is measured by optical density. The minimum inhibitory concentration (MIC) of a compound, resulting in a >90% growth inhibition, can thus be determined (Andrews, 2001). Benefits of this broth-dilution technique include its simplicity and capacity to rapidly test a large number of compounds. The assignment of an MIC allows comparison of multiple compounds against a single bacterial species or even across a number of different species. In addition, the microdilution method utilises only small volumes reducing the requirement for large quantities of compound or

materials. Here we used the broth microdilution method to examine the antibacterial efficacy of 11 chelants.

3.3.1 Media selection

Inoculum concentration, dilution broth and incubation conditions all influence MIC determination (Imani Rad et al., 2017; Wiegand et al., 2008). It is therefore essential that compounds are tested using a single growth medium and consistent parameters to enable legitimate comparisons to be made. For antibiotics, MICs are typically performed in Mueller Hinton Broth (MHB) (European Committee for Antimicrobial Susceptibility Testing, 2000; Wiegand et al., 2008) or Iso-sensitest (ISO) broth (Andrews, 2001). The use of M9 minimal media would have allowed more precise modelling of metal ion content, but previous experiments encountered considerable variability in *E. coli* growth (Marikka Beecroft, personal communication). We also considered the use of Luria Bertani (LB) broth as a widely-used growth medium with no inorganic nutrient restrictions (Sezonov et al., 2007).

To assess how broth composition altered the efficacy of chelating agents against *E. coli*, comparisons were made between LB, ISO, MHB without supplementation and MHB containing the recommended additional calcium and magnesium concentrations. Experiments were performed with three representative chelants, CHA, DTPMP and EDTA against *E. coli* (Fig. 3.2). The *E. coli* K-12 strain BW25113 was chosen to allow comparisons with deletion mutants from the Keio collection, a comprehensive set of single-gene knockout mutants (Baba et al., 2006). With CHA there was little difference in bacterial growth inhibition regardless of the medium used (Fig. 3.2A). However, there were significant differences in the susceptibility of *E. coli* to DTPMP and EDTA (Fig. 3.2B and 3.2C). While supplemented and unsupplemented MHB did behave similarly, there were clear differences between MHB, LB and ISO, presumably due to differences in broth constituents, especially metal content (Ng, 2020). In MHB, *E. coli* was much more susceptible to DTPMP and EDTA, whereas in

ISO the bacteria proved considerably more resistant (Fig. 3.2B and 3.2C).

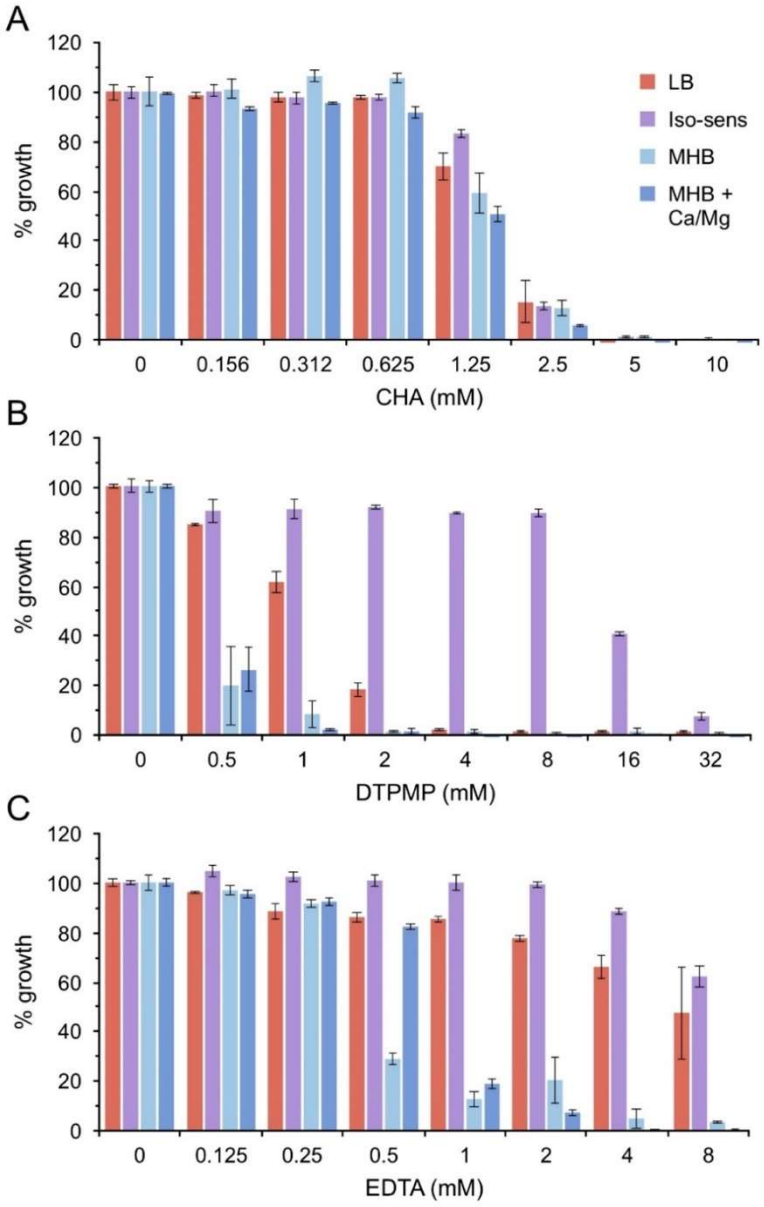

Figure 3.2 Comparison of the effect of selected chelants on *E. coli* growth in different media. The inoculum was cultivated in LB before diluting 1:10 with the appropriate medium for subsequent testing. These were then mixed with 2-fold dilutions of CHA (A), DTPMP (B) or EDTA (C) and incubated at 37°C for 16 h. The optical density was measured at $A_{600\ nm}$ and the percentage growth calculated by normalisation against the control without chelant. Results are the mean and standard deviation of an independent experiment performed in triplicate. LB = Luria-Bertani, Iso-sens = Iso-sensitest, MHB = Muller Hinton Broth and MHB + Ca/Mg = MHB supplemented with calcium and magnesium.

MHB has the potential to be problematic as it needs to be supplemented with additional calcium and magnesium that could alter cellular responses in the presence of chelating agents. Experiments with ISO broth were also occasionally subject to solubility issues leading to precipitation that might interfere with MIC determination. For these reasons, and because DTPMP and EDTA sensitivities with LB were between those found with MHB and ISO (Fig. 3.2B and 3.2C), LB was selected as the growth medium of choice that would allow an assessment of sensitivity to chelants when bacteria are in a robust physiological state.

3.3.2 Inhibition of *E. coli* growth by chelating agents

The effect of each of the 11 chelants on bacterial growth was evaluated using 2-fold serial dilutions of each ligand (Fig. 3.3). The results allowed us to draw some initial conclusions on antibacterial efficacy between each of the structurally distinct chelants.

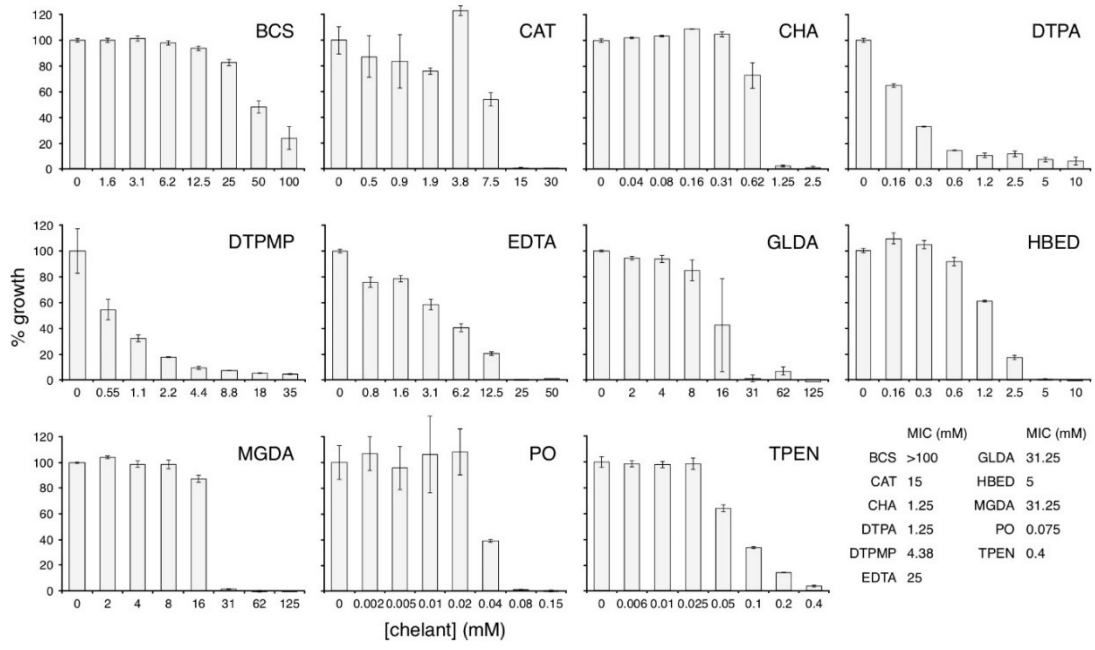

Figure 3.3 Effect of chelants on *E. coli* growth. Bacteria were cultivated in LB media and mixed with appropriate 2-fold dilutions of each chelant and incubated with shaking for 16 h at 37°C. Results are the mean and standard deviation of an independent experiment performed in triplicate; a further two independent

experiments performed in triplicate yielded similar results. MICs in mM are based on >90% growth inhibition, where achieved, as indicated at the bottom right of the figure.

The dose-response curves with different chelants vary. CAT, CHA, GLDA, MGDA and PO show minimal effects on bacterial growth until a threshold concentration is reached, after which bacterial growth drops off rapidly (Fig. 3.3). DTPA, DTPMP and EDTA show more linear effects on growth reduction as concentration is increased. In most cases, high concentrations were required to achieve *E. coli* growth inhibition of >90%. The two chelants with highest efficacy were PO and TPEN with an MIC of 75 and 400 μM, respectively. BCS shows the lowest efficacy, failing to fully inhibit bacterial growth even at the highest concentrations tested (Fig. 3.3).

3.4 Inhibition of *E. coli* growth by chelating agents in combination

Previous work by Beecroft (2019) revealed four distinct classes of effects on *E. coli* cellular metal content with the chelants tested: i) BCS, CAT and CHA produced no apparent alteration in metal composition, ii) DTPA, EDTA, GLDA and MGDA resulted in depletion of manganese alongside reductions in iron and zinc levels, iii) TPEN reduced zinc levels with a modest reduction in manganese, and iv) DTPMP, HBED and PO reduced iron levels coupled with elevated manganese. To gain further insight into their impact on bacterial metal homeostasis, pairs of chelants were tested based on the supposition that those affecting different metalloregulatory pathways should be synergistic when combined. The checkerboard, or 2-dimensional, assay provides a simple way to evaluate inhibitory interactions between two soluble compounds and has been widely used to compare efficacies of different antibiotics in combination (Bollenbach, 2015; Bonapace et al., 2002; Lambert & Lambert, 2003). The microdilution method used for MIC assays was adapted with consideration of published protocols for the interpretation of checkerboard results (Andrews, 2001). The use of checkerboard assays is complicated with chelating agents because in some cases, bacterial growth is never fully inhibited, unlike with many antibiotics. For

instance, BCS at a maximal concentration of 100 mM only inhibits *E. coli* growth by 70-80% (Fig. 3.3). As before, a percentage growth of <10% was chosen as a baseline for minimum inhibitory concentrations, which are needed to calculate a fractional inhibitory concentration (FIC) index. In the case of BCS where <10% growth was not achieved, the maximum concentration of chelant provided the MIC and this should be taken into account when assessing results obtained with this chelant. Representative examples of synergistic, indifferent (or non-interacting) and antagonistic pairings from our studies are illustrated in Figure 3.4A-C.

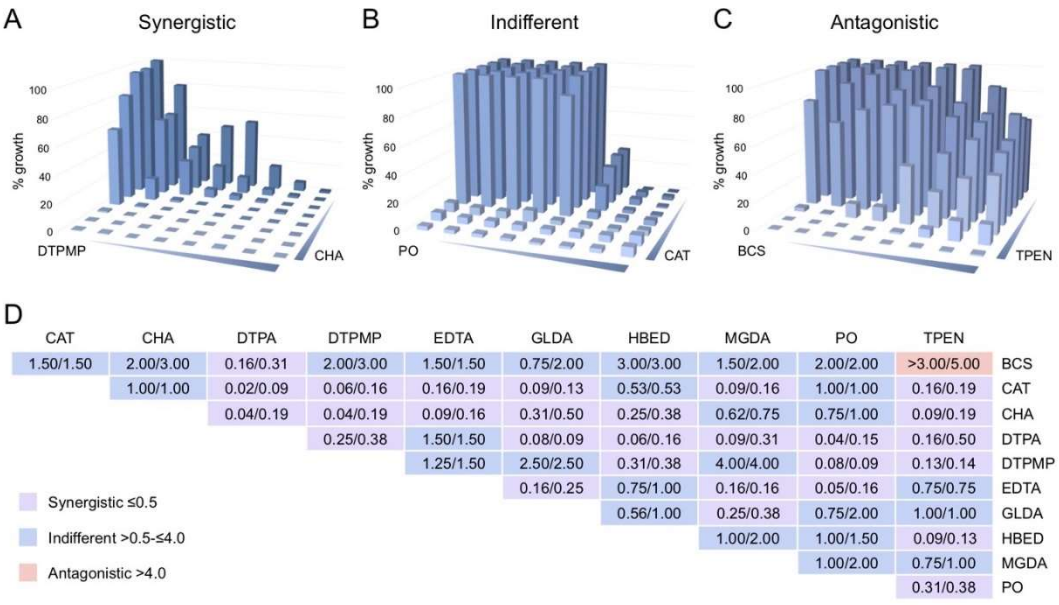

CAT	CHA	DTPA	DTPMP	EDTA	GLDA	HBED	MGDA	PO	TPEN	
1.50/1.50	2.00/3.00	0.16/0.31	2.00/3.00	1.50/1.50	0.75/2.00	3.00/3.00	1.50/2.00	2.00/2.00	>3.00/5.00	BCS
	1.00/1.00	0.02/0.09	0.06/0.16	0.16/0.19	0.09/0.13	0.53/0.53	0.09/0.16	1.00/1.00	0.16/0.19	CAT
		0.04/0.19	0.04/0.19	0.09/0.16	0.31/0.50	0.25/0.38	0.62/0.75	0.75/1.00	0.09/0.19	CHA
			0.25/0.38	1.50/1.50	0.08/0.09	0.06/0.16	0.09/0.31	0.04/0.15	0.16/0.50	DTPA
				1.25/1.50	2.50/2.50	0.31/0.38	4.00/4.00	0.08/0.09	0.13/0.14	DTPMP
					0.16/0.25	0.75/1.00	0.16/0.16	0.05/0.16	0.75/0.75	EDTA
						0.56/1.00	0.25/0.38	0.75/2.00	1.00/1.00	GLDA
							1.00/2.00	1.00/1.50	0.09/0.13	HBED
								1.00/2.00	0.75/1.00	MGDA
									0.31/0.38	PO

Figure 3.4 Chelant combinations analysed by the checkerboard assay. Examples of (A) synergistic, (B) indifferent and (C) antagonistic pairings, for CHA/DTPMP, CAT/PO and BCS/TPEN, respectively, are shown. (D) FIC index (FICI) values are shown for two independent experiments performed in triplicate for each chelant combination. FIC values were calculated based on the lowest concentration of each chelant in combination divided by the MIC for that chelant. Two-fold dilutions (as in an MIC) of chelants were performed in LB broth with *E. coli* BW25113 at 37°C with shaking at 37°C for 16 h. Additional controls for low levels of DMSO, ethanol or water were included where relevant.

Overall 55 chelant pairings were tested and FIC indices determined (Figure 3.4D; Equation 2.1), revealing one antagonistic, 26 indifferent and 28 synergistic combinations by selecting the lowest possible combination of each chelant in cumulative calculations. Some of the checkerboard data contributing to this analysis was obtained from previous work (Beecroft, 2019). Considerably fewer synergistic pairings, only 5 (plus 8 mixed synergistic/indifferent outcomes), were obtained using an average FIC method (Appendix, Figure 9.1), although that is not surprising as such an approach employs much stricter criteria for assigning synergy (Bonapace et al., 2002). DTPA yielded the highest number of synergistic pairings, with 9 partners (Fig. 3.10). BCS produced the lowest number, displaying synergism only with DTPA (Fig. 3.10), perhaps because of its limited capacity to fully inhibit bacterial growth (Fig. 3.3).

3.4.1 Can supplementation with manganese suppress the effects of EDTA on *E. coli*?

The principal effect of the azacarboxylate ligands DTPA, EDTA, GLDA and MGDA is to deplete *E. coli* of manganese, with the reductions ranging from 5- to 15-fold relative to untreated controls (Paterson et al., 2022). It was postulated that supplementing cultures with $MnCl_2$ could perhaps counteract the growth inhibition observed in the presence of EDTA. Hence *E. coli* cultures were grown in the presence of increasing concentrations of both manganese and EDTA (Fig. 3.5). The results show that the presence of either EDTA (Fig. 3.5A) or manganese (Fig. 3.5B) both result in *E. coli* growth inhibition in a concentration-dependent manner. When EDTA and manganese are mixed at different ratios, improved growth can be observed (Fig. 3.5C and 3.5D). However, this appears to simply be a consequence of EDTA-manganese association, with the complexes formed moderating the toxicity associated with the individual components.

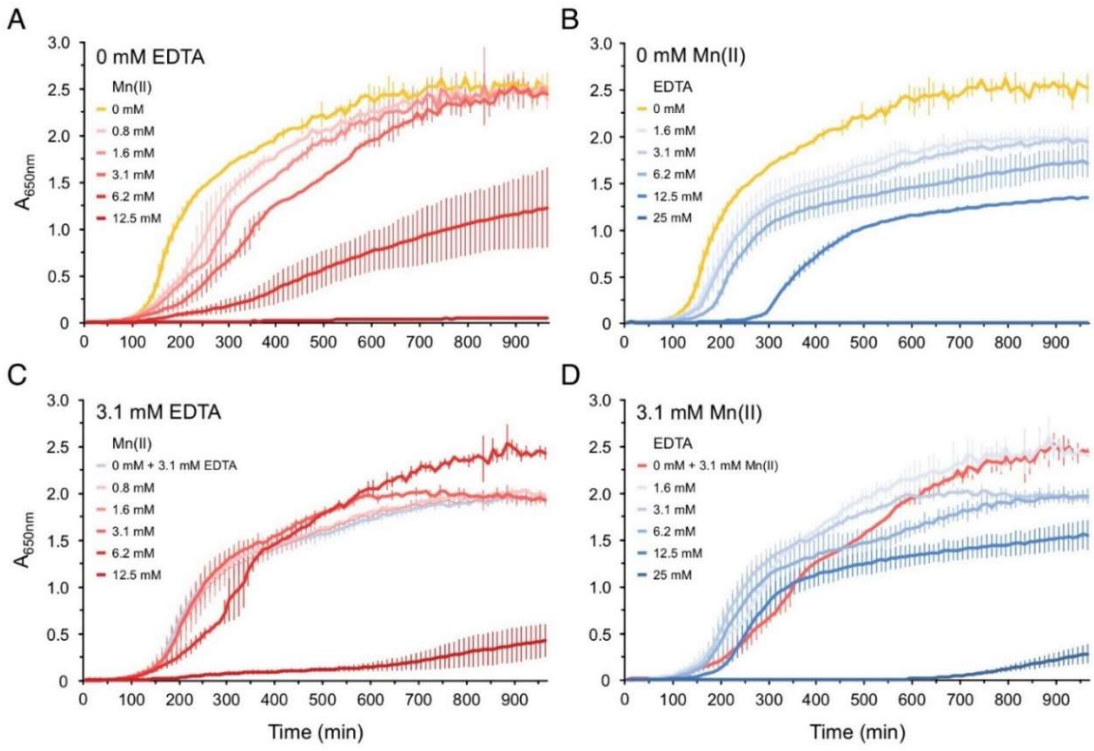

Figure 3.5 Effect of manganese supplementation on *E. coli* growth inhibition by EDTA. Bacteria were cultivated at 37°C in LB supplemented with $MnCl_2$ (red) or EDTA (blue) at the concentrations indicated, with shaking in a plate reader and growth monitored by absorbance at 650 nm. The growth curves presented are the mean of two biological repeats performed in triplicate.

3.4.2 Sensitivity of *E. coli* Keio mutants to PO

To provide insight into the gene products important for tolerating exposure to chelants we next selected one of the iron chelators, PO, in a screen of the *E. coli* Keio collection of single gene deletions to identify mutants with increased susceptibility. This work was performed by Nancy Reeder and Justin Caserta as part of our collaboration with Procter and Gamble. The duplicate set of the Keio collection of 3985 mutants (7970 strains in total) was cultivated in microtitre plates in LB media in the presence of PO at 27 and 34 μM. The growth of each strain exposed to PO relative to untreated controls was determined after overnight incubation and the most sensitive mutants identified (Fig. 3.6A). The influence of EDTA on *E. coli* growth has previously been analysed by inoculating the Keio collection mutants onto LB agar plates (Nichols et al., 2011) and this facilitated comparisons with the data on PO (Fig. 3.6B).

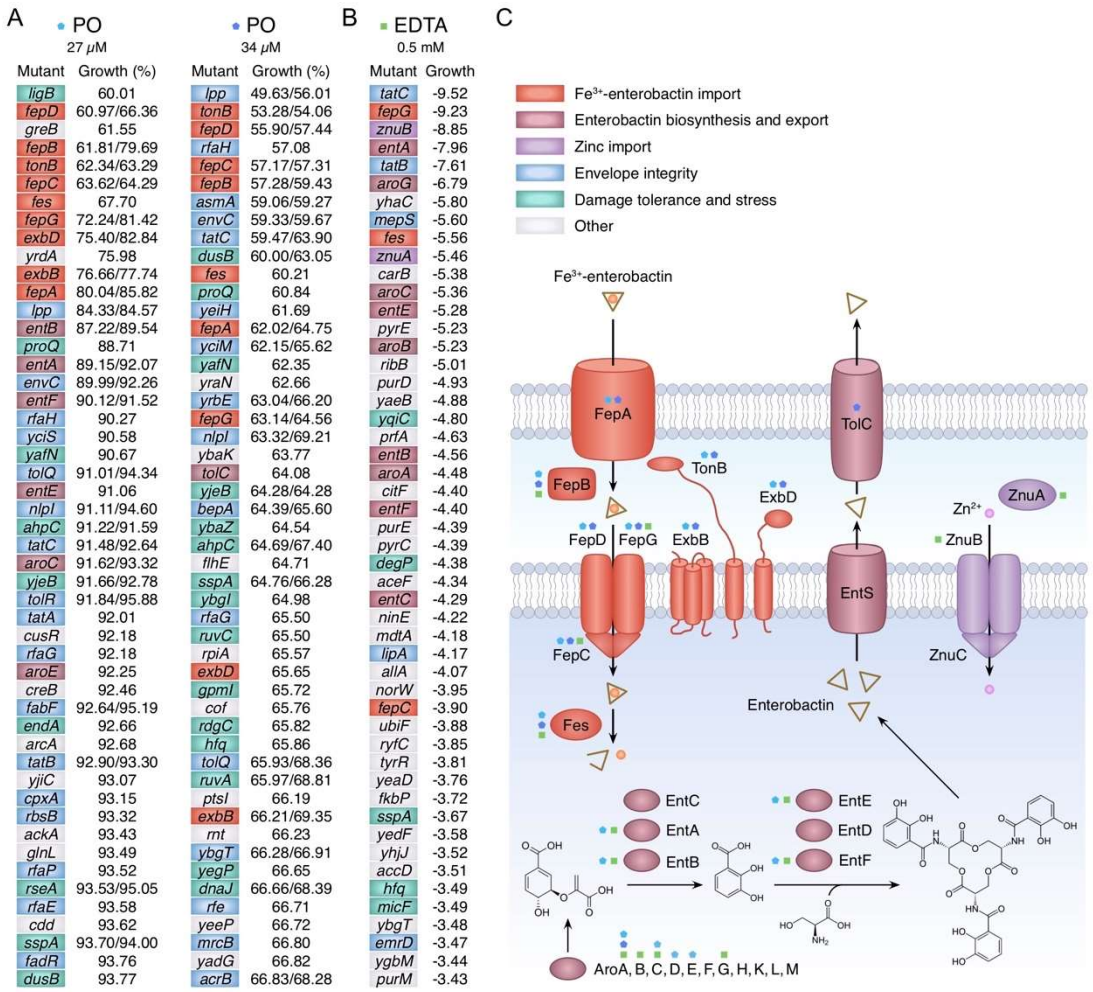

Figure 3.6 Effect of PO on the growth of *E. coli* mutants from the Keio collection. (A) The duplicate set of 3985 Keio library mutants (Baba et al., 2006), 7970 strains in total, were grown in LB media at 37°C with 27 or 34 μM PO for 16 h. Percentage growth was compared to untreated controls for each strain and the top 50 slowest growing mutants are shown. Where two percentages under each condition are shown, these correspond to the presence of both duplicates from the Keio collection in the top 200 slowest growing mutants identified in the screen. Each mutant is colour-coded based on the functional grouping assigned for each gene with the key shown in (C). (B) The 50 slowest growing mutants identified from Keio phenotypic screens using EDTA (Nichols et al., 2011) are shown to facilitate comparisons with PO. The more negative pixel score values correspond to the poorest colony growth on agar plates supplemented with 0.5 mM EDTA. (C) The ferric enterobactin synthesis, export and import system of *E. coli*. Key proteins involved in each part of the iron uptake system are colour-coded according to their roles (Miethke, 2013; Raymond et al., 2003). Outer and inner membranes are depicted as lipid bilayers with the lower portion of the diagram shaded in blue to represent the cytosol. Where substantially-

reduced growth is associated with mutation of key ferric-siderophore synthesis and transport components, these are indicated with cyan and blue (PO) and green (EDTA) symbols.

The Keio screen with PO highlighted the importance of genes involved in iron-siderophore uptake for tolerance of PO (Fig. 3.6A). Mutants affecting enterobactin synthesis (Aro, Ent), export (TolC) and import (FepA-G, ExbBD-TonB and Fes) were among those with the most substantial growth reductions relative to the control following PO exposure (Fig. 3.6A and 3.6C). Deletion mutants affecting envelope integrity, efflux pumps, damage tolerance and stress responses also showed significant sensitivities to PO (Fig. 3.6A), and mutants defective in components of the Znu zinc uptake system showed impaired growth when exposed to EDTA (Fig. 3.6B).

3.4.3 Effect of PO, EDTA and DTPMP on the growth of selected *E. coli* Keio collection mutants

To validate the findings with the Keio screen, we selected a range of the most PO susceptible mutants and others deficient in related iron, manganese and zinc uptake pathways for further testing. All of the mutants affecting enterobactin biosynthesis or uptake (*aroA*, *fepA*, *fepC* and *fes*) (Raymond et al., 2003) exhibited substantially reduced growth relative to the wild-type following exposure to PO (Fig. 3.7A), consistent with the importance of iron acquisition for tolerance of this chelant. Interestingly, a corresponding sensitivity was not found with *fepB* and *fepD* mutants (Fig. 3.7A). Strains lacking integral membrane proteins involved in drug export and envelope integrity (*acrB*, *envC*, *lpp* and *tolC*) also showed increased susceptibility as in the Keio screen with PO (Fig. 3.6 and 3.7A). A *znuC* mutant affecting zinc import (Lonergan & Skaar, 2019) showed some increased sensitivity to PO, although a *znuB* mutant involved in the same uptake system did not (Fig. 3.7A). Mutants affecting components of the Fe^{3+}-citrate (*fecA*, *fecB*, *fecD* and *fecE*) and Fe^{3+}-hydroxamate (*fhuF*) systems (Miethke, 2013) were generally no more susceptible to PO (Fig. 3.8A). Similarly, mutants involved in cysteine (*cysE*) and histidine (*hisI*) biosynthesis that are

highly sensitive to iron starvation (Nichols et al., 2011) showed no increased susceptibility to PO (Fig. 3.8A).

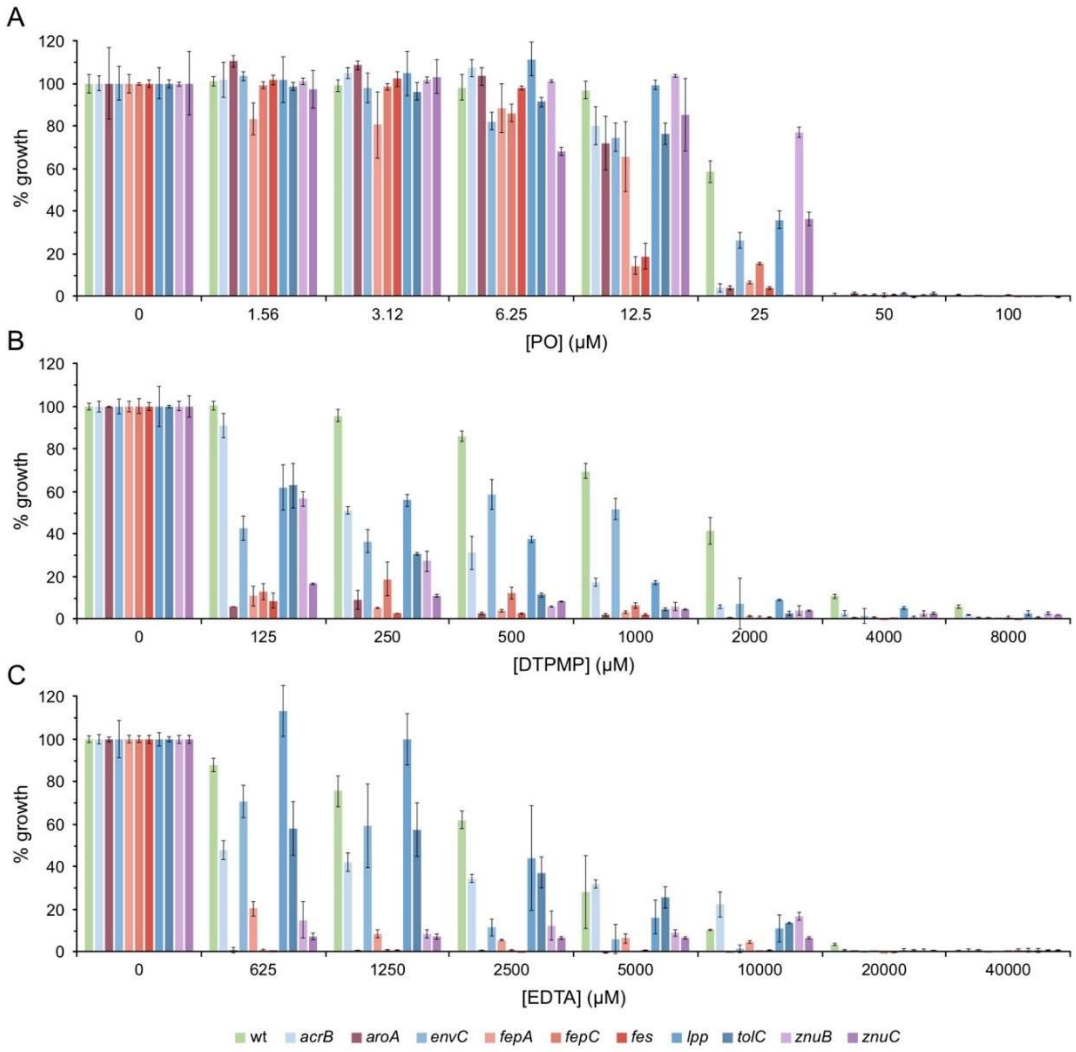

Figure 3.7 Selected *E. coli* mutant sensitivity to three chelants – part 1. Bacteria were incubated with a two-fold serial dilution of (A) PO, (B) DTPMP or (C) EDTA in 100 µl of LB media and incubated with shaking for 16 h at 37°C. Absorbance at 600 nm was recorded and the percentage growth calculated for each strain. Data represent the mean and standard deviation of an independent experiment performed in triplicate. A second biological repeat was performed and a similar pattern of susceptibility was observed.

The same strains were also examined for their susceptibility to DTPMP and EDTA (Fig. 3.7B-C and Fig. 3.8B-C). As with PO, defects in the enterobactin pathway (*aroA*, *fepA*, *fepC* and *fes*) produced the highest sensitivity to these two chelants, underlining

the necessity of this route of iron acquisition for bacterial growth and defence against these chelants. In contrast to PO, the other ferric iron import pathway mutants also showed increased susceptibility, especially with DTPMP (Fig. 3.7B-C). The universal effect of DTPMP is perhaps surprising, but suggests a capacity to bind to a range of different metals, and disrupt a variety of different processes within the cell. Reduced growth following chelant exposure was apparent with mutants affecting membrane integrity functions.

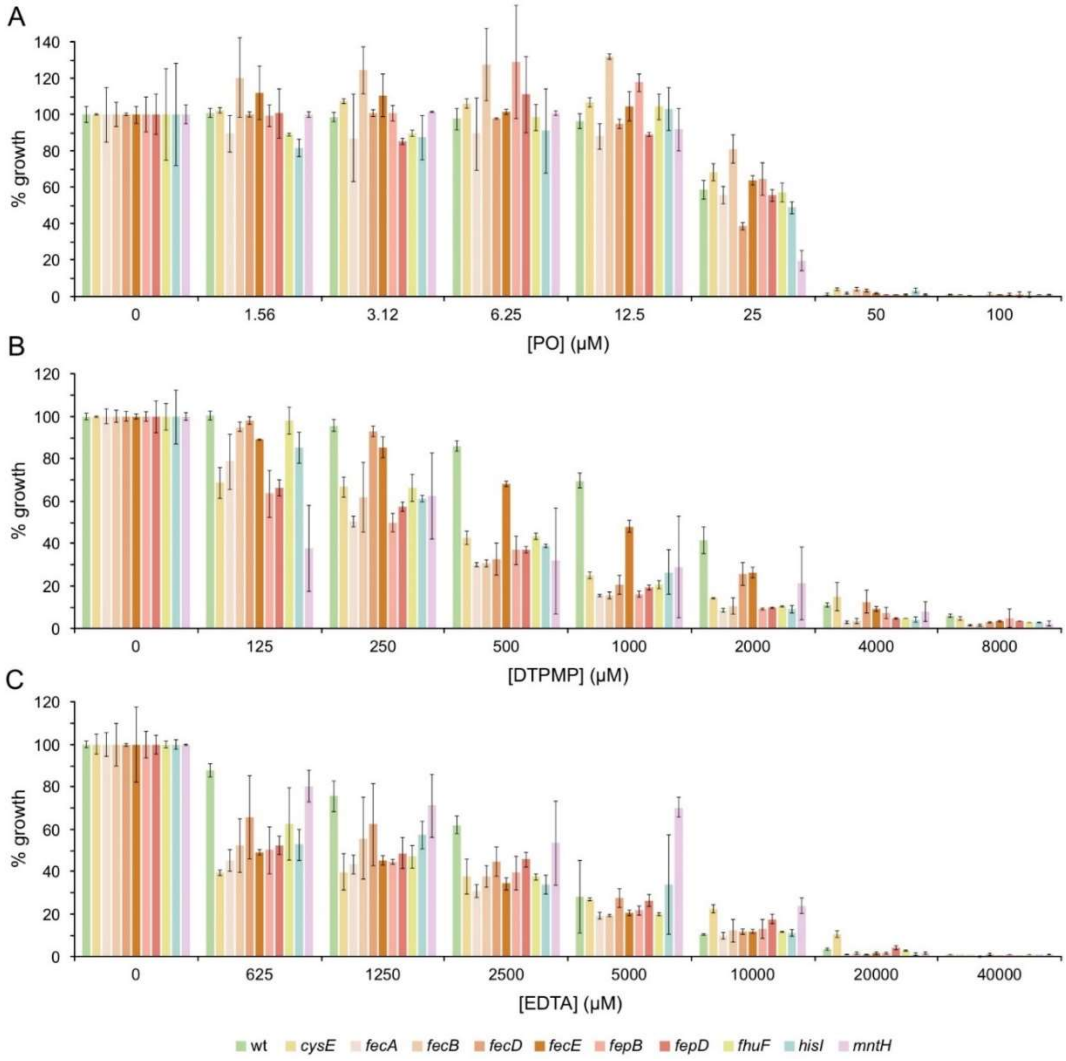

Figure 3.8 Selected *E. coli* mutant sensitivity to three chelants – part 2. Bacteria were incubated with a two-fold serial dilution of (A) PO, B (DTPMP) or (C) EDTA in 100 µl of LB media and incubated with shaking for 16 h at 37°C. Absorbance at 600 nm was monitored and percentage growth determined. Data represent the mean and

standard deviation of one biological repeat performed in triplicate. A second biological repeat was performed in triplicate with a similar pattern of susceptibility observed.

Mutants in the *znuB* and *znuC* zinc import system were much more sensitive to DTPMP and EDTA (Fig. 3.7B-C) than PO (Fig. 3.7A), suggesting that reductions in cellular zinc increase chelant vulnerability. Surprisingly, deletion of the manganese importer, MntH, did not result in decreased growth following EDTA exposure (Fig. 3.8C, Nichols et al., 2011). In fact, in repeat assays, growth was improved following EDTA treatment in an *mntH* knock-out strain (Fig. 3.9). Given that manganese levels are severely constrained by EDTA (Paterson et al., 2022), this observation is surprising and may indicate that it is primarily reductions in iron and zinc that contribute to growth restriction. The *mntH* mutant was more sensitive to the iron chelators DTPMP and PO (Fig. 3.8A-B), in keeping with the demand for manganese import during iron starvation (Anjem et al., 2009; Imlay, 2014).

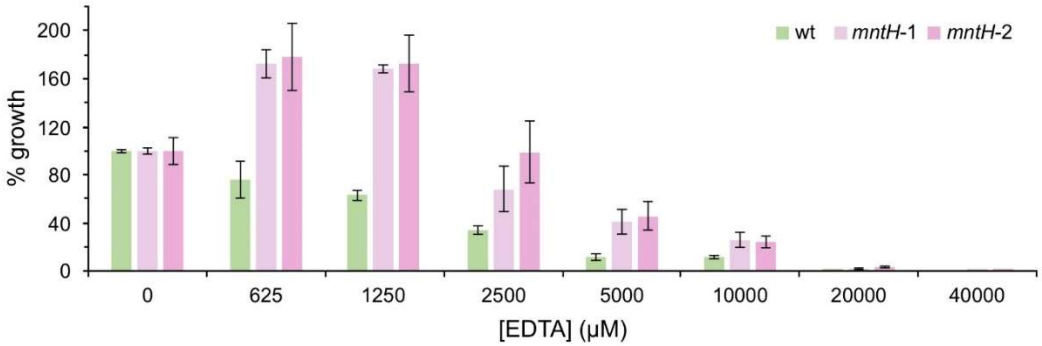

Figure 3.9 Sensitivity of *E. coli ΔmntH* to EDTA. Bacteria were incubated with a two-fold serial dilution of chelant in 100 µl of LB media and incubated with shaking for 16 h at 37°C. Absorbance at 600 nm was monitored and percentage growth determined. Samples of wild-type (BW25113) and *mntH*-1 and *mntH*-2 represent the mean and standard deviation of independent experiments performed in triplicate.

3.5 Discussion and conclusions

3.5.1 Antibacterial activity of individual chelating agents

All of the chelants examined in this chapter inhibited bacterial growth to some extent, although BCS showed limited efficacy even at 100 mM (Fig. 3.2). The dose-response curves with different chelants also varied, with several chelants (CAT, CHA, GLDA, MGDA and PO) exerting little effect on growth until a threshold concentration was reached. Others (DTPA, DTPMP and EDTA) resulted in higher susceptibility at lower chelant concentrations and produced a correspondingly linear reduction in growth (Fig. 3.2). The different sensitivity profiles displayed by this latter group could be an indication of dual antibacterial effects, such as metal starvation coupled with membrane permeabilisation, invoked previously as an explanation for the biphasic inhibition profile of EDTA with *P. aeruginosa* (Lambert et al., 2004). DTPA, DTPMP and EDTA share similar molecular structures (Fig. 3.1) which may correspond to an analogous mechanism of growth inhibition. In the majority of cases high chelant concentrations were required to achieve *E. coli* growth inhibition, with PO and TPEN showing highest efficacy (Fig. 3.2).

There is limited published information on the antibacterial mode of action of most chelating agents. The metal affinity of chelants is anticipated to disrupt metal homeostasis in bacterial cells by selective metal deprivation, and recent work demonstrated that even at 10% growth inhibition chelants have a significant impact on *E. coli* cellular metal levels (Paterson et al., 2022). Each of the 11 chelants studied were categorised according to their effects on specific metals in *E. coli* and this information is helpful in understanding the effects of each chelant individually and in combination.

BCS, CAT and CHA show no significant impact on the metal composition of *E. coli* cells (Paterson et al., 2022). Either they act by a completely different mechanism to restrict bacterial growth (i.e. not involving the perturbation of metal homeostasis) or,

perhaps more likely, they sequester metals within the cell making them inaccessible to the proteins that require them for functionality. This could potentially occur at the inner or outer membrane, the periplasm or in the cytosol, depending on whether the chelator can traverse the cell wall barrier. Based on their lipophilicity, from partition coefficient estimates in their most likely ionisation state at neutral pH, it is feasible that these three chelants readily associate with bacterial membranes. For instance, the long hydrophobic tail and polar head of CHA (Fig. 3.1) could potentially insert into the outer membrane and thereby trap essential metals at the surface so they cannot gain access to the cell.

The principal effect of the azacarboxylate ligands, DTPA, EDTA, GLDA and MGDA, is to deplete *E. coli* of manganese, ranging from 5- to 15-fold reductions relative to untreated controls (Paterson et al., 2022). Both zinc and iron concentrations were also reduced to a lesser extent. There are a number of manganese-dependent enzymes in *E. coli* that could be rendered inactive by manganese starvation, including Mn-superoxide dismutase SodA (Miller, 2012), Mn-dependent ribonucleotide reductase NrdEF (Andrews, 2011) and the haem biosynthetic enzyme coproporphyrinogen III oxidase HemF (Breckau et al., 2003). Mismetallation of these enzymes and loss of the antioxidant properties of manganese could result in cells being more prone to damage by reactive oxygen species (Imlay, 2014; Lisher & Giedroc, 2013). The low levels of manganese may be exacerbated by additional depletion of zinc and iron meaning that multiple metabolic systems are rendered inactive.

DTPMP, HBED and PO affect cells similarly to one another, reducing cellular iron concentration coupled with a substantial increase in manganese (Paterson et al., 2022). There was no significant change in levels of calcium, magnesium or zinc. *E. coli* cells are known to import manganese as a cellular response to iron starvation (Anjem et al., 2009; Imlay, 2014). Manganese-equivalents of iron-redox enzymes, e.g. Mn-superoxide dismutase (Miller, 2012) and Mn-dependent ribonucleotide

reductase (Andrews, 2011), can substitute for iron-containing equivalents, while manganese can functionally substitute for iron in many mononuclear iron enzymes (Imlay, 2014; Juttukonda & Skaar, 2015). Iron and manganese metal homeostasis systems are linked *via* the ferric uptake regulator (Fur) and the proton-dependent manganese importer MntH (Seo et al., 2014). The *E. coli* Fur protein, when complexed with Fe^{2+}, represses the expression of a suite of genes involved in iron uptake, metabolism and bacterial virulence (Sarvan et al., 2018). Thus, when iron levels are limiting, the affinity of Fur for its promoter sites is reduced leading to upregulation of the iron homeostasis network. One such gene negatively regulated by Fur-Fe^{2+} is *mntH*, in accordance with the cellular response that switches to manganese import when iron is scarce (Seo et al., 2014). The manganese superoxide dismutase (MnSOD) is similarly negatively regulated by Fur-Fe^{2+}, whereas Fur-Fe^{2+} activates expression of iron superoxide dismutase, FeSOD (Dubrac & Touati, 2000). Hence, as iron levels in the cell decrease, FeSOD levels decline just as MnSOD levels rise, concomitant with increased manganese uptake. The decreased levels of iron combined with increased manganese induced by DTPMP, HBED and PO can thus probably be explained by bacterial adaptation to protect against iron starvation. PO is capable of traversing eukaryotic membranes to form Fe^{3+} complexes; decreasing mitochondrial metabolism and thereby reducing energy production (Kim et al., 2011). Although it is not known whether PO is similarly capable of penetrating bacterial cells, especially the Gram-negative outer membrane, it may become embedded in the outer membrane, reducing metal availability in the periplasm and cytosol. However, if this were the case there should not be a reduction in absolute iron concentration within the cell (Paterson et al., 2022). This may indicate that PO is capable of destabilising the membrane, either through its insertion, or through chelating the essential stabilising metal ions in a similar mechanism to EDTA. Dual antibacterial effects could potentially explain its relatively low MIC in comparison to the other chelators which show a preference for iron.

The predominant effect of TPEN is to reduce the zinc concentration, consistent with its known affinity for Zn^{2+} (Haase et al., 2013). At higher concentrations of TPEN, manganese levels are also slightly reduced and may contribute to growth inhibition by TPEN (Paterson et al., 2022). Even relatively small reductions in the levels of zinc may adversely affect *E. coli* growth (Graham et al., 2009). Microarray analysis of *E. coli* exposed to TPEN (Sigdel et al., 2006) links chelant exposure with increased expression of genes regulated by the zinc uptake regulator (Zur) (Mikhaylina et al., 2018) but also those controlled by Fur, implying that TPEN may not be entirely selective for zinc.

3.5.2 Antibacterial activity of chelating agents in combination

Chelants were examined in checkerboard assays to provide additional insights into chelant mechanism of action and identify pairings with increased efficacy. Of 55 chelant combinations, 28 synergistic, 26 indifferent and a single antagonistic pair were identified using cumulative calculations (Fig. 3.4 and 3.10). Synergistic, indifferent and antagonistic pairings are listed according to their effect on metal content to facilitate comparisons between groups (Fig. 3.10).

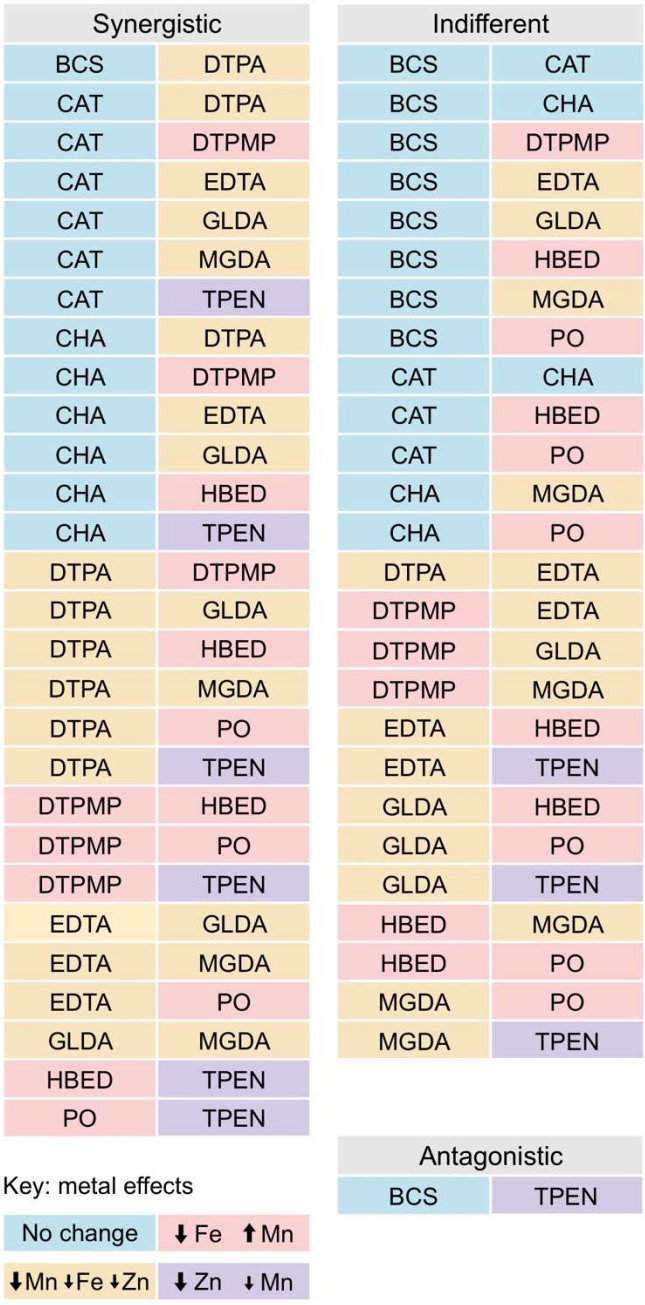

Figure 3.10 Comparison of synergistic, indifferent and antagonistic combinations. The four chelant categories are defined by their distinct effects on total cellular metal concentration in *E. coli*. The effect of each chelant on *E. coli* metal content was determined at concentrations that resulted in 10% growth inhibition (Paterson et al., 2022). Synergistic, indifferent and antagonistic pairs are as defined in Figure 3.4. Bars are colour-coded according to their effect on metals as indicated in the key.

It was predicted that chelant categories that cause similar effects on cellular metal levels would produce indifferent outcomes when combined. Conversely, those with dissimilar effects on metal composition might be expected to yield synergistic results. To some extent this proved to be the case, but there were notable exceptions (Fig. 3.10). Although the majority of the synergistic pairs do indeed match complementary categories of metal deprivation, there are 7 examples (DTPA/GLDA, DTPA/MGDA, DTPMP/HBED, DTPMP/PO, EDTA/GLDA, EDTA/MGDA and GLDA/MGDA) where chelants individually induce analogous cellular responses to metals yet produce synergistic effects in combination. There are also multiple examples of chelants from the different metal effect categories defined earlier that show indifference (e.g. DTPMP/EDTA, GLDA/HBED, and MGDA/TPEN). The results suggest that there are several different ways that chelants function in depriving cells of metals, even for those that appear to have the same overall effect. Preferential removal of metal either from the media or at the bacterial surface as a function of chelant structure may account for some of these differences. Alternatively, there may be effects produced by chelant-metal association at membranes or in the cytosol that influence metal accessibility. It is interesting to note that CAT and CHA display an identical pattern of synergistic and indifferent outcomes with 7 other chelants and are also indifferent with each other (Fig. 3.10). These findings suggest that CAT and CHA are functionally equivalent in depriving cells of the same subset of metals despite their dissimilar structures (Fig. 3.1). This is informative since neither of these chelants appeared to affect total cellular metal content (Paterson et al., 2022).

That only one antagonistic pairing was identified through these assays suggests that the use of chelants in combination may present new therapeutic or commercial solutions for the restriction of bacterial growth. Although the individual efficacy of each chelant is low, synergistic chelant combinations offer a promising antibacterial alternative in product formulations and healthcare applications. Further work is needed to assess whether the patterns of interaction between chelants seen here

also hold true for other bacterial species, especially those with different cell envelope structure and composition.

3.5.3 Effects of EDTA on *E. coli*

In terms of antibacterial efficacy, EDTA is the chelant that has received most attention, with research into its effects on bacteria dating back to the 1960s (Leive, 1965b). It has been assumed that EDTA inhibits bacterial growth by the removal of stabilising Ca^{2+} and Mg^{2+} ions from the outer envelope of Gram-negatives leading to increased vulnerability to osmotic stress and cell lysis (Leive, 1965b). Treatment of *E. coli* with EDTA enhances susceptibility to various compounds, including amines (Voss, 1967) and antibiotics (Leive, 1965a, 1974; Scudamore et al., 1979; Spicer & Spooner, 1974), consistent with interference with outer membrane permeability (Alakomi et al., 2003). Similar observations have been made with other Gram-negatives, including *P. aeruginosa* (Angus et al., 1982; Haque & Russell, 1974; Leive, 1974; Weiser et al., 1968). Cell envelope damage by EDTA has been directly visualized by atomic force microscopy of both *E. coli* (Amro et al., 2000) and *P. aeruginosa* (Alakomi et al., 2006). Destabilisation of artificial lipid membranes has also been reported as a consequence of EDTA exposure (Prachayasittikul et al., 2007). Few reports have been published on the effect of any other chelants on bacteria, and until recently (Paterson et al., 2022), none appeared to have examined their impact on metal homeostasis.

Paterson et al. (2022) demonstrated that EDTA severely reduces manganese, with lesser reductions in iron and zinc. In this chapter, we investigated whether supplementing bacterial cultures with manganese chloride in the presence of EDTA would promote recovery (Figure 3.5). Both EDTA and manganese caused *E. coli* growth inhibition (Figure 3.5A-B), consistent with both compounds causing toxicity. When EDTA and manganese were combined in different ratios improved growth was observed (Figure 3.5C-D). However, this appeared to be largely due to EDTA-Mn^{2+}

complex formation reducing the toxicity of each component. Supplementation of EDTA-treated *P. aeruginosa* and *Salmonella enterica* serovar Typhimurium cells with Ca^{2+} and Mg^{2+} has previously been reported (Alakomi et al., 2003; Brown & Richards, 1965; Leive, 1974), with the positive effects attributed to either membrane stabilisation or alleviation of the detrimental EDTA excess by chelant-metal binding.

The toxic effects of manganese excess have been widely reported, with detrimental effects on bacterial growth attributed to the rewiring of multiple metabolic and regulatory pathways (Kaur et al., 2017). High manganese levels affect the stability of proteins and other macromolecules, along with biogenesis of the cell envelope. Manganese exposure also disrupts the synthesis of iron-sulphur clusters, and haem enzymes, producing secondary iron depletion. Since iron-dependent enzymes are essential for a myriad of processes, including the electron transport chain, an excess of manganese will ultimately result in reduction of adenosine triphosphate (ATP) production and severe energy deficiency (Kaur et al., 2017). Recent work has identified the membrane-localized electron transport chain cytochrome aa_3 haem-copper menaquinol oxidase as a major target of excess manganese in *Bacillus subtilis* (Sachla et al., 2021). In addition, manganese exposure also results in the elevated production of reactive oxygen species (ROS) leading to oxidative stress. Other studies have shown that Mg^{2+}-dependent enzymes can be inhibited or stimulated by Mn^{2+}, and that Mn^{2+} can occupy Mg^{2+}-binding sites in cells. This suggests a link between manganese and magnesium homeostasis within the cell, and reveals Mg^{2+}-dependent processes as targets of manganese toxicity (Hohle & O'Brian, 2014).

3.5.4 *E. coli* mutants with increased susceptibility to chelating agents

The effect of EDTA on the growth of the Keio collection of 3985 single gene deletion mutants (Baba et al., 2006) was previously investigated by printing strains onto LB agar plates supplemented with this chelant (Nichols et al., 2011). To provide further

insight into key genes involved in tolerating exposure to chelants, the iron chelator PO was employed against the Keio collection mutants to screen for effects on growth in LB broth. It was hypothesised that genes involved in iron import, export, and homeostasis would show elevated susceptibility (Fig. 3.6C). These genes include those encoding AroA-M involved in the biosynthesis of chorismate that is converted in steps by EntABC to 2,3-dihydroxybenzoic acid (DHB). EntDEF then catalyses DHB and L-serine linkage and ultimate assembly into enterobactin, which is exported to the extracellular environment by EntS and TolC (Raymond et al., 2003). The ferric-enterobactin complex is recovered by association with the outer membrane receptor FepA. The TonB/ExbBD complex provides energy from the proton motive force to facilitate release of the Fe^{3+}-enterobactin complex from FepA, facilitated by FepB, and delivery to the FepCDG ABC-family, ATP-dependent inner membrane permease (Nagy et al., 2013). Upon reaching the cytosol, Fe^{3+} is released from the siderophore by the Fes esterase. Another ABC-family transporter, ZnuABC, transports Zn^{2+} across the inner membrane (Patzer & Hantke, 1998).

The Keio screen with PO confirmed the importance of genes involved in iron-siderophore uptake for tolerance to PO, with strains defective in the synthesis and trafficking of enterobactin showing substantial reductions in growth following exposure to PO (Fig. 3.6A). Hypersensitivity to PO was also apparent in mutants lacking efflux pumps, along with factors important for maintenance of envelope integrity and tolerance of cellular stress (Fig. 3.6A). This would fit with PO gaining access to the periplasm or cytosol in these strains and exacerbating its effects on growth. These findings were confirmed by examining a selection of the PO-affected mutants in MIC assays (Fig. 3.7A and 3.8A). Mutations in components of the Fe^{3+}-hydroxamate and Fe^{3+}-citrate systems were generally unaffected by PO (Fig. 3.8A). Other mutants which are highly sensitive to iron starvation including those involved in cysteine (*cysE*) and histidine (*hisI*) biosynthesis (Nichols et al., 2011), showed no increased susceptibility to PO (Fig. 3.8A). A similar subset of genes involved in

enterobactin-iron uptake and membrane integrity were also susceptible to EDTA (Nichols et al., 2011) (Fig. 3.6B, 3.7C and 3.8C) and DTPMP (Fig. 3.7B and 3.8B). In contrast to PO, mutants lacking the FecABCDE system which takes up ferric iron in complex with citrate (Miethke, 2013) were relatively much more sensitive to EDTA and DTPMP. Similarly, cells deficient in components of the ZnuABC zinc uptake system were generally unaffected by PO, but were highly susceptible to EDTA and DTPMP (Fig. 3.7 and 3.8). The results are consistent with PO primarily sequestering iron, whereas EDTA restricts the availability of both iron and zinc (Paterson et al., 2022). Surprisingly, bacteria lacking the MntH importer proved more resistant to EDTA (Fig. 3.9) which indicates that the major effects on manganese deprivation (Paterson et al., 2022) are not necessarily responsible for growth impairment. DTPMP appeared to affect a similar suite of mutants as EDTA, despite its primary effects on iron limitation (Paterson et al., 2022). The fact that the *mntH* mutant was much more sensitive to DTPMP and PO (Fig. 3.8A-B) which both primarily target iron (Paterson et al., 2022), may reflect the necessity for increased manganese import under conditions of iron restriction (Anjem et al., 2009; Imlay, 2014). The results highlight major differences in the mechanism of action of these three chelants with effects on different iron acquisition pathways and the importance of zinc acquisition in some cases but not others.

A small number of mutants displayed improved growth relative to untreated controls when PO was incorporated in the growth medium (data not shown). Several of these mutants display growth improvement at both PO concentrations suggesting a genuine advantage in their absence. These mutants correspond to genes linked to regulatory pathways (e.g. *yqhC*, *yieP)*, metabolic processes (e.g. *tnaB*, *gldA*) and oxidative damage repair (e.g. *mutY*, *recQ*). However, the largest group affected are those engaged in flagellar biosynthesis, of which 26 *fli*, *flg* and *flh* genes occur in the 200 mutants that show the most enhanced growth at both PO concentrations. This may represent an alleviation of the substantial energy cost involved in flagellum

assembly and operation (Smith & Chapman, 2010) during the iron limitation imposed by PO. Significantly, flagellar gene deficient mutants do not exhibit the most enhanced growth of the Keio mutant strains under low iron conditions using MOPS media (Nichols et al., 2011), suggesting that PO exerts additional detrimental effects or targets iron depletion with a different cellular specificity.

3.6 Future directions

The results detailed in this chapter show that chelating agents offer significant potential as antibacterial agents against *E. coli* as a representative Gram-negative. Chelant antibacterial efficacy and mode of action were investigated using chelant pairs to compare with previously generated information on how these chelants alter the cellular concentration of metals in *E. coli* (Paterson et al., 2022). For many of the 11 chelants, however, the precise mechanism through which they mediate their antimicrobial effects remains unclear. The chelants clearly restrict the availability of key metals, with iron, manganese and zinc being the most important or potentially associate with the outer membrane to further reduce access of metal-binding proteins and transporters to their cognate metal ions. Previous work has also highlighted that some are capable of disrupting the outer membrane of Gram-negatives making cells prone to increased permeability and ultimately lysis (Haque & Russell, 1974; Leive, 1965b, 1974; Weiser et al., 1968). This may be an important factor when chelants are used in combination, allowing easier intracellular access for one or both ligands.

Further work is needed to more precisely determine the localisation of chelants (and metals) within cells to help reveal their cellular targets. Gathering robust metal ion affinities for chelators to multiple metal ions *in vitro* would allow enhanced prediction capabilities of possible effects on bacterial cell growth. Combining this information would allow comparison with known metal availabilities of metal ions at distinct cellular locations, such as that assembled for the *Salmonella* cytosol (Osman et al., 2019). The subset of Keio collection mutants tested with PO, EDTA and DTPMP

could be harnessed to provide more detail on the effects of the other chelants on the metal uptake pathways examined in this chapter. It is also essential to examine whether bacterial species with different cell wall arrangements exhibit similar cellular responses to chelating agent treatment. To begin to address this latter question, the impact of chelants on Gram-positive and Gram-negative species is examined in Chapter 4 of this thesis.

4 Susceptibility of Gram-negative and Gram-positive bacteria to chelating agents

4.1 Introduction

In the previous chapter, we examined the susceptibility of *E. coli* to 11 chelating agents both singly and in pairwise combinations. Mutant strains were also assessed to help delineate the metal uptake pathways important for tolerance of selective metal deprivation by chelants. In this chapter, we extended our investigation into the effect of chelants by comparing chelant efficacy against three additional bacterial species, *Pseudomonas aeruginosa*, *Bacillus subtilis* and *Staphylococcus aureus*, the latter two as representative Gram-positive species. Three of the chelants studied in Chapter 3 (CHA, DTPMP and EDTA) were retained for this comparison because they produce differing effects on total cellular metal content in *E. coli* (Paterson et al., 2022). Four additional chelants were included, in part, due to commercial interest in their mode of action and also their unique chemistries. After these initial comparisons, the remainder of the chapter is focussed on the effects of these chelants on cellular metal content and membrane permeability in *P. aeruginosa*. Since *P. aeruginosa* is an opportunistic pathogen, chelant-chelant and chelant-antibiotic combinations were evaluated for antibacterial efficacy. Such antibacterial combinations have potential for improved efficacy in commercial products as well as therapeutics to treat bacterial infections.

4.1.1 Chelating agents

In addition to CHA, DTPMP and EDTA which were studied in detail in Chapter 3, an additional four chelating agents were included at this stage (Fig. 4.1). The additional chelants were selected based on their different metal affinities, solubility and chemical structures. Many of these chelating agents are employed as additives in product formulations to extend shelf life. Industrial requirements such as regulatory frameworks and cost were considered in partnership with Procter and Gamble. CHA,

DTPMP and EDTA were previously tested on *E. coli* (Chapter 3), where they differ in their effects on metal homeostasis, and hence were carried forward here to determine whether they elicited similar cellular responses in different bacterial species. The four new chelants were chloroxine (CHL), fusaric acid (FA), hinokitiol (HNK) and tropolone (TRO; Fig. 4.1).

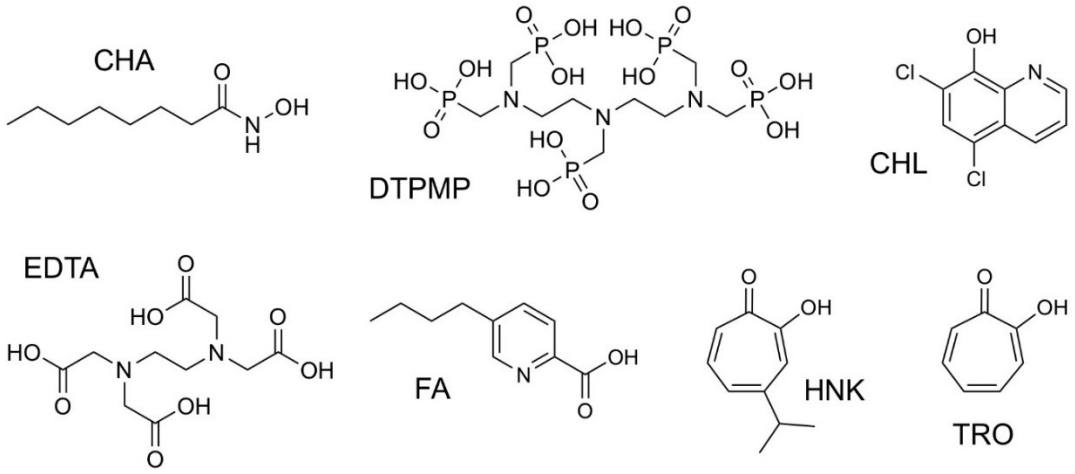

Figure 4.1 Chelating agents used in this chapter. CHA (caprylhydroxamic acid), DTPMP (diethylenetriaminepentamethylene phosphonic acid), CHL (chloroxine, dichlorchinolinolum), EDTA (ethylenediaminetetraacetic acid), FA (fusaric acid, 5-butylpyridine-2-carboxylic acid), HNK (hinokitiol, β-thujaplicin), TRO (tropolone, 2-hydroxycyclohepta-2,4,6-trien-1-one). CHA, DTPMP and EDTA were used in prior analyses (see Chapter 3).

CHL is a small, synthetic dichloroquinolinol which has antibacterial activity against *E. coli* and *S. aureus*, as well as efficacy against various fungal species (Shahabadi et al., 2021). CHL has previously been used in conjunction with ceftazidime to enhance bacterial killing against *Burkholderia thailandensis* and *B. pseudomallei* (Barker et al., 2021). FA is a mycotoxin which has been hypothesised to augment the toxicity of other mycotoxins (Bacon et al., 1996). Its effects on bacteria have previously been examined, with Gram-positive species showing enhanced sensitivity (Crutcher et al., 2017) suggesting that the outer membrane of Gram-negatives provides some protection against this chelant. HNK (β-thujaplicin) also possesses antibacterial activities against both *E. coli* and *S. aureus*. It has been suggested that

its bactericidal activity may be partly due to inhibition of membrane metabolism, resulting in suppression of cellular respiration (Morita et al., 2007). More recent studies have even suggested that HNK could be harnessed for cancer chemotherapy through inhibition of proliferation and colony formation of lung adenocarcinoma cells by causing deoxyribonucleic acid (DNA) damage and disrupting normal autophagy and cell cycle processes (Li et al., 2014; Shih et al., 2013). TRO is closely related in structure to HNK and is a known antibacterial which can inhibit the growth of both Gram-positive and Gram-negative species (Trust, 1975). A recent study highlighted the importance of the action of TRO against CapF, a bifunctional metalloenzyme involved in the production of capsular polysaccharides in *S. aureus*. TRO binds tightly to the Zn^{2+} ion needed by CapF, thereby destabilising the enzyme, halting production of essential polysaccharides and leaving cells vulnerable to lysis (Nakano et al., 2015). PO was included as a control in one of the assays performed here and was examined previously in Chapter 3. It is a commonly used antifungal in product formulations, most notably in shampoos to prevent dandruff caused by *Malassezia globosa*. The mechanism of action of PO is complex, and not well understood, although it is known that this chelant can penetrate fungal cells and form complexes with Fe^{2+} and Fe^{3+} ions (Kim et al., 2011).

4.1.2 Bacterial growth inhibition by chelants

Broth microdilution assays were carried out in LB media to assess the antibacterial activities of the seven chelating agents selected for study (Fig. 4.1). The bacteria chosen were *B. subtilis*, *S. aureus*, *E. coli*, and *P. aeruginosa*; the former two as representative Gram-positive species that possess a single membrane, whereas the latter two are Gram-negatives possessing both an inner and outer membrane. The lipopolysaccharide-rich outer membrane of Gram-negative species serves as an additional protective layer, and is known to present a considerable impermeability

barrier to hydrophobic molecules, including many commonly used antibiotics (Delcour, 2009).

To assess susceptibility, 2-fold serial dilutions of each chelant were performed as in Chapter 3 and incubated with each bacterial species at 37°C for 16 hours before growth was measured by optical density. Percentage growth relative to untreated controls is shown in Figure 4.2 and the MICs for >90% inhibition presented in Table 4.1. The majority of chelants displayed a linear decrease in bacterial growth as concentration is increased, but some chelants such as CHA showed a 'critical concentration' after which bacterial growth suddenly drops. The concentration of chelant required to inhibit growth by >90% differed between the chelants, with CHL, FA, HNK and TRO typically showing greater efficacy than CHA, DTPMP or EDTA (Table 4.1), although there is variation in susceptibility between the species.

While differences were expected between the chelant susceptibility of Gram-positive and Gram-negative species, the presence of an outer membrane does not always confer increased tolerance (Figure 4.2 and Table 4.1). Furthermore, it is striking that the different Gram-negatives and Gram-positives often differ in their sensitivities. *B. subtilis* and *S. aureus* tolerate CHA better than either of the two Gram-negative species (Fig. 4.2A), whereas the reverse is true for CHL (Fig. 4.2B) and TRO (Fig. 4.2G). *E. coli* and *B. subtilis* proved most resistant to DTPMP, while *S. aureus* was the most susceptible to this chelant (Fig. 4.2C). *E. coli* proved >10-fold more resistant to EDTA than the other three species (Fig. 4.2D), whereas *P. aeruginosa* showed the greatest tolerance to FA (Fig. 4.2E). Despite their similarity in chemical structures (Fig. 4.1), HNK and TRO exhibit a different pattern of susceptibility (Fig. 4.2F-G). *P. aeruginosa* and *S. aureus* were most resistant to HNK (Fig. 4.2G).

CHL was omitted from further studies due to poor solubility and discolouration of samples, which at higher concentrations interfered with growth inhibition measurements (Appendix, Fig. 9.2A). Hinokitiol was observed to gradually turn yellow over a period of weeks. This was found to be due to exposure to daylight as samples

kept in the dark did not discolour (Appendix, Fig. 9.2B). The colour change did not impair the ability of hinokitiol to inhibit *P. aeruginosa* growth in samples exposed to light for 1 or 2 months (Appendix, Fig. 9.2C). The colour change in hinokitiol solutions is most likely due to photo-oxidation, as samples of the closely-related tropolone form a tetrameric product that is yellow-red in colour following exposure to peroxidase in the presence of hydrogen peroxide (Kahn & Andrawis, 1985; Zhao & Sakai, 2003).

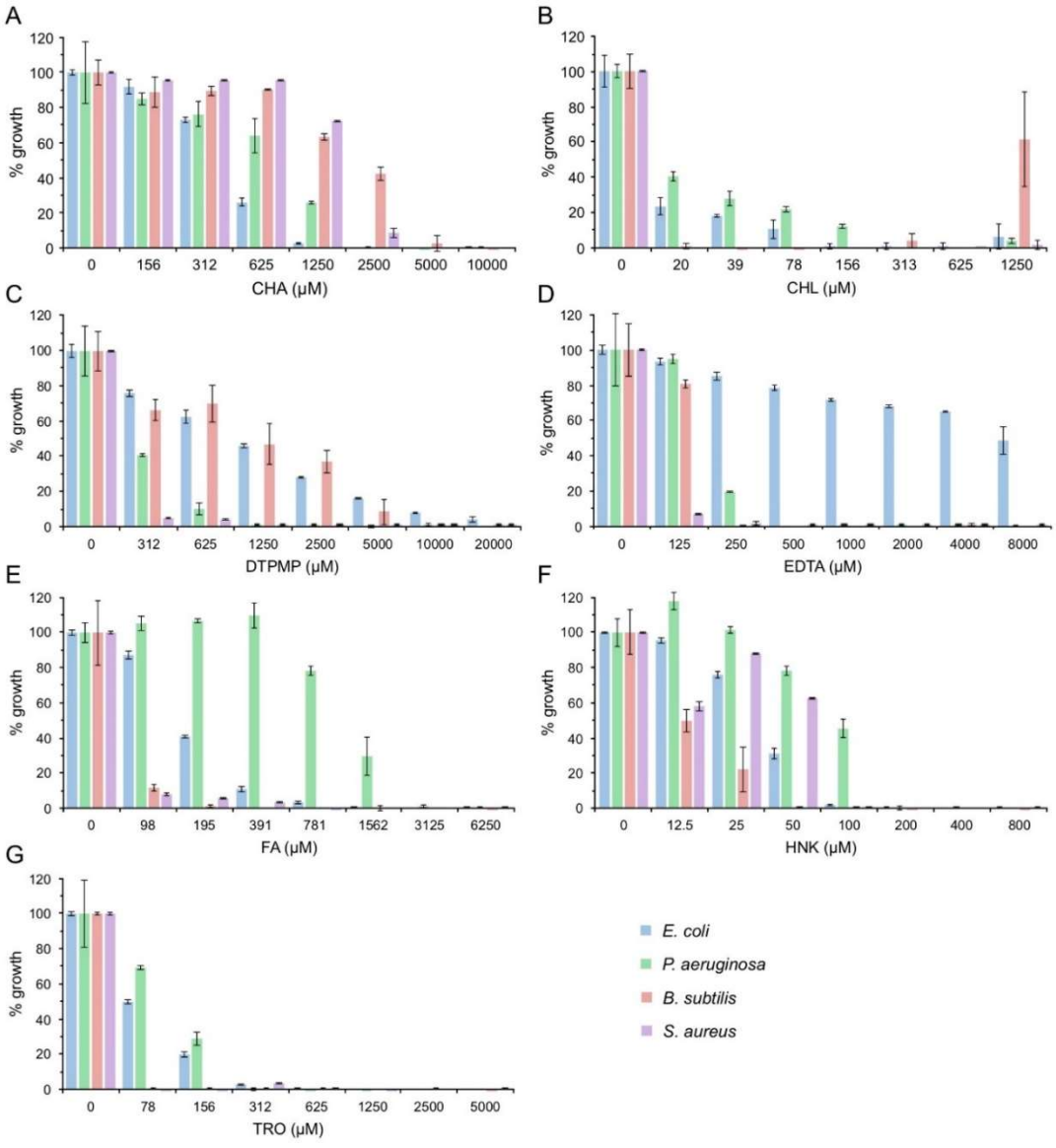

Figure 4.2 Effect of chelants on bacterial growth. Bacteria were incubated with 2-fold serial dilutions of each chelant in 100 µl of LB media and incubated with shaking for 16 h at 37°C. Absorbance at 600 nm was recorded and the percentage growth determined. Data represent the mean and standard deviation of a single biological repeat performed in triplicate.

Whether the chelants exert bacteriostatic or bactericidal effects was estimated for *E. coli*, *P. aeruginosa* and *S. aureus* by determining the minimum bactericidal concentration (MBC; Table 4.1). With each chelant, 10 µl was transferred from wells where growth inhibition was observed to 90 µl of fresh LB broth and incubated at 37°C for 16 h and growth measured at $A_{600\,nm}$. This approach provides a qualitative estimate of MBC and other methods to validate killing would be appropriate (Balouiri et al., 2016; Pfaller et al., 2004). Despite this limitation, there was convincing evidence of bactericidal activity at high chelant concentrations (MBC >4x MIC). DTPMP and EDTA appeared least effective at killing and generally displayed bacteriostatic effects until concentrations 6-8x the MIC were reached (Table 4.1). Chelants showing an MBC twice that of the MIC included CHA with *P. aeruginosa* and *S. aureus*, CHL with *E. coli*, FA with *P. aeruginosa* and TRO with *P. aeruginosa* (Table 4.1). HNK had an MBC identical to the MIC with *S. aureus*, indicating high bactericidal activity. It is interesting to note the variation in chelant susceptibility between the four bacterial species.

Table 4.1 MICs of chelants with four bacterial species.

Chelant	MIC	*E. coli*	*P. aeruginosa*	*B. subtilis*	*S. aureus*
CHA	MIC	1250	2500	5000	5000
	MBC	5000	5000	>10000	10000
CHL	MIC	156	313	10	20
	MBC	313	1250	20	78
DTPMP	MIC	10000	1250	10000	700
	MBC	>32000	8000	10000	4000
EDTA	MIC	17500	500	250	125
	MBC	40000	4000	>500	1000
FA	MIC	781	3125	125	200
	MBC	3125	6250	>250	3125
HNK	MIC	50	200	50	100
	MBC	400	800	>100	100
	MIC	312	312	25	25

TRO	MBC	1250	625	50	78

MICs in µM were defined as inhibition of growth by >90% (MIC_{90}). In wells without growth, 10 µl was transferred and added to 90 µl of fresh medium and incubated at 37°C for 16 h and the MBC defined as inhibition of growth by >90%.

4.2 Effect of chelant-chelant and chelant-antibiotic combinations on *P. aeruginosa* growth

The antibacterial efficacy of chelating agents is often limited, requiring concentrations of 100-10000 µM to substantially inhibit bacterial growth, although CHL, HNK and TRO show promising activity at relatively low concentrations (Table 4.1). As a consequence, chelating agents are typically used in conjunction with other antimicrobial agents in commercial formulations to restrict microbial growth. Combinations of chelants and antibiotics also offer possibilities for therapeutic applications in the limited studies published to date (Chan et al., 2020; Parquet et al., 2018; Vinuesa & McConnell, 2021). To investigate how the seven chelants perform when combined with other antimicrobial agents, or when combined with each other, we again employed the checkerboard assay (see Chapter 3).

4.2.1 Chelant-chelant combinations with *P. aeruginosa*

Comparing the effects of chelant combinations on antibacterial growth helped to identify synergistic combinations with improved antibacterial efficacy against *E. coli*, and also provided some indication of differences in chelant mode of action (Chapter 3). To probe these effects further and establish whether similar results would be obtained with a different Gram-negative species, we examined pairs of six selected chelants in checkerboard assays with *P. aeruginosa* (Fig. 4.3). As with *E. coli*, synergistic (Fig. 4.3A) and indifferent (Fig. 4.3B) combinations were identified, but no antagonistic pairs were found with *P. aeruginosa* using these chelants. FIC indices were determined using the individual or mean methods as described in Chapters 2 and 3. A total of 12 synergistic combinations were identified with the individual method but only 6 with the more restrictive mean approach (Fig. 4.3C and D). Indifference was apparent with two FA combinations (FA/CHA and FA/TRO) and the HNK/TRO pairing, the latter in keeping with their similar chemical structures and presumed mode of action (Fig. 4.3C). DTPMP and EDTA were both synergistic with all of the other chelants, including each other using the individual FIC calculations (Fig. 4.3C). These two chelants also showed most synergistic pairings (3 each) using the mean FIC determination (Fig. 4.3D).

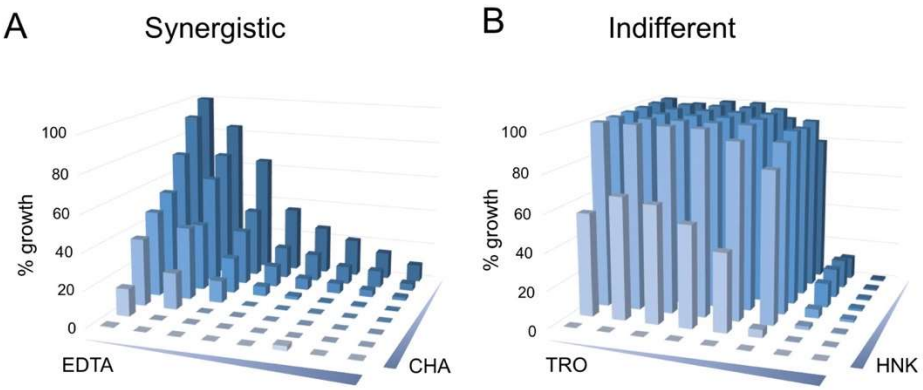

C Individual FIC

DTPMP	EDTA	FA	HNK	TRO	
0.05	0.03	1.00	0.05	0.28	CHA
	0.09	0.09	0.03	0.03	DTPMP
		0.09	0.03	0.08	EDTA
			0.25	1.00	FA
				0.75	HNK

D Mean FIC

DTPMP	EDTA	FA	HNK	TRO	
0.32	0.29	1.00	0.61	0.55	CHA
	0.60	0.64	0.33	0.29	DTPMP
		0.51	0.30	0.41	EDTA
			0.88	0.85	FA
				0.95	HNK

Synergistic ≤0.5
Indifferent >0.5-≤4.0

Figure 4.3 Chelant combinations analysed by the checkerboard assay. Checkerboard assays were performed with 2-fold serial dilutions of chelants (as in MIC determination assays) in LB broth with *P. aeruginosa* at 37°C for 16 h. Additional controls for low levels of DMSO were included where appropriate. Representative examples are shown of CHA/EDTA as a synergistic pairing (A) and HNK/TRO as an indifferent combination (B). FIC index values are shown for two independent experiments performed in triplicate for each chelant combination, calculated using either an individual (C) or mean (D) method. The assay allows the calculation of an MIC for each chelant and the FIC, which provides a measure of the effect of the chelants in combination as synergistic, indifferent or antagonistic. FIC values were calculated based on the lowest concentration of each chelant in combination divided by the MIC for that chelant (see Equation 2.1).

4.2.2 Chelant-antibiotic checkerboards

To evaluate the potential of chelants as potentiators of antibiotic activity, we examined the effect of chelants in combination with antibiotics against *E. coli*, *P. aeruginosa*, *B.*

subtilis and *S. aureus*. Chelants such as EDTA are known known to affect the permeability of the Gram-negative outer membrane and may well act synergistically with antibiotics as a result (Alakomi et al., 2006; Leive, 1965b; Vaara, 1992). The two water-soluble chelants, EDTA and DTPMP, were selected for study as they affect different cellular metals in *E. coli* (Paterson et al., 2022) and also produce the most synergistic combinations in chelant-chelant checkerboards (Fig. 4.3). Six readily available antibiotics were selected for study: a β-lactam (ampicillin) affecting cell wall synthesis, chloramphenicol, tetracycline and three aminoglycosides (kanamycin, streptomycin and spectinomycin), all of which target the ribosome and block protein synthesis (Krause et al., 2016).

Representative examples of synergistic and indifferent (or non-interacting) pairings from these studies are shown in Figure 4.4. For example, the DTPMP-kanamycin pairing shows synergism with *B. subtilis* and *S. aureus* but indifference with *E. coli* and *P. aeruginosa*. With the two latter Gram-negative species there is also evidence of antagonistic effects at certain concentrations of the chelant and antibiotic (Fig. 4.4). Overall 12 chelant-antibiotic pairings were tested for each bacterial species and the FIC indices determined (Fig. 4.5; Equation 2.1), revealing 33 synergistic and 15 indifferent combinations by selecting the lowest possible combination of each chelant in cumulative calculations (Fig. 4.5A). Considerably fewer synergistic pairings, only 9, were obtained using a mean FIC method (Fig. 4.5B), although this is not overly surprising given that such an approach employs much stricter criteria for assigning synergy (Bonapace et al., 2002). *E. coli* and *P. aeruginosa* yielded a similar pattern of results with both EDTA and DTPMP with each antibiotic (Fig.4.5). EDTA was generally synergistic with each antibiotic on both species, consistently so with *P. aeruginosa* using individual or mean FIC estimations. DTPMP produced clear antagonistic effects with all three aminoglycosides, kanamycin, spectinomycin and streptomycin although the overall FIC scores were in the indifferent range (Fig. 4.4 and 4.5). With the two Gram-positives there were different individual FIC outcomes,

though most were indifferent using a mean FIC. The results presumably reflect differences in susceptibility due to cell wall architecture and membrane composition between Gram-negative and Gram-positive bacteria and also within the two groups. The synergistic combinations are consistent with chelants improving the uptake of antibiotics by penetrating or destabilising the outer membrane of Gram-negative species, although they also act as potentiators of antibiotics with Gram-positives.

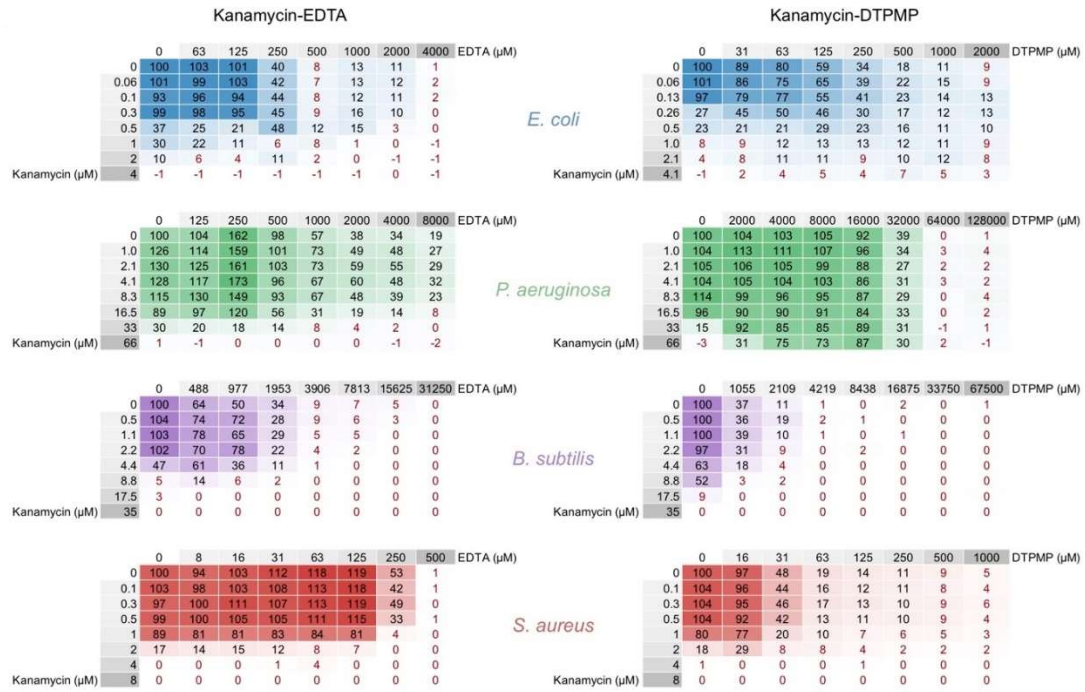

Figure 4.4 Representative combinations of EDTA or DTPMP with kanamycin against four bacterial species. Checkerboard assays were performed with 2-fold serial dilutions of chelants and antibiotics in LB broth with *E. coli* (blue), *P. aeruginosa* (green), *B. subtilis* (purple) and *S. aureus* (red) at 37°C for 16 h.

A

Individual FIC	*E. coli*		*P. aeruginosa*		*B. subtilis*		*S. aureus*	
	EDTA	DTPMP	EDTA	DTPMP	EDTA	DTPMP	EDTA	DTPMP
Ampicillin	0.25	0.28	0.09	0.06	0.14	0.63	0.52	0.09
Chloramphenicol	0.50	0.31	0.05	0.13	0.28	0.19	1.00	0.16
Kanamycin	0.14	2.03*	0.63	2.00*	1.50	0.38	0.38	0.31
Spectinomycin	0.09	1.06*	0.08	0.56*	0.13	0.13	0.38	0.09
Streptomycin	0.13	3.00*	0.27	1.50*	0.09	0.13	2.00	0.56
Tetracycline	0.05	0.56	0.09	0.19	0.05	0.19	0.75	0.27

B

Mean FIC	*E. coli*		*P. aeruginosa*		*B. subtilis*		*S. aureus*	
	EDTA	DTPMP	EDTA	DTPMP	EDTA	DTPMP	EDTA	DTPMP
Ampicillin	0.75	0.77	0.43	0.61	0.65	0.98	1.00	0.57
Chloramphenicol	1.04	0.77	0.24	0.54	0.77	0.73	1.10	0.75
Kanamycin	0.66	2.81*	0.91	1.16*	1.40	0.84	0.94	0.84
Spectinomycin	0.49	1.86*	0.34	1.09*	0.74	0.70	0.95	0.72
Streptomycin	0.86	1.00*	0.43	1.38*	0.47	0.60	1.19	0.95
Tetracycline	0.34	0.93	0.35	0.65	0.56	0.68	1.05	0.59

Figure 4.5 Summary of antibiotic-chelant pairings against four bacterial species. Checkerboard assays were performed with 2-fold serial dilutions of chelants and antibiotics in LB broth with *E. coli*, *P. aeruginosa*, *B. subtilis* and *S. aureus* at 37°C for 16 h. FIC indices were determined by individual (A) or mean (B) methods. Synergistic combinations (≤0.5) are highlighted in lilac and indifferent pairings (>0.5-≤4.0) in blue. An asterisk indicates those combinations that showed evidence of antagonism.

4.3 Effect of chelants on cell permeability

Bacterial uptake of the nonpolar hydrophobic probe 1-N-phenylnaphthylamine (NPN) can be used to monitor the effect of chelants on Gram-negative outer membrane permeability. NPN fluorescence is increased in a glycerophospholipid environment and indicates weakening of the bacterial outer membrane (Alakomi et al., 2006). This approach has been successfully employed to examine the membrane permeabilising effects of EDTA on *Pseudomonas* species (Alakomi et al., 2006). Initial efforts to use NPN to monitor chelant effects by microscopy were not sufficiently reproducible, mainly due to the low fluorescence of NPN with single cells, and therefore a method

was adopted which allowed the monitoring of NPN fluorescence using a microtitre plate reader (Helander & Mattila-Sandholm, 2000).

The NPN fluorescence assay was initially validated by comparing the *E. coli* wild-type (BW25113) with the isogenic *rfaC* (*waaC*) mutant which has a defect in lipopolysaccharide (LPS) formation (Baba et al., 2006; Pagnout et al., 2019) resulting in increased cell permeability (Fig. 4.6A). The *rfaC* mutant exhibited >2-fold increased fluorescence relative to the wild-type consistent with increased uptake of NPN due to increased permeability. Elevated uptake of NPN, as judged by increased fluorescence, in the *E. coli* wild-type strain was apparent following exposure to EDTA (Fig. 4.6B) consistent with published results (Alakomi et al., 2006). NPN uptake was also increased by EDTA in another Gram-negative species, *Serratia marcescens*, although the effect was less marked than *E. coli* and was subject to experimental variability (Fig. 4.6C). No significant increase in fluorescence was detected when the Gram-positive *S. aureus* was mixed with EDTA in the presence of NPN (data not shown).

Eight chelants were investigated for their effects on membrane damage against *P. aeruginosa*. DTPA and PO were included here because of indications that they might associate with the Gram-negative outer membrane or alter membrane permeability in *E. coli* (see Chapter 3). Due to experimental variability, each experiment was performed six times in triplicate although the trends in each case were similar. Representative results of single experiments performed in triplicate with each chelant are shown in Figure 4.6D. Two of the chelants, DTPMP and EDTA, produced a modest increase in NPN fluorescence (Fig. 4.6D). The results with EDTA match those seen previously using this technique with *P. aeruginosa* (Alakomi et al., 2006), although this is the first time that DTPA has been examined and suggests that it shares similar membrane permeabilising effects. In contrast, DTPMP did not alter the levels of NPN fluorescence with *P. aeruginosa*, while CHA, FA, HNK, PO and TRO all resulted in a reduction in fluorescence (Fig 4.6D). Either they associate with NPN

to quench fluorescence or they, somehow, block NPN uptake at the cell surface. Although these experiments appear to confirm that EDTA and DTPA disrupt the outer membrane of *P. aeruginosa* and increase cell permeability, they unfortunately do not provide further insight into the mode of action of the remaining chelants.

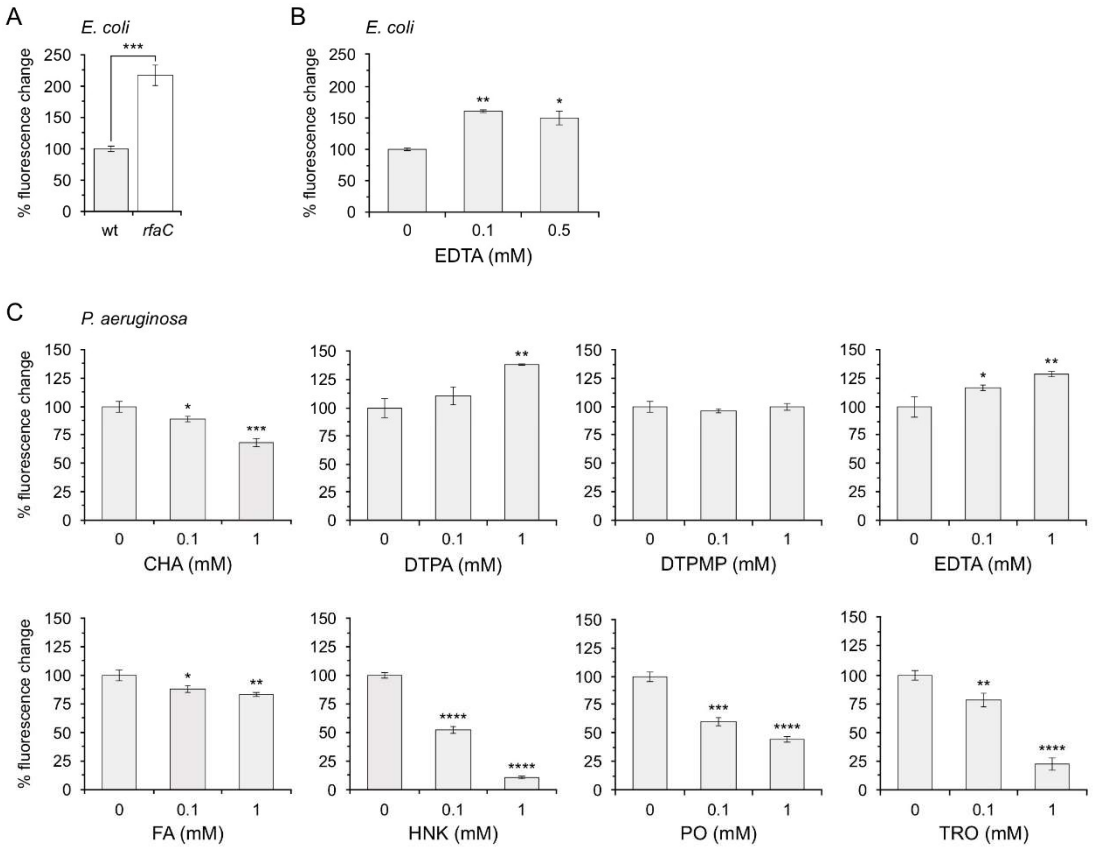

Figure 4.6 Effect of chelants on *P. aeruginosa* membrane permeability. Bacteria were incubated with each chelant at room temperature for 10 minutes before NPN was added at a final concentration of 10 μM. Emission was monitored at 405 nm following excitation at 355 nm. Data represent the mean and standard deviation of a single experiment performed in triplicate. One way ANOVA was used for comparisons between treated and untreated samples; *p<0.05, **p<0.01, ***p<0.001, ****p<0.0001.

4.4 Effect of chelants on *P. aeruginosa* cellular metal content

Previous studies revealed that chelants can selectively deprive *E. coli* cells of metal ions, notably affecting levels of iron, manganese and zinc (Paterson et al., 2022). The effect of chelants on total cellular metal content of *P. aeruginosa* was therefore

investigated to compare the effects of the three chelating agents examined previously (CHA, DTPMP and EDTA) alongside three of the additional compounds, FA, HNK and TRO.

As before (Beecroft, 2019), inductively coupled plasma mass spectrometry (ICP-MS) was employed to accurately determine the total cellular metal content of Ca, Cu, Fe, Mg, Mn and Zn, thus providing information on how chelating agents affect *P. aeruginosa* metal acquisition (Fig. 4.7). Chelant concentrations were chosen that result in approximately 10-15% growth inhibition. At higher levels of chelant cells may begin to lyse, thereby releasing metals which could be acquired by surviving cells, skewing the results. Cellular metal content determination experiments often utilise EDTA in the wash buffer prior to digestion to remove any metal ions bound at the cell surface (Osman et al., 2019; Shen et al., 2019). Since EDTA was one of the chelants to be analysed here, it was omitted from the wash buffer in these experiments. The results presented therefore include metals which are associated with the bacterial outer membrane as well as within the cell.

As previously observed with *E. coli* (Beecroft, 2019), exposure of *P. aeruginosa* to CHA produced no significant change in the cellular metal content of the six metals analysed (Fig. 4.7A). It is possible that CHA traps metal ions at the cell surface by associating with the outer membrane in these two Gram-negative species. Hence the absolute level of metals could remain the same while the intracellular bioavailability is severely constrained, resulting in cell growth inhibition.

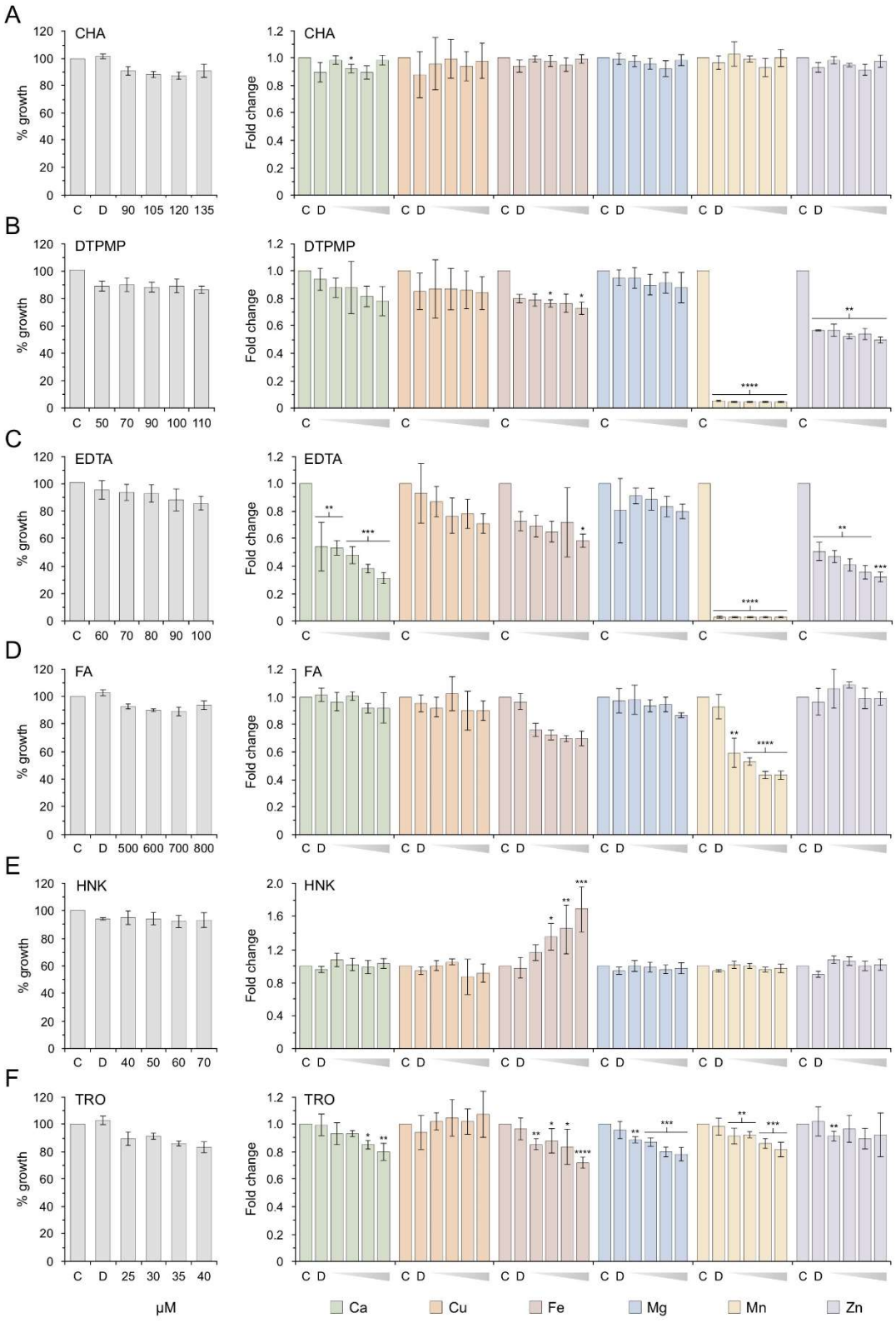

Figure 4.7 Effect of chelants on total cellular metal composition of *P. aeruginosa*. Cells were grown in the presence or absence of chelant in 50 ml of LB broth to mid-log phase ($A_{600\ nm}$ 0.3-0.4; 3-4 hours) in a shaking incubator (125 rpm) at 37°C before determination of metal atoms per cell using ICP-MS. Data are the mean

and standard deviation of 4 independent experiments, except in the case of FA, where 3 biological replicates were performed. One way ANOVA was used to compare each chelant concentration with the untreated control in each case; *p<0.5, **p<0.01, ***p<0.001, ****p<0.0001. The fold-change in metal concentration relative to the untreated control is indicated. Concentrations of chelants in μM are indicated below the graphs on the left showing the level of bacterial growth inhibition. C represents the control without treatment and D, DMSO, where relevant. The full data set can be found in the Appendix, Table 9.2.

Both DTPMP and EDTA (Fig.4.7B and 4.7C, respectively), produced a dramatic reduction (>10-fold) in manganese, with a secondary effect on zinc levels. There was also a reduction in iron in both cases, with EDTA also causing a drop in calcium. These differences were consistent across the four data sets (Appendix, Table 9.2) even when the variation between experiments yielded an overlap in the standard deviation error bars. The impact of EDTA on *P. aeruginosa* is broadly similar to that found with *E. coli* (Paterson et al., 2022), although the reduction in calcium is greater with *P. aeruginosa* (Fig. 4.7C). The effect of DTPMP on *P. aeruginosa* differed markedly from that seen with *E. coli*. In *E. coli*, DTPMP causes a reduction in iron in concert with an increase in manganese, consistent with a cellular response to iron limitation (Paterson et al., 2022). However in *P. aeruginosa,* DTPMP behaves much like EDTA, predominantly limiting manganese levels with lesser reductions in iron and zinc (Fig. 4.7B). That the same chelating agent may induce a different cellular response in different Gram-negatives is interesting and presumably reflects variation in the metal homeostasis systems between the two genera (Chandrangsu et al., 2017).

The inclusion of FA in the growth medium decreased the cellular levels of both manganese and iron in *P. aeruginosa*, leaving the other metals unaffected (Fig. 4.7D). This pattern of metal depletion has not been observed previously with any of the other 11 chelants examined with *E. coli* (Beecroft, 2019). In these previous studies, iron limitation coincided with an influx of manganese with DTPMP, HBED and PO. It is

possible that *P. aeruginosa* does not possess a similar iron-sparing pathway that relies on manganese import. Alternatively, this may be an indication that the affinities of manganese-binding proteins in *P. aeruginosa* are lower than those found in *E. coli*.

Additional unique effects were found with HNK, which caused a significant elevation in iron levels (Fig 4.7E), while TRO resulted in small but reproducible reductions in calcium, iron, manganese and magnesium but no change in copper or zinc (Fig. 4.7F). Not only is it noteworthy that TRO triggers smaller reductions over a broader range of metals (as opposed to most other chelants which have larger effects on a smaller number of metals), but also that TRO and HNK have such differing effects despite the similarity in their chemical structures (Fig. 4.1).

4.5 Discussion

4.5.1 Antibacterial activity of chelating agents

All of the chelants examined in this chapter displayed some capacity to inhibit the growth of representative Gram-negative and Gram-positive bacteria. However, the chelants had differing inhibitory effects on different species, even between those with similar cell wall architectures. The presence of the Gram-negative outer membrane did not always provide enhanced protection against chelating agents, although *E. coli* and *P. aeruginosa* were more resistant to CHL, FA and TRO than the two Gram-positives (Fig. 4.2; Table 4.1). However, *B. subtilis* and *S. aureus* were more resistant to CHA than the two Gram-negatives. In addition, *B. subtilis* shows greater tolerance of DTPMP than *P. aeruginosa*, while *S. aureus* proved more resistant to HNK than *E. coli* (Fig. 4.2; Table 4.1). *E. coli* has >10-fold resistance to EDTA relative to *P. aeruginosa* (Fig. 4.2D) despite both genera sharing inner and outer membranes. The results highlight differences in susceptibility of bacteria that should be taken into account when considering chelants for applications where growth inhibition is desirable. They also indicate that bacteria differ in how they tolerate metal restriction mediated by chelants; this may be affected by the particular cell wall composition and

architecture of the species involved and the functionality of their metal acquisition and regulatory systems. The chelants generally exhibit bacteriostatic activity, although at high concentrations killing is observed indicating that metal starvation, possibly combined with membrane damage, is bactericidal. Three of the chelants added to the study in this chapter, CHL, HNK and TRO, showed promising bactericidal activity and efficacy at relatively low concentrations.

4.5.2 Antibacterial activity of chelant-chelant combinations

Pairwise comparisons of bacterial growth inhibition with seven chelants were conducted with *P. aeruginosa* using checkerboard assays. Of the 15 pairings tested, 12 were synergistic using an individual FIC index calculation method (Fig. 4.3C), but only six with the mean FICI method; no antagonistic pairings were found. Combinations of EDTA and DTPMP with other chelants proved the most effective at restricting bacterial growth and thus represent promising candidates for inclusion together to enhance antibacterial hostility. The structurally-related pair of HNK and TRO did show indifference with each other and only differed in their interaction with FA, consistent with them sharing a similar mode of action. Broadly similar results were obtained in checkerboards using CHA, DTPMP and EDTA with *P. aeruginosa* compared with the results shown in Chapter 3 with *E. coli* (Fig. 3.3). The CHA-DTPMP and CHA-EDTA pairs were synergistic in both species, however, in *E. coli* the DTPMP-EDTA pair was indifferent, whereas in *P. aeruginosa* this combination was synergistic. This difference suggests that the chelants may act differently when combined against these two Gram-negatives. In general, it appears that chelants frequently prove synergistic when combined, although predicting which combinations will be most effective based solely on their structures remains challenging.

4.5.3 Antibacterial activity of chelant-antibiotic combinations

Previous studies have shown that chelating agents can potentiate the antibacterial activity of different antibiotics against Gram-negative bacteria (Brown & Richards,

1965; Chan et al., 2020; Parquet et al., 2018; Vinuesa & McConnell, 2021; Weiser et al., 1968). This effect is thought to arise by disruption of the outer membrane by the chelant, allowing hydrophobic antibiotics greater access to their intracellular targets (Delcour, 2009; Miller, 2016). Synergistic chelant-antibiotic pairings offer considerable therapeutic potential against intransigent Gram-negative bacteria, for instance, in the treatment of *Pseudomonas* wound infections.

Six antibiotics were selected for use in combinations with EDTA and DTPMP against the four bacterial species (Fig. 4.5). These antibiotics correspond to four distinct classes; one β-lactam, one amphenicol, three aminoglycosides, and one tetracycline (Abushaheen et al., 2020). β-lactams disrupt formation of the cell wall through covalent binding to penicillin-binding proteins (PBPs) which are essential in the final stages of cell wall synthesis; cross-linking peptidoglycan in both Gram-positive and Gram-negative bacteria (Bush & Bradford, 2016). The inhibition of bacterial peptidoglycan transpeptidation by penicillin is due to the structural similarity of this antibiotic with the terminal D-Ala-D-Ala dipeptide of nascent peptidoglycan (Tipper & Strominger, 1965; Tooke et al., 2019). The β-lactam ring then interacts with the nucleophilic serine active site within the PBP, leading to opening of the ring and irreversible acylation of the PBP, thus preventing formation transpeptide cross-links between the glycan chains (Tooke et al., 2019). Some β-lactams such as ceftaroline can bind allosteric sites within *S. aureus* PBP2a, resulting in heightened sensitivity of this species to this antibiotic (Tooke et al., 2019). Ampicillin is an aminopenicillin which displays antibacterial action against both Gram-positive and Gram-negative species due to the presence of a positively charged amino group which allows it to pass through porins in the outer membrane of Gram-negative species (Tooke et al., 2019).

Amphenicols inhibit protein synthesis by binding to the bacterial ribosome, thereby inhibiting protein synthesis. Chloramphenicol inhibits the formation of peptide bonds by preventing the aminoacyl-tRNA 3′ end of an elongating protein chain from binding

to the peptidyl transferase centre within the 50S ribosomal subunit (Siibak et al., 2009). Chloramphenicol has several reactive groups that can form hydrogen bonds with various nucleotides of the peptidyl transferase cavity (Schlünzen et al., 2001). The interactions of chloramphenicol with the peptidyl transferase active site within the ribosome are thought to be stabilised by Mg^{2+} ions, highlighting the importance of metal homeostasis in the mode of action of this antibiotic (Schlünzen et al., 2001).

Aminoglycosides and tetracyclines are capable of inhibiting bacterial growth by binding the 30S ribosomal subunit, halting protein synthesis in a manner similar to that of amphenicols (Chopra & Roberts, 2001; Krause et al., 2016). Aminoglycoside antibiotics bind to the 16S rRNA component of the 30S subunit of the bacterial ribosome, causing misincorporation of amino acids into elongating peptide chains (Kohanski et al., 2010; Krause et al., 2016). In contrast to amphenicols which are broadly bacteriostatic, aminoglycosides often display bactericidal effects through production of misfolded proteins which are incorporated in the envelope, increasing cell permeability and thereby increasing drug uptake (Kohanski et al., 2010). For this reason, aminoglycosides have been shown to be broadly synergistic with other antibiotics (Krause et al., 2016). The core structure of aminoglycosides can be altered through addition of various amino and hydroxyl substitutions which will alter both the mechanism of action and the susceptibility of the resultant antibiotic to aminoglycoside-modifying enzymes (Krause et al., 2016; Ramirez & Tolmasky, 2010). Aminoglycosides enter the cell through a multi-step process, the first stage of which involves binding of the polycationic aminoglycoside to negatively charged components of the cell membrane such as phospholipids, lipopolysaccharides, and teichoic acids, followed by removal of stabilising Mg^{2+} ions (Krause et al., 2016; Ramirez & Tolmasky, 2010), once again highlighting the role of metals in antibiotic susceptibility. Tetracyclines are also capable of inhibiting bacterial protein synthesis through inhibition of the association of aminoacyl-tRNA with the bacterial ribosome (Chopra & Roberts, 2001). In order to traverse the cell membrane, negatively charged

tetracycline must first associate with positively charged ions to overcome the repulsion of the negatively charged cell wall (Chopra et al., 1992). It is thought that tetracycline forms cationic coordination complexes with magnesium in order to pass through OmpC and OmpF porins in the Gram-negative outer membrane (Chopra & Roberts, 2001). Association of tetracyclines with the bacterial ribosome is reversible, explaining the bacteriostatic nature of these antibiotics (Chopra et al., 1992).

Of the 48 chelant-antibiotic pairings tested, 33 synergistic and 15 indifferent combinations were identified using individual FIC indices (Fig. 4.5A). As expected, given differences in cell wall structure, the Gram-negatives and Gram-positives displayed different patterns of synergy and indifference. Similar results were also obtained between the Gram-negative *E. coli* and *P. aeruginosa*, whereas *B. subtilis* and *S. aureus* diverged in how they were affected by mixtures of chelant and antibiotic (Fig. 4.5A).

The synergistic effects fit with chelants promoting intracellular antibiotic uptake, although precisely how that occurs is unclear. EDTA is known to damage the outer membrane of Gram-negative bacteria, possibly by removal of stabilising calcium and magnesium, increasing permeability to hydrophobic compounds such as antibiotics (Alakomi et al., 2006; Leive, 1965b; Vaara, 1992). Our experiments examining the effect of chelants on uptake of the hydrophobic, fluorescent NPN support the involvement of EDTA in increasing membrane permeability in *E. coli, S. marcescens* and *P. aeruginosa* (Fig. 4.6). Moreover, DTPA appears to behave in a similar way to EDTA, consistent with their related aminocarboxylate structures (see Chapter 3), although the other chelants could not be assigned a comparable function. Bacteria with deficiencies in the biosynthesis of lipopolysaccharides show elevated susceptibility to antibiotics of multiple different classes including ampicillin, chloramphenicol and spectinomycin (Lambert et al., 2004; Nichols et al., 2011). EDTA is known to potentiate the activity of penicillin G, ampicillin, tetracycline and chloramphenicol against *P. aeruginosa* (Lambert et al., 2004; Weiser et al., 1968), in

keeping with the results described here. Examination of the inhibition profile for EDTA against *P. aeruginosa* revealed a biphasic response (Lambert et al., 2004), which suggests a dual antibacterial mechanism of action – potentially metal starvation by chelation from the medium coupled with outer membrane damage, which may require higher concentrations of the chelant. Because of this nonlinear concentration-dependent inhibition by EDTA, Lambert & Lambert (2003) advise caution when interpreting synergistic interactions in checkerboard analyses with EDTA and antibiotics. They argue that the ΣFIC method is only applicable to mixtures of antimicrobials which individually have similar dose-response curves (Lambert & Lambert, 2003). For mixtures of antimicrobials which display significantly different dose responses, the ΣFIC method may produce synergy or antagonism for substances which may actually confer indifferent physiological responses. However, in the absence of other high-throughput methods for testing and analysis, the ΣFIC method was applied here for chelant-antibiotic pairings, with the caveat that further investigations are appropriate when attempting to assign genuine combinatorial effects.

Interestingly, there was evidence of antagonism in pairings of DTPMP with each of the aminoglycoside antibiotics, kanamycin, spectinomycin and streptomycin with the two Gram-negative species (Fig. 4.4 and 4.5). It is possible that DTPMP blocks association of the antibiotic with the outer membrane or forms complexes with the antibiotic to prevent it from entering the cell. The ferrichrome importer, FhuA, is linked with aminoglycoside uptake (Braun et al., 2001; Volkmar Braun, 1999) and mutations in FhuA are found in strains showing aminoglycoside resistance (Ibacache-Quiroga et al., 2018). Stripping of iron from the antibiotic by DTPMP could potentially prevent aminoglycoside uptake by that route. Alternatively, and perhaps more likely, is that the chelant removes metals such as magnesium, from the outer membrane to restrict aminoglycoside uptake. The aminoglycosides streptomycin and gentamycin are known to utilise metals at the outer membrane to facilitate their intracellular uptake in

P. aeruginosa (Hancock et al., 1981). Aminoglycoside and EDTA resistance can be conferred by increased expression of the outer membrane protein H1 related to levels of metals and their impact on cell envelope charge (Hancock, 1984; Nicas & Hancock, 1980). While EDTA shows synergism with the aminoglycosides (Fig. 4.5A), potentially through combined effects that enhance outer membrane permeability (Hancock, 1984), DTPMP may remove metals required for aminoglycoside penetration, thus explaining the observed antagonism in checkerboard assays.

Although no antagonism was observed between either chelant with tetracycline, this antibiotic is itself known to be a chelating agent, and its antibacterial and pharmacokinetic properties are influenced by chelation of metals (Guerra et al., 2016). Tetracycline appears to traverse the outer membrane of Gram-negative bacteria *via* the OmpF and OmpC porin channels (Ian Chopra & Roberts, 2001; Guerra et al., 2016). Transport requires the antibiotic to acquire an overall positive charge, so it is hypothesised that binding metal cations allows uptake of tetracycline coordination complexes (Ian Chopra & Roberts, 2001). Metal binding by some of the other antibiotics, such as ampicillin (El-Gamel, 2010) and kanamycin (Szczepanik et al., 2004), could also be potentially affected by chelation in antibiotic-chelant pairings (Krause et al., 2016; Ramirez & Tolmasky, 2010).

4.5.4 Impact of chelating agents on total cellular metal concentration

Exposure of *E. coli* to chelating agents produces distinct changes in the levels of specific metal ions in the cell (Paterson et al., 2022). Evaluation of the three chelants studied previously with *E. coli* revealed that CHA and EDTA yielded similar effects in *P. aeruginosa*, whereas DTPMP behaved differently suggesting that cellular responses to metal starvation may not be identical between these two Gram-negatives or that structural variations in outer membrane composition influence chelant action. A diversity of effects on metal composition were also noted with the three additional chelants, FA, HNK and TRO. FA caused reduced iron and

manganese levels, HNK elevated iron concentrations and TRO affected a range of different metals, notably decreasing calcium, iron, magnesium and manganese (Fig. 4.7). The effects of FA, HNK and TRO on cellular metal concentrations expand the diversity of effects observed, although it remains unclear how these effects are implemented. In terms of mode of action, it seems likely that chelants are removing metals from the bacterial cell surface as well as from the growth medium. Chelants, such as DTPA and EDTA, clearly also affect membrane permeability and this is an additional factor to consider when evaluating the antibacterial effect of the other chelants. Knowledge of which metals are primarily impacted by specific chelant treatment, combined with information derived from MIC and checkerboard assays (Figures 4.2 and 4.3) should help identify pairings of chelants that act synergistically to enhance antibacterial efficacy. The capacity of chelants to enhance the antibacterial effects of conventional antibiotics is also encouraging. Chelants could be harnessed as potentiators in combination with antibiotics for the treatment of drug-resistant bacterial infections. The focus on *P. aeruginosa* here has been informative in confirming that chelant-chelant and chelant-antibiotic mixtures exhibit potential for therapeutic applications in skin infections (Allan et al., 2020; Parquet et al., 2018).

4.6 Future work

This chapter analysed the effect of chelating agents and chelant-antibiotic combinations on the growth of four bacterial species as representative Gram-positives and Gram-negatives. Chelant-chelant combinations were only tested against *P. aeruginosa*, hence examination of the other three species may be informative in establishing chelant efficacy as broad-spectrum antibacterials. Bactericidal and bacteriostatic effects were examined for three out of the four species but further work on this aspect is merited. The impact of each chelant on total cellular metal content was only investigated with *P. aeruginosa*. Exploring the effect of chelants on cellular metal content in Gram-positive species is a priority since this

group has been overlooked in previous studies. It will be of interest to see whether iron, manganese and zinc are the key metals needed by Gram-positives, as has been found to be the case with *E. coli* and *P. aeruginosa*. If potent chelant-chelant or chelant-antibiotic pairings are identified then it may be of value to assess their antibacterial effect on a wider range of bacterial species that are problematic in consumer products as well as human infections. This could be taken forward by evaluating efficacy in treatment of *in vivo* skin infection models and wound healing models in mice or other animal systems.

With the majority of chelants examined, the NPN assay was unable to determine whether they had the capacity to penetrate the *P. aeruginosa* outer membrane, possibly due to quenching of fluorescence by chelant-NPN association or prevention of NPN uptake at the cell surface. Other dyes could be employed to evaluate disruption of membrane integrity by chelants, such as propidium iodide or SYTOX Green which fluoresce upon binding to nucleic acids when membrane integrity is compromised (Clementi et al., 2014; Santoscoy & Jarboe, 2019). Fluorescently-tagged chelants may allow tracking of chelant location in or outside the cell, although such modifications are likely to adversely affect metal affinity. Radioisotopic labelling of metals could also be used to monitor their location within the cell (Clementi et al., 2014). Fluorescent probes have been designed which bind to specific metal ions to reveal their intracellular locations without causing damage to the cell. Metals for which probes have been designed include Zn^{2+},Cu^{+}/Cu^{2+}, Fe^{2+}/Fe^{3+}, Mg^{2+}, and Ni^{2+}, though affinity of these probes is not always high enough to provide accurate measurements, and some non-specific binding to other metals may occur (Dean et al., 2012).

5 Isolation and characterisation of *E. coli* chelant-resistant mutants

5.1 Introduction

Chapters 3 and 4 explored the efficacy and antibacterial mode of action of different chelating agents against four different bacterial species. To gain further insight into the cellular targets or secondary effects of chelating agents, we attempted to isolate mutants of *E. coli* and *S. aureus* as representative Gram-negative and Gram-positive bacteria. The isolation and characterisation of these mutants in *E. coli* are presented in this chapter and those from *S. aureus* in the following chapter. Bacteria were cultivated for 15 and 29 days at sub-MIC levels of either EDTA or DTPMP. These chelants were selected because of their differential effects on *E. coli* cellular metal content. EDTA primarily depletes cells of manganese with lesser reductions in iron and zinc, while DTPMP deprives *E. coli* of iron resulting in an influx of manganese (Paterson et al., 2022). Both chelants have high affinities for metals, especially Fe^{3+} in solution (García-Casal et al., 2004) and EDTA is known to have secondary effects on membrane permeability in Gram-negatives (Alakomi et al., 2003; Brown & Richards, 1965; Leive, 1974). The well-characterised K-12 laboratory strain of *E. coli* was chosen because its genome sequence is known (Blattner et al., 1997), and because of the availability of the Keio collection, a single-gene knock-out library (Baba et al., 2006), which allows genes or cellular pathways to be investigated by studying mutant susceptibility to chelants. This chapter details the isolation of *E. coli* chelant-resistant mutants through prolonged sub-lethal exposure to either EDTA or DTPMP, subsequent sequencing of these mutants to identify any heritable changes that have arisen and further investigations into the genes implicated in their resistant phenotype. The experiments testing additional chelants in this chapter were

performed by Lydia Newton as part of her final year MSci project in Natural Sciences and genome sequencing analysis was conducted by Ping Hu (P&G, Cincinnati).

5.2 Isolation and characterisation of *E. coli* chelant-resistant mutants

5.2.1 Isolation of chelant-resistant mutants by experimental evolution

E. coli K12 (BW25113; CGSC7636) was cultivated in the presence of sub-MIC levels of either EDTA or DTPMP for a period of 29 days. Bacteria were initially cultivated in microcentrifuge tubes with daily subculture in either 4 mM EDTA or 1 mM DTPMP (Fig. 5.1A). After 15 days, cultures were purified to single colonies on agar plates, and a single colony of each stored as a frozen stock. Subculturing was continued in microtitre plates, allowing the bacterial population to be exposed to additional higher concentrations of each chelant. After 29 days, these cultures were also recovered and single colonies purified and retained (Fig. 5.1A). Note that Day 15 isolates are not necessarily the direct ancestors of Day 29 cells as single colonies were obtained from a mixed population. Selected strains recovered at 15 and 29 days were tested for resistance to EDTA and DTPMP (Fig. 5.1B and 5.1C).

The three strains isolated at low levels of EDTA (JN161, JN188 and JN192) all showed improved resistance to this chelating agent when compared to the parent strain (Fig. 5.1B). This superior tolerance was readily apparent at higher concentrations of EDTA (8-32 mM), especially with the two strains cultivated for 29 days. In contrast, the DTPMP exposed strains JN165, JN196 and JN198 failed to acquire resistance (Fig. 5.1C), although in some experiments JN165 and JN198 did show improved growth at low DTPMP concentrations (data not shown). None of the EDTA-resistant strains developed tolerance to DTPMP and similarly all of the strains isolated against DTPMP showed susceptibility to EDTA equivalent to the wild-type (Fig. 5.1B and 5.1C).

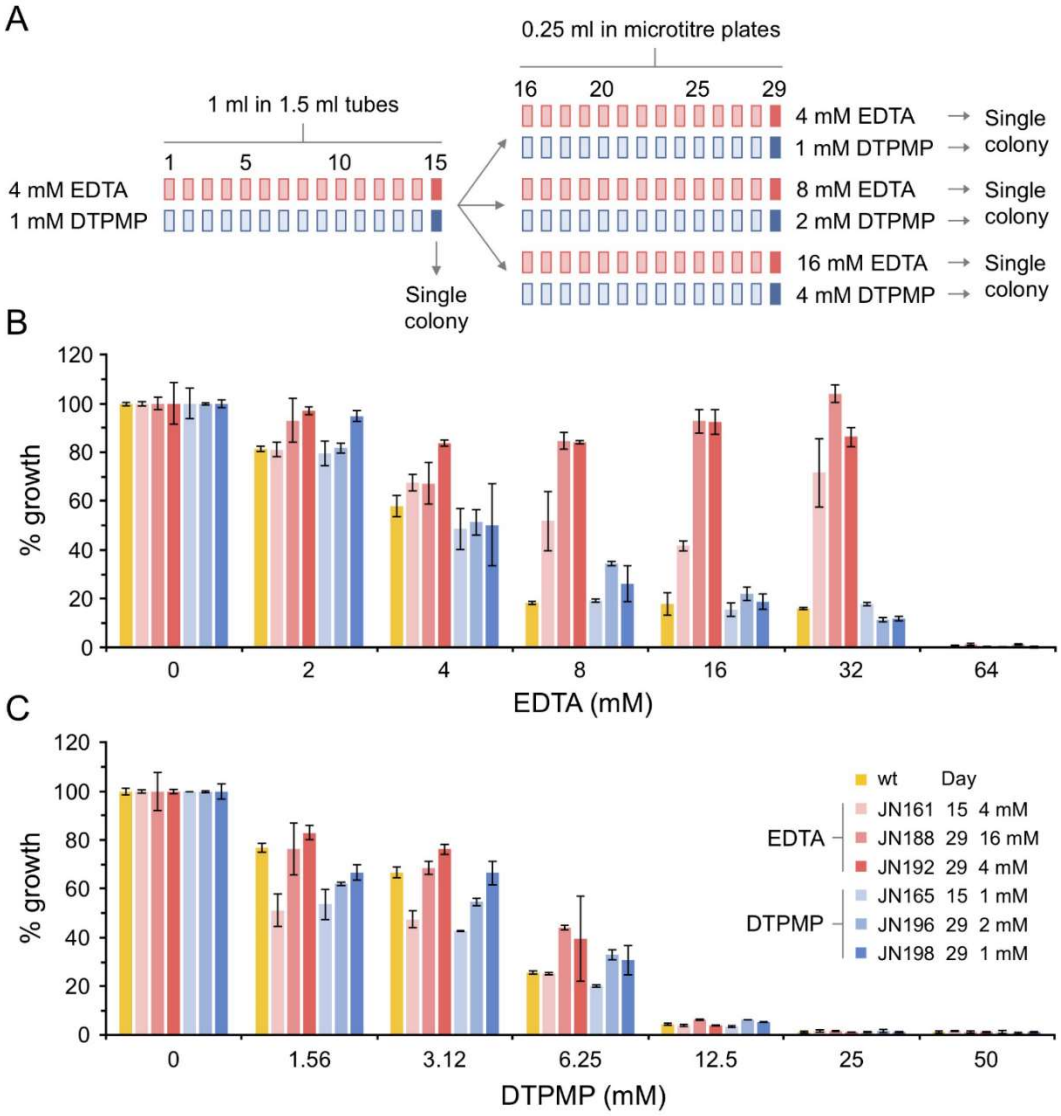

Figure 5.1 Isolation of *E. coli* chelant-resistant mutants. (A) *E. coli* (BW25113) mutants that tolerate either EDTA or DTPMP were obtained by repeated subculture for 15 and 29 days at sub-MIC levels of each chelant. Susceptibility of wild-type and mutant strains to EDTA (B) or DTPMP (C) was examined. Two-fold serial dilutions of each chelant were mixed with each strain and incubated at 37°C with shaking at 150 rpm for 16 h. Growth was measured at $A_{600\,nm}$ at the end point and normalised against controls without chelant to give the percentage growth. Mutants selected against EDTA are shown in shades of pink, while those exposed to DTPMP are in blue. Results represent the mean and standard deviation of an experiment performed in triplicate. Two additional independent repeats produced similar results.

5.2.2 Colony morphology and growth of chelant-resistant mutants

The colony morphology of the *E. coli* strains selected against EDTA and DTPMP was examined. In most cases, there were no marked differences in the colonial

appearance of these strains relative to the parental wild-type , however, large and small colony variants were noted with the three EDTA-resistant strains: JN161, JN188 and JN192 (Fig. 5.2). This feature was most obvious with JN188 (Fig. 5.2H), which was isolated against the highest concentration of EDTA (16 mM). Large and small colonies from these strains streaked onto fresh LB agar plates produced both size variants. This phenomenon is reminiscent of the phenotype resulting from phase variation of surface-exposed antigen 43 and type I fimbria (Hasman et al., 2000). Subsequent sequencing of chelant-resistant strains did provide some indication that the presence or absence of type I fimbriation is responsible for the observed phenotype (see Section 5.3).

The growth of the six chelant-resistant strains was also examined in LB broth without chelant addition (Fig. 5.3). All of the strains, regardless of whether they were isolated against EDTA or DTPMP, displayed a similar slow growth phenotype with a prolonged exponential phase, much slower than the wild-type. The two strains isolated after 15 days (JN161 and JN165) showed slightly faster growth than those obtained after 29 days (Fig. 5.3). Interestingly, this delayed growth phenotype was not evident on solid media (Fig. 5.2).

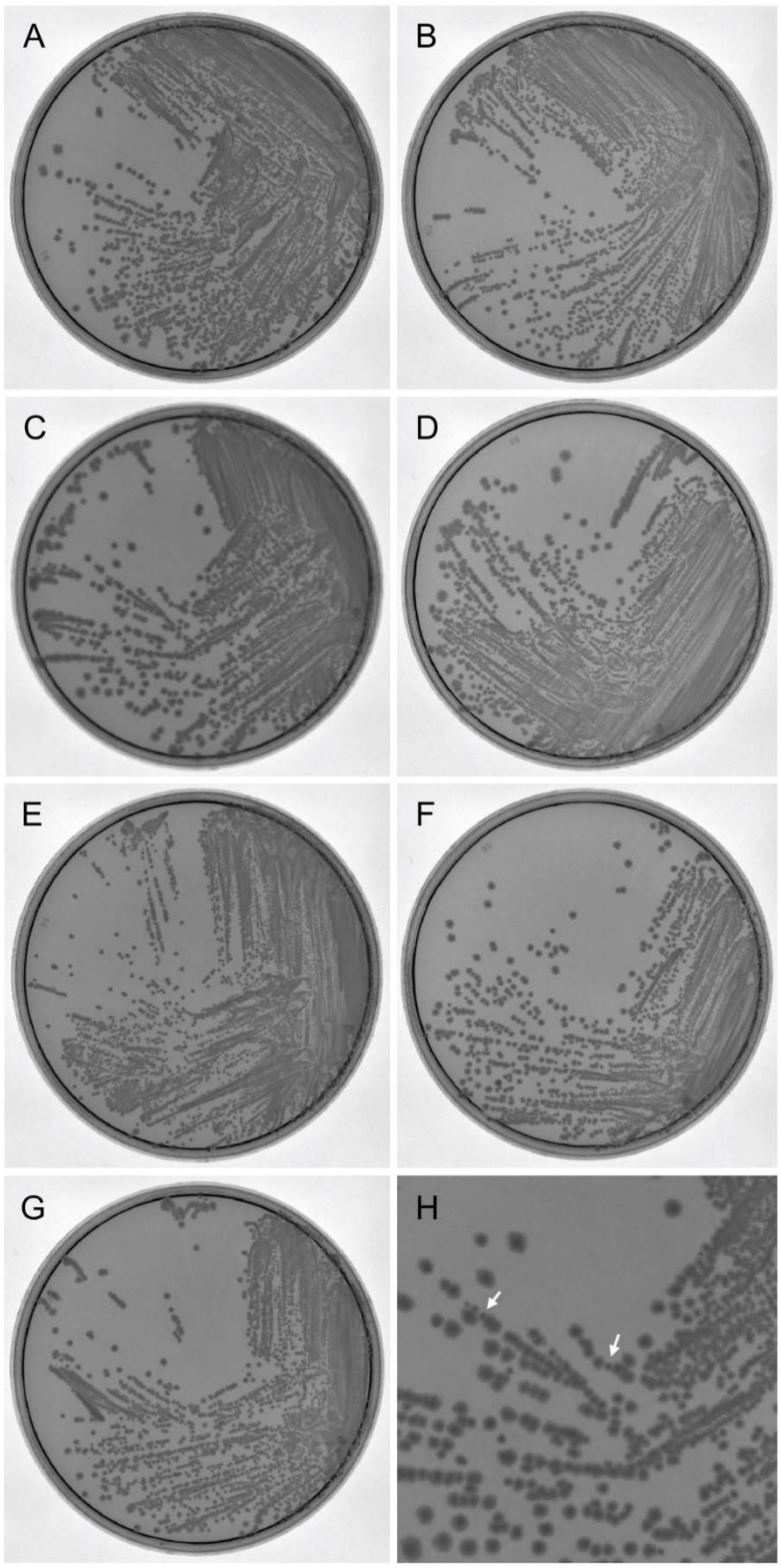

Figure 5.2 Colony morphology of *E. coli* chelant-resistant mutants. Isolated strains were streaked and grown on LB agar at 30°C for 16 hours prior to imaging. BW25113 wild-type (A), JN161 (B), JN188 (C), JN192 (D), JN165 (E), JN196 (F) and JN198 (G). A close-up of JN188 colony morphology is included to highlight the large and small colony variants (H). Two of the small colony types are indicated by arrows.

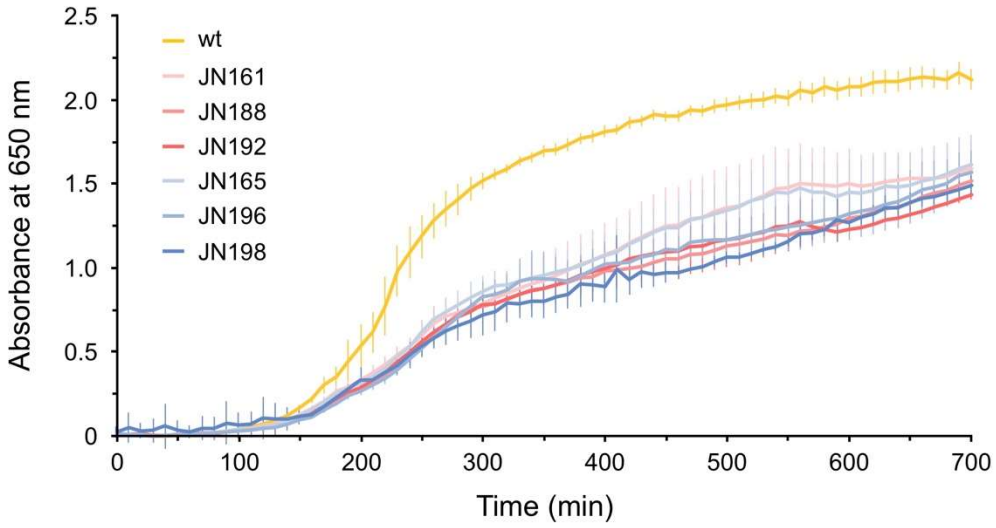

Figure 5.3 Growth curves of *E. coli* chelant-resistant mutants. Strains were cultivated in LB broth at 37°C and absorbance monitored at $A_{650\ nm}$. Those isolated in the presence of EDTA (JN161, JN188 and JN192) are highlighted in pink, while those isolated in the presence of DTPMP (JN165, JN196, JN198) are in blue. The results are the mean and standard deviation of a single experiment performed in triplicate.

5.2.3 Susceptibility of EDTA and DTPMP chelant resistant mutants to other chelants

To assess whether the strains exposed to EDTA and DTPMP had acquired tolerance to additional chemically-unrelated chelants, the strains were mixed with 2-fold serial dilutions of six of the chelants introduced in Chapters 3 and 4. The results of the wild-type and mutant strains exposed to CHA, DTPA, FA, HNK, PO and TRO are shown in Figure 5.4. With CHA, JN188 showed a slightly increased susceptibility, while the remainder of the mutants behaved like the wild-type (Fig. 5.4A). At low concentrations of DTPA (0.5-1 mM) the EDTA-resistant strains grew less well than the wild-type (Fig. 5.4B). In contrast, the DTPMP-selected mutants were sensitive at all DTPA concentrations; in fact, JN196 and JN198 showed an 8-fold lower MIC than the wild-type (Fig. 5.4B). The mutant strains behaved much like the wild-type against FA (Fig. 5.4C) and PO (Fig. 5.4E) with, minor variations. Significantly, the two Day 29 EDTA-resistant strains, JN188 and JN192, showed improved resistance to HNK (Fig. 5.4D) and TRO (Fig. 5.4F) producing a similar dose response. The results suggest that the

mutant strains carry genetic changes that can promote resistance to some chelants but increase the susceptibility to others, in keeping with different mechanisms of chelant action.

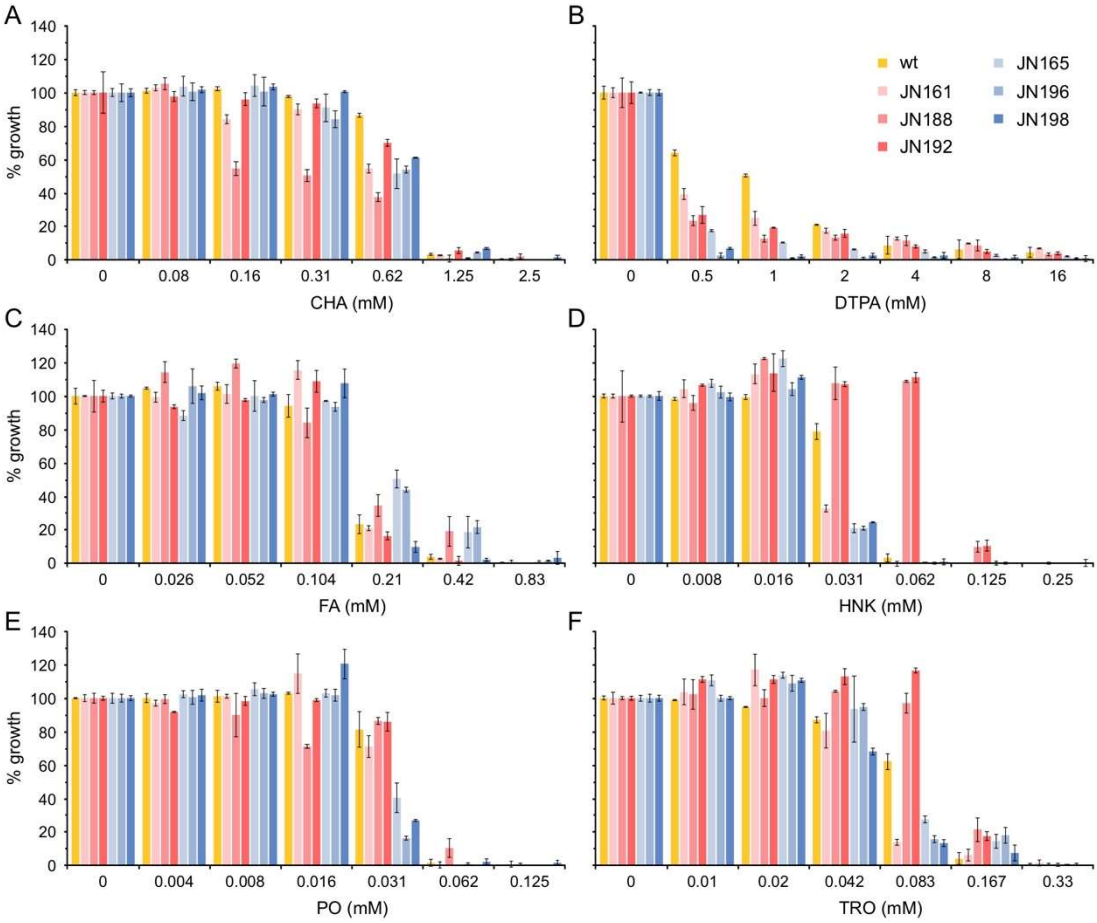

Figure 5.4 Susceptibility of *E. coli* chelant-resistant mutants to CHA, DTPA, FA, HNK, PO and TRO. Sensitivity of wild-type and mutant strains to CHA (A), DTPA (B), FA (C), HNK (D), PO (E) and TRO (F) was examined using two-fold serial dilutions of each chelant which were mixed with each strain and incubated at 37°C with shaking at 150 rpm for 16 h. Growth was measured at $A_{600\,nm}$ at the end point and normalised against controls without chelant to give the percentage growth. Mutants selected against EDTA are shown in shades of pink, while those exposed to DTPMP are in blue. Results represent the mean and standard deviation of an experiment performed in triplicate. An additional independent repeat performed in triplicate produced similar results. These experiments were performed by Lydia Newton as part of her final year MSci project in Natural Sciences.

5.3 Identification of mutations in chelant-resistant strains

To identify mutations responsible for the improved tolerance of *E. coli* to EDTA, the genome sequence of each strain, including the BW25113 parent strain and the chelant-selected strains, was determined using an Illumina MiSeq platform with 30 times coverage by MicrobesNG. An annotation pipeline was devised and differences between the parent and mutants identified by Ping Hu at P&G. The mutations found are summarised in Figure 5.5. Significantly, two of the mutations are associated with genes affecting iron (*fepA-entD*) and zinc (*yeiR*) homeostasis consistent with improved survival following exposure to EDTA. A number of membrane bound or exported proteins (*cadC, ydbA, yahJ*) and a variety of cytosolic enzymes were also identified (Fig. 5.5). Several of the changes are amino acid substitutions which may affect protein functionality, while others lie upstream of genes and may alter levels of transcription.

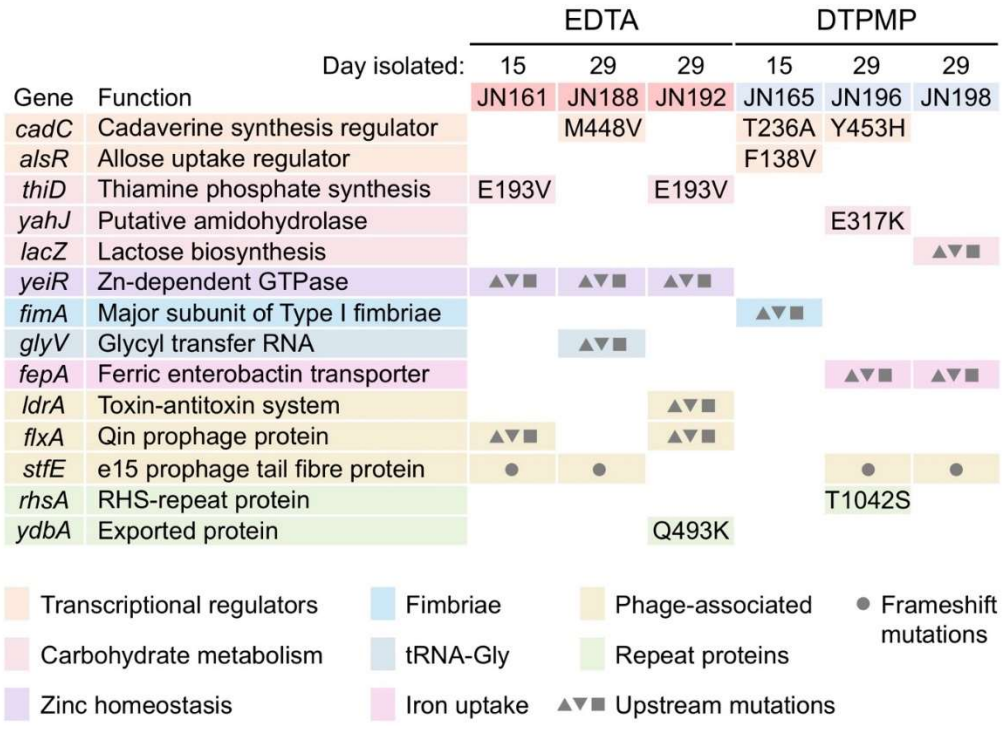

Figure 5.5 Mutations identified by genome sequencing of six *E. coli* chelant-resistant mutants. The genes affected are grouped according to function and specific mutations listed for each strain. Missense mutations that change amino acid sequences of the gene product are shown. JN192 *ydbA* also has an Ile485Met

substitution. Gene *stfE* carries several different frameshift mutations as indicated by the circle symbol. Base changes upstream of genes are indicated by triangular and square symbols reflecting potential upregulation, downregulation or no effect on adjacent gene expression. Synonymous changes affecting *gcvT* (x1), *rhsA* (x4) and *ydbA* (x7) are not listed.

None of the mutations were found in every strain, although those upstream of *yeiR* were present in all EDTA-resistant isolates (Fig. 5.5). The diversity of mutations suggests that there may be different pathways to chelant resistance in these strains and perhaps the mutations act collectively to confer tolerance. It is likely that identical mutations arose early in the period of cultivation and were inherited by subsequent generations. The most promising candidates for a role in chelant resistance included an acid tolerance regulator (*cadC*), a zinc-dependent GTPase (*yeiR*) and genes involved in iron uptake (*fepA*-*entD*). Substitution mutations affecting gene products are described first, followed by several genes that may be upregulated to aid chelant resistance.

AlsR (RpiR) is a transcriptional repressor of the D-allose uptake and catabolism regulon. Although the AlsR Phe138Val mutation found in JN165 occurs in the SIS sugar isomerase domain (Bateman, 1999), this portion of the domain is not especially well conserved. The ThiD Asp193Val substitution in JN161 and JN192 is conserved and lies on the surface of the hydroxymethylpyrimidine (HMP) kinase (Cheng et al., 2002) involved in thiamine biosynthesis; this residue is not located near the HMP binding site or dimer interface but its mutation could potentially affect the arrangement of residues required for ATP binding (Appendix, Fig. 9.3; Cheng et al., 2002; Nodwell et al., 2014). JN196 is the only strain to carry a Glu317Lys substitution in YahJ, an uncharacterised metal-dependent amidohydrolase that appears to possess a signal sequence for export. The amino acid substitutions in RhsA (Thr1042Ser) and YdbA (Asn493Lys and Ile485Met) are found in JN196 and JN192, respectively, alongside multiple synonymous changes that are likely due to frequent genetic rearrangements

between the repeated sequences characteristic of these two proteins (Fig. 5.5). The *stfE* gene, encoding an uncharacterised phage tail fibre protein, carries multiple frameshift mutations in four out of six chelant-resistant strains that are likely to inactivate the gene. However, it is unlikely that loss of StfE function nor any of the other substitutions listed above are primary factors in chelant tolerance, although they may help in combination with the other changes present in each mutant. The three amino acid substitutions in CadC will be discussed later.

Upstream mutations were found in all of the strains that could potentially amplify gene expression levels to help alleviate chelant toxicity. The genetic changes upstream of *fimA* in JN165 are a consequence of site-specific flipping of the 314 bp invertible segment responsible for type I fimbrial gene phase variation (Abraham et al., 1985; Hasman et al., 2000). In JN165, this inverts the orientation of the promoter to switch on expression of the entire *fim* operon (*fimAICDFGH*). Although JN165 was not one of the EDTA-resistant strains associated with colony size variation, it does highlight that genetic changes affecting the *fim* operon are a likely source of the colony size variants in these strains (Fig. 5.2). The mutations adjacent to *glyV*, *flxA* (downstream of the convergently transcribed *flxA* and *ydfW* phage genes), *ldrA* (also in a downstream region) and *lacZ* do not appear to affect any key transcriptional elements and are therefore unlikely to contribute to chelant tolerance. BW25113 has an insertion (∆*lacZ4787*) that disrupts the *lacZ* gene (Baba et al., 2006).

In contrast, two distinct mutations are located in the 5' leader mRNA of *yeiR* (Fig. 5.6A) in the EDTA-resistant strains that could be associated with chelant tolerance. JN161 and JN192 have an A-T mutation at +40 in the *yeiR* transcript, whereas JN188 has a C-T change at +43 (Fig. 5.6A). The fact that these two mutations have arisen independently supports the notion that this region contains important regulatory features that are altered beneficially for chelant resistance. The *E. coli yeiR* gene product is a Zn-dependent G3E (COG0523) family P-loop GTPase involved in zinc homeostasis (Blaby-Haas et al., 2012; Young et al., 2021). Moreover, Δ*yeiR* mutants

are hypersensitive to EDTA, especially when combined with a Δ*znuABC* mutant that lacks the zinc uptake machinery (Blaby-Haas et al., 2012). Increased expression of YeiR might therefore be expected to help these strains tolerate deprivation of zinc in the presence of low levels of EDTA. Similarly, upregulation of the *fepA-entD* operon, encoding components of the enterobactin pathway for iron import (Raymond et al., 2003), could potentially improve iron retrieval following DTPMP exposure in JN196 and JN198. The G-T transversion in the *fepA* promoter region occurs in the -10 sequence of the weaker of the two *fepA* promoters (Fig. 5.6B) and appears to produce a more favourable σ70 RNA polymerase binding site (5'-TAGAGT-3'). In Chapter 3, *fepA* mutants proved sensitive to both EDTA and DTPMP indicative of a requirement for ferric-enterobactin uptake in response to iron starvation (Fig. 3.7).

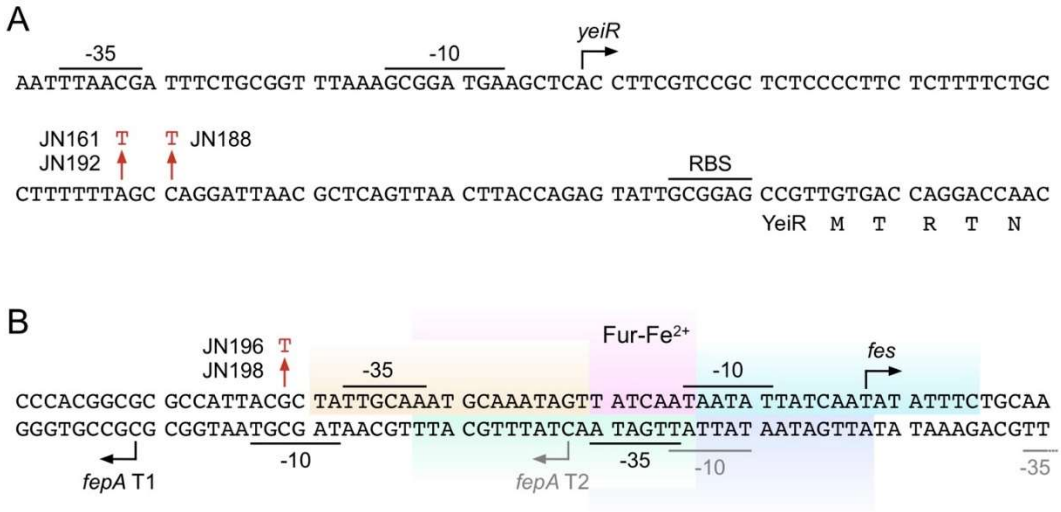

Figure 5.6 Location of upstream mutations in the *yeiR* and *fepA-entD* promoter regions. (A) The promoter region of *yeiR*. The -35 and -10 sites of the σF (σ28) promoter for *yeiR* with the transcript start site indicated by a rightward arrow. Single nucleotide substitutions found in JN161 and JN192 (A to T) and JN188 (C to T) are highlighted in red. The predicted ribosome binding site (RBS) and start of the *yeiR* gene are also shown. (B) The promoter region of the divergently transcribed *fepA-entD* and *fes-ybdZ-entF-fepE* operons. The -10 and -35 sites indicate the differently-orientated promoters for *fepA* and *fes.* Transcript start sites are indicated by arrows, including the minor (T1) and major (T2) transcripts for *fepA*; the latter signals distinguished in grey (Escolar et al., 1998; Hunt et al., 1994). Five overlapping binding sites for the Fur-Fe^{2+} repressor (Chen et al., 2007) are indicated by shaded areas in

different colours. The single nucleotide substitution (G to T) found in JN196 and JN198 is highlighted in red. Additional Fnr, H-NS and Crp binding sites are not shown.

5.3.1 Increased expression of *fepA* or *entD* may contribute to chelant tolerance

The upstream mutations identified in the screen for chelant-resistant mutants (Fig. 5.5) could be responsible for upregulation of adjacent gene expression. To investigate the possibility that increased production of specific gene products could confer chelant resistance, the *entD* and *fepA* genes were cloned in pET22b(+) which permits their controlled expression in appropriate strains. The wild-type versions of the genes for *thiD* and *yahJ* were also inserted in this vector for further characterisation of their effects, even though these two genes are associated with substitution mutations (Fig. 5.5). The mutation in ThiD was found in EDTA-resistant strains, whereas those affecting *entD*, *fepA* and *yahJ* were isolated from *E. coli* exposed to DTPMP. All four constructs along with the pET22b(+) vector control were introduced into the *E. coli* strain BL21-AI and their effects on EDTA and DTPMP resistance investigated (Fig. 5.7). Gene expression can be selectively induced by addition of arabinose and IPTG, which can be controlled by varying the concentration of these two inducers.

Levels of EDTA resistance were similar in all of the BL21-AI carrying each clone and the vector control in uninduced cells (Fig. 5.7A). In the same strains, expression of genes cloned in pET22b(+) were induced by addition of 0.5 mM and 0.1% arabinose (Fig. 5.7B). Under induced conditions, all of the cells grew relatively less well than the uninduced cultures after exposure to EDTA. BL21-AI carrying pYahJ was more sensitive to EDTA suggesting its product has some toxicity when expression levels are increased. However, pEntD and pFepA showed improved growth compared with the vector control consistent with higher expression of these two proteins helping in EDTA resistance, although there is some variability in the results with improvements mainly seen between 0.62 and 5 mM EDTA (Fig. 5.7B). A similar pattern was apparent with DTPMP, although the improvements with pEntD

and pFepA in induced conditions were even less marked (Fig. 5.7C and 5.7D). With DTPMP, the pYahJ construct produced the best growth at high chelant concentrations and does not show the toxicity evident in EDTA experiments (Fig. 5.7). No significant differences between pThiD and pET22b(+) were noted in uninduced or induced conditions with either chelant (Fig. 5.7).

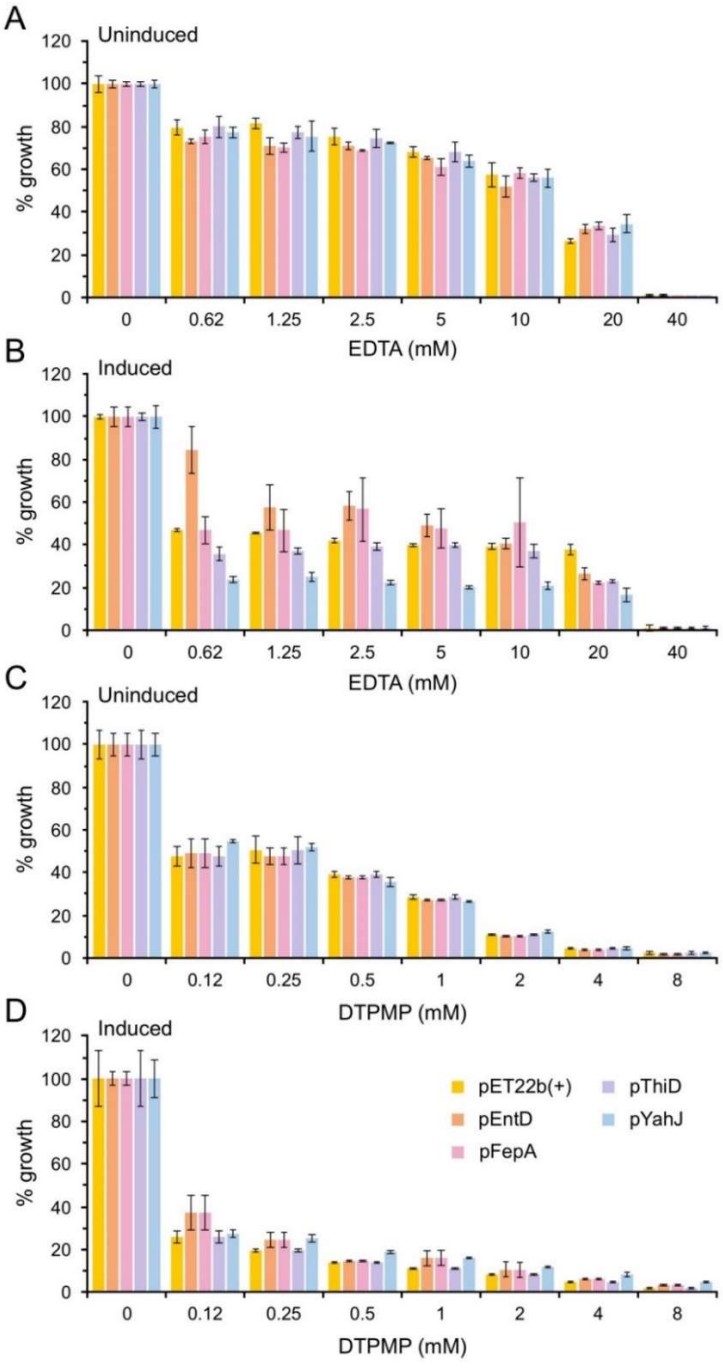

Figure 5.7 Effect of increased expression of EntD, FepA, ThiD and YahJ on EDTA and DTPMP resistance in *E. coli*. BL21-AI cells carrying wild-type *entD*, *fepA*,

thiD and *yahJ* genes inserted in pET22b(+) were assessed for susceptibility to EDTA (A and B) and DTPMP (C and D). pET22b(+) served as a negative control in conditions without induction of gene expression (A and C; labelled uninduced) and with addition of 0.5 mM IPTG and 0.1% arabinose to induce low-level gene expression (B and D, labelled induced). Two-fold serial dilutions of each chelant were mixed with each strain and incubated at 37°C with shaking at 150 rpm for 16 h. Growth was measured at $A_{600\ nm}$ at the end point and normalised against controls without chelant to give the percentage growth. Mutants selected against EDTA are shown in shades of pink, while those exposed to DTPMP are in blue. Results represent the mean and standard deviation of an experiment performed in triplicate. An additional independent repeat performed in triplicate produced similar results.

5.3.2 Mutations in CadC and their influence on chelant resistance

The three unique amino acid substitution mutations found in CadC were the most intriguing of the changes identified in the screen for resistant mutations against DTPMP and EDTA (Fig. 5.5). CadC is a sensor and regulator of acid stress that is bound to the inner membrane and has a periplasmic domain responsible for signalling low pH in association with LysP (Fig. 5.8A; Jung et al., 2018). Under non-inducing conditions, the lysine-specific transporter LysP inhibits CadC. When cells are exposed to low pH in the presence of lysine, the interaction between LysP and CadC is weakened, rendering CadC susceptible to protonation and capable of activating expression of the *cadBA* operon. *cadB* encodes a lysine/cadaverine antiporter and *cadA* a lysine decarboxylase that converts lysine to the more alkaline cadaverine to increase both intracellular and extracellular pH. The end-product of decarboxylation, cadaverine, exported to the periplasm by CadB acts in a feedback loop to deactivate CadC as a transcriptional activator of the *cadBA* operon (Fig. 5.8A; Küper & Jung, 2006).

The three CadC substitutions found in JN165, JN188 and JN196 appear to have occurred independently in these strains in response to either EDTA or DTPMP exposure (Fig. 5.5). Strikingly, the three mutations cluster in the C-terminal periplasmic domain of CadC at the interface between dimer subunits (Fig. 5.8B and

5.8C). Five negatively-charged residues in CadC located nearby along this surface (Fig. 5.8B and 5.8C) are essential for activation of CadC at low pH, most likely by protonation that reduces charge repulsion and allows the subunit association that triggers binding to the *cadBA* promoter inside the cell (Haneburger et al., 2011, 2012; Küper & Jung, 2006). Tyr453 (mutated to His in JN196) is essential for cadaverine-dependent inhibition of CadC (Haneburger et al., 2012). Substitution of Tyr453 with alanine, isoleucine or phenylalanine revealed that the aromatic character at this position is necessary for feedback inhibition by cadaverine. This highlights the possibility that the Tyr453His mutant, and potentially also the other two substitutions, produces a CadC that is not deactivated by cadaverine. Met448Val is also close to Glu447 and important for cadaverine binding within the central cavity of CadC (Haneburger et al., 2012). The presence of more activated CadC in chelant-resistant strains could help in tolerating EDTA or DTPMP, potentially *via* the increased production of the polyamine cadaverine which could directly or indirectly reduce chelant toxicity. Interestingly, mutations in CadC were also found in experimental evolution of *E. coli* exposed to the antibacterial agent triclosan (Leyn et al., 2021), although these mutations were not located at the subunit interface (Fig. 5.8B and 5.8C). It is possible that CadC is important more generally in cellular stress responses and modification of its activities promotes survival in response to various environmental stressors.

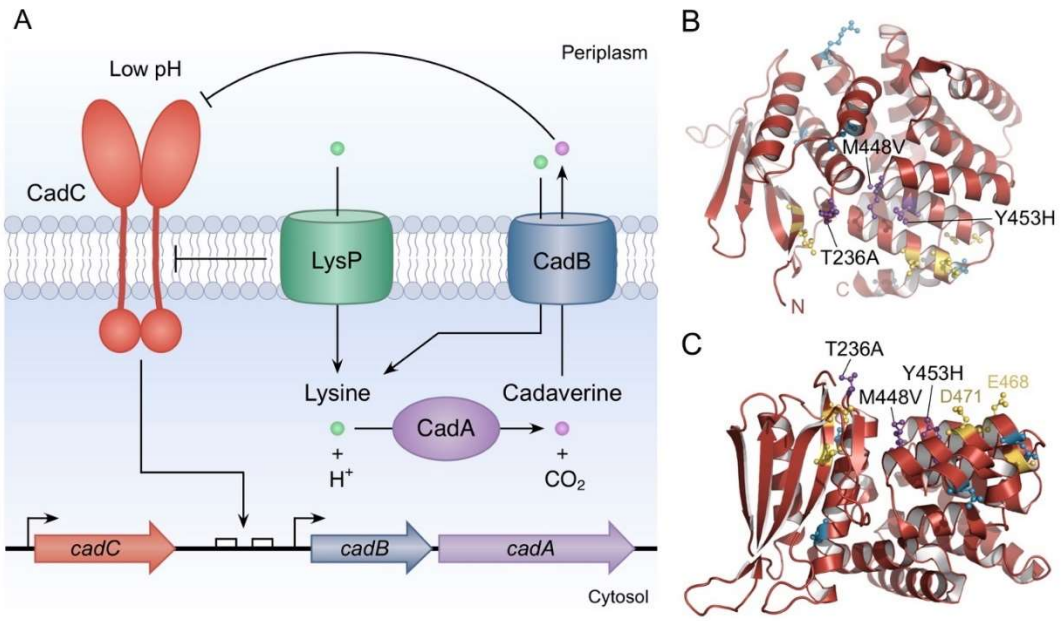

Figure 5.8 The CadCAB acid tolerance system and location of CadC mutants at the C-terminal periplasmic domain dimer interface. (A) In response to acid stress (pH <6.8) and in the presence of lysine, the CadC transcriptional activator induces the expression of the *cadBA* operon. *cadB* encodes a lysine/cadaverine antiporter and *cadA* a lysine decarboxylase, the latter combines lysine and a proton to generate the more alkaline cadaverine and carbon dioxide to increase the intracellular pH. CadB imports lysine to the cytosol and exports cadaverine to the periplasmic space where it helps increase the extracellular pH. LysP is a lysine-specific importer but is also a co-sensor and inhibitor of CadC. Exported cadaverine acts as a feedback inhibitor of CadC activation. The *cadC* gene is located immediately upstream of the *cadBA* operon and two CadC binding sites are located within the *cadBA* promoter. Adapted from Brameyer et al. (2019) and Jung et al. (2018). (B) and (C) Structure of the periplasmic domain of *E. coli* CadC (Protein Data Bank: 3LY7; Eichinger et al., 2011) highlighting mutated residues. The CadC monomer is orientated in (C) so that the dimer interface lies along the top surface of the protein. Residues mutated in chelant-resistant strains are highlighted in purple (Thr236Ala in JN165; Met448Val in JN188 and Tyr453His in JN196). Negatively charged residues at the dimer interface important in detection of low pH are coloured in yellow (Asp198, Asp200, Glu461, Glu468, and Asp471; Haneburger et al., 2011). Residues mutated after exposure to triclosan are highlighted in cyan (Ala220Thr, Met322Thr, Arg333Ser, Asn466Tyr and Asp506Glu; Leyn et al., 2021). Protein structures were generated in Pymol.

As with the clones described above, the wild-type *cadC* gene was inserted into pET22b(+) to facilitate an examination of effects on chelant resistance. The three substitution mutations were introduced in this construct by site-directed mutagenesis to give pCadC T236A, M448V and Y453H and these were examined alongside negative (pET22b(+)) and positive controls (pCadC wt). The BW25113 parent strain was transformed with each of the plasmids and these were assessed for sensitivity to both EDTA and DTPMP (Fig. 5.9). This strain lacks T7 RNA polymerase and so expression of the cloned genes depends on fortuitous expression, although this is more likely given the high copy number of the vector. There appeared to be some improved resistance to EDTA in the Y453H mutant over pCadC wt, T236A, M448V and pET22b(+) (Fig. 5.9A), although the differences were small. There was little difference between these constructs and the vector when tested against DTPMP (Fig. 5.9B). A Δ*cadC* mutant (JW4094) was transformed with these clones in case the wild-type chromosomal copy of *cadC* was masking the effect of the plasmid-encoded *cadC* mutants. However, no significant change in chelant resistance was found with the CadC mutants against EDTA or DTPMP (data not shown). Given that *cadC* mutations were only found in three of six chelant-selected strains (Fig. 5.5), it may be that additional mutations in these strains confer a greater effect on chelant tolerance and that the *cadC* changes provide only a supplementary benefit. Alternatively, the experiments performed were affected by the levels of CadC produced from the constructs used in chelant susceptibility assays with BW25113 and JW4094 (Δ*cadC*).

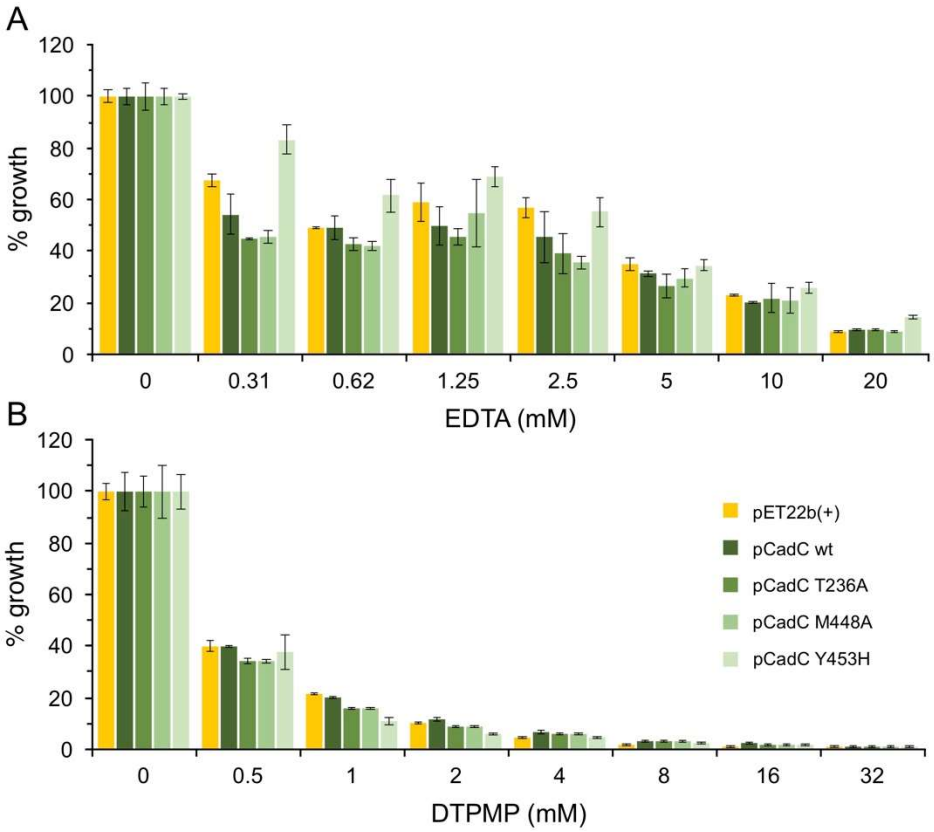

Figure 5.9 Effect of plasmids carrying CadC mutations on the susceptibility of *E. coli* to EDTA and DTPMP. BW25113 cells carrying wild-type and mutant *cadC* genes inserted in pET22b(+) were assessed for susceptibility to EDTA (A) and DTPMP (B). pET22b(+) served as a negative control. Two-fold serial dilutions of each chelant were mixed with each strain and incubated at 37°C with shaking at 150 rpm for 16 h. Growth was measured at $A_{600\ nm}$ at the end point and normalised against controls without chelant to give the percentage growth. Results represent the mean and standard deviation of an experiment performed in triplicate. An additional independent repeat performed in triplicate produced similar results.

5.4 Discussion and conclusions

After prolonged sub-lethal exposure to chelating agents, *E. coli* BW25113 acquired several mutations that reduced its susceptibility to EDTA, and to a lesser extent DTPMP (Fig. 5.1). Genome sequencing of these mutants identified a relatively small number of alterations that affect the products of genes and potentially the level of expression of others, most significantly those linked to zinc and iron homeostasis and acid tolerance.

5.4.1 Colony morphology and growth rate of chelant-resistant mutants

No significant difference in growth rate was noted on solid media with the six mutants isolated. However, the EDTA-resistant strains did show differences in colony morphology (Fig. 5.2), consistent with phase variation of type I fimbrial gene expression (Abraham et al., 1985; Hasman et al., 2000). These phenotypic changes were not obvious with the wild-type and DTPMP-resistant strains. It is unclear why increased switching might occur in these strains and whether that could also influence chelant resistance. In liquid media, all of the mutants showed a reduction in growth rate relative to the wild-type (Fig. 5.3). Mutants isolated at Day 15 (JN161 and JN165) grew slightly better than those recovered at Day 29. The extended lag phase in these mutants may contribute to chelant tolerance by giving cells longer to resolve problems arising from metal starvation or to manufacture specific proteins involved in regulating growth prior to cell division. For example, in *Salmonella enterica* Serovar Typhimurium, genes expressed during the lag phase include those involved in metal transport and iron-sulphur cluster formation (Rolfe et al., 2012). Accumulation of manganese, calcium and iron seem to be particularly important for progression to exponential growth, with concentrations of these metals being highest at the end of lag phase (Rolfe et al., 2012). It is not clear which mutations are responsible for growth reduction in each of the isolated strains. Several of the genes affected by mutation, including *thiD*, *rhsA*, *yeiR*, *flxA* and *ydbA*, show modest growth defects in LB when they are deleted (Baba et al., 2006), but it is also likely that increased expression of selected genes or functional modifications could also produce the observed slower growth phenotype.

5.4.2 Susceptibility of chelant resistant mutants to other chelants

The *E. coli* mutants isolated following exposure to EDTA and DTPMP showed differing sensitivities to additional chelating agents (Fig. 5.4). All strains exhibited increased susceptibility to DTPA, despite EDTA and DTPA showing a similar pattern

of decreases in manganese, iron and zinc (Paterson et al., 2022), suggesting some difference in the mode of action of these two chelants. Interestingly, the two EDTA-resistant mutants obtained after 29 days (JN188 and JN192), but not the Day 15 strain (JN161), showed improved resistance to both HNK and TRO (Fig. 5.4D and 5.4F). It is not clear which of the mutations are important for these effects as JN188 and JN192 have different mutations in addition to the shared *yeiR* changes (Fig. 5.5). Mutant tolerance of EDTA, TRO and HNK implies that these chelants may have a similar mechanism of action.

5.4.3 Significance of mutations affecting *fepA-entD*, *yeiR* and *cadC*

A diverse range of genes were affected by the mutations found in the chelant-exposed strains and several, such as the single amino acid substitutions, may well contribute to chelant tolerance (Fig. 5.5). Several of those found are membrane-associated or exported proteins which may affect chelant binding at the surface or ability to penetrate the Gram-negative outer membrane. Assays using cytochrome *c* to assess differences in bacterial cell surface charge failed to detect any changes between the wild-type and the six mutants (Lydia Newton, personal communication). Expression of two of these genes (ThiD and YahJ) failed to significantly increase EDTA or DTPMP resistance of BL21-AI in either uninduced or induced conditions (Fig. 5.7). Preliminary experiments (not shown) examining single gene knock-outs from the Keio collection (Baba et al., 2006) of many of the genes found in the chelant-resistant strains did not reveal increased sensitivity or resistance to EDTA or DTPMP but this data needs to be repeated. However, a previous screen of the Keio collection (Nichols et al., 2011) found that *fepA* and *yeiR* mutants are hypersensitive to EDTA. Of the other genes listed in Figure 5.5, the *flxA, thiD*, *rhsA* and *stfE* knockouts displayed modest EDTA sensitivities (Nichols et al., 2011). The experiments described in Chapter 3 confirmed that *fepA* mutants are highly sensitive to both EDTA and DTPMP (Fig. 3.7B and 3.7C).

A mutation found in both strains isolated after 29 days exposure to DTPMP affects the promoter region of the Fur-Fe^{2+}-regulated *fepA-entD* operon (Fig. 5.6B) with potential to increase downstream gene expression. Increased expression of FepA or EntD did seem to improve resistance to EDTA, and to a lesser extent DTPMP, in plasmid constructs when gene expression was induced (Fig. 5.7). EntD fulfils an essential role in enterobactin biosynthesis, a siderophore produced by *E. coli* for iron sequestration (Raymond et al., 2003). Exported enterobactin complexed with iron is then recovered by the integral outer membrane receptor FepA before delivery to FepBCDG and import to the cytosol (Barnard et al., 2001); Chapter 3, Fig. 3.6C). Although the strains exposed to DTPMP showed only weak, if any, resistance to this chelant (Fig. 5.1C), it makes sense that increased expression of FepA and EntD would improve survival at sub-MIC concentrations of DTPMP. It also suggests that iron deprivation is an important factor in the mechanism of action of this chelant, which fits with earlier studies on the metals affected by DTPMP (Paterson et al., 2022).

All of the EDTA resistant strains carry a mutation in the untranslated leader region of the *yeiR* gene (Fig. 5.6A), which encodes a zinc-dependent GTPase with an undefined role in zinc homeostasis (Blaby-Haas et al., 2012; Young et al., 2021). Since *yeiR* mutants are known to be susceptible to EDTA (Blaby-Haas et al., 2012; Nichols et al., 2011), it seems logical that the two distinct mutations found here would lead to increased expression of the *yeiR* gene and this aids in coping with reductions in zinc availability in the presence of EDTA (Paterson et al., 2022). YeiR belongs to the COG0523 subset of the G3E GTPase superfamily that appear to be metal chaperones associated with cobalt, iron and zinc delivery (Edmonds et al., 2021; Haas et al., 2009). YeiR is highly selective for zinc (Blaby-Haas et al., 2012; Nichols et al., 2011) and is likely to serve an important role in distributing zinc to essential metalloenzymes under limiting conditions, such as exposure to EDTA. Deletion of other members of the COG0523 family also results in susceptibility to EDTA, including

B. subtilis yciC, although this is only evident when cells are also missing the zinc transport-associated protein YcdH (Gaballa et al., 2002; Gaballa & Helmann, 1998).

Three unique mutations were isolated in the *cadC* gene whose product serves as an activator of the *cadBA* operon in response to acid conditions (Jung et al., 2018; Küper & Jung, 2006). Note that *E. coli* CadC is distinct from the cadmium-responsive regulator CadC found in the plasmid pI258 of *S. aureus* (Ye et al., 2005). Significantly the three mutations found in the chelant-adapted strains cluster together at the dimer interface (Fig. 5.8B and 5.8C) and include Tyr453 an aromatic residue essential for binding cadaverine, the feedback inhibitor of CadC activation (Haneburger et al., 2012). It is possible that all three mutants are incapable of binding cadaverine which would result in elevated expression of *cadAB*, thus increasing cadaverine production and acid tolerance. A more alkaline external pH produced by cadaverine would affect association of EDTA or DTPMP with metals due to deprotonation which might make them more effective at sequestering metals at the cell surface. In the case of EDTA, this might protect the outer membrane from damage (Alakomi et al., 2003; Brown & Richards, 1965; Leive, 1974) or make metal acquisition easier, however this remains unclear. Alternatively, the chelants may have detrimental effects themselves as acids that are ameliorated in the presence of cadaverine.

Mutations in *cadC* were also found in *E. coli* exposed to low levels of the antibacterial agent triclosan (Leyn et al., 2021) and also carvacrol (Al-Mnaser & Woodward, 2020). Triclosan is an inhibitor of the FabI, NADH-dependent enoyl-[acyl carrier protein] reductase required for fatty acid synthesis (Heath et al., 1998; McMurry et al., 1998). Although the triclosan mutations were located in different parts of *cadC* from those identified with chelants (Fig. 5.8B and 5.8C), it does raise the possibility that *cadC* acts in a general fashion to signal cell stress, perhaps affecting the cell outer membrane *via* sensing in the periplasm. As was found here with chelant-associated strains (Fig. 5.9), there was no indication that the individual CadC substitutions conferred resistance to triclosan (Leyn et al., 2021), however, they may

well provide complementary benefits in combination with additional genomic alterations.

5.5 Future directions

EDTA and DTPMP were selected due to their widespread commercial use, distinct chemical structures and differing effects on cellular metals. It may be valuable to repeat this experimental evolution approach with additional chelating agents whose mode of action is uncharacterised. For instance, BCS, CAT and CHA would good candidates as no differences in total cellular metal were detected with these chelants in *E. coli* (Paterson et al., 2022). The next chapter details a similar approach to isolate EDTA- and DTPMP-resistant mutants of *S. aureus,* but other problematic species in industrial or clinical settings, such as *P. aeruginosa,* would merit investigation.

Using ICP-MS, it would be helpful to assess whether the chelant-resistant mutants have improved capacity to acquire metals in the presence or absence of EDTA and DTPMP. Confirmation that *yeiR*, *fepA* and *entD* gene expression is increased in the relevant mutant strains could be confirmed by RT-PCR or qPCR. Further study of YeiR is also needed as effects on its overexpression on EDTA resistance has not been explored. Similarly, the induced expression of CadC and its mutant variants could be re-examined in BL21-AI following induction of gene expression. The effect of cadaverine on EDTA and DTPMP toxicity with *E. coli* would be simple to test and may yield insights into whether the *cadC* mutations could protect against chelants by increasing cadaverine expression. Finally, the effect of HNK and TRO on cellular metal content has been determined for *P. aeruginosa* (Fig. 4.7) but not *E. coli*. It would be of interest to see if there were any similar effects on metals with these two chelants on *E. coli* since JN188 and JN192 showed resistance to HNK and TRO in addition to EDTA.

6 Isolation and characterisation of *S. aureus* chelant-resistant mutants

6.1 Introduction

In the previous chapter, we examined the effects of prolonged sub-lethal chelant treatment on *E. coli* as a representative Gram-negative with the aim of identifying the cellular targets of DTPMP and EDTA. In this chapter, we adopted the same approach in an effort to isolate chelant-resistant mutants of the Gram-positive species *S. aureus*. The majority of previously published work on the antibacterial effects of chelating agents has focussed on Gram-negatives (see Chapter 4), where certain chelants exert damaging effects on the lipopolysaccharide-rich outer membrane. It was hoped that studying a model Gram-positive would provide new insights into how bacteria with a radically different cell envelope architecture and metal uptake pathways respond to chelants. *S. aureus* mutants were isolated at 15 and 29 days in the presence of sub-MIC levels of DTPMP and EDTA as before. In this chapter, genome sequencing analysis was performed by Ping Hu (P&G, Cincinnati), Zeta potential by Elizabeth Bromley (Department of Physics, Durham University), salt sensitivity experiments in broth by Rebecca Lee, as part of her final year MBiol research project, and peptidoglycan cross-linking analysis by Waldemar Vollmer (The Centre for Bacterial Cell Biology, Newcastle University).

6.2 Isolation and characterisation of *S. aureus* chelant-resistant mutants

6.2.1 Isolation of chelant-resistant mutants by experimental evolution

Drug-naïve *S. aureus* (FDA209P) was cultivated in the presence of sub-MIC levels of either EDTA or DTPMP for periods of 15 and 29 days, as described previously with

E. coli (Chapter 5, Section 5.2.1). Experiments with *E. coli* and *S. aureus* were conducted in parallel with the same approach used in both cases (Fig. 6.1A), although different chelant concentrations were chosen in keeping with the differing sensitivities of the two species. FDA209P is widely used as a methicillin-sensitive *S. aureus* (MSSA) reference strain in antibiotic susceptibility assays and its complete genome sequence is available (Singh et al., 2015).

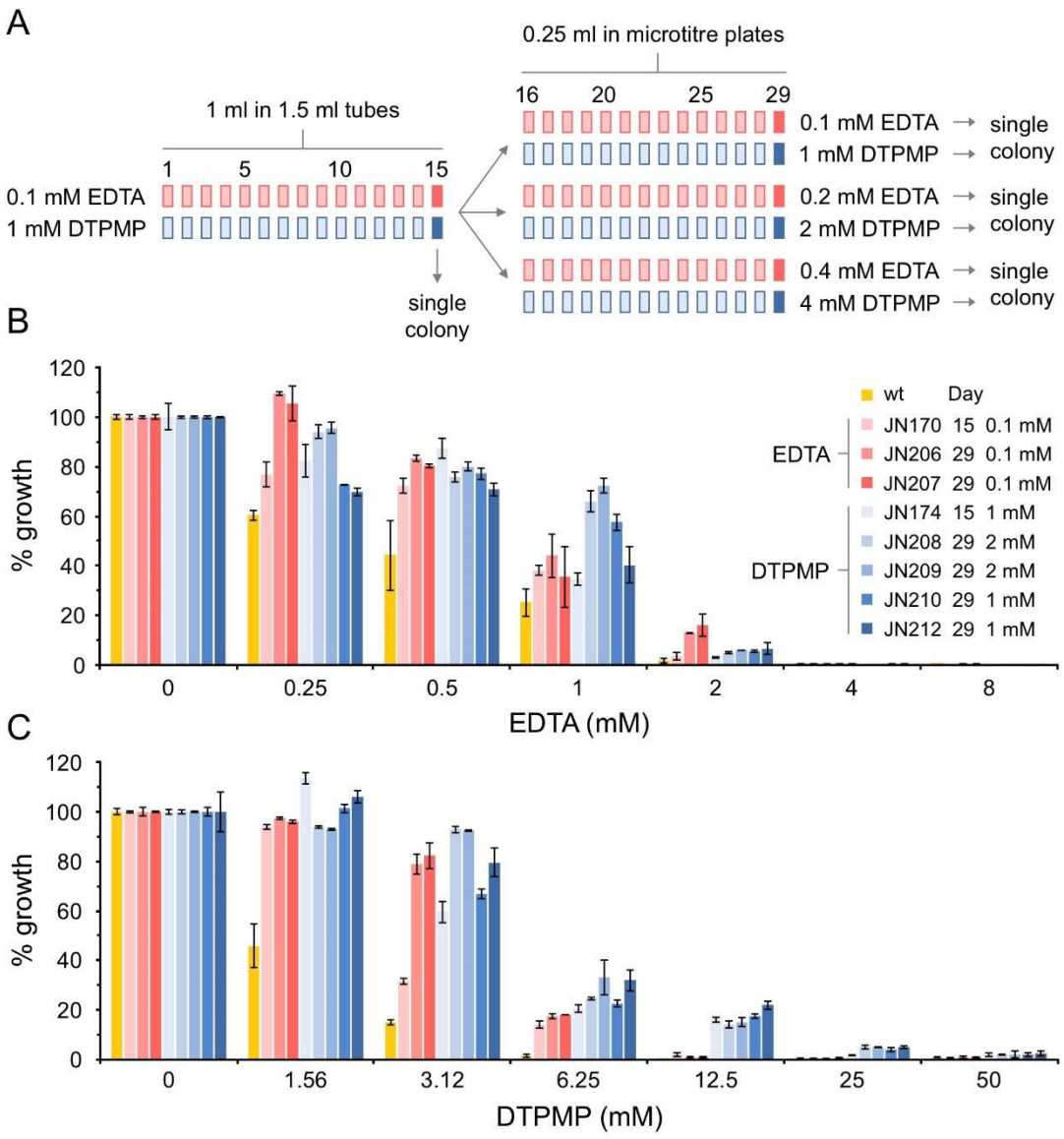

Figure 6.1 Isolation of *S. aureus* chelant-resistant mutants. (A) *S. aureus* (FDA209P) mutants that tolerate either EDTA or DTPMP were obtained by repeated subculture for 15 and 29 days at sub-MIC levels of each chelant. Susceptibility of wt and mutant strains to EDTA (B) or DTPMP (C) was examined. Two-fold serial

dilutions of each chelant were mixed with each strain and incubated at 37°C with shaking at 150 rpm for 16 h. Growth was measured at $A_{600\ nm}$ at the end point and normalised against controls without chelant to give the percentage growth. Mutants selected against EDTA are shown in shades of pink, while those exposed to DTPMP are in blue. Results represent the mean and standard deviation of an experiment performed in triplicate. Two additional independent repeats produced similar results.

Selected strains recovered at 15 and 29 days were assessed for their capacity to tolerate EDTA and DTPMP compared to the parental wild-type (Fig. 6.1B and 6.1C). All eight mutants showed a significant improvement in resistance to EDTA relative to the parental strain at all concentrations tested (Fig. 6.1B), even those strains isolated in the presence of DTPMP. EDTA-isolated strains (JN170, JN206 and JN207) showed the highest levels of EDTA resistance, especially with the two strains obtained after 29 days (Fig. 6.1B). Enhanced tolerance in the isolated strains was even more evident with DTPMP, with >2-fold improvements in growth seen with all mutants in comparisons with the parental strain, regardless of which chelant they were exposed to during the selection process (Fig. 6.1C). DTPMP-isolated mutants (JN174, JN208, JN209, JN210 and JN212) displayed a 4-fold increase in resistance to this chelant relative to the starting wild-type (Fig. 6.1C). These results contrast with *E. coli*, where it was not possible to isolate mutants with increased resistance to DTPMP using the same approach (Chapter 5, Fig. 5.1C). The discovery that resistance to both DTPMP and EDTA can arise following exposure to either of the chelants in *S. aureus* is intriguing. It could indicate a more generalised mechanism of adaptation that allows tolerance to both chelants or that the cellular impact of these two chelants is actually similar in this species.

6.2.2 Colony morphology and growth of chelant-resistant mutants

The colony morphology of the *S. aureus* strains selected against EDTA and DTPMP were examined by streaking onto LB agar plates (Fig. 6.2). DTPMP-isolated strains JN174, JN210 and JN212 produced smaller colonies after overnight incubation

consistent with slower growth (Fig. 6.2E, H and I). Despite this modest growth defect, no other phenotypic differences between these three mutants and the others (including the wild-type) were observed even after an extended incubation period (Fig. 6.2).

The growth rate of the chelant-resistant strains was also examined in LB broth in the absence of chelating agents (Fig. 6.3). The fastest growth was found with the parental strain which transitions between the exponential and stationary phase at around 5 hours. The JN174, JN208, and JN209 DTPMP-isolated mutants produced a similar pattern of growth, alongside JN170, an EDTA isolate, that displays a slight growth reduction relative to the wild-type. In contrast, JN206 and JN207, also isolated against EDTA, show an extended lag phase and slower exponential phase, but ultimately reach a similar optical density as JN170 after 9 hours. The remaining DTPMP-isolated strains, JN210 and JN212, exhibit a significantly reduced growth rate, failing to achieve the same optical density as the parent strain even after 12 hours incubation (Fig 6.3).

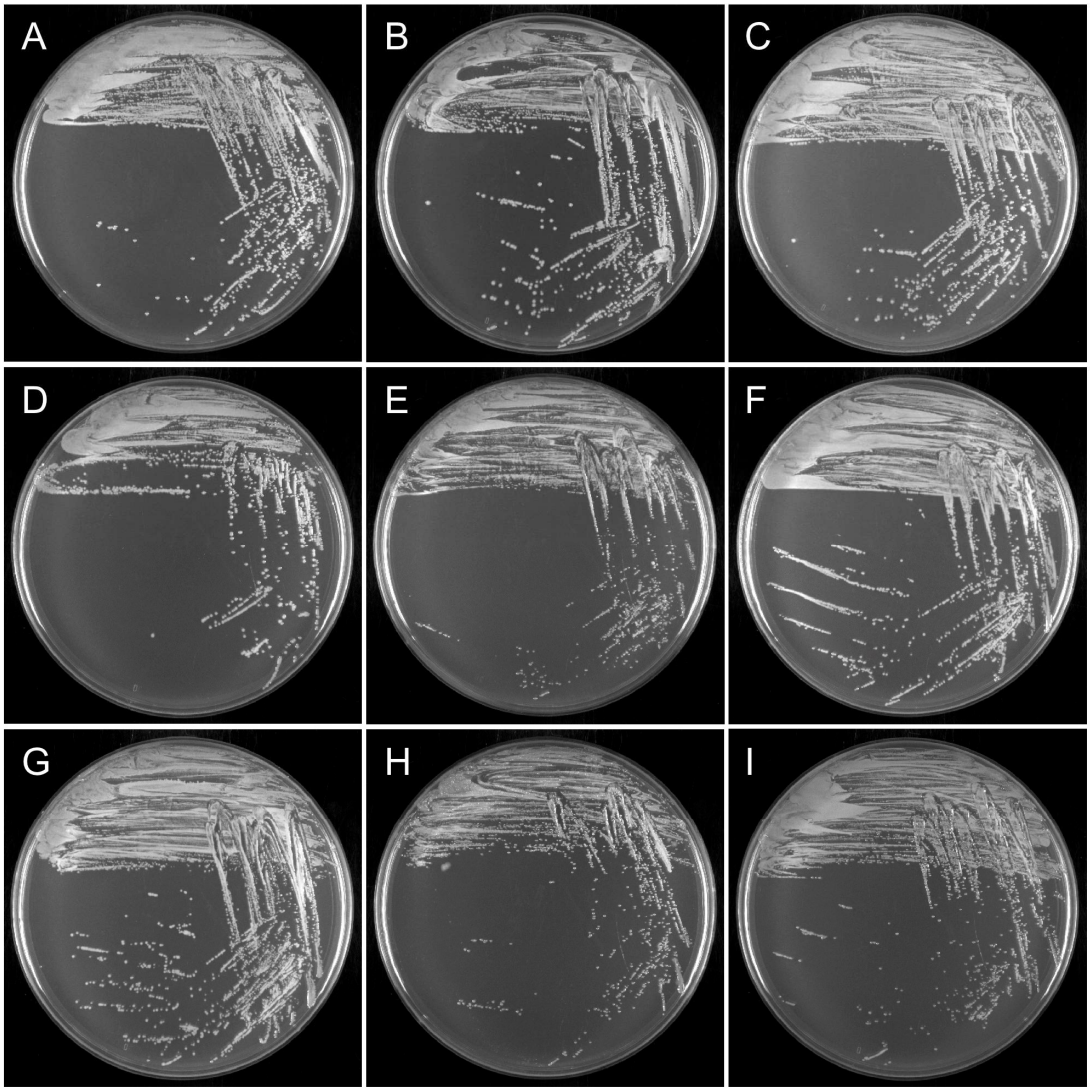

Figure 6.2 Colony morphology of *S. aureus* chelant-resistant mutants. Isolated strains were streaked and grown on LB agar at 30°C for 20 hours prior to imaging. FDA209P wt (A), JN170 (B), JN206 (C), JN207 (D), JN174 (E), JN208 (F), JN209 (G), JN210 (H), JN212 (I).

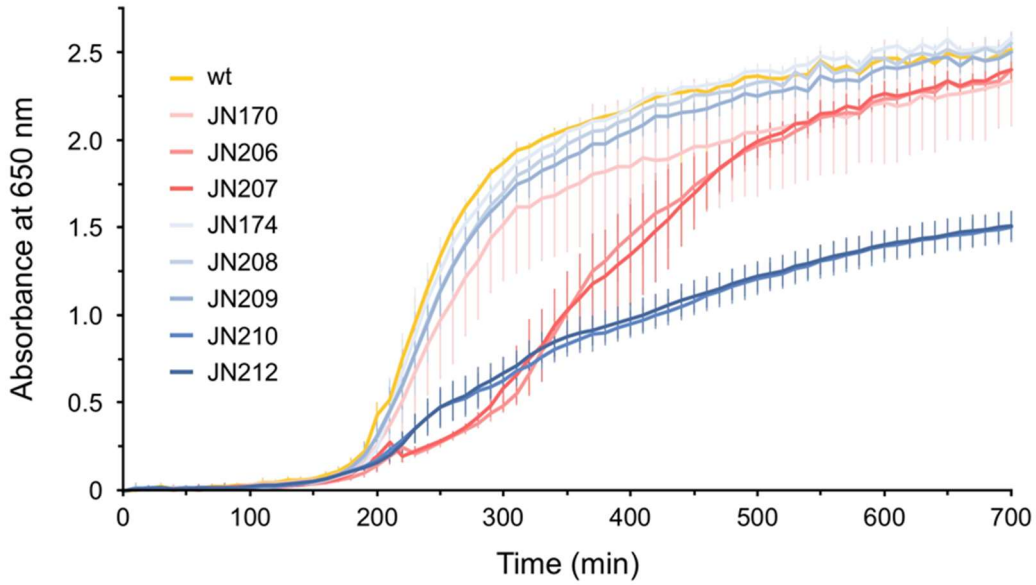

Figure 6.3 Growth curves of *S. aureus* chelant-resistant mutants. Strains were cultivated in LB broth at 37°C and absorbance monitored at $A_{650\ nm}$. Those isolated in the presence of EDTA (JN170, JN206 and JN207) are highlighted in pink, while those isolated in the presence of DTPMP (JN174, JN208, JN209, JN210 and JN212) are in blue. The results are the mean and standard deviation of a single experiment performed in triplicate.

6.3 Identification of mutations in chelant-resistant strains

To identify the mutations responsible for the enhanced EDTA and DTPMP tolerance of these mutants, the genome sequence of each strain, including the FDA209P parent, was determined using an Illumina MiSeq platform with 30 times coverage by MicrobesNG (as described for *E. coli*; Chapter 5, Section 5.3). An annotation pipeline was devised and differences between the parent and mutant strains identified by Ping Hu at P&G. The mutations found are summarised in Figure 6.4.

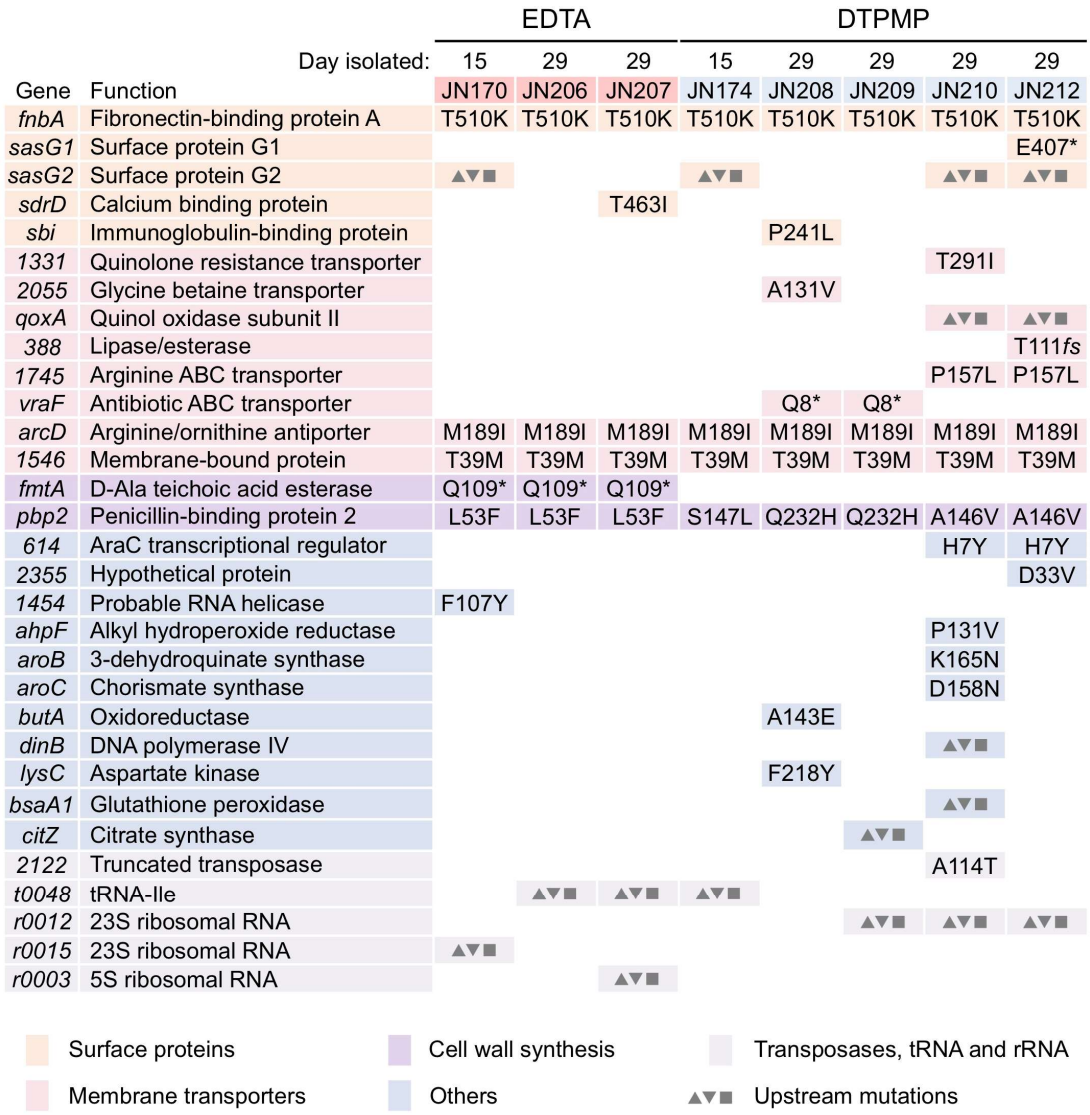

Figure 6.4 Mutations identified by genome sequencing of eight *S. aureus* chelant-resistant mutants. The genes affected are grouped according to function and the specific mutations listed for each strain. Missense mutations that change amino acid sequences of the gene product are shown, replacement of an amino acid with a stop codon is indicated by an asterisk. A single mutation, affecting gene *388*, is a frameshift (fs) and mutations upstream of genes that could potentially affect gene expression are labelled accordingly. Base changes upstream of genes are indicated by triangular and square symbols reflecting potential upregulation, downregulation or no effect on adjacent gene expression. Synonymous changes affecting *uvrA*, *sdrC*, *tnpA*, *recU*, *pheT*, *infB*, *gapB*, *fmtA*, *clfB* (x4) and *arlS* are not listed.

Mutations affecting genes in all eight chelant-resistant strains were noteworthy since they could be responsible for the changes that result in tolerance. These include

amino acid substitutions in FnbA (fibronectin binding protein), ArcD (an arginine:ornithine antiporter), PBP2 (penicillin binding protein 2) and 1546 (an uncharacterised membrane bound protein). Additional mutations of interest included stop codons disrupting *fmtA*, encoding a teichoic acid esterase present in all three EDTA-isolated strains, and *vraF* that encodes an antibiotic efflux pump found in JN208 and JN209, two of the strains selected against DTPMP (Fig. 6.4). Mutations in a putative arginine ABC transporter, *1745*, were unique to JN210 and JN212. Surprisingly, these changes all affect cell surface molecules, membrane-bound transporters and the cell wall synthesis machinery, rather than the anticipated metal uptake systems. The mutations and their potential effects are summarised briefly in the remainder of this section and the more important ones discussed more fully at the end of the chapter. Several genes that may be upregulated to promote chelant resistance are described first followed by those that alter gene products or prevent their translation.

A relatively small number of mutations upstream of genes were identified that could influence expression (Fig. 6.4), although none were found in all of the strains indicating that they either do not contribute to chelant resistance or that they provide only a supplemental benefit. Multiple different point mutations were found in JN170, JN174, JN210 and JN212 upstream of the *sasG2* gene. SasG is a repeat protein, involved in host tissue adhesion and biofilm formation, that in some strains consists of 1637 amino acids (Gruszka et al., 2012). In FDA209P *sasG* is split into two with *sasG2* lacking the N-terminal signal peptide required for export. The presence of repeat sequences may encourage localised rearrangements and perhaps explain why so many mutations are located in this region. A substitution and stop codon were located at the extreme C-terminal end of *sasG1*, perhaps for similar reasons. Upstream mutations in DTPMP-selected strains were also found linked to *qoxA* (quinol oxidase subunit II, which belongs to the cytochrome *c* oxidase family as a component of the respiratory chain) in JN210, *dinB* (DNA polymerase IV, involved in

translesion synthesis) in JN210, *bsaA1* (glutathione peroxidase, involved in detoxifying hydrogen peroxide) also in JN210, and *citZ* (citrate synthase as part of carbohydrate metabolism) in JN209. The mutations upstream of tRNA and rRNA genes could potentially help more generally in managing protein translation in response to growth restriction and metal starvation imposed by chelants.

The majority of genetic alterations in the chelant-isolated strains are missense, frameshift or nonsense mutations affecting a wide array of genes (Fig. 6.4). Those located in a single strain, often found only in DTPMP-selected mutants, may not contribute to chelant resistance at all but some may provide minor benefits in combination with the other changes in that strain. Several of these genes (*ahpF*, *butA*), alongside others mentioned above that might affect expression (*dinB*, *bsaA1*), may be linked to oxidative stress tolerance associated with chelant exposure. The mutation in AhpF (Pro131Val) is adjacent to a redox-active disulphide (Cys127-Cys130), based on its homology with its equivalent from *Salmonella enterica* Serovar Typhimurium (Wood et al., 2001), and could potentially modify its activity.

Changes in surface proteins may affect the charge on the exterior of the cell and potentially influence metal or chelant binding. These include missense, nonsense or frameshift mutations affecting *fnbA*, *sasG1*, *sdrD* and *sbi* (Fig. 6.4). The stop codon in SasG1 removes the last 8 residues of the protein (ELDHRSIA) which could alter the charge at the outer surface. The fibronectin binding protein FnbA adds an additional positive charge through replacement of threonine with lysine and may be important as the substitution is carried by all chelant-resistant strains. The change lies within one of the fibronectin-binding repeats (FnBPA-1), immediately adjacent to a conserved glycine (Bingham et al., 2008). Other mutations of interest, include the frameshift in gene *388*, which removes the bulk of the product, a putative lipase that could be involved in cell wall metabolism. JN208 and JN209 have a stop codon in *vraF* (Gln8*), which renders it non-functional (Fig. 6.4). The VraFG ABC transporter participates in the export of cationic antimicrobial peptides, antibiotics and

bacteriocins and is regulated by the two-component GraRS sensory network (Meehl et al., 2007). Identical substitution mutations in *arcD* and the *1546* gene product are present in all mutants. The mutation in the uncharacterised 1546 protein lies in the first of two predicted membrane spanning regions (residues 32-53 and 58-84). The protein consists of only 94 residues but the second of transmembrane helix shares homology with KdpF, a stabilising component of the KdpFABC potassium importer (Gründling, 2013; Huang et al., 2017). It may be that 1546 can associate and influence KdpABC activity or associate with alternative ion channel. ArcD is transmembrane arginine-ornithine antiporter which enables import of arginine and export of ornithine in a 1:1 ratio. It is part of the arginine deiminase system that incorporates an arginine deiminase (*arcA*), ornithine transcarbamylase (*arcB*) and carbamate kinase (*arcC*) (Driessen et al., 1987; Zhu et al., 2007). ArcD has 13 predicted transmembrane helices and the mutated residue lies in a loop between helices 6 and 7.

All of the EDTA-isolated strains carry a mutation in *fmtA* that removes the bulk of the 397-residue protein, likely inactivating the gene product. FmtA is a membrane bound protein that interacts with teichoic acids, and has two conserved motifs typically found in penicillin binding proteins (PBPs) and β-lactamases, SXXK and S(Y)XN (where X is any residue), leading to the proposal that it might play a role in cell wall synthesis (Navratna et al., 2010). There are two types of teichoic acids in *S. aureus*: lipoteichoic acids (LTAs) which are attached to the outer leaflet of the cytoplasmic membrane and wall teichoic acids (WTAs) which are covalently linked to peptidoglycan (Percy & Gründling, 2014). Both teichoic acid polyol-phosphate polymers undergo postsynthetic modification by glycosylation in the cytosol (LTAs) or extracellular esterification (WTAs). The net negative charge of teichoic acids is partially masked when D-Ala is added to the teichoic acids through esterification. FmtA hydrolyses the ester bond between D-Ala and the teichoic acid backbone,

thereby modulating cell surface charge according to physiological requirements (Rahman et al., 2016).

All of the chelant-resistant strains also have mutations in PBP2 (Fig. 6.5). PBPs are involved in the synthesis and maintenance of peptidoglycan and *S. aureus* has four PBPs in total (PBP1-4), with PBP1 and PBP2 being essential for viability (Sauvage et al., 2008; Stapleton & Taylor, 2002). PBP2 is unique in *S. aureus* in catalysing both transpeptidation, the cross-linking between glycan chains, and transglycosylation, the polymerisation of the glycan strands from lipid II precursors (Fig. 6.5A) (Stapleton & Taylor, 2002). The presence of four distinct substitution mutations in PBP2 in each of the eight chelant-resistant strains suggests that they fulfil an important role in EDTA and DTPMP tolerance. Three of these mutations (Ala146Val, Ser147Leu and Gln232His), found only in the DTPMP isolates, cluster near the active site Glu114 and Glu171 residues of PBP2 in a channel where N-acetylglucosamine (NAG or GlcNAc) and N-acetylmuramic acid (NAM or MurNAc) pairs are fused to assemble the glycan polymer (Fig. 6.5B) (Lovering et al., 2007). All three substitutions are located within highly conserved motifs responsible for PBP2 glycosyltransferase (transglycosylase) activity (Fig. 6.5C). The EDTA strains all carry a different mutation (Leu53Phe) in the transmembrane helix that spans the lipid bilayer and positions PBP2 for peptidoglycan synthesis (Lovering et al., 2007).

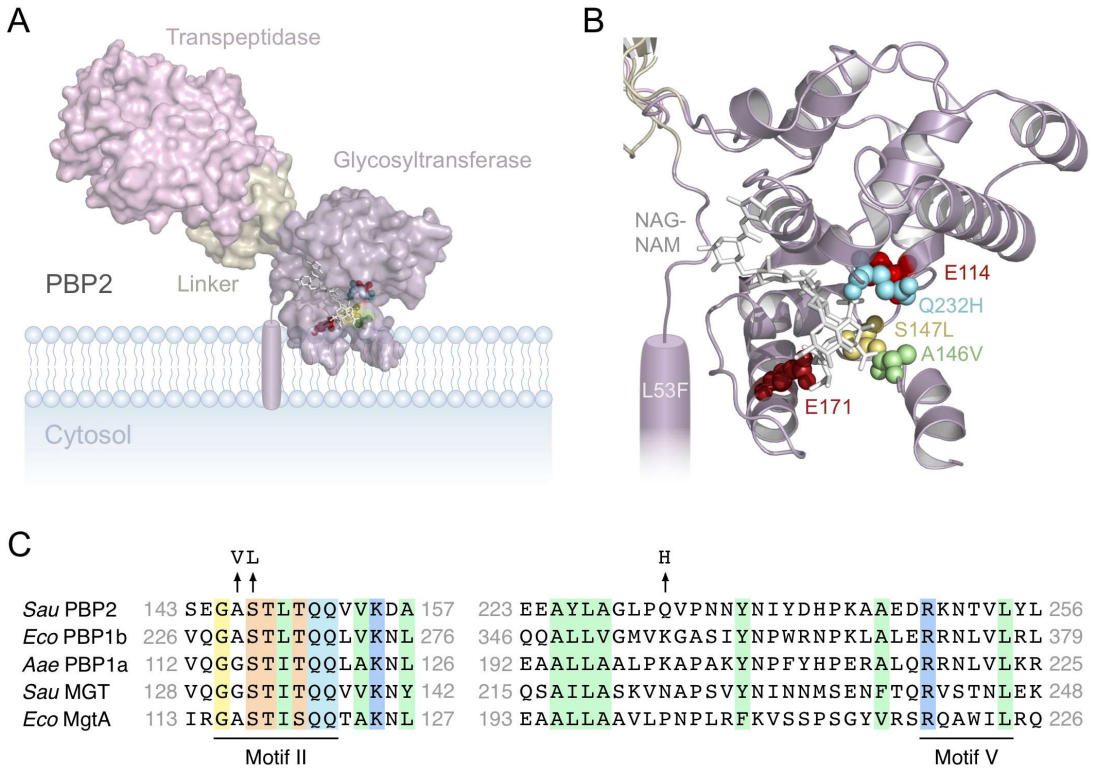

Figure 6.5 Location of substitution mutations in the PBP2 glycosyltransferase domain. (A) Structure of PBP2 (PDB: 2OLV) and its position in the bacterial cytoplasmic membrane. The transpeptidase, glycosyltransferase (transglycosylase) and intervening linker domains are highlighted (Lovering et al., 2007). A single transmembrane helix tethers PBP2 to the membrane. (B) Location of PBP2 glycosyltransferase active site residues and mutations identified in this study. Active site glutamates (E114 and E171) are coloured red. Three mutations (A146V, S147L, Q232H) found in DTPMP isolates cluster close to the active site where the sugar backbone of peptidoglycan is assembled. This is labelled NAG-NAM but here is actually the substrate analogue moenomycin represented in stick format. A fourth mutation, present in EDTA-isolated mutants (L53F), is located in the transmembrane helix that spans the lipid bilayer. (C) Sequence alignment of the relevant GT_{51} conserved motifs in selected bacterial glycosyltransferases highlighting the location of the A146V, S147L and Q232H mutations (Goffin & Ghuysen, 1998; Huang et al., 2012; Lovering et al., 2007). *S. aureus* (*Sau*), *E. coli* (*Eco*) and *Aquifex aeolicus* (*Aae*). Conserved residues present in all sequences are highlighted and GT_{51} motifs II and V are labelled. Residue positions within each of the protein sequences is indicated and accession numbers are: PBP2 (F4NA87), PBP1b (P02919), PBP1a (O66874), MGT (Q93Q23) and MgtA (P46022). Structures were generated in Pymol.

6.4 Characterisation of *S. aureus* chelant-resistant mutants by assessing phenotypic changes at the cell surface

6.4.1 Probing changes in envelope properties with antibiotics that target the bacterial cell wall

The mutation profile in chelant-resistant isolates suggested that changes in bacterial cell wall architecture might be responsible for the improved resistance to EDTA and DTPMP (Fig. 6.4). Antibiotics that target different stages in *S. aureus* cell wall biosynthesis can be employed as tools to interrogate any structural alterations. Here we utilised a selection of β-lactams, vancomycin and moenomycin to probe mutant susceptibility. All of the isolated strains contain amino acid substitutions in PBP2, located either in the transmembrane helix or within the glycosyltransferase active site (Fig. 6.5). Penicillin binding proteins (PBPs) are required for the construction and maintenance of the peptidoglycan sacculus that encloses the Gram-positive cell wall providing osmotic stability and protection from environmental stressors. A number of β-lactam antibiotics specifically inhibit the activity of PBPs and were selected to examine changes in chelant-resistant strains. Penicillin G, also known as benzylpenicillin, is the original molecule extracted from *Penicillium chrysogenum* and targets the transpeptidase active site of Gram-positive PBPs (Lobanovska & Pilla, 2017). This antibiotic, along with related second and third generation cephalosporins, cefoxitin, cefotaxime and cefsulodin were chosen as they target different subsets of the four PBPs found in *S. aureus* (Fontana et al., 2000; Sauvage et al., 2008). In *S. aureus*, cefoxitin preferentially targets PBP1, whereas cefotaxime and Penicillin G favour binding to PBP4 (Fontana et al., 2000) which may explain the differences in concentrations of each antibiotic required to provide growth inhibition. MIC assays were again used to facilitate rapid and simple comparison between the susceptibilities of the mutant strains (Fig. 6.6).

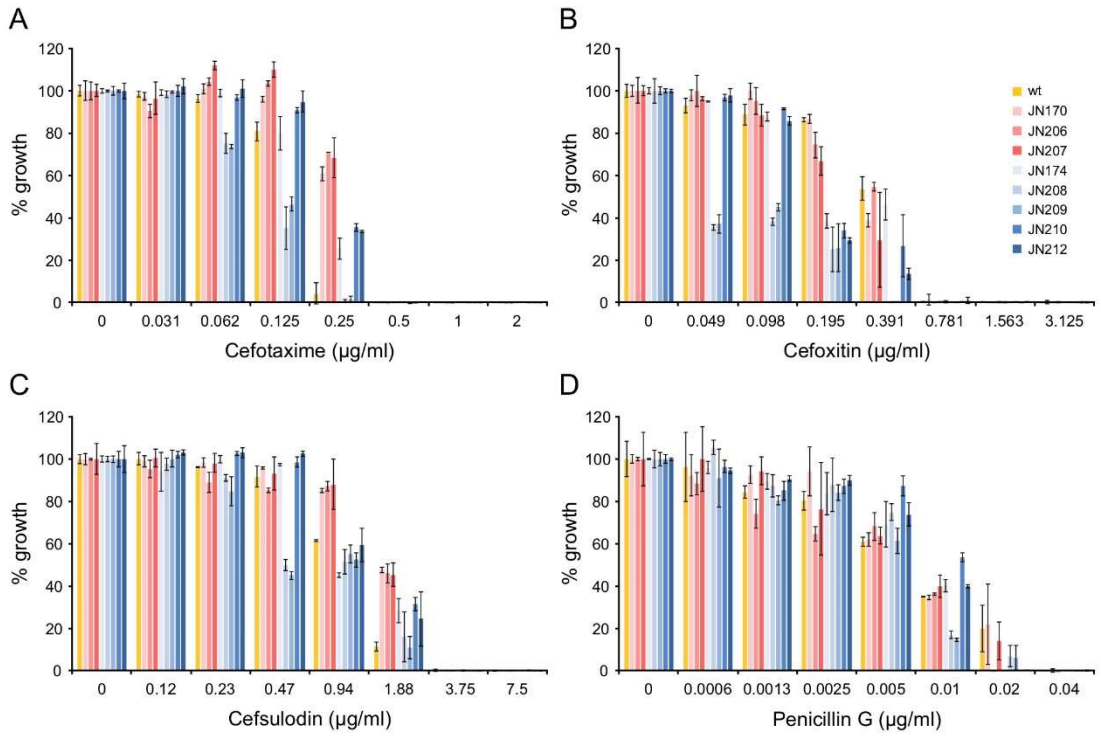

Figure 6.6 Susceptibility of *S. aureus* chelant-resistant mutants to β-lactam antibiotics in liquid culture. Sensitivity of wt and mutant strains to cefotaxime (A), cefoxitin (B), cefsulodin (C) and Penicillin G (D) was examined using two-fold serial dilutions of each antibiotic which were mixed with each strain in LB and incubated at 37°C with shaking at 150 rpm for 16 h. Growth was measured at $A_{600\ nm}$ at the end point and normalised against controls without antibiotic to give the percentage growth. Mutants selected against EDTA are shown in shades of pink, while those exposed to DTPMP are in blue. Results represent the mean and standard deviation of an independent experiment performed in triplicate. An additional independent repeat produced similar results.

The EDTA-selected isolates (JN170, JN206 and JN207) showed a modest increase in resistance to cefotaxime and cefsulodin relative to the wild-type, but no significant changes with cefoxitin and penicillin G (Fig. 6.6). These three strains carry unique mutations in *pbp2* and *fmtA*, alongside other genetic changes present in all of the mutant strains (Fig. 6.4). JN210 and JN212, two of the DTPMP-isolated mutants, also showed indications of improved tolerance of cefotaxime (Fig. 6.6A) but also some sensitivity to cefoxitin (Fig. 6.6B). Little change in susceptibility was apparent with JN174, whereas the remaining DTPMP-selected strains, JN208 and JN209,

proved significantly more sensitive to all four antibiotics, especially cefoxitin (Fig. 6.6). In general, the mutants showed fewer differences compared to the wild-type with penicillin G (Fig. 6.6D). The enhanced susceptibility of JN208 and JN209 may correlate with its unique *pbp2* mutation and/or the elimination of the *vraF* drug efflux pump found only in these strains (Fig. 6.4).

In addition to MICs, the sensitivity of these mutants to three of the four β-lactams, penicillin G, cefoxitin and cefotaxime was also examined using antibiotic discs placed onto overlays seeded with each of the relevant strains. Representative images of the results are shown in the Appendix (Fig. 9.4) and the measured zones of inhibition summarised in Figure 6.7. Although the differences were small, an increased susceptibility to penicillin G and cefoxitin of the DTPMP-isolated mutants was apparent. Of these strains, only JN208 and JN209 showed additional increased sensitivity to cefotaxime. There were indications that the EDTA-isolated mutants (JN170, JN206, and JN207) were more resistant to these three antibiotics but the overlapping error bars mean the results are inconclusive (Fig. 6.7).

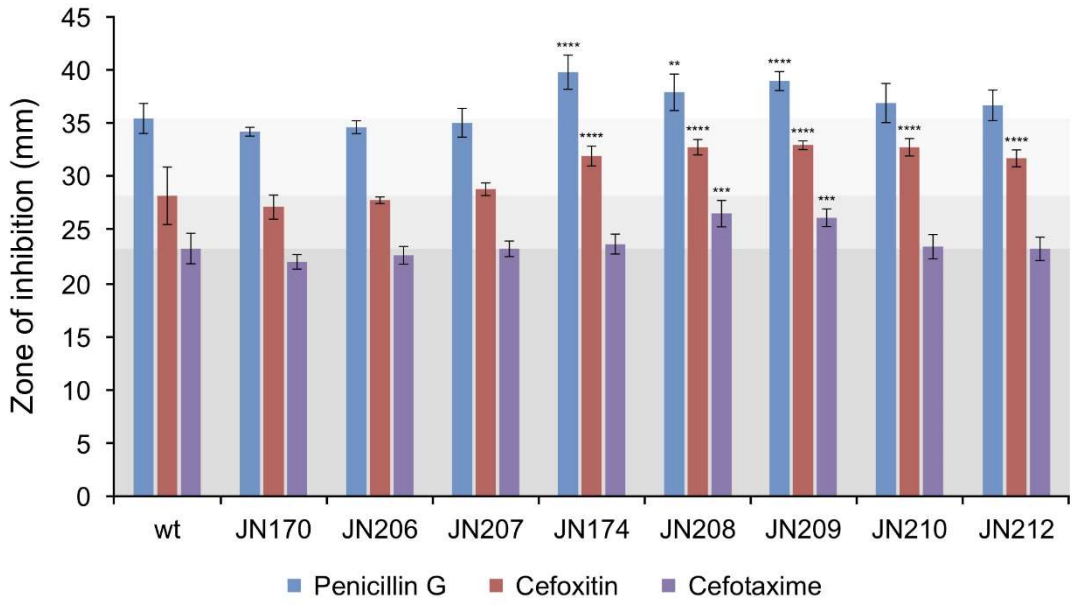

Figure 6.7 Susceptibility of *S. aureus* chelant-resistant mutants to β-lactam antibiotic discs. Susceptibility to penicillin G (10 U), cefoxitin (30 µg) and cefotaxime (30 µg) was measured through application of antibiotics discs to bacterial overlays. Discs were applied aseptically to LB agar plates with an overlay of 7.5 ml 0.6% LB

agar and 200 µl of an overnight culture of each strain. Plates were incubated for 16 h at 37°C and the diameter of growth inhibition measured using Fiji (Image J). The grey shaded background indicates the zone diameter of the wild-type with each antibiotic to facilitate comparisons with each mutant. The student t-test was used to compare mutant strains to the wild-type; *p<0.5, **p<0.01, ***p<0.001, ****p<0.0001. Results are the mean and standard deviation of three independent experiments.

Vancomycin is a glycopeptide antibiotic which binds the terminal D-Ala-D-Ala peptide side chain of lipid II, preventing access of PBPs and thus inhibiting polymerisation and crosslinking of peptidoglycan (Kapoor et al., 2017). Moenomycin belongs to a unique family of antibiotics which mimics the growing sugar-chain substrate or product, preventing peptidoglycan glycan chain polymerisation by association with glycosyltransferases (Lovering et al., 2007; Zuegg et al., 2015). Specific mutations in the glycosyltransferase active site of PBP2 confer resistance of *S. aureus* to moenomycin by reducing antibiotic binding (Rebets et al., 2014). Given the nature of their targets, both vancomycin and moenomycin were chosen to further probe the differences in cell wall structure between the mutant strains and the potential significance of the glycosyltransferase mutations present in PBP2 (Fig. 6.8). All of the chelant-resistant mutants showed increased susceptibility to vancomycin in comparison to the wild-type, with the DTPMP-isolated mutants showing considerably greater sensitivity than the EDTA-selected strains(Fig. 6.8A). As with the β-lactams (Fig. 6.6), JN208 and JN209 again showed the greatest susceptibility of all the isolates with reduced growth evident at 0.188 µg/ml vancomycin (Fig. 6.8A). With moenomycin, the EDTA-isolated strains displayed a similar sensitivity profile to the wild-type (Fig. 6.8B). In contrast, the DTPMP-isolated mutants exhibited a 4-fold increase in sensitivity to this antibiotic (Fig 6.8B). Interestingly the DTPMP-isolated mutants, JN208 and JN209, which had previously shown an enhanced susceptibility to all of the tested antibiotics, showed improved resistance to moenomycin relative to the other DTPMP-isolates (Fig. 6.8B).

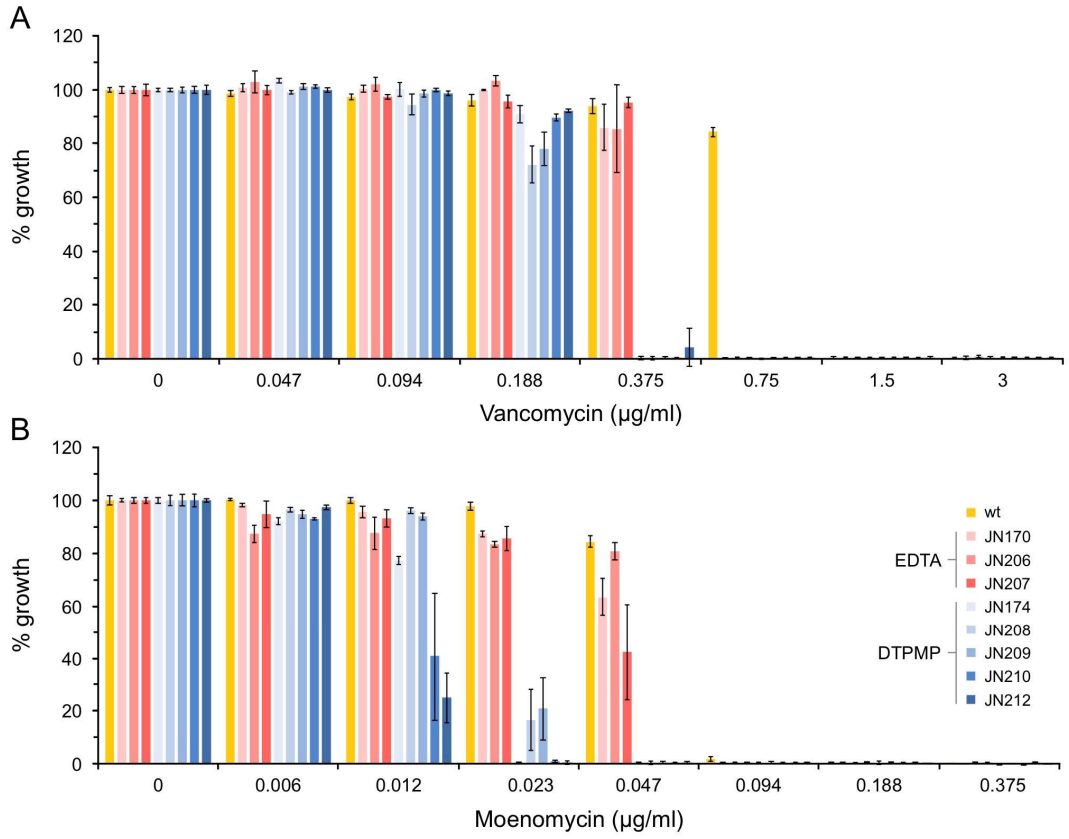

Figure 6.8 Susceptibility of *S. aureus* chelant-resistant mutants to vancomycin and moenomycin. Two-fold serial dilutions of vancomycin (A) or moenomycin (B) were mixed with each strain and incubated at 37°C with shaking at 150 rpm for 16 h. Growth was measured at $A_{600\ nm}$ at the end point and normalised against controls without antibiotic to give the percentage growth. Results represent the mean and standard deviation of an independent experiment performed in triplicate. Two additional independent repeats produced similar results.

To confirm these results, bacterial susceptibility to moenomycin incorporated in agar plates was investigated by applying serial dilutions of *S. aureus* grown to mid-log phase for each of the strains (Fig. 6.9). As in the MIC assays conducted in liquid culture (Fig. 6.8), none of the EDTA-isolated strains exhibited any increased susceptibility to moenomycin. However, the DTPMP-isolated strains proved exceedingly susceptible to moenomycin under these conditions (Fig. 6.9). The slow-growth phenotype of JN174, JN210 and JN212 observed previously (Fig. 6.2) is apparent here without moenomycin (Fig. 6.9), but cannot account for the slight

improvement in growth with JN208 and JN209, which can be attributed to modest resistance consistent with the MIC assays (Fig. 6.8B).

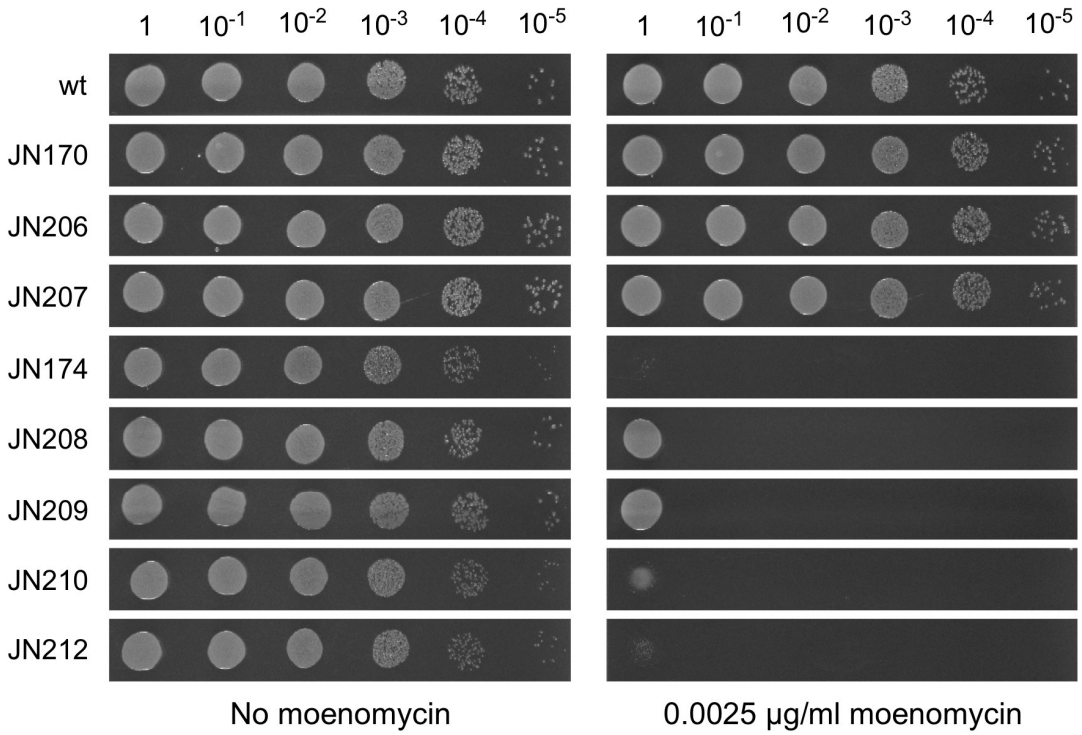

Figure 6.9 Susceptibility of *S. aureus* chelant-resistant mutants to moenomycin on solid media. Strains were grown to an $A_{600\ nm}$ of 0.4, serial 10-fold dilutions performed and 10 µl volumes applied to the surface of LB agar plates in the presence or absence of 0.0025 µg/ml moenomycin. Similar results were obtained in two additional independent experiments.

6.4.2 Susceptibility of *S. aureus* chelant-resistant mutants to other cell wall disrupting agents

Various other agents that target the bacterial cell wall can also be used to probe changes that alter membrane or peptidoglycan composition and structure. These include the non-ionic detergent Triton X-100 and two enzymes that target peptidoglycan directly, lysostaphin and lysozyme. Triton X-100 is widely used as a membrane permeabiliser for cell lysis and the extraction of organelles and membrane proteins (Koley & Bard, 2010). The cellular toxicity of Triton X-100 results from insertion of the polar head of the Triton molecule into the outer leaflet of the lipid

bilayer, disrupting hydrogen bonding within the lipid membrane and compromising its integrity without disrupting protein-protein interactions. In *S. aureus*, Triton X-100 specifically stimulates the release of acylated intracellular lipoteichoic acids (LTAs), inducing bacterial autolysis as a consequence of reduced cross-linking and digestion of peptidoglycan (Komatsuzawa et al., 1994). Lysostaphin is a Class III bacteriocin secreted by *Staphylococcus simulans* biovar *staphylolyticus* in stationary phase to kill competitor staphylococci (Bastos et al., 2010; Schindler & Schuhardt, 1964). It consists of an N-terminal glycyl-glycine endopeptidase domain and C-terminal cell wall targeting domain. The latter recognises pentaglycine bridges in cross-linked peptidoglycan, while the peptidase cleaves between third and fourth glycines (Gründling & Schneewind, 2006), weakening cell wall osmotic stability and inducing lysis (Kusuma et al., 2007). Lysozyme is a muramidase produced by animals in various mucosal tissues as part of the innate immune response. It cleaves peptidoglycan chains between the glycosidic β-1,4-linked residues of NAG and NAM (Bera et al., 2005) producing bacterial cell lysis (Ragland & Criss, 2017). Pathogenic *Staphylococcus* species are relatively tolerant of lysozyme due to O-acetylation of the sugars by OatA which restricts access of lysozyme to the NAG-NAM substrate (Bera et al., 2005, 2006). However, the FDA209P strain appears to lack the *oatA* gene encoding this peptidoglycan O-acetyltransferase.

Each of the three antimicrobial agents were used in turn to investigate differences in the cell wall structure of the *S. aureus* chelant-resistant mutants. Autolysis of whole cells by Triton X-100 was examined by loss of turbidity following the protocol described by Mani et al., (1993). Strains were grown to mid-log phase before addition of Triton X-100 (0.1%) and bacterial cell turbidity monitored over time. The wild-type gradually lost turbidity over several hours as cell autolysis occurred (Fig. 6.10A). A similar trend was observed with the DTPMP-isolated strains (Fig. 6.10A), suggesting their susceptibility to this detergent is comparable to the wild-type, although the Day 15 mutant, JN174, did show some improved resistance. In contrast, all of the EDTA-

isolated mutants showed increased susceptibility to Triton X-100 (Fig. 6.10A), indicating that they have acquired cell wall modifications that more readily expose the bacterial membrane to surfactant attack.

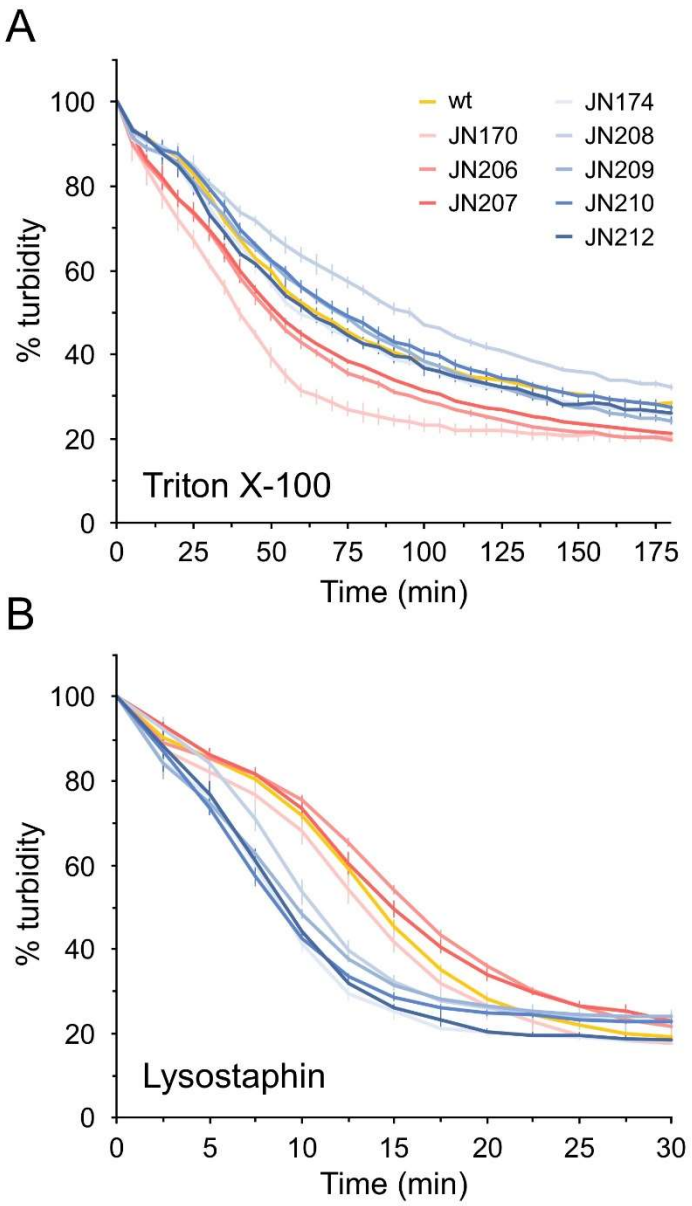

Figure 6.10 Susceptibility of *S. aureus* chelant-resistant mutants to select lytic agents. Cells were grown in LB at 37°C in a shaking incubator to an $A_{650\ nm}$ of 0.6, harvested and washed three times in PBS. Triton X-100 (0.1%) (A) or lysostaphin (2.5 µg/ml) (B) was added to the cell suspension and turbidity monitored at $A_{650\ nm}$ at room temperature. Those isolated in the presence of EDTA (JN170, JN206 and JN207) are highlighted in pink, while those isolated in the presence of DTPMP (JN174, JN208, JN209, JN210, JN212) are in blue. Results represent the mean and standard

deviation of an experiment performed in triplicate. An additional independent repeat produced similar results.

A similar assay was conducted to assess susceptibility to the peptidoglycan endopeptidase lysostaphin (Fig. 6.10B). In contrast to detergent-exposed cells, it was the DTPMP-isolated mutants that displayed increased sensitivity to lysostaphin (Fig. 6.10B). The EDTA-isolated mutants behaved much like the wild-type, although a slight improvement in resistance was evident at later time points with JN206 and JN207 (Fig. 6.10B). The results with Triton X-100 and lysostaphin highlight significant differences between the EDTA and DTPMP isolates, despite the fact that both sets of mutants have acquired dual chelant resistance.

Lysozyme, which cleaves glycosidic bonds between NAG and NAM sugars in peptidoglycan, was applied to the surface of bacterial overlays on agar plates containing the chelant-isolated strains with the wild-type for comparison. *S. aureus* resistance to lysozyme was observed with the wild-type and majority of the mutants, although the lysozyme precipitated on the plate surface makes it more difficult to visualise growth inhibition (Fig. 6.11). However, JN208 and JN209, two of the DTPMP isolates, clearly failed to grow in the vicinity of the spots, a feature especially visible at 12.5 and 25 mg/ml lysozyme (Fig. 6.11). The EDTA-isolated strains, JN170, JN206, and JN207 showed a discrete ring around the edges of the spotted lysozyme (Fig. 6.11), although similar zones of lysozyme precipitation have been seen in related agar diffusion assays (Bera et al., 2006).

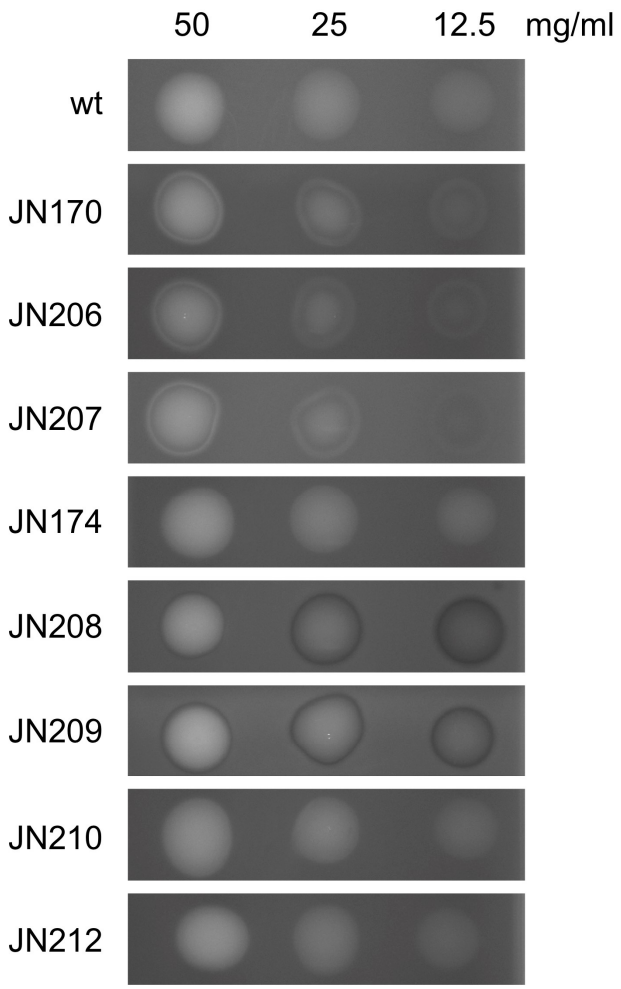

Figure 6.11 Sensitivity of *S. aureus* chelant-resistant mutants to lysozyme. 20 µl of lysozyme at 50, 25, and 12.5 mg/ml was applied to LB agar plates with an overlay of 7.5 ml 0.6% LB agar and 200 µl of an overnight culture of each strain. Plates were incubated for 16 h at 37°C. Results above are representative of three independent experiments.

6.5 Changes in cell surface charge of *S. aureus* chelant-resistant mutants

Mutations affecting cell surface proteins and molecules in the *S. aureus* chelant-isolated strains could alter the net surface charge, potentially repelling the charged phosphonates and carboxylates of DTPMP and EDTA, respectively, to promote chelant tolerance. Bacterial resistance to cationic antimicrobial peptides (CAMPs), for example, can arise by mutations that increase the positive charge at the cell surface

to restrict CAMP binding (Band & Weiss, 2014; Joo & Otto, 2015) . To investigate this possibility, binding of cells to the positively-charged cytochrome *c* and direct measurement of surface electrostatic charge by zeta potential was undertaken with wild-type and chelant-isolated strains.

6.5.1 Cytochrome *c* binding by chelant-resistant *S. aureus* mutants

Cytochrome *c* is a small mitochondrial haemoprotein that plays a vital role in the respiratory chain and also in signalling cell apoptosis (Garrido et al., 2006). Because of its net positive charge and distinctive red colour, it can be used to monitor the net surface charge of cells in a simple photometric assay (Peschel et al., 1999). The assay relies on the fact that cells that are more negatively charged will bind more of the available cytochrome *c*. As bacterial cells are pelleted by centrifugation they remove cytochrome *c* from the solution, reducing the amount of colour detected.

Cells from wild-type and chelant-resistant mutants were mixed with cytochrome *c*, subjected to centrifugation and the supernatant assayed for the presence of pigment. The wild-type cells removed approximately half of the cytochrome *c* from solution in keeping with its negative surface charge (Fig. 6.12A). Remarkably, almost all of the cytochrome *c* was removed from solution when mixed with any of the three EDTA-selected mutants (Fig. 6.12A). The results suggest that these strains, JN170, JN206 and JN207, have a considerably more negatively-charged surface than the wild-type. A similar effect, if not quite so marked, was observed with two of DTPMP-isolated mutants, JN208 and JN209 (Fig. 6.12A). The remainder of the DTPMP strains (JN174, JN210 and JN212) behaved much like the parent strain (Fig. 6.12A), suggesting that the acquisition of a negatively-charged outer surface charge is not essential for the development of chelant resistance.

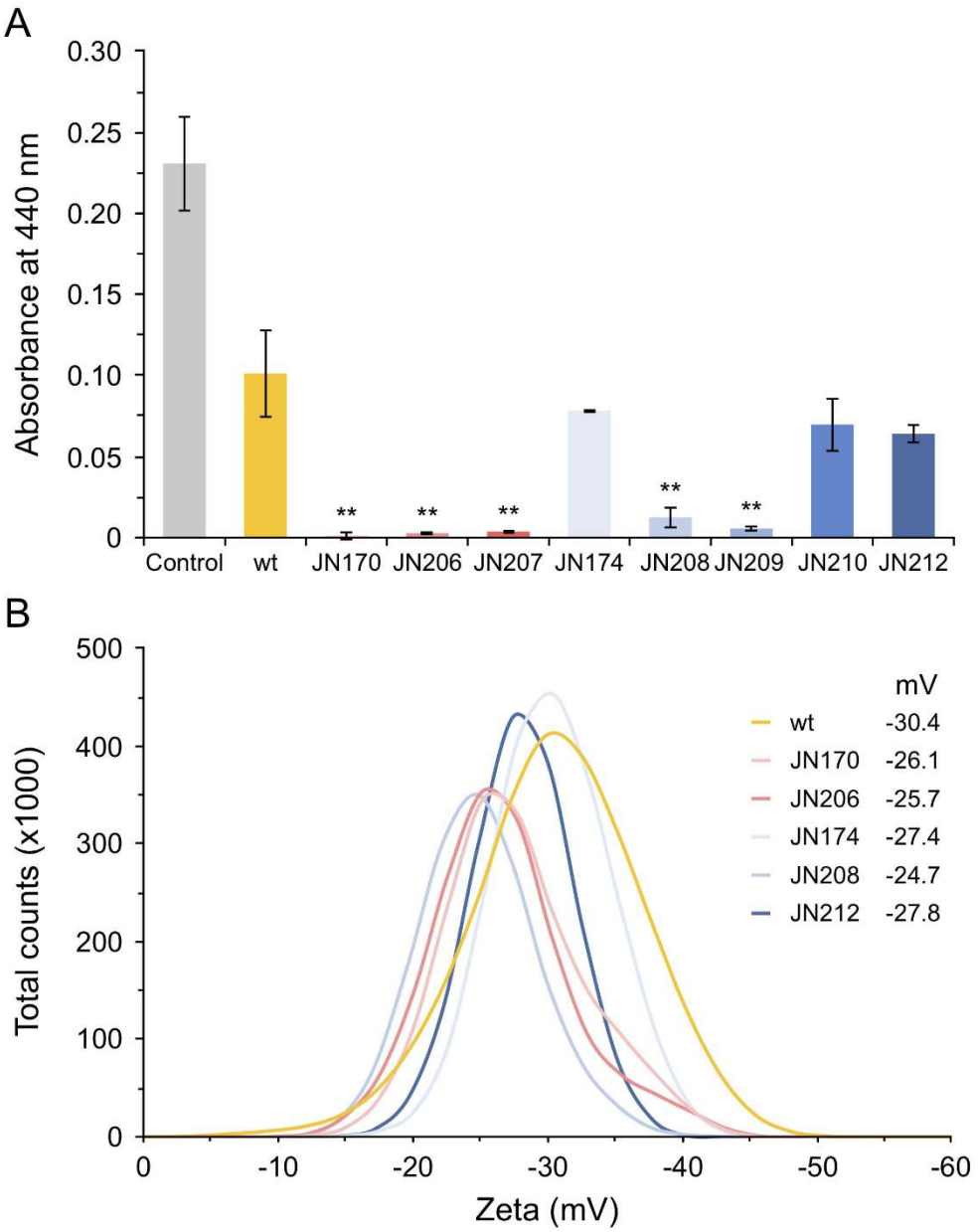

Figure 6.12 Changes in cell surface charge in *S. aureus* chelant-resistant mutants. (A) Cytochrome *c* binding assay. Cells were grown in LB at 37°C in a shaking incubator to an $A_{600\ nm}$ of 1, harvested and washed three times in 20 mM MOPS buffer pH7. Concentrated cells were normalised to the same optical density and 5 mg/ml cytochrome *c* added. Cells were incubated at room temperature for 15 min, pelleted and the supernatant measured at $A_{440\ nm}$ to detect unbound cytochrome *c*. The results are the mean and standard deviation of an experiment performed in triplicate. The student t-test was used to compare mutant strains to the wild-type; *p<0.5, **p<0.01. A second independent experiment showed similar results. (B) Zeta potential analysis. Cells were grown in LB at 37°C in a shaking incubator at 150 rpm for 16 h, harvested and washed three times in 0.5 mM sodium phosphate pH7 buffer.

Cells were adjusted to give an $A_{600\ nm}$ of 0.4 before measuring the zeta potential. Those isolated in the presence of EDTA (JN170, JN206 and JN207) are highlighted in pink, while those isolated in the presence of DTPMP (JN174, JN208, JN209, JN210 and JN212) are in blue. The results shown are the average of 20 measurements. An independent experiment yielded a similar pattern of results.

6.5.2 Zeta potential of chelant-resistant *S. aureus* mutants

Measurement of zeta potential allows a more quantitative assessment of the cell surface charge of bacterial species (Ayala-Torres et al., 2014; Halder et al., 2015). We therefore examined a smaller subset of the mutants to validate the changes in cell surface charge indicated by the cytochrome *c* assay (Fig. 6.12B). The zeta potential is the electric potential of a charged particle at the solid-liquid interface (Wilson et al., 2001). The results show that the wild-type is negatively charged with an average zeta potential of -30.4 mV (Fig. 6.12B), similar to the -35.6 mV determined in other studies with *S. aureus* MTCC 96 (Halder et al., 2015). In contrast to results from the cytochrome *c* assay, the two EDTA-isolated mutants (JN170 and JN206) and the DTPMP isolate (JN208) displayed a more positive charge relative to the wild-type (Fig. 6.12B). JN174 and JN212 behaved more like the wild-type, although they also showed a slight increase in zeta potential (Fig. 6.12B). These results are the inverse of those observed with cytochrome *c*, suggesting a greater positive rather than a greater negative charge for the respective strains.

6.6 Changes in peptidoglycan structure in *S. aureus* chelant-resistant mutants

Peptidoglycan monomers are synthesized as lipid-linked precursors (lipid II) which are transported across the cytoplasmic membrane before being inserted into the sacculus network by PBPs (Egan et al., 2020). In *S. aureus*, important modifications to lipid II include (i) the addition of the pentaglycine branches by amino acid transferases and (ii) the amidation of glutamic acid by the aminotransferase MurT/GatD to form glutamine (Turner et al., 2014). The latter steps of peptidoglycan

biosynthesis are catalysed by PBPs which are essential for the manufacture of a functional cell wall. Of the four PBPs in *S. aureus*, only PBP1 and PBP2 are essential; the function of PBP3 remains largely unknown, while PBP4 plays an important role in the synthesis of highly cross-linked peptidoglycan, and may also be important in β-lactam resistance in community-acquired MRSA (Reed et al., 2015). PBP2 has both transglycosylase and transpeptidase activities required for elongation of glycan chains and formation of peptide bonds, respectively (Turner et al., 2014). One of the characteristics of staphylococcal peptidoglycan is its high degree of cross-linking with up to 90% of its muropeptides linked to adjacent glycan chains in the peptidoglycan mesh (Loskill et al., 2014). Alongside glycan strand length, peptidoglycan cross-linking is often assessed by examining the ratios of dimers, trimers and multimers as a percentage of all muropeptides.

Since all of the chelant-resistant mutants carry mutations in PBP2, the degree of peptidoglycan cross-linking was examined in selected strains in comparison with the parental wild-type (Fig. 6.13A). All of the mutants tested showed a significant reduction in cross-linking relative to the wild-type, with the DTPMP-isolated strain JN208 showing the greatest reduction in cross-linked oligomers larger than trimers (Fig. 6.13B). The large bulge in higher oligomers seen with the wild-type is much reduced in the chelant-resistant strains and these mutants showed a corresponding increase in the proportion of monomer, dimer and trimer species (Fig. 6.13A). Given that the mutations in PBP2 are within or in the vicinity of the glycosyltransferase domain rather than the transpeptidase, this difference is consistent with a reduction in peptidoglycan chain length. It is interesting that EDTA-isolated strains, which carry the same Leu53Phe substitution in the transmembrane helix of PBP2, showed a similar defect as the DTPMP mutants that carry three different mutations in the glycosyltransferase active site (Fig. 6.13B). This indicates that all of the PBP2 mutations give rise to equivalent phenotypes with potential benefits for improved metal uptake or prevention of chelant binding or accessibility.

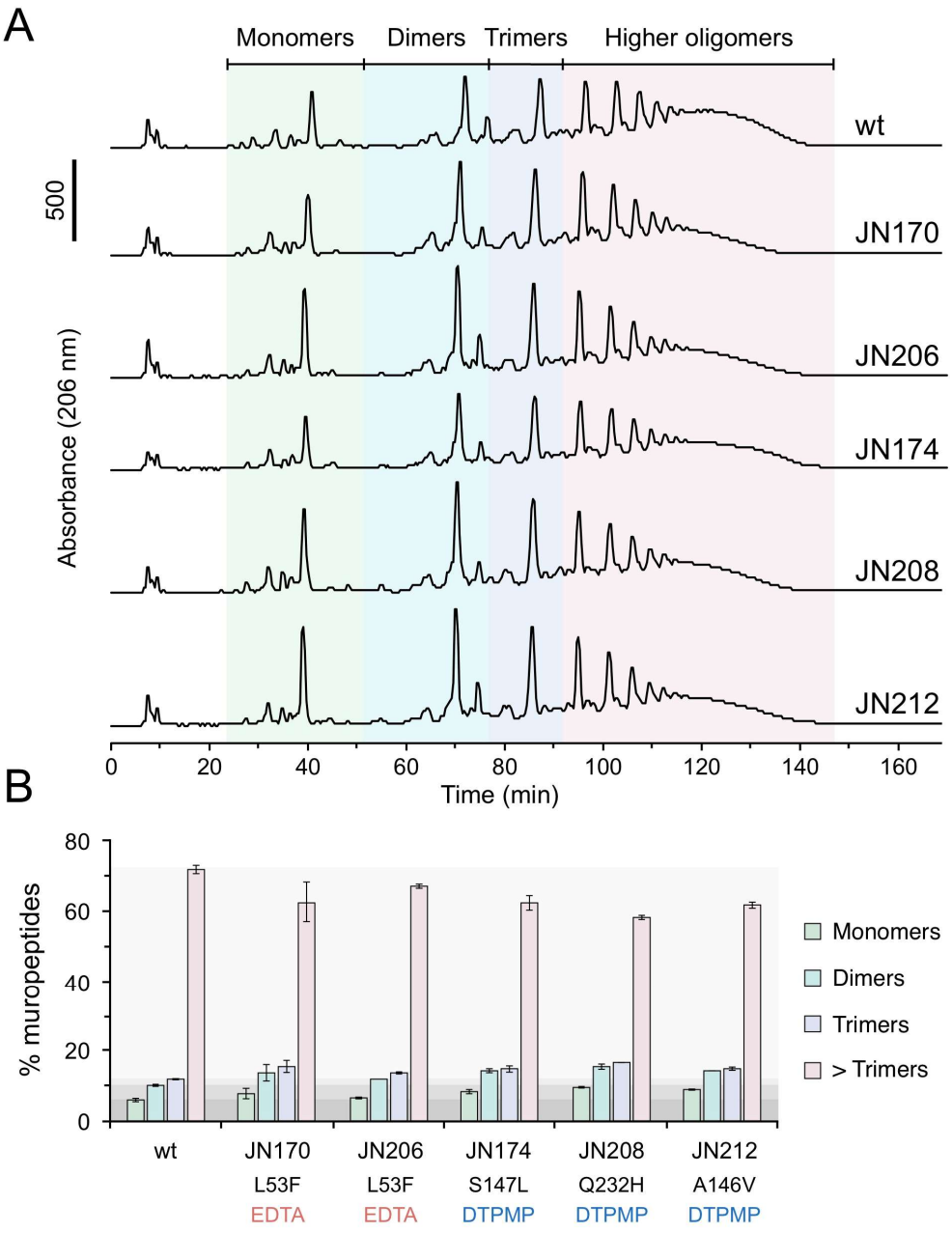

Figure 6.13 Peptidoglycan cross-linking in *S. aureus* chelant-resistant mutants with substitutions in PBP2. (A) Peptidoglycan from selected mutants was purified as described in the methods section (Chapter 2, Section 2.4.7). The extent of cross-linking was determined by analysis of muropeptides by high performance liquid chromatography. A representative data set is shown; two independent experiments yielded similar results. (B) The relative proportion of monomer, dimer, trimers and higher oligomers of cross-linked chains in the wild-type and chelant resistant mutants. Results are the mean and standard deviation of two independent repeats.

6.7 *S. aureus* chelant-resistant mutant response to osmotic stress

The cell wall of *S. aureus* is essential for maintenance of osmotic pressure, ensuring the preservation of appropriate concentrations of solutes and preventing cell lysis (Stewart et al., 2005). *S. aureus* has a relatively high salt tolerance in comparison to other bacterial species, even Gram-negatives, mediated through its ability to increase turgor, initially through elevation of intracellular osmolytes, such as potassium and glycine betaine (Stewart et al., 2005). Tolerance also depends on cell wall integrity and alterations in peptidoglycan and teichoic acids have been linked to the capacity of *S. aureus* to withstand osmotic stress. A recent study (Schuster et al., 2020) identified a gene (*SAUSA300_0957*) important for sodium chloride tolerance, which when deleted increased peptidoglycan cross-linking and reduced susceptibility to oxacillin. Significantly, the salt sensitivity of this mutant could be suppressed by amino acid substitutions in the transglycosylase domain of PBP2, restoring peptidoglycan cross-linking to the same level as the wild-type (Schuster et al., 2020). One of the Δ*975* suppressor mutations in PBP2 was Ser147Leu, identical to that found in the DTPMP-resistant strain, JN174 (Fig. 6.4). Like the suppressor mutant (Schuster et al., 2020), JN174 also exhibited a reduction in peptidoglycan cross-linking (Fig. 6.13). The links between PBP2, peptidoglycan cross-linking and osmotic stress, encouraged us to assess the chelant-resistant mutants for their capacity to tolerate high salt concentrations (Fig. 6.14).

The growth of bacteria cultured in standard LB (0.1M NaCl) and high salt LB broth (0.5M NaCl) was examined (Fig. 6.14). The wild-type showed significantly impaired growth in the high salt medium (Fig. 6.14A) and all five of the DTPMP-isolated strains exhibited a similar level of sensitivity (Fig. 6.14D and Appendix, Fig. 9.5). In contrast, all of the EDTA-isolated mutants were much more tolerant of osmotic stress, with JN206 and JN207 growing almost as well in LB containing 0.5M NaCl as the standard LB (Fig. 6.14B-D and Appendix, Fig. 9.5).

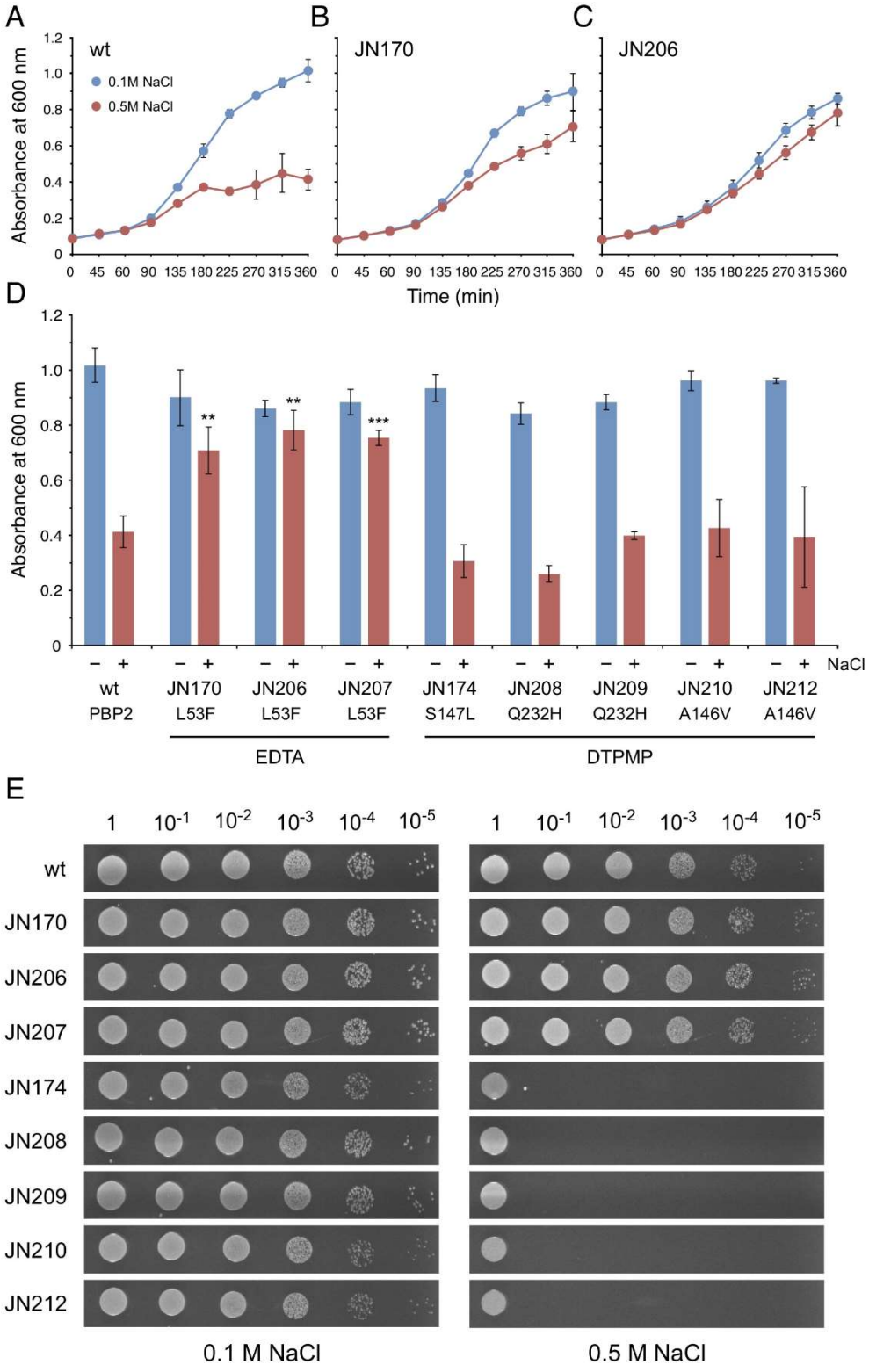

Figure 6.14 Differing responses of *S. aureus* chelant-resistant mutants to osmotic stress. (A-C) Salt tolerance of EDTA-isolated mutants in LB broth. Bacteria were cultivated in LB containing either 0.1 M or 0.5 M NaCl at 37°C in a shaking incubator and growth monitored at $A_{600\,nm}$. Representative growth curves for wild-type, JN170 and JN206 are shown. (D) Growth ($A_{600\,nm}$) of wild-type and chelant-isolated

mutants after 6 h at 37°C in LB with 0.1 M (–) or 0.5 M (+) NaCl. Experiments in A-D are the mean and standard deviation of independent experiments performed in triplicate. The data in (D) are the end point of the growth curves shown in Appendix, Fig. 9.5 and are reproduced here to aid comparisons and summarise the results. These experiments were performed by Rebecca Lee as part of her final year MBiol research project. The student t-test was used to compare mutant strains to the wild-type in either 0.1 or 0.5 M NaCl LB as appropriate; **p<0.01, ***p<0.001. (E) Susceptibility of *S. aureus* mutants to high salt in agar plates. Strains were grown to an $A_{600\ nm}$ of 0.4, serial 10-fold dilutions performed and 10 µl volumes applied to the surface of LB agar plates containing 0.1 or 0.5 M NaCl. Similar results were obtained from 2 additional independent experiments.

The susceptibility of strains to high salt was also investigated using LB agar plates containing 0.1M and 0.5M NaCl (Fig. 6.14E). A slight improvement in growth of the EDTA-isolated mutants in high salt conditions can be observed relative to the wild-type (Fig. 6.14E; compare growth at the 10^{-5} dilution), although it is much less obvious than that seen in the LB broth experiments (Fig. 6.14A-D). In contrast, the DTPMP-isolated strains displayed an extreme salt sensitivity (Fig. 6.14E), which was not apparent in liquid culture (Fig. 6.14D and Appendix, Fig. 9.5). The results from these assays are consistent with mutations in PBP2 resulting in changes in susceptibility to osmotic stress, although other mutations in each of the strains may also contribute to these phenotypes. It is significant that all of the tested chelant-resistant mutants showed a similar reduction peptidoglycan cross-linking, but yet the EDTA and DTPMP isolates behaved differently in response to osmotic stress. Notably, the latter all have mutations in the glycosyltransferase domain of PBP2, whereas the EDTA-isolated strains carry mutations in the transmembrane helix of PBP2.

6.8 Discussion and conclusions

6.8.1 Altered phenotype of chelant-resistant strains

Selected mutants of *S. aureus* grown at sub-MIC levels of EDTA or DTPMP were recovered at 15 and 29 days and had acquired resistance to their respective chelants.

Surprisingly, strains selected against EDTA also showed improved resistance against DTPMP, and vice versa, implying a common mechanism that promotes resistance to both chelants (Fig. 6.1). This tolerance did not extend to four other chelants used in Chapter 4, CHA, FA, HNK or TRO, which retained a similar sensitivity profile as the wild-type (Rebecca Lee, unpublished results). No changes in colony morphology were apparent (Fig. 6.2), although three of the DTPMP mutants displayed a slower rate of growth (Figs. 6.2 and 6.3). The reduced growth was not essential for chelant tolerance and is probably associated with mutations unique to those strains. The two DTPMP-isolated mutants, JN210 and JN212, showed the slowest growth in liquid culture and carry a range of additional mutations (Fig. 6.4). A slower growth rate could be advantageous in providing extended time for metabolic processes and genome maintenance prior to cell division (Lewis, 2007; Mok & Brynildsen, 2018). Protein turnover is reduced at a slower metabolic rate and protein requirements may drop considerably. In slow growing *B. subtilis* cells, for example, only a single protease is needed to maintain cellular function and growth (Gray et al., 2019). The formation of small colony variants (SCVs) in response to antibiotic exposure has been documented in other studies (Johns et al., 2015; Tuchscherr et al., 2016).

6.8.2 The altered cell envelope of chelant-resistant mutants

Genome sequencing of the chelant-resistant mutants identified mutations that were associated with changes in surface proteins, membrane transporters and cell wall metabolism instead of the expected metal uptake systems. The most significant of these were *fnbA*, *pbp2*, *1546* and *arcD* present in all strains (Fig. 6.4). In addition, mutations in *fmtA* were found in all EDTA strains, and *vraF* and *1745* in different pairs of DTPMP isolates cultivated for 29 days (Fig. 6.4). Of these, *fmtA* and *vraF* are likely null mutants, containing premature termination codons at residues 109 and 9, respectively. As a result, a range of cell wall targeting agents were employed to investigate any alterations in the cell envelope of chelant-resistant strains. The

different EDTA and DTPMP isolates are discussed with reference to the mutations present in each strain and how these correlate with the phenotypes observed.

6.8.2.1 EDTA-selected strains

The three EDTA-isolated strains, JN170, JN206 and JN207, showed very similar phenotypic responses and carry a similar suite of mutations. The only major differences were in the slower initial growth rate of JN206 and JN207 (Fig. 6.3) and the slightly higher susceptibility of JN170 to autolysis in the presence of Triton X-100 (Fig. 6.10A). It is not entirely clear what changes are responsible for these differences, although JN170 has additional mutations affecting *sasG2* and 23S rRNA gene expression and a Phe107Tyr substitution in gene *1454* (Fig. 6.4). JN206 and JN207 share a single mutation upstream of tRNA-Ile that is absent from JN170. There are five other mutations carried by all three strains (FnbA Thr510Lys, ArcD Met189Ile, 1546 Thr39Met, FmtA Gln109* and Pbp2 Leu53Phe), several or all of which must contribute to improved chelant tolerance and the other phenotypic changes affecting the cell envelope. The DTPMP-isolated strains share identical mutations in *fnbA*, *arcD* and *1546* but lack a mutation in *fmtA* and although they also have *pbp2* mutations, these are located in the glycosyltransferase catalytic site rather than the adjacent transmembrane helix in EDTA strains (Fig. 6.4 and 6.5).

The *fmtA* mutation is unique to the EDTA isolates and introduces a stop codon in place of Gln109 in the 397-residue protein. This change eliminates the esterase catalytic site, including the conserved SXXK and Y(S)XN motifs, and is therefore likely to constitute a null mutant (Dalal et al., 2019). *S. aureus* lacking *fmtA* displays increased susceptibility to Triton X-100 (Komatsuzawa et al., 1997, 1999; Qamar & Golemi-Kotra, 2012), which fits with the sensitivity observed in EDTA-isolated strains (Fig. 6.10A). Relative to wild-type MRSA, *fmtA* mutants show a reduced MIC with methicillin and other β-lactam antibiotics (Komatsuzawa et al., 1997). In contrast, the EDTA isolates displayed some resistance to third generation cephalosporins,

cefsulodin and cefotaxime, whereas there was no difference in comparison with the parent strain against penicillin G or the second generation cephalosporin, cefoxitin (Fig. 6.6). As with penicillin, cephalosporins are a class of β-lactams that bind the transpeptidase domain of PBPs in order to inhibit peptidoglycan synthesis (Krause et al., 2016; Livermore, 1987). It is possible that the absence of *fmtA* does affect cefsulodin and cefotaxime susceptibility, perhaps by reducing access for these β-lactams, however, the presence of a *pbp2* mutation in these strains may also contribute to the observed resistance.

FmtA is a teichoic acid D-alanine esterase, meaning that Δ*fmtA* mutants possess elevated levels of D-Ala in their wall teichoic acids compared to *fmtA*$^{+}$ strains (Rahman et al., 2016). The positive charge on D-Ala partially masks the negative charge of the polyol-phosphate backbone of teichoic acids, hence *fmtA* cells would be expected to exhibit a more positive external charge. Consistent with the loss of FmtA activity, two of the EDTA strains were tested and found to have a more positive charge following Zeta potential analysis (Fig. 6.12B). However, experiments conducted with cytochrome *c* suggested that EDTA-selected strains were actually more negatively-charged than the wild-type since they removed almost all of the positively-charged protein from solution (Fig. 6.12A). Despite these apparently contradictory findings, it remains possible that both outcomes are actually correct. Zeta potential determines the outer surface charge of the cell at its interface with solution where wall teichoic acids reside and would be expected to be enriched with the positively-charged D-Ala in cells lacking *fmtA*. The additional positive charge here could produce a greater negative charge closer to the cell membrane where cytochrome *c* may preferentially assemble. Alternatively, changes brought about by mutation of PBP2 could increase the negative charge of the peptidoglycan layer and promote cytochrome *c* association. Clearly, the methodology employed in cell surface charge measurements is important and may not always reflect the complexities of the altered Gram-positive envelope. *S. aureus* and *B. subtilis* cells defective in *dlt* operon genes, and as a result

lacking D-Ala modified teichoic acids, produce cells that more readily bind cytochrome *c*, implying an increased negative charge (Peschel et al., 1999; Wecke et al., 1997). The replacement of threonine with a lysine in the surface-exposed fibronectin binding protein, FnbA (Fig. 6.4), adds an additional positive charge that could also influence cell surface charge in EDTA-selected strains.

As mentioned, all three of the EDTA isolates also carry a mutation in the transmembrane helix that secures PBP2 to the cytoplasmic membrane (Fig. 6.5). This mutation could alter the positioning of the PBP2 glycosyltransferase domain to reduce the efficacy of glycan polymer synthesis, which might account for the reduced peptidoglycan crosslinking evident in EDTA mutants (Fig. 6.13) due to shorter chains being produced. The resulting cells may have a reduced cell wall thickness, although the integrity and overall structure may not be compromised as cells do not show significantly increased susceptibility to the peptidoglycan-targeting lysostaphin (Fig. 6.10B) or lysozyme (Fig. 6.11). Although there was a slight increased sensitivity to vancomycin (Fig. 6.8A), none of the EDTA-selected mutants showed increased sensitivity to moenomycin (Fig. 6.8B). Similarly, the Leu53Phe substitution in PBP2 could be responsible for the improved salt tolerance of these mutants (Fig. 6.14) as the extent of peptidoglycan cross-linking has been linked to cellular osmostability and mutations in PBP2 (Schuster et al., 2020). However, it should be noted that *fmtA* mutants also show reduced peptidoglycan cross-linking (Komatsuzawa et al., 1999). The Thr39Met substitution in the uncharacterised gene *1546* present in these strains (Fig. 6.4) could also potentially affect salt tolerance. The *1546* product is predicted to have two membrane spanning helices, one of which resembles the short polypeptide KdpF involved in potassium uptake (Gründling, 2013; Huang et al., 2017). Potassium is an osmolyte that aids osmotic stress survival (Gründling, 2013), however, further work is needed to establish the precise function of the *1546* product. Interestingly, one of the DTPMP mutants (JN208) has a substitution mutation in a transporter (*2055*, Ala131Val); Fig. 6.4), that imports glycine betaine, another potent osmolyte

(Graham & Wilkinson, 1992). It is unclear what role the *arcD* mutation fulfils in the phenotypes examined, although effects on charge are a possibility. In *S. aureus, arcD* encodes an arginine-ornithine antiporter and its inactivation completely inhibits uptake of arginine (Zhu et al., 2007) and also reduces the capacity to tolerate acidic conditions in *Streptococcus suis* (Fulde et al., 2014). Interestingly, *S. aureus* surface charge can be reduced through incorporation of L-lysine into membrane phosphatidylglycerols, a process mediated by MprF (FmtC) (Peschel et al., 2001). Mutations in *fmtC,* or *lysC* involved in arginine biosynthesis, result in an increased negative surface charge and enhanced susceptibility to antibiotics, including vancomycin and moenomycin (Nishi et al., 2004).

6.8.2.2 DTPMP-selected strains

The five DTPMP-isolated mutants, JN174, JN208, JN209, JN210 and JN212, generally showed similar phenotypic responses, however, there were some clear differences between the JN208/209 pairing and JN174, JN210 and JN212. Some of these can be linked to specific mutations in these strains. All of the DTPMP strains carry the same *fnbA*, *1546* and *arcD* mutations, as do the EDTA isolates (Fig. 6.4). However, the only additional shared mutation in JN208/209 absent from all others is the stop codon in *vraF*. JN210/212 also have additional shared missense mutations in *1745* (a possible arginine ABC transporter) and *614* (an AraC family transcriptional regulator) and upstream mutations affecting *sasG2*, *qoxA* and *r0012* (Fig. 6.4). While all five DTPMP mutants have substitutions in the glycosyltransferase domain of PBP2, these affect different amino acids between JN174 and the other two pairs of strains isolated at Day 29 (Fig. 6.5).

In terms of growth, JN210 and JN212 are the only DTPMP strains that exhibit significantly reduced growth in liquid culture compared to the wild-type (Fig. 6.3). Presumably, the mutations associated with these two strains mentioned above must be responsible for this effect. This slow growth phenotype was mirrored on agar

plates, although JN174 additionally showed much slower colony growth under these conditions (Fig. 6.2). JN174, JN210 and JN212 all behaved similarly in response to all other treatments suggesting that the core mutations in *fnbA*, *1546, arcD* and *pbp2* are primarily responsible for the behaviour of these strains.

JN174, JN210 and JN212 showed little or no significant elevated susceptibility to penicillin G and the three other cephalosporins in MIC assays (Fig. 6.6), although they proved more sensitive to penicillin G and cefoxitin, but not cefotaxime, in experiments with antibiotic discs (Fig. 6.7). Since these related antibiotics target transpeptidation, it seems likely that the mutations in these strains (A146V and S147L), located in the same conserved motif (Fig. 6.5C), may be responsible for the increased susceptibility. These three DTPMP mutants also show increased susceptibility to vancomycin and moenomycin (Fig. 6.8 and 6.9), also in keeping with mutations affecting PBP2. All of the DTPMP strains displayed greater sensitivity to lysostaphin (Fig. 6.10B) and high salt (Fig. 6.14) than the wild-type, but no increased susceptibility to Triton X-100 (Fig. 6.10A). JN174, JN210 and JN212 were also unaffected by lysozyme (Fig. 6.11). No major differences in surface charge were detected between these mutants and the wild-type (Fig. 6.12) but the two strains tested, JN174 and JN210, both showed reduced peptidoglycan cross-linking (Fig. 6.13). Interestingly, an equivalent of S147L (S132A) in the *S. aureus* MGT glycosyltransferase (Fig. 6.5C) also has a defect in peptidoglycan cross-linking (Huang et al., 2012). An S147L mutation in PBP2 is also linked to salt tolerance and reduced crosslinking from another study (Schuster et al., 2020).

In contrast, JN208 and JN209, which have an additional mutation that eliminates *vraF*, showed much higher sensitivity to penicillin G and the three cephalosporins (Fig. 6.6 and 6.7) and additional susceptibility to lysozyme (Fig, 6.11). They also displayed improved binding of cytochrome *c* and a reduced negative charge in zeta potential assays (Fig. 6.12), behaviour that more closely resembles the EDTA-isolated strains. The differences between the two sets of DTPMP-selected strains can

be attributed to the mutations affecting *pbp2* and *vraF*. JN208 and JN209 have a Gln232His substitution mutation in PBP2 that is located adjacent to the conserved motif V (Fig. 6.5C). This mutated residue lies adjacent to a conserved proline (P231) that resides within a cleft in PBP2 where the glycan chain is positioned during polymerisation (Lovering et al., 2008). Another surface-exposed proline (P234) when mutated to glutamine produces moenomycin resistance and reduced glycan chain length (Rebets et al., 2014). The increased sensitivity of JN208 and JN209 to β-lactams could be due to improved binding at the PBP2 transpeptidase active site as a result of the Q232H mutation. Alternatively, the absence of *vraF*, and the antibiotic resistance pump it encodes, may allow higher concentrations of the β-lactams to accumulate. The VraFG ABC transporter participates in the export of antibiotics and bacteriocins and is regulated by the GraRS sensory system (Meehl et al., 2007). GraRS and VraFG are overexpressed in vancomycin-intermediate *S. aureus* (VISA) strains and mutations in *graR* and *vraG* confer hypersensitivity to vancomycin and polymixin B (Meehl et al., 2007). JN208 and JN209 are sensitive to vancomycin but no more so than the other three DTPMP strains, possibly linking vancomycin sensitivity to the PBP2 glycosyltransferase mutations in these strains. Significantly, *vraF* deletion in isolation does not significantly alter the zeta potential or D-alanine incorporation of this mutant relative to the wild-type (Vestergaard et al., 2017). This suggests that the altered cell surface charge in JN208 and JN209 (Fig. 6.12), is primarily due to the specific alteration in PBP2 rather than *vraF*.

The lysozyme-susceptibility of JN208 and JN209, but not any of the other mutants, implies additional alterations in the cell wall of these strains that improve enzyme access to the β-1,4 glycosidic bond that links adjacent NAG-NAM subunits. C-type lysozymes can also insert into membranes, and form pores in negatively charged bacterial membranes, thereby acting in a similar manner to cationic antimicrobial peptides (CAMPs) (Herbert et al., 2007; Ragland & Criss, 2017). For this reason, genes involved in resistance to CAMPs, such as *vraFG* (Li et al., 2007), and

alterations in cell surface charge (Joo & Otto, 2015) are both implicated in the susceptibility of these mutants to lysozyme.

The mutations specifically in the glycosyltransferase domain in PBP2 may also account for the increased lysostaphin sensitivity of the DTPMP mutants (Fig. 6.10B). The EDTA strains do not show this susceptibility and also have a mutation that affects peptidoglycan crosslinking but it is not located in the glycosyltransferase active site (Fig. 6.5). Lysostaphin specifically cleaves the pentaglycine bridges in the *S. aureus* cell wall (Schindler & Schuhardt, 1964) and the reduced number of cross bridges in peptidoglycan may have a greater impact on these mutants than it does on the wild-type. EDTA-selected strains also have reduced peptidoglycan cross-linking but the charge differences associated with the additional loss of *fmtA* may affect the phenotypes observed. Increased lysostaphin sensitivity is evident in *S. aureus sigB* mutants which possess thinner cell walls (Bastos et al., 2010). The PBP2 glycosyltransferase mutations in the DTPMP-isolated mutants could result in a similarly reduced thickness in the peptidoglycan layer, thus increasing susceptibility to lysostaphin (Fig. 6.10B) and the majority of the cell-wall targeting antibiotics (Fig. 6.7-6.9). Improved binding of moenomycin, and perhaps also the glycan chain, in the three glycosyltransferase mutants may also account for the extreme susceptibility to this antibiotic (Fig. 6.9). Tighter binding to lipid II precursors could potentially reduce the efficiency of peptidoglycan synthesis and explain the reduced cross-linking observed in these strains. In keeping with this, moenomycin-resistant mutants possessed longer peptidoglycan chains than their more susceptible MRSA COL parent strain and also showed increased tolerance of vancomycin (Nishi et al., 2003).

The alterations in cell surface charge and cell wall structure uncovered in this chapter show some correlation with increased resistance to EDTA and DTPMP. Chelating agents are negatively charged at physiological pH and have high affinities for positively charged metal ions. It may be that cells with a more negative net surface charge are more capable of repelling these two chelating agents, thereby minimising

their impact. However, those charges will be neutralised if chelants bind their preferred metals before they reach the cell surface. Alternatively, the more accessible or thinner cell wall, as exemplified by differing susceptibilities to antibiotics and cell wall-targeting agents, may make metal acquisition easier. A combination of chelant binding to wall teichoic acids *via* a more positive charge in EDTA-selected strains, combined with a more negative charge at the cell surface attracting essential metals could promote chelant resistance. In DTPMP-selected strains the effects are probably different, although a thinner layer of peptidoglycan may increase cell permeability and be sufficient to promote improved metal uptake. Such effects may explain the increased sensitivity of these strains to high salt. Overall, the results reiterate and further reveal the importance of cell wall architecture and surface charge in tolerating antibiotics, osmotic stress and chelating agents. Further work is needed to identify and characterise the principal factors responsible for EDTA and DTPMP resistance and whether improved metal uptake is indeed a feature of these mutant strains.

6.9 Future directions

The experiments described in this chapter highlight the importance of cell surface charge and cell wall structure in resistance to the respective carboxylate and phosphonate chelating agents, EDTA and DTPMP. A relatively small number of genes are linked to improved chelant tolerance, however, additional experiments would be helpful in defining the contribution of each mutant and how they function in concert.

The reduced muropeptide cross-linkage experiments (Fig. 6.13) indicate that there may be changes in the cell wall thickness which could be readily visualised by transmission electron microscopy (TEM). Cell surface charge could be investigated further by assessing sensitivity to cationic antimicrobial peptides, given their requirement for negatively charged membrane targets (Joo & Otto, 2015; Peschel et al., 1999). Sensitivity of the mutants to additional antibiotics with intracellular targets

could by employed as a means to probe alterations in cell permeability. For example, several of the chelant-resistant strains show increased susceptibility to kanamycin and tetracycline which target the 30S subunit of the ribosome (data not shown). Cell permeability could be further probed with NPN as in Chapter 5 or by monitoring the uptake of propidium iodide. A more quantitative assay for *S. aureus* cell lysis mediated by lysozyme (Bera et al., 2006) could be employed to validate the sensitivities observed here. In addition, the zeta potential and cytochrome *c* assays are worth repeating to validate the findings on cell surface charge. Different buffer conditions can affect zeta potential measurements (Ng & Ting, 2017), although the results presented here likely do reflect genuine differences in cell surface charge.

Overproduction, purification and characterisation of PBP2 proteins carrying the four mutations identified in this study would provide insight into any defects in glycosyltransferase or transpeptidase activities *in vitro* (Egan et al., 2015). The effect of chelants, antibiotics and metals on PBP2 activity could be informative in understanding the phenotypes observed in each of the chelant-resistant mutants. Fluorescent probes can also be used for this purpose, as in previous work with *Streptococcus pneumoniae* (Kocaoglu et al., 2015). Transferring the *pbp2* alleles to an *S. aureus* wild-type would allow the significance of the different mutations to be examined in the absence of the other mutations present in the chelant-selected strains. This would be particularly helpful in distinguishing the contribution of *fmtA* and *pbp2* mutations in EDTA-selected strains. The availability of similar mutations in the glycosyltransferase domain from the salt tolerance study (Schuster et al., 2020) is another option; it would be valuable to assess whether the other mutations isolated in PBP2 also confer chelant resistance.

The effect on metal starvation of *S. aureus* of EDTA and DTPMP has yet to be determined. It may be that these two chelants deprive cells of the same metals as was found with *P. aeruginosa* (Chapter 4), in contrast to the results obtained with *E. coli* (Paterson et al., 2022). Furthermore, it is also not known whether the

modifications in chelant-resistant strains allow these cells to acquire the metals needed for growth. It is possible that *S. aureus* may be able to import other metals to compensate for those which are depleted in the presence of chelating agents, as in *E. coli* when manganese pathways are utilised under conditions of iron starvation (Kaur et al., 2017; Lisher & Giedroc, 2013). It is unclear whether such alternative pathways exist in *S. aureus*, but examining alterations in metal concentrations in response to chelating agents may begin to reveal more about the mechanisms through which chelants inhibit bacterial growth in *S. aureus*. As with *P. aeruginosa*, monitoring the expression levels of key metal uptake pathway components by qPCR or RT-PCR might be a better approach to assessing cellular responses to different chelating agents in terms of metal starvation.

7 Phenotypic analysis of selected *S. aureus* USA 300 mutants

7.1 Introduction

In Chapter 6, chelant-resistant mutants of the *S. aureus* (MSSA) strain FDA209P were isolated by repeated culture at sub-MIC levels of either EDTA or DTPMP. Genome sequencing of the selected strains identified a relatively small number of mutations that affected genes primarily involved in peptidoglycan synthesis, teichoic acid modification and various membrane bound proteins and transporters. Exposure of the mutant strains to a range of cell wall-targeting agents and antibiotics, alongside other analyses, confirmed that changes in cell surface charge and alterations in peptidoglycan architecture had occurred. Although, many of the phenotypes could be assigned to specific mutations, interpretation of the findings was complicated by the presence of multiple mutations in each strain. Ideally, these mutations would be studied separately, however, generating such strains is not necessarily straightforward. However, the availability of a collection of insertion mutants in *S. aureus*, the Nebraska Transposon Mutant Library (Fey et al., 2013), means that single genes of interest can be studied. The library consists of 1,952 strains, each containing a transposon insertion within a non-essential gene of the epidemic community-associated methicillin-resistant *S. aureus* (CA-MRSA) isolate USA300. Selected mutants, alongside the parental wild-type strain, were kindly provided by Dr Kevin Waldron (Biosciences Institute, Newcastle University). We chose six mutants of greatest interest and these are listed in Table 7.1. In the previous chapter, missense mutations in *fnbA*, *arcD* and *1546* were found in all eight chelant-resistant strains (Chapter 6, Fig. 6.4). Truncated proteins resulted from nonsense mutations in *fmtA* (in all EDTA-selected mutants) and *vraF* (in the DTPMP isolates, JN208 and JN209). Lastly, a substitution in the *1745* gene product was only found in JN210 and JN212, both DTPMP-selected strains. The *pbp2* gene is essential so insertions in this gene

were unavailable from the USA300 strain collection. For simplicity, the gene names assigned in the *S. aureus* FDA209P strain are used henceforth, instead of the numbers for the equivalent genes in USA300.

Table 7.1 USA300 mutants selected for further study

FDA209P gene	USA300 gene	Protein identity (%)	FDA209P mutation	Known or predicted function
arcD	*2568*	99	Met189Ile	Arginine permease
fmtA	*959*	100	Gln109*	Teichoic acid D-Ala esterase
fnbA	*2441*	84	Thr510Lys	Fibronectin-binding protein A
1745	*1807*	100	Pro157Leu	Arginine ABC transporter
vraF	*647*	100	Gln8*	ABC drug transporter
1546	*1607*	100	Thr39Met	Unknown, membrane bound

S. aureus genes from strain FDA209P are annotated with the prefix SAFDA_, those from USA300 with SAUSA300_. The percentage identity between the relevant FDA209P and USA300 gene products is shown to highlight their similarity. An asterisk denotes a stop codon.

7.2 Phenotypic analysis of USA300 mutants

The CA-MRSA USA300 mutants listed in Table 7.1 were initially examined for their potential to confer resistance to EDTA and DTPMP. Susceptibility to antibiotics that target the cell wall were examined next, followed by sensitivity to lysostaphin and osmotic stress. Finally, changes in cell surface charge were assessed by utilising the cytochrome *c* binding assay. These experiments allowed a comparison with the data presented in Chapter 6 to further evaluate the contribution of specific genes in chelant resistance and phenotypic changes affecting the *S. aureus* cell envelope.

7.2.1 Susceptibility of USA300 mutants to EDTA and DTPMP

All eight of the *S. aureus* FDA209P strains isolated following exposure to low levels of EDTA and DTPMP had acquired improved resistance to both chelants (Chapter 6, Fig. 6.1). The six USA300 insertion mutants were therefore examined for their susceptibility to these two chelating agents (Fig. 7.1). Four of the USA300 mutants showed improved growth relative to the wild-type strain at 0.125 mM EDTA (Fig. 7.1A). These were *fmtA*, *1745*, *1546* and *vraF*, although there was some variability in growth of the latter. In comparison with the wild-type, these same four strains also showed significantly improved resistance to DTPMP over a range of concentrations (Fig. 7.1B). The *arcD* and *fnbA* mutants behaved much like the wild-type strain when exposed to EDTA (Fig. 7.1A) or DTPMP (Fig. 7.1B), suggesting that elimination of these genes does not help in chelant tolerance.

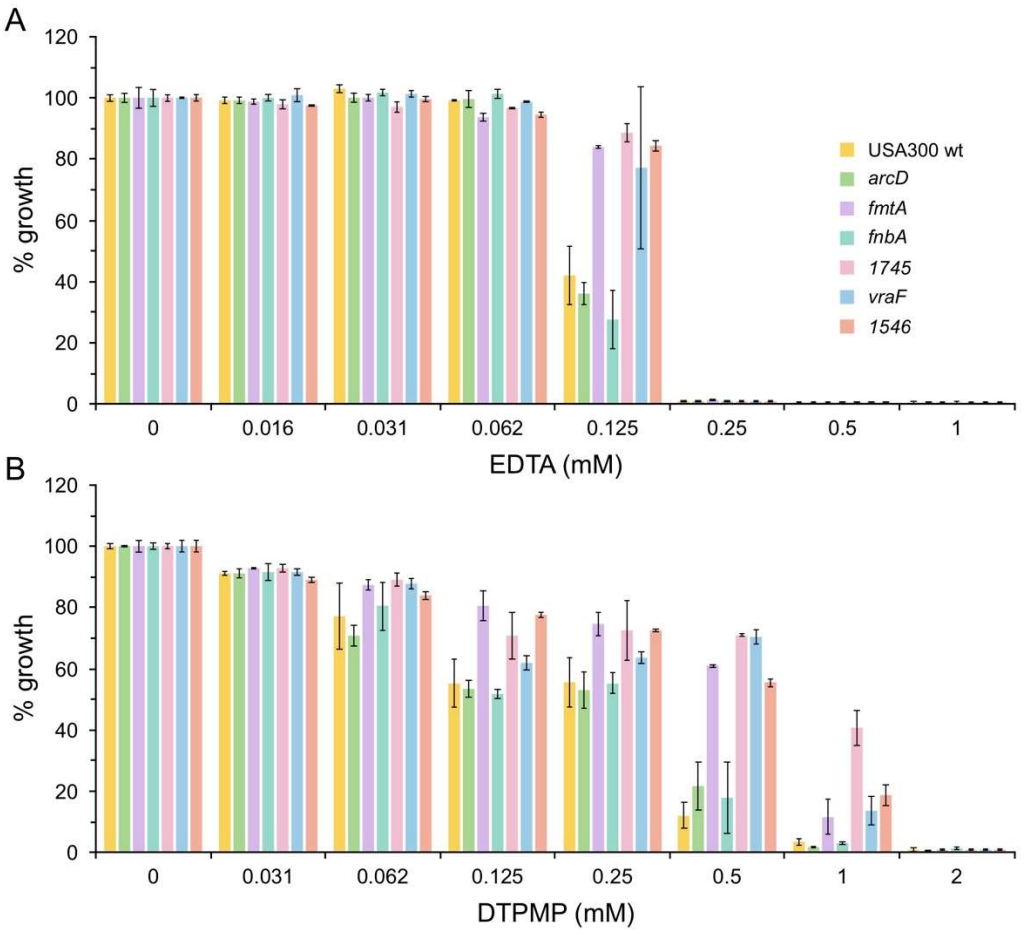

Figure 7.1 Susceptibility of selected *S. aureus* USA300 mutants to EDTA and DTPMP. Two-fold serial dilutions of EDTA (A) or DTPMP (B) were mixed with each strain and incubated at 37°C with shaking at 150 rpm for 16 h. Growth was measured at $A_{600\ nm}$ at the end point and normalised against controls without treatment to give the percentage growth. Results represent the mean and standard deviation of an independent experiment performed in triplicate. Two additional independent repeats produced similar results.

7.2.2 Susceptibility of USA300 mutants to vancomycin and moenomycin

The FDA209P DTPMP isolates displayed increased susceptibility to vancomycin (Chapter 6, Fig. 6.8A), and were highly susceptible to moenomycin, in contrast to EDTA-selected strains (Chapter 6, Fig. 6.8B). The four USA300 mutants that demonstrated improved chelant tolerance, *fmtA*, *1745*, *1546* and *vraF* (Fig. 7.1), all showed increased sensitivity to vancomycin (Fig. 7.2A). Conversely, three of these mutants, *1745, vraF* and *1546,* proved more resistant to moenomycin than the wild-type (Fig. 7.2B). The *fmtA* strain was perhaps slightly more sensitive to moenomycin relative to the wild-type (Fig. 7.2B). As in the EDTA and DTPMP MIC assays (Fig 7.1), the *arcD* and *fnbA* mutants behaved much like the wild-type following exposure to vancomycin (Fig. 7.2A) and moenomycin (Fig. 7.2B).

The experiments were repeated with moenomycin incorporated into agar plates as in Chapter 6, Figure 6.9. Again, *arcD* and *fnbA* behaved liked the wild-type, although there appeared to be a slight improvement in growth compared with the wild-type (Fig. 7.3). In these experiments, *fmtA*, *1745*, *1546* and *vraF* all grew much better than the wild-type in the presence of moenomycin, with *1745* and *vraF* displaying the greatest improvement in growth (Fig. 7.3). The enhancement in moenomycin tolerance with *fmtA* in agar plates was not evident in liquid media (Fig. 7.2B), although there was consistency in resistance with *1745, vraF* and *1546* between the two assays.

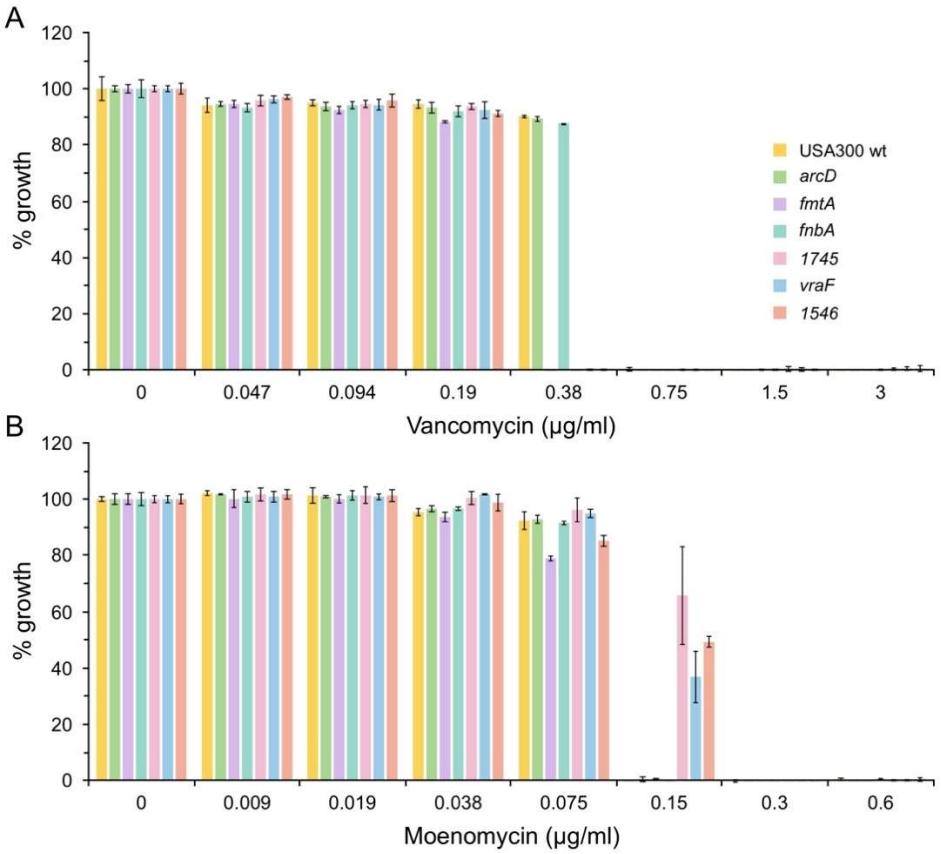

Figure 7.2 Susceptibility of selected *S. aureus* USA300 mutants to vancomycin and moenomycin. Two-fold serial dilutions of vancomycin (A) or moenomycin (B) were mixed with each strain and incubated at 37°C with shaking at 150 rpm for 16 h. Growth was measured at $A_{600\ nm}$ at the end point and normalised against controls without treatment to give the percentage growth. Results represent the mean and standard deviation of an independent experiment performed in triplicate. Two additional independent repeats produced similar results.

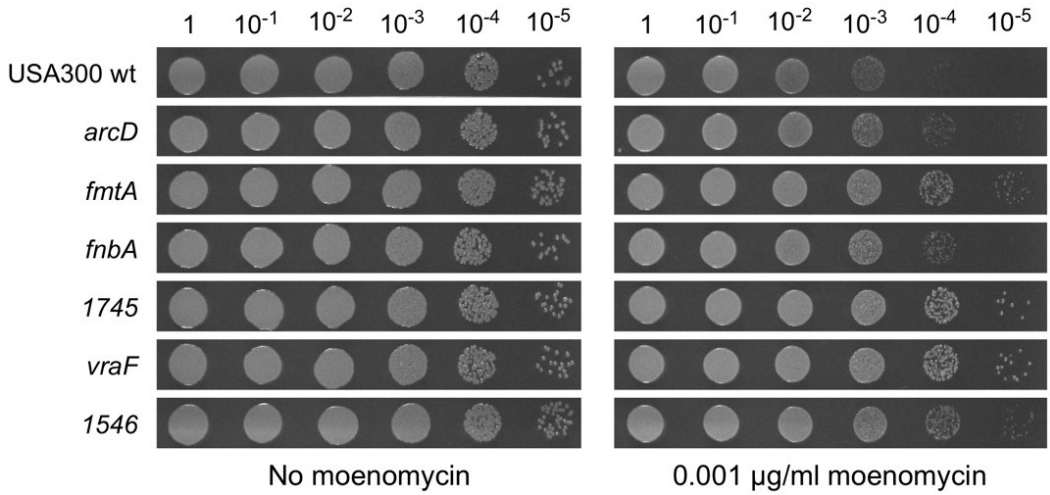

Figure 7.3 Susceptibility of selected *S. aureus* USA300 mutants to moenomycin. Strains were grown to an $A_{600\ nm}$ of 0.4, serial 10-fold dilutions performed and 10 µl volumes applied to the surface of LB agar plates in the presence or absence of moenomycin. Similar results were obtained in two additional independent experiments.

7.2.3 Susceptibility of USA300 mutants to lysostaphin

In the previous chapter, the EDTA-selected strains behaved much like the wild-type following exposure to lysostaphin, while all of the DTPMP isolates displayed much greater susceptibility (Chapter 6, Fig. 6.10B). These experiments were repeated with the USA300 mutants (Fig. 7.4). Most of the mutants produced a similar sensitivity profile as the wild-type in response to exposure to this peptidoglycan endopeptidase. However, *fmtA* and *1546* exhibited a small increased susceptibility to lysostaphin after about 60 minutes incubation (Fig. 7.4).

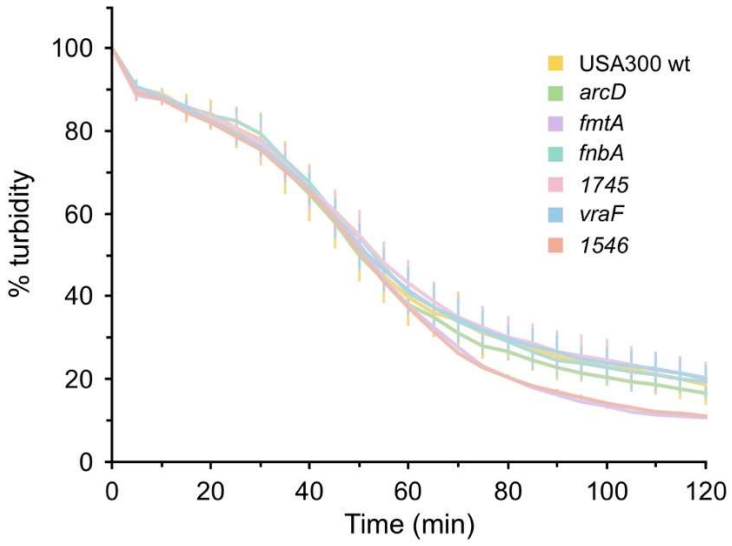

Figure 7.4 Susceptibility of selected *S. aureus* USA300 mutants to lysostaphin. Cells were grown in LB at 37°C in a shaking incubator to an $A_{650\ nm}$ of 0.6, harvested and washed three times in phosphate-buffered saline (PBS). Lysostaphin (2.5 µg/ml) was added to the cell suspension and turbidity monitored at $A_{650\ nm}$ at room temperature. Results represent the mean and standard deviation of an experiment performed in triplicate. Two additional independent repeats produced similar results.

7.2.4 Susceptibility of USA300 mutants to osmotic stress

The EDTA-selected mutants all showed improved tolerance of osmotic stress relative to the wild-type, whereas the DTPMP-selected strains showed elevated sensitivity (Chapter 6, Fig. 6.14). Experiments using high salt concentrations were conducted by incorporating additional salt in LB agar plates as before (Fig. 6.14E). However, *S. aureus* USA300 proved much more tolerant of 0.5M NaCl than the FDA209P strain (data not shown), and so experiments were performed with LB agar containing 1 M NaCl (Fig. 7.5). Interestingly, none of the six USA300 mutants showed any change in sensitivity to osmotic stress in response to 1 M NaCl (Fig. 7.5).

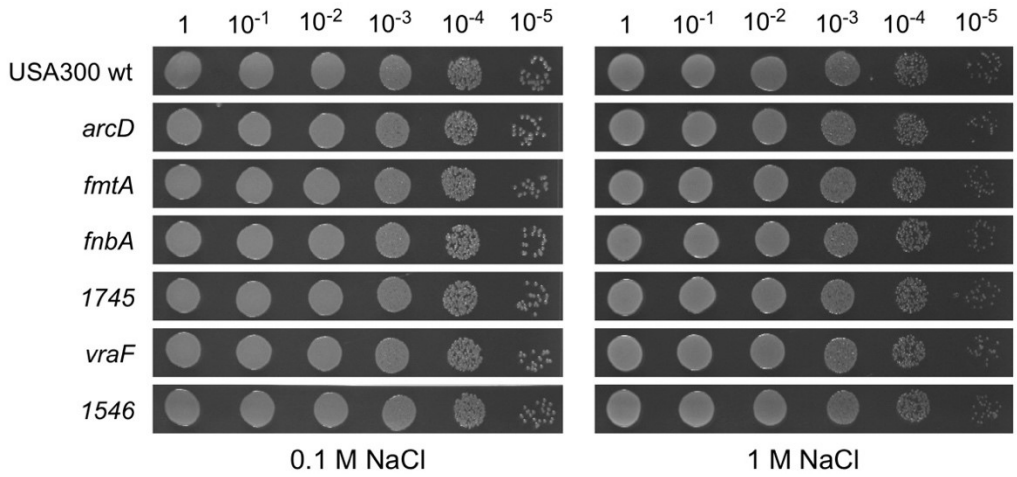

Figure 7.5 Susceptibility of selected *S. aureus* USA300 mutants to osmotic stress. Strains were grown to an $A_{600\,nm}$ of 0.4, serial 10-fold dilutions performed and 10 µl volumes applied to the surface of LB agar plates containing 0.1 or 1 M NaCl. Similar results were obtained in two additional independent experiments.

7.2.5 Cell surface charge of USA300 mutants

Previous experiments to monitor cell surface charge by association with cytochrome *c* revealed that all of the EDTA-selected mutants and two of the DTPMP strains, JN208 and JN209, appeared to have acquired an increased negative charge when compared to the parental FDA209P wild-type (Chapter 6, Fig. 6.12A). Although conflicting results were obtained when zeta potential was determined (Fig. 6.12B), an inverse pattern emerged that may well fit with an increased negative charge near the bacterial membrane that causes improved binding to the positively-charged cytochrome *c*, along with a more positive charge at the outer surface of the cell that is preferentially detected by zeta potential.

A similar cytochrome *c* experiment was conducted with the six USA300 strains (Fig. 7.6). The *fmtA* mutant showed significant removal of cytochrome *c* from the solution consistent with an increased negative charge. The *1745*, *vraF* and *1546* mutants also showed improved binding of cytochrome *c* relative to the wild-type, although the effect was less dramatic (Fig. 7.6). As in other assays, the *arcD* and *fnbA* strains behaved much as the wild-type (Fig. 7.6).

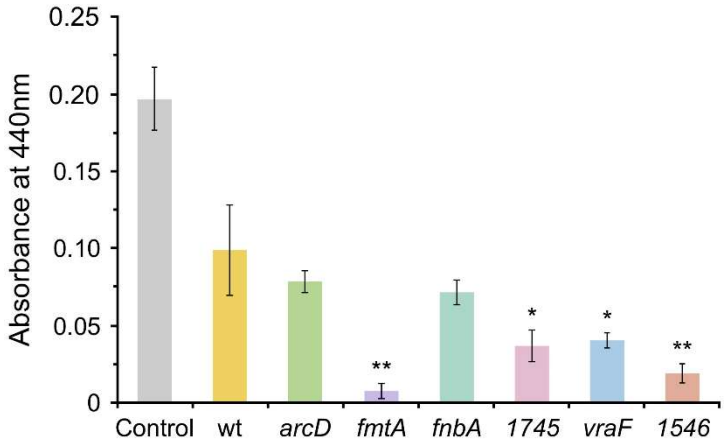

Figure 7.6 Selected *S. aureus* USA300 mutant binding to cytochrome *c*. Cells were grown in LB at 37°C in a shaking incubator to an $A_{600\ nm}$ of 1, harvested and washed three times in 20 mM MOPS buffer pH7. Concentrated cells were normalised to the same optical density and 5 mg/ml cytochrome *c* added. Cells were incubated at room temperature for 15 min, pelleted and the supernatant measured at $A_{440\ nm}$ to detect unbound cytochrome *c*. The results are the mean and standard deviation of three independent experiments performed in triplicate. The student t-test was used to compare mutant strains to the wild-type; *p<0.5, **p<0.01.

7.3 Discussion and conclusions

In the previous chapter, several genes linked to EDTA and DTPMP tolerance were identified from screens of the *S. aureus* strain FDA209P with the aim of identifying cellular targets of these chelants. In this chapter, the provision of six mutants, obtained by insertional mutagenesis from the USA300 Nebraska Transposon Mutant Library, enabled an examination of the contribution of each of these genes individually on a number of phenotypes associated with changes in cell wall architecture. When considering these results it is important to note that the mutations in the FDA209P chelant isolates are not all null alleles and each strain possesses a unique suite of mutations that may be collectively responsible for the phenotypes observed. Hence the conclusions concerning *fnbA*, *arcD*, *1745* and *1546* should take this into account, although FDA209P *fmtA* and *vraF* can be considered equivalent null mutations. It should also be noted that the FDA209P (MSSA) and USA300 (CA-MRSA) strains

may not behave exactly in the same fashion under the conditions tested as some differences in gene complement and expression patterns are inevitable.

7.3.1 Comparison of FDA209P and USA300 phenotypes

The six USA300 mutants were examined for their susceptibility to EDTA, DTPMP, vancomycin, moenomycin, lysostaphin and osmotic stress. The results with USA300 *fmtA*, *1745* and *vraF* mutants are summarised in Table 7.2 and compared with the three groups of FDA209P strains that carry these same three mutations.

Table 7.2 *S. aureus* FDA209P and USA300 *fmtA*, *1745* and *vraF* phenotypes

	Strains	JN170, 206, 207	JN210, 212	JN208, 209
	Mutation	*fmtA*	*1745*	*vraF*
EDTA	FDA209P	Resistant	Resistant	Resistant
	USA300	Resistant	Resistant	Resistant
DTPMP	FDA209P	Resistant	Resistant	Resistant
	USA300	Resistant	Resistant	Resistant
Vancomycin	FDA209P	Sensitive	Sensitive	Sensitive
	USA300	Sensitive	Sensitive	Sensitive
Moenomycin	FDA209P	As wild-type	Sensitive	Sensitive
	USA300	Resistant	Resistant	Resistant
Lysostaphin	FDA209P	As wild-type	Sensitive	Sensitive
	USA300	Sensitive	As wild-type	As wild-type
High salt	FDA209P	Resistant	Sensitive	Sensitive
	USA300	As wild-type	As wild-type	As wild-type

The FDA209P chelant-selected strains are listed on the top row and each contain mutations in either *fmtA*, *1745* or *vraF*, along with a range of other mutations (Chapter 6).

Significantly, the *fmtA*, *1745*, *vraF* and *1546* insertion mutants all showed improved resistance to the two chelants, EDTA and DTPMP (Fig. 7.1). Missense mutations in *1745*, found only in JN210 and JN212, and *1546* present in all of the original chelant-selected strains, while nonsense mutations in *fmtA* and *vraF* are found in all three EDTA-isolates and two of the DTPMP strains (JN208 and JN209), respectively (Chapter 6, Fig. 6.4). The results provide an indication that all four mutations reduce

or inactivate the activity of the proteins encoded by these FDA209P genes and directly link this loss of function to chelant resistance.

Some of the other phenotypes observed previously can also be connected to the elimination of these genes. Mutation of USA300 *fmtA*, *1745*, *vraF* and *1546* conferred modest susceptibility to vancomycin (Fig. 7.2 and 7.3). The sensitivity to vancomycin seen with these four mutants could explain the susceptibility to vancomycin in the chelant-resistant strains (Table 7.2). The *fmtA* insertion mutant showed increased sensitivity to vancomycin; *fmtA* mutation has previously been shown to increase susceptibility to vancomycin in *S. aureus* (Rajagopal et al., 2016).

In contrast, there are major differences between USA300 and the DTPMP-selected FDA209P with respect to moenomycin, especially with reference to strains carrying the *1745* and *vraF* alleles (Table 7.2). The USA300 *fmtA*, *1745*, *vraF* and *1546* mutants all promoted moenomycin resistance (Fig. 7.3), unlike the DTPMP-selected strains which proved highly sensitive to moenomycin (Chapter 6, Fig. 6.9). In addition, the fmtA insertion mutant showed increased sensitivity to moenomycin (Fig. 7.2), although not when the moenomycin was included in agar plates, where improved resistance was evident (Fig. 7.3). This argues that other mutations found in the DTPMP strains are responsible for moenomycin sensitivity, with a mutation in the glycosyltransferase domain of PBP2 being the only candidate present in every case (Chapter 6, Fig. 6.4). Because the USA300 *1745* and *vraF* mutants behave like the wild-type in response to lysostaphin and osmotic stress rather than showing elevated susceptibility (Table 7.2), these same *pbp2* mutations must also be responsible for the lysostaphin and high salt sensitivities observed in DTPMP-selected strains (Chapter 6, Fig. 6.10B and 6.14E). This is in accordance with the interpretation of results in the discussion section of Chapter 6, whereby specific mutations in the glycosyltransferase active site of PBP2 were linked to susceptibility to moenomycin, lysostaphin and osmotic stress. Although the EDTA-selected strains also have a mutation in PBP2 (Leu53Phe), this does not impinge upon the glycosyltransferase

active site and is associated instead with high salt tolerance and wild-type levels of sensitivity to moenomycin and lysostaphin (Table 7.2). Although the mutations in *fmtA* and *1546*, the latter present in all strains, do show some increased susceptibility to lysostaphin (Fig. 7.4), this may not significantly influence the phenotype observed with this enzyme in EDTA-isolated strains.

The USA300 *fnbA* and *arcD* mutants behaved like the wild-type strain in all of the experiments described in this chapter. This could indicate that the mutations in these genes, present in all of the chelant-selected strains, do not contribute to chelant tolerance or the other phenotypes explored in Chapter 6. However, the situations are not comparable as the FDA209P mutations are amino acid substitutions rather than null alleles. Hence the changes in FnbA (Thr510Lys) and ArcD (Met189Ile) could cause a change of function that does contribute to the various phenotypes observed, especially those related to cell surface charge. However, it does seem reasonable to conclude that even if they are involved, they are more likely to fulfil secondary roles.

7.3.2 Alterations in USA300 mutant cell surface charge

The surface charge of the six USA insertion mutants was also investigated using the cytochrome *c* assay. Cells from the *fmtA* mutant bound almost all of the cytochrome *c* in the sample, consistent with an increased negative charge relative to the wild-type (Fig. 7.6). In the same assay, the EDTA-selected mutants, all of which harbour an *fmtA* null mutation, similarly bound almost all of the cytochrome *c* present (Chapter 6, Fig. 6.12A), suggesting that loss of *fmtA* is largely responsible for the surface charge changes in these strains. Smaller effects on cytochrome *c* levels were also noted with the *1745*, *vraF* and *1546* insertion mutants (Fig. 7.6) and these also indicate some increased negative charge in these strains. Collectively, these may also contribute to cell surface changes in the chelant-resistant strains; this is more difficult to evaluate with *1745* and *1546* as the FDA209P strains carry missense rather than null mutations (Chapter 6, Fig. 6.4). JN208 and JN209, which are the only strains that lack *vraF,*

both display an apparent increase in negative charge (Chapter 6, Fig. 6.12A). Hence, all three of these mutations may be involved in electrostatic effects, perhaps alongside the specific *pbp2* mutation in these strains (Chapter 6, Fig. 6.4).

7.4 Future directions

The preliminary findings in this chapter leave considerable scope for additional experiments, many of which were performed previously with the chelant-resistant strains isolated in Chapter 6. Further analyses with the six USA300 mutants would be helpful in defining the contribution of specific genes in several phenotypes, including autolysis in the presence of Triton X-100, susceptibility to β-lactams and to lysozyme, and evaluation of cell surface charge by zeta potential. Further work on the resistance of these mutants to osmotic stress could be informative, perhaps initially using liquid culture rather than agar plates. The viability experiments (Fig. 7.5) could be repeated using higher salt concentrations to more clearly distinguish any differences between the wild-type and mutant strains. The growth of these strains in liquid culture in the absence of chelating agent, as in Chapter 6, Figure 6.3, has also yet to be examined. Mutant susceptibility to additional chelating agents may also be useful in helping understanding chelant mode of action as well as the tolerance mechanisms employed by *S. aureus*. Several other genes affected by mutation in the chelant-resistant strains (Chapter 6, Fig. 6.4) could be examined by assessing additional insertion mutants from the Nebraska Transposon Mutant Library. High throughput screening of the entire library might also identify other genes of interest involved in *S. aureus* chelant resistance, perhaps including those required for metal uptake pathways as found in studies with *E. coli* (Chapters 3 and 5). Further insights could be obtained by studying double-mutants to help unravel the contribution of each mutation when combined. For example, a *vraF 1546* double mutant, might yield insight into the unique behaviour of the DTPMP-isolated strains, JN208 and JN209, the only strains that exhibited sensitivity to lysozyme (Chapter 6, Fig. 6.11).

It would be worthwhile to examine the USA300 insertion mutants by transmission electron microscopy in the presence and absence of selected antibacterial agents to probe changes in cell wall architecture. Increased cell wall thickness is proposed to confer resistance to vancomycin by increasing the number of 'trapped' vancomycin molecules, preventing antibiotic access to the D-Ala-D-Ala substrate (Nishi et al., 2003). Moenomycin-resistant strains with mutations in the glycosyltransferase catalytic site of PBP2 possess significantly thicker cell walls and associated deficiencies in normal cell division (Nishi et al., 2003; Rebets et al., 2014). In addition, muropeptide analysis of USA300 mutants would be help in assessing whether these genes affect glycan chain length and the degree of peptidoglycan cross-linking or whether this is this primarily due to the *pbp2* mutations present in each of the chelant-resistant strains.

Determining any differences in cellular metal content by ICP-MS would be especially helpful since four of the mutants, *fmtA*, *1745*, *vraF* and *1546*, are resistant to EDTA and DTPMP (Fig. 7.1). These experiments should be conducted in the presence and absence of the two chelants and will hopefully confirm changes in these mutants that enable them to acquire metals more readily under chelant-mediated metal depletion conditions.

8 Conclusions

8.1 Efficacy of chelants as antibacterials

8.1.1 Individual effects of chelating agents

All of the chelants examined in this thesis inhibited bacterial growth to some degree and therefore offer potential benefits as antibacterial agents (Chapters 3 and 4). Bactericidal effects in addition to bacteriostatic were apparent (Table 4.1). The dose-response curves through which these different chelants inhibited growth varied, with some chelants exerting little detrimental effect on growth until reaching a particular threshold concentration after which growth dropped off dramatically (Fig. 3.3). Others provided higher levels of growth inhibition at lower chelant concentrations (e.g. PO and TPEN), producing a more linear reduction in growth (Fig. 3.3). These different sensitivity profiles could be linked to chelant molecular structures and metal selectivity, or may be an indication of dual antibacterial effects, such as metal deprivation coupled with membrane permeabilization, the latter supported by the increased uptake of NPN in experiments with EDTA and DTPA (Fig. 4.6). For most of the chelants tested, the concentrations required to provide >90% growth inhibition were significantly higher than most contemporary antibiotics. However, bacteria may find it more challenging to develop resistance to these synthetic chelating agents compared to more conventional antibiotics, as exemplified by *E. coli* exposed to DTPMP in experimental evolution experiments where no significant tolerance was developed (Chapter 5). This feature may be due to the presence of multiple cellular targets, limited biodegradability and the essential need to populate metalloenzymes with the correct metals.

In Chapter 4, we investigated the effect of chelants on selected Gram-negatives and Gram-positives. Previous studies have primarily focussed on Gram-negatives and effects on the outer membrane (Alakomi et al., 2006; Haque & Russell, 1974;

Vaara, 1992), which typically offers protection from antibacterial agents (Leive, 1974; Miller, 2016). However, the chelants tested often exerted unexpected inhibitory effects on these species, even within the same grouping. For example, *B. subtilis* and *S. aureus* proved more resistant to CHA than the two Gram-negative species and *E. coli* had at least a 10-fold greater resistance to EDTA than *P. aeruginosa* (Fig. 4.2).

EDTA is the best-characterised chelant in terms of antibacterial effects, although work has tended to focus on its damaging effects on the Gram-negative outer membrane, attributed to removal of stabilising metal ions (Alakomi et al., 2006; Alakomi et al., 2003; Leive, 1965), rather than cellular metal starvation. The mechanism of action of the remainder of the chelants has not been explored previously. Hence the work presented in this thesis, building upon Beecroft (2019), provides the first investigation into the effect of chelants on selective metal deprivation. A diversity of effects are indicated, including removal of metals from the growth medium, trapping of metals bound to chelants at the cell surface, metal restriction and potential mismetallation of intracellular enzymes and selective metal removal affecting iron, manganese and zinc (Paterson et al., 2022).

8.1.2 Chelating agents in combination

Combinations of chelants were also investigated with a view to identifying synergistic and indifferent interactions that might help in distinguishing chelants with similar or dissimilar modes of action. Synergistic pairings with improved antibacterial efficacy have the potential to be adopted in industrial commercial processes, consumer goods and healthcare settings. Multiple chelant combinations were evaluated using *E. coli* and *P. aeruginosa* (Chapters 3 and 4 respectively), as Gram-negative species tend to be more difficult to eradicate in such environments. With consideration of clinical applications in wound dressings and other skin infections, combinations of chelants with a range of antibiotics were also evaluated with representative Gram-positive and Gram-negative bacteria.

8.1.2.1 Chelant-chelant pairings

Overall, 55 chelant pairings were tested against *E. coli* revealing one antagonistic, 26 indifferent and 28 synergistic combinations (Fig. 3.10). DTPA yielded the highest number of synergistic pairings, while BCS produced the lowest number, likely due to its limited capacity to inhibit bacterial growth. Previous work had revealed the cellular response of *E. coli* to each of these chelants (Beecroft, 2019), allowing pairings to be analysed according to their effects on metal concentrations. The majority of synergistic pairings were found among chelants with differing individual effects on cellular metals (Fig. 3.10). Significantly however, there were seven pairings in which chelants from the same class also showed synergism, and only four examples in which chelants from the same class show indifference (Fig. 3.10), highlighting the difficulties in predicting synergism based on structural properties or effects on cellular metal concentrations in *E. coli*. Only one antagonistic pairing was found in these assays, suggesting that the use of combinations of chelants in either commercial or therapeutic applications may prove advantageous, particularly against species which display resistance to other antimicrobials. Further work is needed, however, to determine whether these synergistic, indifferent or antagonistic chelant interactions are similar in other Gram-negative species and also in Gram-positives.

Bacterial growth inhibition was analysed in pairwise combinations with seven different chelants against *P. aeruginosa,* including three pairings which were examined in *E. coli*. Of the 15 pairings tested, 12 were found to be synergistic (Fig. 4.3C) and no antagonistic combinations were identified. Combinations of EDTA and DTPMP with other chelants proved the most effective at restricting bacterial growth and thus represent promising candidates for inclusion together to enhance bacterial hostility. The pairing of structurally related HNK and TRO resulted in indifference with each other and these chelants only differed in their interaction with FA, suggesting that they may share a similar mode of action. Broadly similar results were obtained in checkerboards using CHA, DTPMP and EDTA with *P. aeruginosa* compared with the

results shown in Chapter 3 with *E. coli* (Fig. 3.3). The CHA-DTPMP and CHA-EDTA pairs were synergistic in both species, however, in *E. coli* the DTPMP-EDTA pair was indifferent, whereas in *P. aeruginosa* this combination was synergistic. This difference suggests that the chelants may act differently when combined against these two Gram-negatives. In general, it appears that chelants frequently prove synergistic when combined, although predicting which combinations will be most effective based solely on their structures remains challenging at this stage.

8.1.2.2 Chelant-antibiotic pairings

Six antibiotics from four distinct classes were selected for use in combinations with EDTA and DTPMP against four species representing both Gram-positive and Gram-negative bacteria: *B. subtilis*, *E. coli*, *P. aeruginosa*, and *S. aureus* (Fig. 4.5). Of the 48 chelant-antibiotic pairings tested, 33 synergistic and 15 indifferent combinations were identified (Fig. 4.5A), with Gram-negatives and Gram-positives displaying different patterns of synergy and indifference. Synergistic effects may indicate that chelants promote intracellular antibiotic uptake; EDTA has previously been shown to enhance antibiotic uptake in Gram-negative species through the predicted removal of stabilising calcium and magnesium ions in the outer membrane (Alakomi et al., 2006; Leive, 1965; Vaara, 1992) and is known to potentiate the activity of ampicillin, chloramphenicol, penicillin G and tetracycline against *P. aeruginosa* (Lambert et al., 2004; Weiser et al., 1968).

Interestingly, there was evidence of antagonism in pairings of DTPMP with kanamycin, spectinomycin and streptomycin with *E. coli* and *P. aeruginosa* (Fig. 4.4 and 4.5). DTPMP may be able to bind to these aminoglycoside antibiotics or prevent their association with the outer membrane to prevent them from entering the cell. The aminoglycosides, streptomycin and gentamycin use metals at the outer membrane to facilitate their intracellular uptake in *P. aeruginosa* (Hancock et al., 1981) and it may be more likely that DTPMP removes metals such as magnesium from the outer

membrane to restrict aminoglycoside uptake. Tetracycline is itself a chelating agent which traverses the outer membrane of Gram-negatives *via* porin channels (Chopra & Roberts, 2001; Guerra et al., 2016). This transport requires the antibiotic to acquire an overall positive charge, so it is hypothesised that binding metal cations allows the uptake of tetracycline coordination complexes (Chopra & Roberts, 2001). Pairing chelants with antibiotics may also affect the metal binding of some of the other antibiotics, such as ampicillin (El-Gamel, 2010) and kanamycin (Szczepanik et al., 2004) through metal restriction (Krause et al., 2016; Ramirez & Tolmasky, 2010).

8.2 Effects of chelants on cellular metal concentrations in *E. coli* and *P. aeruginosa*

The mechanisms through which the majority of chelating agents exert their antimicrobial activity has received little attention in the literature, although interference with normal cellular metal homeostasis has been observed in *E. coli* (Paterson et al., 2022). BCS, CAT and CHA were shown to have no significant impact on the metal composition of *E. coli* cells, indicating that they may use alternative mechanisms to inhibit bacterial growth or perhaps sequester metals within the cell to reduce accessibility to cellular proteins. PO is known to be capable of traversing eukaryotic membranes (Kim et al., 2011), and may therefore also be able to penetrate bacterial cell membranes, or become embedded within them, causing destabilisation of the membrane through physical disruption or chelation of stabilising ions. TPEN predominantly disrupts zinc concentrations in *E. coli*; even relatively small reductions in the levels of zinc adversely affect *E. coli* growth (Graham et al., 2009).

Analysis by ICP-MS with a novel selection of chelants against *P. aeruginosa* provided additional insight into how these chelants inhibit bacterial growth, revealing restriction of various metals within the cell. As found with *E. coli* (Paterson et al., 2022), CHA displayed no apparent effect on cellular metal concentrations (Fig. 4.7A). EDTA also yielded similar effects in *P. aeruginosa* as with *E. coli*, causing a dramatic

depletion of manganese alongside lesser reductions in levels of zinc, iron and calcium (Fig. 4.7C). DTPMP however behaved differently between the two species, causing decreased iron and elevated manganese in *E. coli*, but resulting in a dramatic reduction in manganese, with lesser reductions in the levels of iron and zinc in *P. aeruginosa* (Fig. 4.7B). This demonstrates that metals which are restricted by chelants may differ between species, presumably reflecting differences in the affinities of the metal acquisition pathways of each of these Gram-negative species and in their cellular responses to metal depletion. FA causes a reduction iron and manganese, HNK causes an increase in iron concentration and TRO affects a range of different metals, most notably decreasing calcium, iron, magnesium and manganese (Fig. 4.7). The mode of action of these chelants remains unclear, however, it seems likely that these chelants are removing metals from both the growth medium and the bacterial cell surface. Knowledge of which metals are primarily impacted by specific chelant exposure may help in chelant selection for specific applications, although as previously mentioned, chelants with differing effects on cellular metal concentrations do not always behave in a synergistic fashion.

8.3 Resistance to chelating agents

Single gene deletion mutants from the Keio collection were examined for sensitivity to chelating agents, building upon data from previous screens carried out against EDTA by Nichols et al. (2011) and as described here with PO by Nancy Reeder and Justin Caserta at P&G (Fig. 3.6). Results from these screens highlighted genes involved in enterobactin biosynthesis and ferric-enterobactin uptake as important in EDTA and PO tolerance. Subsequent experimental evolution experiments revealed that both *E. coli* and *S. aureus* are capable of developing some degree of enhanced resistance to EDTA and DTPMP after prolonged sub-lethal exposure. Sequencing of the resulting mutants highlighted cell surface proteins, membrane transporters and

proteins involved in cell wall metabolism as those with greatest impact on the development of tolerance to these two chelants.

8.3.1 Genes highlighted by Keio single gene knock-out screening

The screens mentioned above and examined in detail in Chapter 3, revealed significant differences in the levels of EDTA or PO susceptibility in *E. coli* single gene disrupted strains. The EDTA screen (Nichols et al., 2011) highlighted proteins involved in enterobactin biosynthesis, import and export as particularly significant in tolerance of this chelant, along with those involved in zinc import and cell envelope integrity (Fig. 3.6). It was surprising, therefore, that ICP-MS analysis of *E. coli* exposed to EDTA revealed a significant decrease in cellular levels of manganese, with lesser reductions in iron and zinc (Paterson et al., 2022). In contrast, PO results in manganese influx coupled with reductions in cellular iron concentrations (Paterson et al., 2022), and it was therefore anticipated that the PO screen with the Keio collection would primarily reveal the importance of genes involved in manganese and iron transport. The importance of iron uptake for tolerance of PO was confirmed, with mutants lacking genes affecting the synthesis and import of enterobactin most adversely affected (Fig. 3.6). Significant sensitivity was also noted in mutants with defects in proteins which are essential for maintenance of cell membrane integrity, suggesting that the absence of these proteins permits easier access of PO to the periplasm or cytosol. Some of the genes most strongly implicated in PO sensitivity were also found in the EDTA screen carried out by Nichols et al. (2011), including those involved in the uptake of enterobactin, however, mutants defective in components of the Znu zinc uptake system also showed significantly impaired growth when exposed to EDTA, whereas they displayed some tolerance to PO (Fig. 3.7). The results suggest that EDTA has broader effects on iron, manganese and zinc, whereas PO has selectivity for iron, consistent with findings from ICP-MS for these

two chelants in *E. coli* (Paterson et al., 2022) and in *P. aeruginosa* for EDTA (Chapter 4).

Surprisingly, deletion of *mntH* did not substantially alter growth in the presence of EDTA (Fig. 3.8C) (Nichols et al., 2011), despite previous data showing that cellular manganese concentrations are severely restricted by this chelant (Beecroft, 2019). An *mntH* mutant actually showed enhanced growth in the presence of EDTA (Fig. 3.9), but increased sensitivity to DTPMP and PO (Fig. 3.8A-B) which preferentially target iron, suggesting that EDTA-mediated growth inhibition may be caused primarily by reductions in iron and zinc, despite the major depletion of manganese.

With a few notable exceptions, levels of resistance or sensitivity resulting from deletion of a single gene were relatively modest, indicating that a broad range of genes may be responsible for determining levels of chelant tolerance in *E. coli*, reflecting the extensive significance of metal acquisition and homeostasis for a myriad of purposes within the cell.

8.3.2 Genes of significance in *E. coli* resistance to EDTA and DTPMP

A broad range of genes were affected in *E. coli* following prolonged exposure to the chelants EDTA and DTPMP. Several of the mutations acquired by these chelant-resistant strains were found to affect proteins associated with the outer membrane, and mirrored results seen in the previously described Keio screens which showed that deletion of *fepA* or *yeiR* results in hypersensitivity to EDTA, along with more modest increases in susceptibility in *flxA, rhsA*, *stfE* and *thiD* knockouts (Nichols et al., 2011). The experiments detailed in Chapter 3 confirmed that *fepA* mutations greatly increase sensitivity to both EDTA and DTPMP (Fig. 3.7B and 3.7C).

A mutation found in both strains isolated after 29 days exposure to DTPMP affects the promoter region of the *fepA-entD* operon (Fig. 5.6B), which is regulated in an iron-dependent manner. Increased expression of FepA or EntD did seem to improve resistance to EDTA, and DTPMP to a lesser extent (Fig. 5.7). EntD fulfils an essential

role in enterobactin biosynthesis (Raymond et al., 2003), while the outer membrane receptor FepA is involved in enterobactin recovery and delivery to the cytosol (Barnard et al., 2001; Chapter 3, Fig. 3.6C). This data suggests that iron deprivation is an important factor in the mechanism of action of both of these chelants, which fits with earlier studies on the metals affected by DTPMP in *E. coli* (Beecroft, 2019).

All of the EDTA-selected strains carried a mutation in the leader region of *yeiR* (Fig. 5.6A), a protein which plays a yet undefined role in zinc homeostasis (Blaby-Haas et al., 2012; Young et al., 2021); likely distributing zinc to essential metalloenzymes under limiting conditions, such as those resulting from EDTA exposure.

Three unique mutations were isolated in the *cadC* gene which responds to acidic conditions (Jung et al., 2018; Küper & Jung, 2006). Each of these mutations is found within the dimer interface (Fig. 5.8B and 5.8C) including a mutation in Tyr453 which is essential for cadaverine binding in a feedback loop which inhibits CadC (Haneburger et al., 2012). Reduction in cadaverine binding prevents this feedback loop and therefore increases cadaverine production and acid tolerance. Mutations in *cadC* were also found in *E. coli* exposed to low levels of triclosan (Leyn et al., 2021) or carvacrol (Al-Mnaser & Woodward, 2020), suggesting that *cadC* may play a role in signalling cell stress. Mutations in *cadC* may therefore enhance bacterial tolerance to cell stress in combination with additional genomic alterations.

8.3.3 Genes of significance in *S. aureus* resistance to EDTA and DTPMP

Prolonged exposure of *S. aureus* to EDTA resulted in mutants with improved resistance to both EDTA and DTPMP, and *vice versa*, implying a common chelant-resistance mechanism (Fig. 6.1), although improved growth was not evident in the presence of other chelants (CHA, FA, HNK or TRO; data not shown). Genome sequencing of the EDTA and DTPMP resistant mutants revealed a variety of mutations in cell surface proteins, membrane transporters and proteins involved in

cell wall metabolism (Fig. 6.4), with different combinations of mutations present depending on which chelant was used in the selection process.

8.3.3.1 EDTA-isolated strains

The three EDTA-selected *S. aureus* strains harboured five identical mutations, with a null mutation in *fmtA* being present in all EDTA isolates and none of the DTPMP-selected strains. *S. aureus fmtA* mutants show increased susceptibility to Triton X-100 (Komatsuzawa et al., 1997, 1999; Qamar & Golemi-Kotra, 2012) and also to β-lactam antibiotics (Komatsuzawa et al., 1997). These EDTA-isolated mutants carrying the *fmtA* mutant allele displayed the expected increased Triton X-100 susceptibility, but surprisingly exhibited some resistance to β-lactams (Fig 6.6), potentially due to additional shared mutations in PBP2 (Fig. 6.4).

Investigations into the cell surface charge of these EDTA isolates revealed a significant difference between two of these mutants compared to the parental wild-type (Fig. 6.12). These changes could be due to mutations within the fibronectin binding protein (FnbA) which is also mutated in these EDTA-selected strains (Fig. 6.4) or again associated with cell wall changes resulting from mutations in PBP2. All of the EDTA isolates harbour Leu53Phe substitution mutations within the transmembrane helix of PBP2 (Fig. 6.5), which may alter the position of the glycosyltransferase domain. This, along with their shared *fmtA* mutation (Komatsuzawa et al., 1999), may help explain the reduction in peptidoglycan crosslinking (Fig. 6.13) and the improved salt tolerance of these mutants (Schuster et al., 2020, Fig. 6.14). This PBP2 mutation may have an impact on cell wall thickness, although no increased sensitivity to lysostaphin (Fig. 6.10B) or lysozyme (Fig. 6.11) was evident, indicating that cell wall integrity has not been majorly compromised. The function and contribution of additional shared mutations within *arcD* and the uncharacterised *1546* gene (Fig. 6.4) have yet to be determined.

8.3.3.2 DTPMP-isolated strains

The five DTPMP-isolated mutants harbour the same *fnbA*, *1546* and *arcD* mutations seen in the EDTA isolates in addition to other unique mutations (Fig. 6.4). Two of these mutants, JN208 and JN209, possess a unique phenotype from the other DTPMP-isolates, and share a null mutation in *vraF* (Fig. 6.4). JN210 and JN212 share additional missense mutations in *614*, *1745* and upstream mutations affecting *sasG2*, *qoxA* and *r0012* (Fig 6.4), all of which may contribute to their own unique phenotype. Again, all isolated strains carried substitution mutations within PBP2, however in contrast to EDTA isolates, these were located within the glycosyltransferase domain (Fig. 6.5), with the precise mutation differing between the DTPMP-selected strains.

JN174, JN210 and JN212 displayed an increased sensitivity to penicillin G and cefoxitin (Fig. 6.7), as well as vancomycin and moenomycin (Fig. 6.8 and 6.9) which may be due to shared mutations within the same PBP2 motif (Fig. 6.5C). In addition, the DTPMP-isolated strains tested (JN174 and JN210) also showed a reduction in peptidoglycan cross-linking (Fig. 6.13), despite showing no alteration in susceptibility to lysozyme (Fig. 6.11).

The additional null mutation in *vraF* found in JN208 and JN209 resulted in a much higher sensitivity to penicillin G and the three cephalosporins (Fig. 6.6 and 6.7), additional susceptibility to lysozyme (Fig, 6.11) and alterations in cell surface charge (Fig. 6.12). These features more closely resemble the EDTA-isolated strains (section 8.3.3.1), and suggests that the phenotypic differences between these groups of DTPMP isolates are likely due to mutations in *vraF* and *pbp2.* None of the DTPMP-selected strains showed changes in susceptibility to Triton X-100 (Fig. 6.10A), despite showing increased sensitivity to lysostaphin (Fig. 6.10B) and high salt concentrations (Fig. 6.14), suggesting that the precise location of the mutations within the glycosyltransferase domain of PBP2 is responsible for this phenotype which was not observed in EDTA-isolated mutants.

The mutations found in *S. aureus* chelant-isolated strains highlight the significance of genes involved in regulation of the cell wall and net cell surface charge in determining tolerance to chelants, antibiotics and increased osmotic stress rather than pathways responsible for metal uptake.

8.3.4 Use of selected *S. aureus* USA300 mutants to examine genes implicated in *S. aureus* FDAP209 chelant resistance

Genes implicated in the experimental evolution of *S. aureus* were further examined using the CA-MRSA USA300 Nebraska Transposon Mutant Library (Chapter 7). This analysis was complicated by the fact that mutations arising following prolonged chelant exposure did not always result in elimination of the gene and all of the strains possessed more than one mutation that could influence the phenotypes observed (Fig. 6.4). Despite this limitation, the results gained from these investigations proved helpful in dissecting the roles that each gene plays in the *S. aureus* mutants isolated in Chapter 6. The findings were summarised in Table 7.2.

USA300 mutants with transposon insertions in *fmtA*, *1745*, *vraF* and *1546* all displayed enhanced tolerance of EDTA and DTPMP (Fig. 7.1), suggesting that the mutations found in chelant-isolated mutants may well eliminate functionality of these genes. Each of these mutations also produced modest improvements in moenomycin resistance (Fig. 7.2) in parallel with increased susceptibility to vancomycin (Fig. 7.3). Surprisingly, there were major differences between the DTPMP-isolated mutants and their USA300 equivalents. The chelant-isolated strains showed a significant increase in moenomycin sensitivity (Fig. 6.9), whereas USA300 *fmtA*, *1745*, *vraF* and *1546* mutants displayed a contrasting increased resistance to this antibiotic (Fig. 7.3). This indicates that additional mutations shared by all DTPMP isolates must be responsible for this enhanced moenomycin sensitivity, with the most promising candidates being mutations within the glycosyltransferase domain of PBP2 (Fig. 6.4). Similar levels of tolerance to osmotic stress and lysostaphin between the wild-type and USA300 *vraF*

and *1745* mutants (Fig. 7.3 and 7.4) were noted, indicating that *pbp2* mutations are again responsible for the elevated susceptibility of DTPMP isolates to these two factors (Fig. 6.14E and 6.10).

Mutation of *fmtA* in the USA300 background did result in cells with an increased net negative charge (Fig 7.6), consistent with the data obtained with the EDTA-selected strains (Fig. 6.12A). Importantly, there were no phenotypic differences between the wild-type and the USA300 *fnbA* and *arcD* mutants, suggesting that although these genes were mutated in all chelant-isolated strains, they do not play a significant role in determining any of the phenotypes revealed in Chapter 6.

8.4 Final remarks

The work encompassed within this thesis has built and expanded upon our current knowledge of the effect of chelating agents on bacterial growth and selective metal deprivation in four different bacterial species. The effects of a novel collection of chelants have been examined against two Gram-positives (*B. subtilis* and *S. aureus*) and two Gram-negatives (*E. coli* and *P. aeruginosa*), with many chelant pairings assessed with the latter two species to identify antagonistic, indifferent and synergistic pairings. We also examined the effect of these chelants in combination with widely-used antibiotics with known mechanisms of action to determine whether they could enhance antibacterial efficacy and gain further insights into the possible modes of action of each chelant. The impact of a selection of these chelants on cellular metal concentrations in *P. aeruginosa* was examined using ICP-MS, revealing a new suite of effects on bacterial metal homeostasis when compared with previous work on *E. coli*. This allowed similarities and differences to be identified between these two species with similar overall cell wall and membrane structures.

In addition to this, an experimental evolution approach was employed to isolate *E. coli* and *S. aureus* mutants which had acquired resistance to either EDTA or DTPMP. Genetic analysis of these mutants revealed genes of particular importance in

determining levels of tolerance to these chelating agents. Iron and zinc uptake pathways were primarily affected in *E. coli*, while proteins involved in the maintenance of cell surface charge and cell wall metabolism were the main targets in *S. aureus*. Informed by the genetic analysis of these chelant-isolated mutants, we also studied the levels of resistance of single gene mutants from both the Keio collection and NARSA library to examine the significance of single genes in determining chelant and antibiotic resistance in *E. coli* and *S. aureus* respectively.

In conclusion, the results presented within this thesis reveal new insights into the mechanisms of bacterial growth inhibition by chelants, showcasing their potential as antibacterial agents and highlighting their value as probes to study selective metal deprivation in bacteria. Further work, expanding upon that covered in this thesis, will enable a better understanding of the mechanisms utilised by different bacteria to acquire essential metals and maintain a healthy balance in metal replete conditions and in situations where metals are scarce. A more complete grasp of the mechanisms through which chelants mediate growth inhibition and how differences in cell wall composition affect metal uptake should allow a more targeted application of these agents in industrial processes, consumer products and also as antimicrobial potentiators in healthcare to assist in the treatment of drug-resistant pathogens.

9 Appendix

9.1 Additional tables and figures

Table 9.1 Estimated metal ion affinities of selected chelants.

Ligand	Ca^{2+}	Cu^{+}	Cu^{2+}	Fe^{2+}	Fe^{3+}	Mg^{2+}	Mn^{2+}	Zn^{2+}
BCS	18.8		7.1, 10.8	6.4, 23.2				10.1, 14.9
CAT	1.7		8.09		18.52	1.98	7.52	9.50
CHA					11.24			
DTPA	10.7		21.5	15.97	28.7	9.3	14.31	18.61
DTPMP	7.11		19.47			6.4	11.15	16.45
EDTA	10.61		18.7	14.27	25.0	8.83	13.81	16.44
GLDA	5.9		13.1		15.35	5.2	7.6	11.5
HBED	9.29		22.95		39.68	10.51	14.78	18.95
MGDA	7.0		13.9	8.1	16.5	5.8	8.4	10.9
TPEN			20.6	14.6			10.27	15.58

The stability or equilibrium constant (*K*), expressed as log *K* are shown where known. Values were obtained from the IUPAC Stability Constants Database (Pettit, 2009) and were determined at 25°C, I = 0.1 M. The first value for BCS with Cu^{2+} and Zn^{2+} refers to ML complex formation, also for BCS with Fe^{2+}, the second refers to ML_2 complex formation; BCS with Ca^{2+} refers to ML_3 complex formation. The second value for BCS with Fe^{2+} corresponds to ML_3 complex formation. Note that formation constants for ML_2 and ML_3 complexes are not directly comparable with ML values.

Figure 9.1 Chelant combinations analysed by the checkerboard assay using a mean FIC methodology. FIC indices from two independent experiments were calculated from checkerboard data. In eight instances different outcomes were found between the two experiments and these have been conservatively assigned as indifferent. MICs were determined for individual chelants as before with FIC values averaged from the boundaries between growth and <10% *E. coli* growth of chelants in combination.

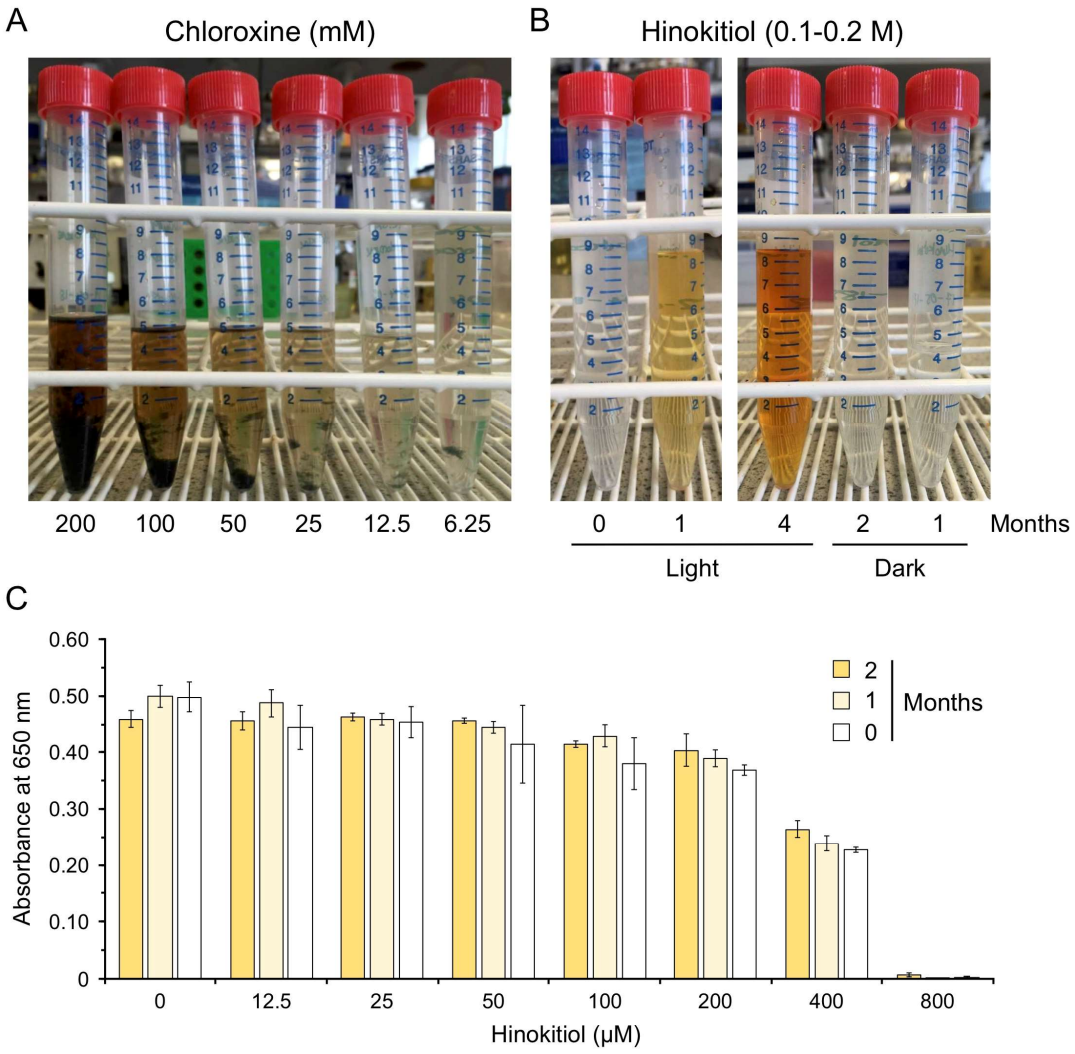

Figure 9.2 Chloroxine and hinokitiol in solution. (A) Solubility and colour of chloroxine in DMSO. Chloroxine produces a dark brown solution that is poorly soluble in DMSO and prone to precipitation even at 6.25 mM concentration. Chloroxine is not soluble in water and also poorly soluble in ethanol. (B) Hinokitiol develops a yellow colouration following light exposure. Hinokitiol dissolved in DMSO (0.1 M) gradually turns yellow over a month if exposed to light and progressively darkens to orange after 4 months. Samples of hinokitiol in DMSO (0.2M) do not change colour if kept in the dark for 1 or 2 months. (C) The hinokitiol colour change does not affect antibacterial activity with *P. aeruginosa*. The efficacy of freshly prepared hinokitiol was compared with samples prepared at 1-month and 2-month intervals and exposed to daylight. Bacteria were mixed with serial 2-fold dilutions of hinokitiol samples and incubated with shaking at 150 rpm at 37°C for 16 hr.

Table 9.2 Effect of chelants on the total cellular metal content of *P. aeruginosa.*

	Metal concentration in atoms per cell at 10-15% growth inhibition					
Chelant (µM)	**Ca**	**Cu**	**Fe**	**Mg**	**Mn**	**Zn**
CHA CONT (0)	2.18×10^7 1.94×10^7 2.42×10^7 2.34×10^7	2.34×10^5 2.60×10^5 2.30×10^5 2.74×10^5	1.80×10^6 1.68×10^6 1.62×10^6 1.60×10^6	1.05×10^8 1.01×10^8 1.18×10^8 1.16×10^8	2.50×10^5 2.50×10^5 2.56×10^5 2.36×10^5	7.34×10^5 7.36×10^5 8.60×10^5 8.16×10^5
DMSO CONT (0)	1.72×10^7 1.83×10^7 2.26×10^7 2.12×10^7	2.40×10^5 2.36×10^5 2.14×10^5 1.77×10^5	1.50×10^6 1.62×10^6 1.58×10^6 1.48×10^6	9.72×10^7 1.05×10^8 1.19×10^8 1.16×10^8	2.48×10^5 2.36×10^5 2.32×10^5 2.36×10^5	7.18×10^5 6.78×10^5 7.82×10^5 7.44×10^5
90	2.06×10^7 1.98×10^7 2.36×10^7 2.28×10^7	2.82×10^5 2.52×10^5 2.02×10^5 2.06×10^5	1.71×10^6 1.69×10^6 1.60×10^6 1.59×10^6	9.62×10^7 1.01×10^8 1.15×10^8 1.14×10^8	2.76×10^5 2.44×10^5 2.38×10^5 2.58×10^5	7.38×10^5 7.12×10^5 8.16×10^5 8.04×10^5
105	1.98×10^7 1.85×10^7 2.24×10^7 2.08×10^7	2.54×10^5 2.54×10^5 2.50×10^5 2.16×10^5	1.67×10^6 1.59×10^6 1.60×10^6 1.61×10^6	9.54×10^7 9.64×10^7 1.12×10^8 1.16×10^8	2.40×10^5 2.46×10^5 2.62×10^5 2.30×10^5	7.06×10^5 6.84×10^5 8.14×10^5 7.60×10^5
120	1.86×10^7 1.68×10^7 2.14×10^7 2.26×10^7	2.32×10^5 2.48×10^5 2.34×10^5 2.16×10^5	1.65×10^6 1.55×10^6 1.48×10^6 1.61×10^6	9.46×10^7 9.88×10^7 9.88×10^7 1.11×10^8	2.28×10^5 2.38×10^5 2.16×10^5 2.38×10^5	6.70×10^5 6.76×10^5 7.34×10^5 7.70×10^5
135	2.14×10^7 1.81×10^7 2.46×10^7 2.28×10^7	2.54×10^5 2.78×10^5 2.06×10^5 2.26×10^5	1.71×10^6 1.64×10^6 1.66×10^6 1.60×10^6	1.05×10^8 1.02×10^8 1.08×10^8 1.13×10^8	2.68×10^5 2.50×10^5 2.36×10^5 2.36×10^5	7.64×10^5 7.16×10^5 7.98×10^5 7.80×10^5
DTPMP CONT (0)	2.32×10^7 1.90×10^7 2.35×10^7 2.62×10^7	3.11×10^5 2.56×10^5 4.53×10^5 3.20×10^5	2.29×10^6 1.88×10^6 2.43×10^6 2.71×10^6	1.15×10^8 9.10×10^7 1.11×10^8 1.31×10^8	2.70×10^5 2.32×10^5 2.70×10^5 3.06×10^5	7.70×10^5 5.80×10^5 8.75×10^5 8.75×10^5
50	2.13×10^7 1.99×10^7 2.03×10^7 2.24×10^7	2.67×10^5 2.40×10^5 2.98×10^5 3.00×10^5	1.81×10^6 1.44×10^6 2.05×10^6 2.10×10^6	1.08×10^8 8.10×10^7 1.14×10^8 1.20×10^8	1.42×10^4 1.32×10^4 1.52×10^4 1.57×10^4	4.32×10^5 3.30×10^5 4.86×10^5 4.98×10^5
70	2.08×10^7 1.53×10^7 2.14×10^7 2.18×10^7	2.65×10^5 2.88×10^5 2.75×10^5 2.81×10^5	1.93×10^6 1.45×10^6 1.87×10^6 2.01×10^6	1.08×10^8 8.05×10^7 1.17×10^8 1.18×10^8	1.37×10^4 1.15×10^4 1.21×10^4 1.30×10^4	4.79×10^5 3.30×10^5 4.56×10^5 4.82×10^5

90	1.77×10^{7} 1.51×10^{7} 2.59×10^{7} 2.02×10^{7}	2.92×10^{5} 2.26×10^{5} 2.91×10^{5} 3.15×10^{5}	1.72×10^{6} 1.36×10^{6} 1.89×10^{6} 2.08×10^{6}	9.70×10^{7} 7.65×10^{7} 1.12×10^{8} 1.14×10^{8}	1.12×10^{4} 1.14×10^{4} 1.16×10^{4} 1.20×10^{4}	3.96×10^{5} 2.95×10^{5} 4.53×10^{5} 4.81×10^{5}
100	2.07×10^{7} 1.41×10^{7} 1.91×10^{7} 1.97×10^{7}	2.66×10^{5} 2.25×10^{5} 3.06×10^{5} 3.22×10^{5}	1.87×10^{6} 1.26×10^{6} 1.92×10^{6} 2.05×10^{6}	1.07×10^{8} 7.55×10^{7} 1.11×10^{8} 1.15×10^{8}	1.13×10^{4} 9.40×10^{3} 1.09×10^{4} 1.17×10^{4}	4.31×10^{5} 2.84×10^{5} 4.70×10^{5} 5.05×10^{5}
110	1.61×10^{7} 1.37×10^{7} 2.08×10^{7} 1.96×10^{7}	2.68×10^{5} 2.42×10^{5} 3.03×10^{5} 2.82×10^{5}	1.62×10^{6} 1.35×10^{6} 1.90×10^{6} 1.83×10^{6}	9.25×10^{7} 7.30×10^{7} 1.16×10^{8} 1.11×10^{8}	1.02×10^{4} 1.00×10^{4} 1.08×10^{4} 1.04×10^{4}	3.59×10^{5} 2.88×10^{5} 4.58×10^{5} 4.37×10^{5}
EDTA CONT (0)	1.89×10^{7} 1.66×10^{7} 2.23×10^{7} 2.38×10^{7}	7.45×10^{4} 8.50×10^{4} 3.52×10^{5} 2.62×10^{5}	1.64×10^{6} 1.72×10^{6} 2.54×10^{6} 2.38×10^{6}	8.55×10^{7} 7.90×10^{7} 1.05×10^{8} 1.08×10^{8}	2.06×10^{5} 2.06×10^{5} 2.86×10^{5} 2.80×10^{5}	5.35×10^{5} 5.90×10^{5} 8.20×10^{5} 7.35×10^{5}
60	1.24×10^{7} 8.85×10^{6} 1.53×10^{7} 6.90×10^{6}	6.35×10^{4} 5.70×10^{4} 3.51×10^{5} 3.12×10^{5}	1.25×10^{6} 1.06×10^{6} 1.94×10^{6} 1.76×10^{6}	7.50×10^{7} 5.95×10^{7} 1.13×10^{8} 5.60×10^{7}	6.00×10^{3} 5.35×10^{3} 8.20×10^{3} 7.55×10^{3}	2.77×10^{5} 2.36×10^{5} 4.49×10^{5} 3.98×10^{5}
70	1.03×10^{7} 9.70×10^{6} 1.18×10^{7} 1.11×10^{7}	6.05×10^{4} 6.20×10^{4} 3.45×10^{5} 2.42×10^{5}	1.12×10^{6} 1.05×10^{6} 2.02×10^{6} 1.60×10^{6}	7.75×10^{7} 7.00×10^{7} 1.04×10^{8} 9.20×10^{7}	5.45×10^{3} 5.10×10^{3} 9.10×10^{3} 6.75×10^{3}	2.51×10^{5} 2.38×10^{5} 4.03×10^{5} 3.60×10^{5}
80	8.85×10^{6} 9.15×10^{6} 1.03×10^{7} 9.55×10^{6}	5.85×10^{4} 5.60×10^{4} 2.31×10^{5} 2.43×10^{5}	1.04×10^{6} 9.40×10^{5} 1.67×10^{6} 1.75×10^{6}	7.55×10^{7} 6.35×10^{7} 1.04×10^{8} 9.25×10^{7}	5.20×10^{3} 5.00×10^{3} 6.30×10^{3} 7.60×10^{3}	2.21×10^{5} 2.04×10^{5} 3.51×10^{5} 3.30×10^{5}
90	7.20×10^{6} 6.70×10^{6} 8.75×10^{6} 8.05×10^{6}	6.00×10^{4} 5.20×10^{4} 3.02×10^{5} 2.21×10^{5}	9.70×10^{5} 8.90×10^{5} 1.70×10^{6} 2.57×10^{6}	6.60×10^{7} 5.95×10^{7} 9.50×10^{7} 9.30×10^{7}	4.71×10^{3} 4.53×10^{3} 6.80×10^{2} 6.80×10^{2}	1.85×10^{5} 1.73×10^{5} 3.04×10^{5} 3.00×10^{5}
100	5.70×10^{6} 5.90×10^{6} 6.65×10^{6} 6.25×10^{6}	5.00×10^{4} 5.40×10^{4} 2.80×10^{5} 1.84×10^{5}	9.20×10^{5} 9.30×10^{5} 1.65×10^{6} 1.40×10^{6}	6.40×10^{7} 6.10×10^{7} 9.10×10^{7} 8.55×10^{7}	6.10×10^{3} 4.75×10^{3} 6.70×10^{3} 5.90×10^{3}	1.58×10^{5} 1.60×10^{5} 2.73×10^{5} 2.57×10^{5}
FA CONT (0)	2.32×10^{7} 2.36×10^{7} 2.38×10^{7}	4.48×10^{5} 3.50×10^{5} 3.89×10^{5}	1.66×10^{6} 2.22×10^{6} 2.39×10^{6}	1.12×10^{8} 1.12×10^{8} 1.23×10^{8}	2.64×10^{5} 2.61×10^{5} 2.74×10^{5}	7.72×10^{5} 7.52×10^{5} 8.25×10^{5}
DMSO	2.24×10^{7} 2.45×10^{7}	4.55×10^{5} 3.30×10^{5}	1.51×10^{6} 2.26×10^{6}	9.80×10^{7} 1.17×10^{8}	2.21×10^{5} 2.54×10^{5}	6.59×10^{5} 7.73×10^{5}

	2.50×10^{7}	3.50×10^{5}	2.30×10^{6}	1.24×10^{8}	2.72×10^{5}	8.38×10^{5}
500	2.14×10^{7} 2.49×10^{7} 2.33×10^{7}	4.54×10^{5} 3.69×10^{5} 3.54×10^{5}	1.23×10^{6} 1.84×10^{6} 1.81×10^{6}	9.76×10^{7} 1.22×10^{8} 1.22×10^{8}	1.52×10^{5} 2.05×10^{5} 1.86×10^{5}	7.61×10^{5} 9.39×10^{5} 8.45×10^{5}
600	2.18×10^{7} 2.26×10^{7} 2.39×10^{7}	4.75×10^{5} 3.16×10^{5} 3.17×10^{5}	1.34×10^{6} 1.66×10^{6} 1.76×10^{6}	9.89×10^{7} 1.09×10^{8} 1.17×10^{8}	1.50×10^{5} 1.60×10^{5} 1.69×10^{5}	8.26×10^{5} 8.17×10^{5} 8.55×10^{5}
700	2.38×10^{7} 2.29×10^{7} 2.47×10^{7}	5.27×10^{5} 3.52×10^{5} 3.50×10^{5}	1.24×10^{6} 1.57×10^{6} 1.70×10^{6}	1.01×10^{8} 1.13×10^{8} 1.17×10^{8}	1.36×10^{5} 1.49×10^{5} 1.45×10^{5}	8.11×10^{5} 8.80×10^{5} 8.63×10^{5}
800	2.40×10^{7} 1.92×10^{7} 2.16×10^{7}	4.13×10^{5} 3.35×10^{5} 3.19×10^{5}	1.26×10^{6} 1.45×10^{6} 1.67×10^{6}	9.54×10^{7} 9.87×10^{7} 1.09×10^{8}	1.05×10^{5} 1.17×10^{5} 1.24×10^{5}	7.26×10^{5} 7.83×10^{5} 8.22×10^{5}
HNK CONT (0)	2.50×10^{7} 2.55×10^{7} 2.20×10^{7} 2.26×10^{7}	4.53×10^{5} 4.03×10^{5} 3.50×10^{5} 4.03×10^{5}	1.92×10^{6} 1.79×10^{6} 2.45×10^{6} 2.45×10^{6}	1.17×10^{8} 1.14×10^{8} 1.10×10^{8} 1.23×10^{8}	2.77×10^{5} 2.60×10^{5} 3.41×10^{5} 3.41×10^{5}	8.05×10^{5} 7.24×10^{5} 9.52×10^{5} 9.20×10^{5}
0 DMSO	2.40×10^{7} 2.31×10^{7} 2.19×10^{7} 2.16×10^{7}	4.29×10^{5} 3.96×10^{5} 3.23×10^{5} 3.51×10^{5}	1.86×10^{6} 2.02×10^{6} 2.04×10^{6} 2.24×10^{6}	1.11×10^{8} 1.09×10^{8} 1.05×10^{8} 1.07×10^{8}	2.59×10^{5} 2.47×10^{5} 3.20×10^{5} 3.11×10^{5}	7.25×10^{5} 6.86×10^{5} 8.29×10^{5} 8.03×10^{5}
40	2.73×10^{7} 2.43×10^{7} 2.45×10^{7} 2.53×10^{7}	4.55×10^{5} 4.35×10^{5} 3.39×10^{5} 3.84×10^{5}	2.40×10^{6} 2.13×10^{6} 2.84×10^{6} 2.50×10^{6}	1.23×10^{8} 1.10×10^{8} 1.15×10^{8} 1.13×10^{8}	2.99×10^{5} 2.65×10^{5} 3.35×10^{5} 3.33×10^{5}	8.91×10^{5} 7.94×10^{5} 9.59×10^{5} 9.68×10^{5}
50	2.35×10^{7} 2.44×10^{7} 2.42×10^{7} 2.36×10^{7}	4.61×10^{5} 4.02×10^{5} 3.73×10^{5} 4.32×10^{5}	2.65×10^{6} 2.81×10^{6} 2.90×10^{6} 3.13×10^{6}	1.05×10^{8} 1.13×10^{8} 1.16×10^{8} 1.24×10^{8}	2.63×10^{5} 2.67×10^{5} 3.43×10^{5} 3.45×10^{5}	7.98×10^{5} 7.90×10^{5} 9.90×10^{5} 1.02×10^{6}
60	2.20×10^{7} 2.44×10^{7} 2.32×10^{7} 2.36×10^{7}	4.05×10^{5} 4.50×10^{5} 2.88×10^{5} 2.48×10^{5}	2.86×10^{6} 3.29×10^{6} 2.80×10^{6} 3.20×10^{6}	1.10×10^{8} 1.13×10^{8} 1.10×10^{8} 1.08×10^{8}	2.60×10^{5} 2.63×10^{5} 3.24×10^{5} 3.17×10^{5}	8.07×10^{5} 7.83×10^{5} 9.16×10^{5} 8.84×10^{5}
70	2.62×10^{7} 2.37×10^{7} 2.34×10^{7} 2.32×10^{7}	4.73×10^{5} 3.81×10^{5} 2.95×10^{5} 3.19×10^{5}	3.42×10^{6} 3.62×10^{6} 3.48×10^{6} 3.69×10^{6}	1.18×10^{8} 1.14×10^{8} 1.07×10^{8} 1.06×10^{8}	2.83×10^{5} 2.56×10^{5} 3.22×10^{5} 3.08×10^{5}	8.59×10^{5} 7.73×10^{5} 9.32×10^{5} 8.67×10^{5}
TRO CONT (0)	2.31×10^{7} 2.14×10^{7} 2.55×10^{7} 2.48×10^{7}	3.10×10^{5} 4.27×10^{5} 3.98×10^{5} 3.46×10^{5}	2.18×10^{6} 2.11×10^{6} 2.32×10^{6} 2.28×10^{6}	1.13×10^{8} 1.08×10^{8} 1.17×10^{8} 1.08×10^{8}	2.80×10^{5} 2.64×10^{5} 2.77×10^{5} 2.64×10^{5}	7.40×10^{5} 7.42×10^{5} 7.11×10^{5} 7.12×10^{5}

0 DMSO	2.44×10^7 2.19×10^7 2.23×10^7 2.44×10^7	2.84×10^5 3.79×10^5 3.31×10^5 3.85×10^5	2.29×10^6 2.10×10^6 2.01×10^6 2.16×10^6	1.11×10^8 1.08×10^8 1.02×10^8 1.04×10^8	2.76×10^5 2.71×10^5 2.46×10^5 2.66×10^5	8.49×10^5 7.76×10^5 6.55×10^5 6.62×10^5
25	1.87×10^7 2.06×10^7 2.47×10^7 2.41×10^7	3.39×10^5 4.33×10^5 3.81×10^5 3.38×10^5	1.76×10^6 1.89×10^6 1.96×10^6 1.89×10^6	9.62×10^7 9.57×10^7 1.04×10^8 9.74×10^7	2.31×10^5 2.50×10^5 2.53×10^5 2.49×10^5	6.41×10^5 7.04×10^5 6.53×10^5 6.50×10^5
30	2.09×10^7 2.04×10^7 2.38×10^7 2.28×10^7	3.79×10^5 4.47×10^5 3.61×10^5 3.45×10^5	1.78×10^6 2.05×10^6 2.13×10^6 1.78×10^6	9.72×10^7 9.67×10^7 9.61×10^7 9.44×10^7	2.55×10^5 2.50×10^5 2.48×10^5 2.39×10^5	8.00×10^5 7.26×10^5 6.77×10^5 5.99×10^5
35	1.95×10^7 1.89×10^7 2.05×10^7 2.13×10^7	3.56×10^5 4.08×10^5 3.77×10^5 3.47×10^5	2.23×10^6 1.65×10^6 1.81×10^6 1.70×10^6	9.56×10^7 8.42×10^7 9.02×10^7 8.59×10^7	2.44×10^5 2.23×10^5 2.24×10^5 2.33×10^5	7.17×10^5 6.97×10^5 5.89×10^5 5.85×10^5
40	1.80×10^7 1.84×10^7 1.81×10^7 2.01×10^7	4.03×10^5 4.58×10^5 3.69×10^5 3.41×10^5	1.62×10^6 1.57×10^6 1.53×10^6 1.61×10^6	9.14×10^7 8.67×10^7 8.30×10^7 8.40×10^7	2.26×10^5 2.26×10^5 2.02×10^5 2.21×10^5	8.02×10^5 7.47×10^5 5.66×10^5 5.46×10^5

Total cellular metal concentration was monitored for *P. aeruginosa* with 10-15% growth inhibition over a range of chelant concentrations. *P. aeruginosa* was grown in 50 ml of LB media at 37°C in a shaking incubator in the presence or absence of chelant to mid log-phase ($A_{650\ nm}$ of 0.3-0.4, 3-4 hours). Data are the mean and standard deviation of four independent experiments (3 for FA). Red text indicates a reduction in total cellular metal content of 1.5-2 fold (■), 2-3 fold (■) or >3 fold (■), whereas blue text indicates an increase in metal content of 1.5-2-fold (■), 2-3 fold (■) or >3 fold (■).

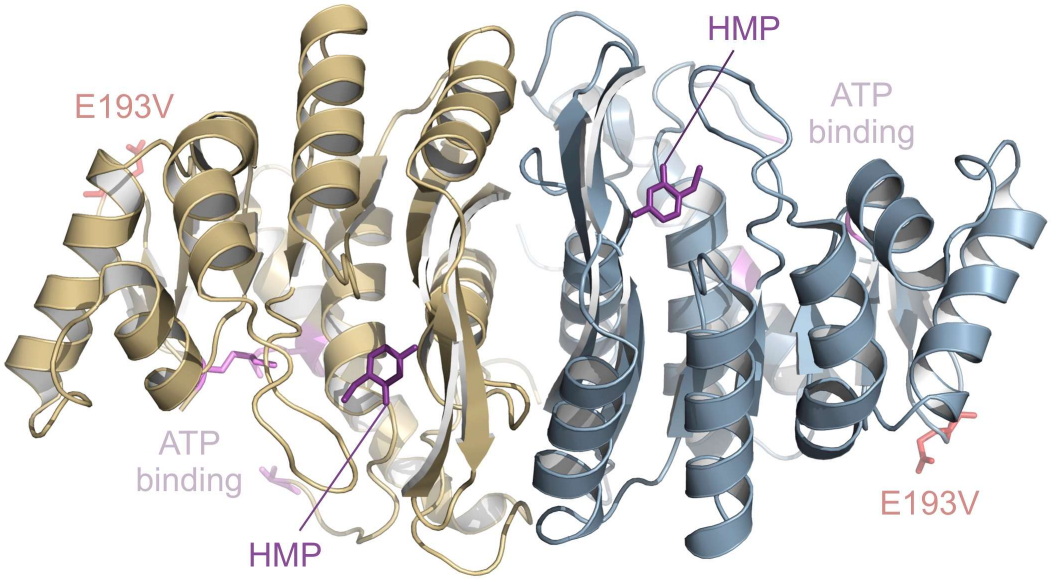

Figure 9.3 Location of the E193K mutation in ThiD. Structure of *Salmonella enteriditis* serovar Typhimurium ThiD protein in complex with hydroxymethylpyrimidine (HMP; Protein Data Bank (PDB): 1JXI; Cheng et al., (2002) Structure 10: 225-235). Residues (Lys176, Arg202 and Lys237) involved in ATP binding are shown in pink. The location of the Glu193Val substitution found in the EDTA-resistant strains JN161 and JN192 is highlighted in red. The protein structure was generated in Pymol.

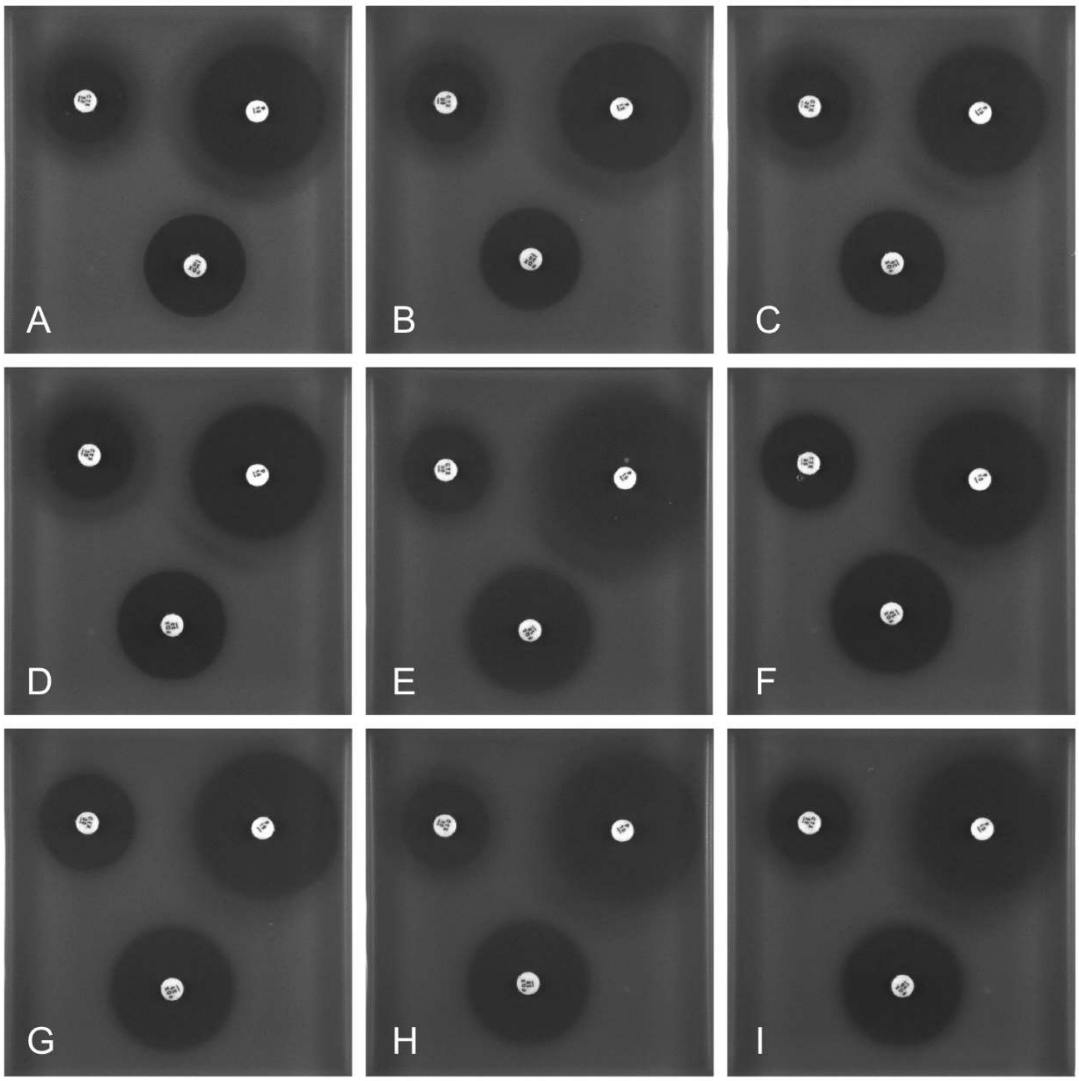

Figure 9.4 Sensitivity of *S. aureus* chelant-resistant mutants to cefotaxime, cefoxitin and penicillin G. (A) wt, (B) JN170,(C) JN206, (D) JN207, (E) JN174, (F) JN208, (G) JN209, (H) JN210, (I) JN212. Discs were placed on agar plates with a bacterial overlay of each strain. Cefotaxime (30 µg, top left), cefoxitin (30 µg, bottom) and penicillin G (10 U, top right) of each plate. LB agar plates were incubated for 24 h at 37°C.

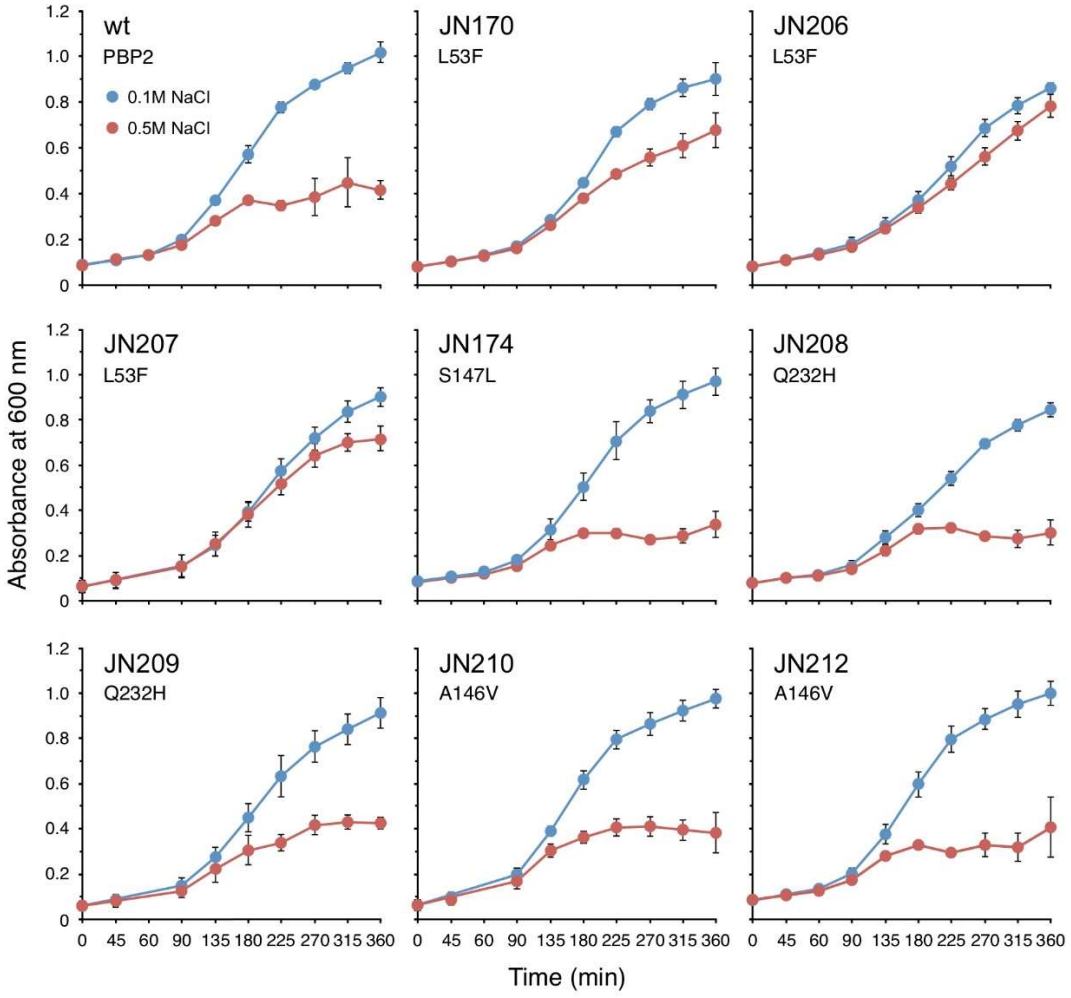

Figure 9.5 Salt tolerance of *S. aureus* chelant-resistant mutants. Bacteria were cultivated in LB containing either 0.1 M or 0.5 M NaCl at 37°C in a shaking incubator and growth monitored at $A_{600\ nm}$. Data are the mean and standard deviation of three independent experiments. The wild-type, JN170 and JN206 are presented in Chapter 6, Figure 6.14 but are reproduced here to facilitate comparisons. These experiments were carried out by Rebecca Lee as part of her final year MBiol research project.

References

Abraham, J. M., Freitag, C. S., Clements, J. R., & Eisenstein, B. I. (1985). An invertible element of DNA controls phase variation of type 1 fimbriae of *Escherichia coli*. *Proceedings of the National Academy of Sciences*, *82*(17), 5724–5727. https://doi.org/10.1073/PNAS.82.17.5724

Abushaheen, M. A., Muzaheed, Fatani, A. J., Alosaimi, M., Mansy, W., George, M., Acharya, S., Rathod, S., Divakar, D. D., Jhugroo, C., Vellappally, S., Khan, A. A., Shaik, J., & Jhugroo, P. (2020). Antimicrobial resistance, mechanisms and its clinical significance. *Disease-a-Month*, *66*(6), 100971. https://doi.org/10.1016/j.disamonth.2020.100971

Ackermann, L., Virtanen, H., Korhonen, L., Laukkanen, A., Huilaja, L., Riekki, R., & Hasan, T. (2017). An epidemic of allergic contact dermatitis caused by a new allergen, caprylhydroxamic acid, in moisturizers. *Contact Dermatitis*, *77*(3), 159–162. https://doi.org/10.1111/cod.12787

Al-Mnaser, A. A., & Woodward, M. J. (2020). Sub-lethal concentrations of phytochemicals (carvacrol and oregano) select for reduced susceptibility mutants of *Escherichia coli* O23:H52. *Polish Journal of Microbiology*, *69*(1), 121. https://doi.org/10.33073/PJM-2020-003

Alakomi, H. L., Paananen, A., Suihko, M. L., Helander, I. M., & Saarela, M. (2006). Weakening effect of cell permeabilizers on Gram-negative bacteria causing biodeterioration. *Applied and Environmental Microbiology*, *72*(7), 4695–4703. https://doi.org/10.1128/AEM.00142-06

Alakomi, H. L., Saarela, M., & Helander, I. M. (2003). Effect of EDTA on *Salmonella enterica* serovar Typhimurium involves a component not assignable to lipopolysaccharide release. *Microbiology*, *149*(8), 2015–2021. https://doi.org/10.1099/mic.0.26312-0

Allan, D. S., Del Carmen Parquet, M., Savage, K. A., & Holbein, B. E. (2020). Iron sequestrant DIBI, a potential alternative for nares decolonization of methicillin-resistant *Staphylococcus aureus*, is anti-infective and inhibitory for mupirocin-resistant isolates. *Antimicrobial Agents and Chemotherapy*, *64*(3). https://doi.org/10.1128/AAC.02353-19

Andrews, J. . (2001). Determination of minimum inhibitory concentrations. *Journal of Antimicrobial Chemotherapy*, *48*, 15–16.

Andrews, S. C. (2011). Making DNA without iron - induction of a manganese-dependent ribonucleotide reductase in response to iron starvation. *Molecular Microbiology*, *80*(2), 286–289. https://doi.org/10.1111/j.1365-2958.2011.07594.x

Angus, B. L., Carey, A. M., Caron, D. A., Kropinski, A. M., & Hancock, R. E. (1982). Outer membrane permeability in *Pseudomonas aeruginosa*: comparison of a wild-type with an antibiotic-supersusceptible mutant. *Antimicrobial Agents and Chemotherapy*, *21*(2), 299. https://doi.org/10.1128/AAC.21.2.299

Anjem, A., Varghese, S., & Imlay, J. A. (2009). Manganese import is a key element of the OxyR response to hydrogen peroxide in *Escherichia coli*. *Molecular Microbiology*, *72*(4), 844–858. https://doi.org/10.1111/j.1365-2958.2009.06699.x

Ayala-Torres, C., Hernández, N., Galeano, A., Novoa-Aponte, L., & Soto, C. Y. (2014). Zeta potential as a measure of the surface charge of mycobacterial cells. *Annals of Microbiology*, *64*(3), 1189–1195. https://doi.org/10.1007/s13213-013-0758-y

Baba, T., Ara, T., Hasegawa, M., Takai, Y., Okumura, Y., Baba, M., Datsenko, K. A., Tomita, M., Wanner, B. L., & Mori, H. (2006). Construction of *Escherichia coli* K-12 in-frame, single-gene knockout mutants: the Keio collection. *Molecular Systems Biology*, *2*, 2006.0008. https://doi.org/10.1038/msb4100050

Bacon, C. W., Porter, J. K., Norred, W. P., & Leslie, J. F. (1996). Production of fusaric acid by

Fusarium species. *Applied and Environmental Microbiology*, *62*(11), 4039–4043. http://aem.asm.org/

Balouiri, M., Sadiki, M., & Ibnsouda, S. K. (2016). Methods for in vitro evaluating antimicrobial activity: A review. *Journal of Pharmaceutical Analysis*, *6*(2), 71–79. https://doi.org/10.1016/j.jpha.2015.11.005

Band, V. I., & Weiss, D. S. (2014). Mechanisms of antimicrobial peptide resistance in Gram-negative bacteria. *Antibiotics*, *4*(1), 18–41. https://doi.org/10.3390/antibiotics4010018

Banin, E., Brady, K. M., & Greenberg, E. P. (2006). Chelator-induced dispersal and killing of *Pseudomonas aeruginosa* cells in a biofilm. *Applied and Environmental Microbiology*, *72*(3), 2064–2069. https://doi.org/10.1128/AEM.72.3.2064-2069.2006

Barker, S., Harding, S. V., Gray, D., Richards, M. I., Atkins, H. S., & Harmer, N. J. (2021). Drug screening to identify compounds to act as co-therapies for the treatment of *Burkholderia* species. *PLoS ONE*, *16*(3), e0248119. https://doi.org/10.1371/journal.pone.0248119

Barnard, T. J., Watson, J., & McIntosh, M. A. (2001). Mutations in the *Escherichia coli* receptor FepA reveal residues involved in ligand binding and transport. *Molecular Microbiology*, *41*(3), 527–536. https://doi.org/10.1046/j.1365-2958.2001.02473.x

Bastos, M. do C. de F., Coutinho, B. G., & Coelho, M. L. V. (2010). Lysostaphin: A staphylococcal bacteriolysin with potential clinical applications. *Pharmaceuticals*, *3*(4), 1139–1161. https://doi.org/10.3390/ph3041139

Bateman, A. (1999). The SIS domain: a phosphosugar-binding domain. *Trends in Biochemical Sciences*, *24*(3), 94–95. https://doi.org/10.1016/S0968-0004(99)01357-2

Beasley, F. C., Marolda, C. L., Cheung, J., Buac, S., & Heinrichs, D. E. (2011). *Staphylococcus aureus* transporters Hts, Sir, and Sst capture iron liberated from human transferrin by Staphyloferrin A, Staphyloferrin B, and catecholamine stress hormones, respectively, and contribute to virulence. *Infection and Immunity*, *79*(6), 2345. https://doi.org/10.1128/IAI.00117-11

Beecroft, M. S. (2019). *Antimicrobial Chelators and their Mechanism of Action* [PhD thesis, Durham University]. http://etheses.dur.ac.uk/12933/http://etheses.dur.ac.uk

Bera, A., Biswas, R., Herbert, S., & Götz, F. (2006). The presence of peptidoglycan O-acetyltransferase in various *Staphylococcal* species correlates with lysozyme resistance and pathogenicity. *Infection and Immunity*, *74*(8), 4598. https://doi.org/10.1128/IAI.00301-06

Bera, A., Herbert, S., Jakob, A., Vollmer, W., & Götz, F. (2005). Why are pathogenic staphylococci so lysozyme resistant? The peptidoglycan O-acetyltransferase OatA is the major determinant for lysozyme resistance of *Staphylococcus aureus*. *Molecular Microbiology*, *55*(3), 778–787. https://doi.org/10.1111/j.1365-2958.2004.04446.x

Bingham, R., Rudiño-Piñera, E., Meenan, N., Schwarz-Linek, U., Turkenburg, J., Höök, M., Garman, E., & Potts, J. (2008). Crystal structures of fibronectin-binding sites from *Staphylococcus aureus* FnBPA in complex with fibronectin domains. *Proceedings of the National Academy of Sciences of the United States of America*, *105*(34), 12254–12258. https://doi.org/10.1073/PNAS.0803556105

Blaby-Haas, C. E., Flood, J. A., Crécy-Lagard, V. de, & Zamble, D. B. (2012). YeiR: a metal-binding GTPase from *Escherichia coli* involved in metal homeostasis. *Metallomics*, *4*(5), 488–497. https://doi.org/10.1039/C2MT20012K

Blattner, F. R., Plunkett, G., Bloch, C. A., Perna, N. T., Burland, V., Riley, M., Collado-Vides, J., Glasner, J. D., Rode, C. K., Mayhew, G. F., Gregor, J., Davis, N. W., Kirkpatrick, H. A., Goeden, M. A., Rose, D. J., Mau, B., & Shao, Y. (1997). The complete genome sequence of *Escherichia coli* K-12. *Science*, *277*(5331), 1453–1462. https://doi.org/10.1126/science.277.5331.1453

Bollenbach, T. (2015). Antimicrobial interactions: mechanisms and implications for drug discovery and resistance evolution. *Current Opinion in Microbiology*, *27*, 1–9. https://doi.org/10.1016/J.MIB.2015.05.008

Bonapace, C. R., Bosso, J. A., Friedrich, L. V., & White, R. L. (2002). Comparison of methods of interpretation of checkerboard synergy testing. *Diagnostic Microbiology and Infectious Disease*, *44*(4), 363–366. https://doi.org/10.1016/S0732-8893(02)00473-X

Brameyer, S., Rösch, T. C., Andari, J. El, Hoyer, E., Schwarz, J., Graumann, P. L., & Jung, K. (2019). DNA-binding directs the localization of a membrane-integrated receptor of the ToxR family. *Communications Biology 2019 2:1*, *2*(1), 1–10. https://doi.org/10.1038/s42003-018-0248-7

Braun, V., Bös, C., Braun, M., & Killmann, H. (2001). Outer membrane channels and active transporters for the uptake of antibiotics. *Journal of Infectious Diseases*, *183*(SUPPL. 1), S12–S16. https://doi.org/10.1086/318840

Braun, Volkmar. (1999). Active transport of siderophore-mimicking antibacterials across the outer membrane. *Drug Resistance Updates*, *2*(6), 363–369. https://doi.org/10.1054/drup.1999.0107

Breckau, D., Mahlitz, E., Sauerwald, A., Layer, G., & Jahn, D. (2003). Oxygen-dependent coproporphyrinogen III oxidase (HemF) from *Escherichia coli* is stimulated by manganese. *Journal of Biological Chemistry*, *278*(47), 46625–46631. https://doi.org/10.1074/jbc.M308553200

Brickman, T. J., & Mcintosh, M. A. (1992). Overexpression and purification of ferric enterobactin esterase from *Escherichia coli*. *Journal of Biological Chemistry*, *267*(17), 12350–12355. https://doi.org/10.1016/S0021-9258(19)49846-3

Brown, M. R. W., & Richards, R. M. E. (1965). Effect of ethylenediamine tetraacetate on the resistance of *Pseudomonas aeruginosa* to antibacterial agents. *Nature*, *207*(5004), 1391–1393. https://doi.org/10.1038/2071391a0

Cardiano, P., Cigala, R. M., Cordaro, M., De Stefano, C., Milea, D., & Sammartano, S. (2017). On the complexation of metal cations with “pure” diethylenetriamine-N,N,N′,N″,N″-pentakis(methylenephosphonic) acid. *New Journal of Chemistry*, *41*(10), 4065–4075. https://doi.org/10.1039/c7nj00118e

Cassat, J. E., & Skaar, E. P. (2013). Iron in Infection and Immunity. *Cell Host & Microbe*, *13*(5), 509–519. https://doi.org/10.1016/j.chom.2013.04.010

Caza, M., & Kronstad, J. (2013). Shared and distinct mechanisms of iron acquisition by bacterial and fungal pathogens of humans. *Frontiers in Cellular and Infection Microbiology*, *NOV*, 80. https://doi.org/10.3389/FCIMB.2013.00080

Cerasi, M., Ammendola, S., & Battistoni, A. (2013). Competition for zinc binding in the host-pathogen interaction. *Frontiers in Cellular and Infection Microbiology*, *DEC*, 108. https://doi.org/10.3389/FCIMB.2013.00108

Cerasi, M., Liu, J. Z., Ammendola, S., Poe, A. J., Petrarca, P., Pesciaroli, M., Pasquali, P., Raffatellu, M., & Battistoni, A. (2014). The ZupT transporter plays an important role in zinc homeostasis and contributes to *Salmonella enterica* virulence. *Metallomics : Integrated Biometal Science*, *6*(4), 845. https://doi.org/10.1039/C3MT00352C

Chan, D. C. K., Guo, I., & Burrows, L. L. (2020). Forging new antibiotic combinations under iron-limiting conditions. *Antimicrobial Agents and Chemotherapy*, *64*(3). https://doi.org/10.1128/AAC.01909-19

Chandrangsu, P., Rensing, C., & Helmann, J. D. (2017). Metal homeostasis and resistance in bacteria. *Nature Reviews. Microbiology*, *15*(6), 338–350. https://doi.org/10.1038/nrmicro.2017.15

Chen, Z., Lewis, K. A., Shultzaberger, R. K., Lyakhov, I. G., Zheng, M., Doan, B., Storz, G., & Schneider, T. D. (2007). Discovery of Fur binding site clusters in *Escherichia coli* by

information theory models. *Nucleic Acids Research*, *35*(20), 6762–6777. https://doi.org/10.1093/NAR/GKM631

Cheng, G., Bennett, E. M., Begley, T. P., & Ealick, S. E. (2002). Crystal structure of 4-amino-5-hydroxymethyl-2- methylpyrimidine phosphate kinase from *Salmonella* typhimurium at 2.3 Å resolution. *Structure*, *10*(2), 225–235. https://doi.org/10.1016/S0969-2126(02)00708-6

Choby, J. E., & Skaar, E. P. (2016). Heme synthesis and acquisition in bacterial pathogens. *Journal of Molecular Biology*, *428*(17), 3408. https://doi.org/10.1016/J.JMB.2016.03.018

Chopra, I., Hawkey, P. M., & Hinton, M. (1992). Tetracyclines, molecular and clinical aspects. *Journal of Antimicrobial Chemotherapy*, *29*(3), 245–277. https://doi.org/10.1093/jac/29.3.245

Chopra, Ian, & Roberts, M. (2001). Tetracycline antibiotics: mode of action, applications, molecular biology, and epidemiology of bacterial resistance. *Microbiology and Molecular Biology Reviews*, *65*(2), 232–260. https://doi.org/10.1128/mmbr.65.2.232-260.2001

Clementi, E. A., Marks, L. R., Roche-Håkansson, H., & Håkansson, A. P. (2014). Monitoring changes in membrane polarity, membrane integrity, and intracellular ion concentrations in *Streptococcus pneumoniae* using fluorescent dyes. *Journal of Visualized Experiments*, *84*(84), 51008. https://doi.org/10.3791/51008

Corbin, B. D., Seeley, E. H., Raab, A., Feldmann, J., Miller, M. R., Torres, V. J., Anderson, K. L., Dattilo, B. M., Dunman, P. M., Gerads, R., Caprioli, R. M., Nacken, W., Chazin, W. J., & Skaar, E. P. (2008). Metal chelation and inhibition of bacterial growth in tissue abscesses. *Science*, *319*(5865), 962–965. https://doi.org/10.1126/science.1152449

Cronin, S. J. F., Woolf, C. J., Weiss, G., & Penninger, J. M. (2019). The role of iron regulation in immunometabolism and immune-related disease. *Frontiers in Molecular Biosciences*, *6*, 116. https://doi.org/10.3389/fmolb.2019.00116

Crutcher, F. K., Puckhaber, L. S., Stipanovic, R. D., Bell, A. A., Nichols, R. L., Lawrence, K. S., & Liu, J. (2017). Microbial resistance mechanisms to the antibiotic and phytotoxin fusaric acid. *Journal of Chemical Ecology*, *43*(10), 996–1006. https://doi.org/10.1007/s10886-017-0889-x

Cullen, T. W., Schofield, W. B., Barry, N. A., Putnam, E. E., Rundell, E. A., Trent, M. S., Degnan, P. H., Booth, C. J., Yu, H., & Goodman, A. L. (2015). Antimicrobial peptide resistance mediates resilience of prominent gut commensals during inflammation. *Science*, *347*(6218), 170–175. https://doi.org/10.1126/science.1260580

Dalal, V., Kumar, P., Rakhaminov, G., Qamar, A., Fan, X., Hunter, H., Tomar, S., Golemi-Kotra, D., & Kumar, P. (2019). Repurposing an ancient protein core structure: structural studies on FmtA, a novel esterase of *Staphylococcus aureus*. *Journal of Molecular Biology*, *431*(17), 3107–3123. https://doi.org/10.1016/J.JMB.2019.06.019

Dean, K. M., Qin, Y., & Palmer, A. E. (2012). Visualizing metal ions in cells: an overview of analytical techniques, approaches, and probes. *Biochimica et Biophysica Acta - Molecular Cell Research*, *1823*(9), 1406–1415. https://doi.org/10.1016/j.bbamcr.2012.04.001

Delcour, A. H. (2009). Outer membrane permeability and antibiotic resistance. *Biochimica et Biophysica Acta - Proteins and Proteomics*, *1794*(5), 808–816. https://doi.org/10.1016/j.bbapap.2008.11.005

Djoko, K. Y., & McEwan, A. G. (2013). Antimicrobial action of copper is amplified *via* inhibition of heme biosynthesis. *ACS Chemical Biology*, *8*(10), 2217–2223. https://doi.org/10.1021/CB4002443

Djoko, K. Y., Phan, M.-D., Peters, K. M., Walker, M. J., Schembri, M. A., & McEwan, A. G. (2017). Interplay between tolerance mechanisms to copper and acid stress in *Escherichia coli*. *Proceedings of the National Academy of Sciences*, *114*(26), 6818–

6823. https://doi.org/10.1073/PNAS.1620232114

Djoko, K. Y., Y. Ong, C. L., Walker, M. J., & McEwan, A. G. (2015). The role of copper and zinc toxicity in innate immune defense against bacterial pathogens. *Journal of Biological Chemistry*, *290*(31), 1854–1861. https://doi.org/10.1074/jbc.R115.647099

do Couto, F. M. M., do Nascimento, S. C., Júnior, S. F. P., da Silva, V. K. A., Leal, A. F. G., & Neves, R. P. (2016). Antifungal activity of the piroctone olamine in experimental intra-abdominal candidiasis. *SpringerPlus*, *5*(1). https://doi.org/10.1186/s40064-016-2130-8

Driessen, A. J. M., Poolman, B., Kiewiet, R., & Konings, W. N. (1987). Arginine transport in *Streptococcus lactis* is catalyzed by a cationic exchanger (secondary solute transport/arginine:ornithine antiport). *Proceedings of the National Academy of Sciences of the United States of America*, *84*, 6093–6097.

Dubrac, S., & Touati, D. (2000). Fur positive regulation of iron superoxide dismutase in *Escherichia coli*: Functional analysis of the *sodB* promoter. *Journal of Bacteriology*, *182*(13), 3802–3808. https://doi.org/10.1128/JB.182.13.3802-3808.2000

Edmonds, K. A., Jordan, M. R., & Giedroc, D. P. (2021). COG0523 proteins: A functionally diverse family of transition metal-regulated G3E P-loop GTP hydrolases from bacteria to man. *Metallomics*, *3*(8). https://doi.org/10.1093/MTOMCS/MFAB046

Egan, A. J. F., Biboy, J., Veer, I. van't, Breukink, E., & Vollmer, W. (2015). Activities and regulation of peptidoglycan synthases. *Philosophical Transactions of the Royal Society B: Biological Sciences*, *370*(1679). https://doi.org/10.1098/RSTB.2015.0031

Egan, A. J. F., Errington, J., & Vollmer, W. (2020). Regulation of peptidoglycan synthesis and remodelling. *Nature Reviews Microbiology 2020 18:8*, *18*(8), 446–460. https://doi.org/10.1038/s41579-020-0366-3

Eichinger, A., Haneburger, I., Koller, C., Jung, K., & Skerra, A. (2011). Crystal structure of the sensory domain of *Escherichia coli* CadC, a member of the ToxR-like protein family. *Protein Science : A Publication of the Protein Society*, *20*(4), 656. https://doi.org/10.1002/PRO.594

Eijkelkamp, B. A., McDevitt, C. A., & Kitten, T. (2015). Manganese uptake and streptococcal virulence. *BioMetals*, *28*(3), 491. /pmc/articles/PMC5800397/

El-Gamel, N. E. A. (2010). Metal chelates of ampicillin versus amoxicillin: Synthesis, structural investigation, and biological studies. *Journal of Coordination Chemistry*, *63*(3), 534–543. https://doi.org/10.1080/00958970903494157

Escolar, L., Pérez-Martín, J., & Lorenzo, V. de. (1998). Coordinated repression in vitro of the divergent *fepA-fes* promoters of *Escherichia coli* by the iron uptake regulation (Fur) protein. *Journal of Bacteriology*, *180*(9), 2579. /pmc/articles/PMC107206/

European Committee for Antimicrobial Susceptibility Testing, T. (2000). Determination of minimum inhibitory concentrations (MICs) of antibacterial agents by agar dilution. *Clinical Microbiology and Infection*, *6*(9), 509–515. https://doi.org/10.1046/j.1469-0691.2000.00142.x

Fey, P. D., Endres, J. L., Yajjala, V. K., Widhelm, T. J., Boissy, R. J., Bose, J. L., & Bayles, K. W. (2013). A genetic resource for rapid and comprehensive phenotype screening of nonessential *Staphylococcus aureus* genes. *MBio*, *4*(1). https://doi.org/10.1128/mBio.00537-12

Finnegan, S., & Percival, S. L. (2015). EDTA: an antimicrobial and antibiofilm agent for use in wound care. *Advances in Wound Care*, *4*(7), 415–421. https://doi.org/10.1089/wound.2014.0577

Flora, S. J. S., & Pachauri, V. (2010). Chelation in metal intoxication. *International Journal of Environmental Research and Public Health*, *7*(7), 2745–2788. https://doi.org/10.3390/ijerph7072745

Fontana, R., Cornaglia, G., Ligozzi, M., & Mazzariol, A. (2000). The final goal: Penicillin-binding proteins and the target of cephalosporins. *Clinical Microbiology and Infection*, *6*(S3), 34–40. https://doi.org/10.1111/j.1469-0691.2000.tb02038.x

Foster, A. W., Osman, D., & Robinson, N. J. (2014). Metal preferences and metallation. *Journal of Biological Chemistry*, *289*(41), 28095–28103. https://doi.org/10.1074/jbc.R114.588145

Fritsche, G., Nairz, M., Libby, S. J., Fang, F. C., & Weiss, G. (2012). Slc11a1 (Nramp1) impairs growth of *Salmonella enterica* serovar typhimurium in macrophages via stimulation of lipocalin-2 expression. *Journal of Leukocyte Biology*, *92*(2), 353–359. https://doi.org/10.1189/jlb.1111554

Fulde, M., Willenborg, J., Huber, C., Hitzmann, A., Willms, D., Seitz, M., Eisenreich, W., Valentin-Weigand, P., & Goethe, R. (2014). The arginine-ornithine antiporter arcD contributes to biological fitness of *Streptococcus suis*. *Frontiers in Cellular and Infection Microbiology*, *4*(AUG), 107. https://doi.org/10.3389/fcimb.2014.00107

Gaballa, A., & Helmann, J. D. (1998). Identification of a zinc-specific metalloregulatory protein, Zur, controlling zinc transport operons in *Bacillus subtilis*. *Journal of Bacteriology*, *180*(22), 5815. /pmc/articles/PMC107652/

Gaballa, A., & Helmann, J. D. (2002). A peroxide-induced zinc uptake system plays an important role in protection against oxidative stress in *Bacillus subtilis*. *Molecular Microbiology*, *45*(4), 997–1005. https://doi.org/10.1046/J.1365-2958.2002.03068.X

Gaballa, A., Wang, T., Ye, R. W., & Helmann, J. D. (2002). Functional analysis of the Bacillus subtilis Zur regulon. *Journal of Bacteriology*, *184*(23), 6508. https://doi.org/10.1128/JB.184.23.6508-6514.2002

Gammoh, N. Z., & Rink, L. (2017). Zinc in infection and inflammation. *Nutrients*, *9*(6), 624. https://doi.org/10.3390/nu9060624

García-Casal, M. N., Leets, I., & Layrisse, M. (2004). Ethylenediaminetetraacetic acid (EDTA) does not increase iron uptake or ferritin synthesis by Caco-2 cells. *Journal of Nutritional Biochemistry*, *15*(5), 261–266. https://doi.org/10.1016/j.jnutbio.2003.10.004

Garénaux, A., Caza, M., & Dozois, C. M. (2011). The ins and outs of siderophore mediated iron uptake by extra-intestinal pathogenic *Escherichia coli*. *Veterinary Microbiology*, *153*(1–2), 89–98. https://doi.org/10.1016/J.VETMIC.2011.05.023

Garrido, C., Galluzzi, L., Brunet, M., Puig, P. E., Didelot, C., & Kroemer, G. (2006). Mechanisms of cytochrome *c* release from mitochondria. *Cell Death and Differentiation*, *13*(9), 1423–1433. https://doi.org/10.1038/sj.cdd.4401950

Ghelardi, E., Celandroni, F., Gueye, S. A., Salvetti, S., Campa, M., & Senesi, S. (2013). Antimicrobial activity of a new preservative for multiuse ophthalmic solutions. *Journal of Ocular Pharmacology and Therapeutics*, *29*(6), 586–590. https://doi.org/10.1089/jop.2012.0041

Goffin, C., & Ghuysen, J.-M. (1998). Multimodular penicillin-binding proteins: an enigmatic family of orthologs and paralogs. *Microbiology and Molecular Biology Reviews*, *62*(4), 1079. /pmc/articles/PMC98940/

Graham, A. I., Hunt, S., Stokes, S. L., Bramall, N., Bunch, J., Cox, A. G., McLeod, C. W., & Poole, R. K. (2009). Severe zinc depletion of *Escherichia coli*: roles for high affinity zinc binding by ZinT, zinc transport and zinc-independent proteins. *The Journal of Biological Chemistry*, *284*(27), 18377. https://doi.org/10.1074/JBC.M109.001503

Graham, J. E., & Wilkinson, B. J. (1992). *Staphylococcus aureus* osmoregulation: roles for choline, glycine betaine, proline, and taurine. *Journal of Bacteriology*, *174*(8), 2711. https://doi.org/10.1128/JB.174.8.2711-2716.1992

Gray, D. A., Dugar, G., Gamba, P., Strahl, H., Jonker, M. J., & Hamoen, L. W. (2019). Extreme slow growth as alternative strategy to survive deep starvation in bacteria. *Nature*

Communications, *10*(1), 1–12. https://doi.org/10.1038/s41467-019-08719-8

Griffiths, E. (1991). Iron and bacterial virulence - a brief overview. *Biology of Metals*, *4*(1), 7–13. https://doi.org/10.1007/BF01135551

Grim, K. P., San Francisco, B., Radin, J. N., Brazel, E. B., Kelliher, J. L., Párraga Solórzano, P. K., Kim, P. C., McDevitt, C. A., & Kehl-Fie, T. E. (2017). The metallophore staphylopine enables *Staphylococcus aureus* to compete with the host for zinc and overcome nutritional immunity. *MBio*, *8*(5). https://doi.org/10.1128/mBio.01281-17

Gründling, A. (2013). Potassium uptake systems in *Staphylococcus aureus*: new stories about ancient systems. *MBio*, *4*(5). https://doi.org/10.1128/MBIO.00784-13

Gründling, A., & Schneewind, O. (2006). Cross-linked peptidoglycan mediates lysostaphin binding to the cell wall envelope of *Staphylococcus aureus*. *Journal of Bacteriology*, *188*(7), 2463–2472. https://doi.org/10.1128/JB.188.7.2463-2472.2006

Gruszka, D. T., Wojdyla, J. A., Bingham, R. J., Turkenburg, J. P., Manfield, I. W., Steward, A., Leech, A. P., Geoghegan, J. A., Foster, T. J., Clarke, J., & Potts, J. R. (2012). Staphylococcal biofilm-forming protein has a contiguous rod-like structure. *Proceedings of the National Academy of Sciences of the United States of America*, *109*(17), E1011. https://doi.org/10.1073/PNAS.1119456109

Guerra, W., Silva-Caldeira, P. P., Terenzi, H., & Pereira-Maia, E. C. (2016). Impact of metal coordination on the antibiotic and non-antibiotic activities of tetracycline-based drugs. *Coordination Chemistry Reviews*, *327–328*, 188–199. https://doi.org/10.1016/j.ccr.2016.04.009

Haas, C. E., Rodionov, D. A., Kropat, J., Malasarn, D., Merchant, S. S., & Crécy-Lagard, V. de. (2009). A subset of the diverse COG0523 family of putative metal chaperones is linked to zinc homeostasis in all kingdoms of life. *BMC Genomics*, *10*, 470. https://doi.org/10.1186/1471-2164-10-470

Haase, H., Hebel, S., Engelhardt, G., & Rink, L. (2013). Application of Zinpyr-1 for the investigation of zinc signals in *Escherichia coli*. *BioMetals*, *26*(1), 167–177. https://doi.org/10.1007/s10534-012-9604-0

Halder, S., Yadav, K. K., Sarkar, R., Mukherjee, S., Saha, P., Haldar, S., Karmakar, S., & Sen, T. (2015). Alteration of Zeta potential and membrane permeability in bacteria: a study with cationic agents. *SpringerPlus*, *4*(1), 1–14. https://doi.org/10.1186/s40064-015-1476-7

Hancock, R. D. (1992). Chelate ring size and metal ion selection: the basis of selectivity for metal ions in open-chain ligands and macrocycles. *Journal of Chemical Education*, *69*(8), 615–621. https://doi.org/10.1021/ed069p615

Hancock, R. D., & Martell, A. E. (1989). Ligand design for selective complexation of metal ions in aqueous solution. *Chemical Reviews*, *89*(8), 1875–1914. https://doi.org/10.1021/cr00098a011

Hancock, R. E. (1984). Alterations in outer membrane permeability. *Annual Review of Microbiology*, *38*, 237–264. https://doi.org/10.1146/annurev.mi.38.100184.001321

Hancock, R. E. W., Raffle, V. J., & Nicas, T. I. (1981). Involvement of the outer membrane in gentamicin and streptomycin uptake and killing in *Pseudomonas aeruginosa*. *Antimicrobial Agents and Chemotherapy*, *19*(5), 777–785. https://doi.org/10.1128/AAC.19.5.777

Haneburger, I., Eichinger, A., Skerra, A., & Jung, K. (2011). New insights into the signaling mechanism of the pH-responsive, membrane-integrated transcriptional activator CadC of *Escherichia coli*. *Journal of Biological Chemistry*, *286*(12), 10681–10689. https://doi.org/10.1074/JBC.M110.196923

Haneburger, I., Fritz, G., Jurkschat, N., Tetsch, L., Eichinger, A., Skerra, A., Gerland, U., & Jung, K. (2012). Deactivation of the *E. coli* pH stress sensor CadC by cadaverine.

Journal of Molecular Biology, *424*(1–2), 15–27. https://doi.org/10.1016/J.JMB.2012.08.023

Haque, H., & Russell, A. D. (1974). Effect of chelating agents on the susceptibility of some strains of Gram-negative bacteria to some antibacterial agents. *Antimicrobial Agents and Chemotherapy*, *6*(2), 200–206. https://doi.org/10.1128/AAC.6.2.200

Hasman, H., Schembri, M. A., & Klemm, P. (2000). Antigen 43 and type 1 fimbriae determine colony morphology of *Escherichia coli* K-12. *Journal of Bacteriology*, *182*(4), 1089. https://doi.org/10.1128/JB.182.4.1089-1095.2000

Heath, R. J., Yu, Y.-T., Shapiro, M. A., Olson, E., & Rock, C. O. (1998). Broad spectrum antimicrobial biocides target the FabI component of fatty acid synthesis. *Journal of Biological Chemistry*, *273*(46), 30316–30320. https://doi.org/10.1074/JBC.273.46.30316

Helander, I. M., & Mattila-Sandholm, T. (2000). Fluorometric assessment of Gram-negative bacterial permeabilization. *Journal of Applied Microbiology*, *88*(2), 213–219. https://doi.org/10.1046/j.1365-2672.2000.00971.x

Herbert, S., Bera, A., Nerz, C., Kraus, D., Peschel, A., Goerke, C., Meehl, M., Cheung, A., & Götz, F. (2007). Molecular basis of resistance to muramidase and cationic antimicrobial peptide activity of lysozyme in *Staphylococci*. *PLoS Pathogens*, *3*(7), e102. https://doi.org/10.1371/journal.ppat.0030102

Hidaka, H., Nagatsu, T., Takeya, K., Takeuchi, T., Suda, H., Kojiri, K., Matsuzaki, M., & Umezawa, H. (1969). Fusaric acid, a hypotensive agent produced by fungi. *Journal of Antibiotics*, *22*(5), 228–230. https://doi.org/10.7164/antibiotics.22.228

Hohle, T. H., Franck, W. L., Stacey, G., & O'Brian, M. R. (2011). Bacterial outer membrane channel for divalent metal ion acquisition. *Proceedings of the National Academy of Sciences of the United States of America*, *108*(37), 15390. https://doi.org/10.1073/PNAS.1110137108

Hohle, T. H., & O'Brian, M. R. (2014). Magnesium-dependent processes are targets of bacterial manganese toxicity. *Molecular Microbiology*, *93*(4), 736–747. https://doi.org/10.1111/mmi.12687

Hood, M. I., & Skaar, E. P. (2012). Nutritional immunity: transition metals at the pathogen-host interface. *Nature Reviews Microbiology*, *10*(8), 525–537. https://doi.org/10.1038/nrmicro2836

Horn, D., & Barrientos, A. (2008). Mitochondrial copper metabolism and delivery to cytochrome *c* oxidase. *IUBMB Life*, *60*(7), 421–429. https://doi.org/10.1002/iub.50

Huang, C.-S., Pedersen, B. P., & Stokes, D. L. (2017). Crystal structure of the potassium importing KdpFABC membrane complex. *Nature*, *546*(7660), 681. https://doi.org/10.1038/NATURE22970

Huang, C.-Y., Shih, H.-W., Lin, L.-Y., Tien, Y.-W., Cheng, T.-J. R., Cheng, W.-C., Wong, C.-H., & Ma, C. (2012). Crystal structure of *Staphylococcus aureus* transglycosylase in complex with a lipid II analog and elucidation of peptidoglycan synthesis mechanism. *Proceedings of the National Academy of Sciences*, *109*(17), 6496–6501. https://doi.org/10.1073/PNAS.1203900109

Hunt, M., Pettis, G., & McIntosh, M. (1994). Promoter and operator determinants for fur-mediated iron regulation in the bidirectional *fepA-fes* control region of the *Escherichia coli* enterobactin gene system. *Journal of Bacteriology*, *176*(13), 3944–3955. https://doi.org/10.1128/JB.176.13.3944-3955.1994

Ibacache-Quiroga, C., Oliveros, J. C., Couce, A., & Blázquez, J. (2018). Parallel evolution of high-level aminoglycoside resistance in *Escherichia coli* under low and high mutation supply rates. *Frontiers in Microbiology*, *9*(MAR), 427. https://doi.org/10.3389/fmicb.2018.00427

Ido, Y., Muto, N., Inada, A., Kohroki, J., Mano, M., Odani, T., Itoh, N., Yamamoto, K., &

Tanaka, K. (1999). Induction of apoptosis by hinokitiol, a potent iron chelator, in teratocarcinoma F9 cells is mediated through the activation of caspase-3. *Cell Proliferation*, *32*(1), 63–73. https://doi.org/10.1046/j.1365-2184.1999.3210063.x

Imani Rad, H., Arzanlou, M., Ranjbar Omid, M., Ravaji, S., & Peeri Doghaheh, H. (2017). Effect of culture media on chemical stability and antibacterial activity of allicin. *Journal of Functional Foods*, *28*, 321–325. https://doi.org/10.1016/j.jff.2016.10.027

Imlay, J. A. (2014). The mismetallation of enzymes during oxidative stress. *Journal of Biological Chemistry*, *289*(41), 28121–28128. https://doi.org/10.1074/jbc.R114.588814

Jain, S., Sengupta, M., Sarkar, S., Ghosh, S., Nandi Mitra, A., Sinha, A., & Chakravroty, S. (2016). Can EDTA change MRSA into MSSA? A future prospective! *Journal of Clinical and Diagnostic Research*, *10*(2), 22–25. https://doi.org/10.7860/JCDR/2016/17944.7280

Janulczyk, R., Ricci, S., & Björck, L. (2003). MtsABC is important for manganese and iron transport, oxidative stress resistance, and virulence of *Streptococcus pyogenes*. *Infection and Immunity*, *71*(5), 2656. https://doi.org/10.1128/IAI.71.5.2656-2664.2003

Jesionek, W., Móricz, Á. M., Alberti, Á., Ott, P. G., Kocsis, B., Horváth, G., & Choma, I. M. (2015). TLC-direct bioautography as a bioassay guided method for investigation of antibacterial compounds in *Hypericum perforatum* L. *Journal of AOAC International*, *98*(4), 1013–1020. https://doi.org/10.5740/jaoacint.14-233

Johns, B. E., Purdy, K. J., Tucker, N. P., & Maddocks, S. E. (2015). Phenotypic and genotypic characteristics of small colony variants and their role in chronic infection. *Microbiology Insights*, *8*, 15–23. https://doi.org/10.4137/mbi.s25800

Joo, H. S., & Otto, M. (2015). Mechanisms of resistance to antimicrobial peptides in *Staphylococci*. *Biochimica et Biophysica Acta - Biomembranes*, *1848*(11), 3055–3061. https://doi.org/10.1016/j.bbamem.2015.02.009

Jung, K., Fabiani, F., Hoyer, E., & Lassak, J. (2018). Bacterial transmembrane signalling systems and their engineering for biosensing. *Open Biology*, *8*(4). https://doi.org/10.1098/RSOB.180023

Juttukonda, L. J., & Skaar, E. P. (2015). Manganese homeostasis and utilization in pathogenic bacteria. *Molecular Microbiology*, *97*(2), 216–228. https://doi.org/10.1111/mmi.13034

Kahn, V., & Andrawis, A. (1985). Tropolone as a substrate for horseradish peroxidase. *Phytochemistry*, *24*(5), 909–913. https://doi.org/10.1016/S0031-9422(00)83151-9

Kapoor, G., Saigal, S., & Elongavan, A. (2017). Action and resistance mechanisms of antibiotics: a guide for clinicians. *Journal of Anaesthesiology Clinical Pharmacology*, *33*(3), 300–305. https://doi.org/10.4103/joacp.JOACP_349_15

Kaur, G., Kumar, V., Arora, A., Tomar, A., Ashish, Sur, R., & Dutta, D. (2017). Affected energy metabolism under manganese stress governs cellular toxicity. *Scientific Reports*, *7*(1), 1–11. https://doi.org/10.1038/s41598-017-12004-3

Kehl-Fie, T. E., & Skaar, E. P. (2010). Nutritional immunity beyond iron: a role for manganese and zinc. *Current Opinion in Chemical Biology*, *14*(2), 218–224. https://doi.org/10.1016/j.cbpa.2009.11.008

Kehl-Fie, T. E., Zhang, Y., Moore, J. L., Farrand, A. J., Hood, M. I., Rathi, S., Chazin, W. J., Caprioli, R. M., & Skaar, E. P. (2013). MntABC and MntH contribute to systemic *Staphylococcus aureus* infection by competing with calprotectin for nutrient manganese. *Infection and Immunity*, *81*(9), 3395–3405. https://doi.org/10.1128/IAI.00420-13

Kehres, D. G., & Maguire, M. E. (2003). Emerging themes in manganese transport, biochemistry and pathogenesis in bacteria. *FEMS Microbiology Reviews*, *27*(2–3), 263–290. https://doi.org/10.1016/S0168-6445(03)00052-4

Kehres, D. G., Zaharik, M. L., Finlay, B. B., & Maguire, M. E. (2000). The NRAMP proteins of *Salmonella typhimurium* and *Escherichia coli* are selective manganese transporters

involved in the response to reactive oxygen. *Molecular Microbiology*, *36*(5), 1085–1100. https://doi.org/10.1046/J.1365-2958.2000.01922.X

Kim, Y., Alpmann, P., Blaum-Feder, S., Krämer, S., Endo, T. T., Lu, D., CARSON, D., & Schmidt-Wolf, I. G. H. (2011). Increased *in vivo* efficacy of lenalidomide by addition of piroctone olamine. *In Vivo*, *25*(1), 99–103.

Kocaoglu, O., Tsui, H. C. T., Winkler, M. E., & Carlson, E. E. (2015). Profiling of β-lactam selectivity for penicillin-binding proteins in *Streptococcus pneumoniae* D39. *Antimicrobial Agents and Chemotherapy*, *59*(6), 3548–3555. https://doi.org/10.1128/AAC.05142-14

Koh, E. I., Hung, C. S., Parker, K. S., Crowley, J. R., Giblin, D. E., & Henderson, J. P. (2015). Metal selectivity by the virulence-associated yersiniabactin metallophore system. *Metallomics*, *7*(6), 1011–1022. https://doi.org/10.1039/c4mt00341a

Kohanski, M. A., Dwyer, D. J., & Collins, J. J. (2010). How antibiotics kill bacteria: from targets to networks. *Nature Reviews Microbiology*, *8*(6), 423–435. https://doi.org/10.1038/nrmicro2333

Koley, D., & Bard, A. J. (2010). Triton X-100 concentration effects on membrane permeability of a single HeLa cell by scanning electrochemical microscopy (SECM). *Proceedings of the National Academy of Sciences of the United States of America*, *107*(39), 16783–16787. https://doi.org/10.1073/pnas.1011614107

Komatsuzawa, H., Ohta, K., Labischinski, H., Sugai, M., & Suginaka, H. (1999). Characterization of *fmtA*, a gene that modulates the expression of methicillin resistance in *Staphylococcus aureus*. *Antimicrobial Agents and Chemotherapy*, *43*(9), 2121–2125. https://doi.org/10.1128/aac.43.9.2121

Komatsuzawa, H., Sugai, M., Ohta, K., Fujiwara, T., Nakashima, S., Suzuki, J., Lee, C. Y., & Suginaka, H. (1997). Cloning and characterization of the *fmt* gene which affects the methicillin resistance level and autolysis in the presence of Triton X-100 in methicillin-resistant *Staphylococcus aureus*. *Antimicrobial Agents and Chemotherapy*, *41*(11), 2355–2361.

Komatsuzawa, H., Suzuki, J., Sugai, M., Miyake, Y., & Suginaka, H. (1994). The effect of Triton X-100 on the *in vitro* susceptibility of methicillin-resistant *Staphylococcus aureus* to oxacillin. *Journal of Antimicrobial Chemotherapy*, *34*(6), 885–897. https://doi.org/10.1093/jac/34.6.885

Krause, K. M., Serio, A. W., Kane, T. R., & Connolly, L. E. (2016). Aminoglycosides: an overview. *Cold Spring Harbor Perspectives in Medicine*, *6*(6). https://doi.org/10.1101/cshperspect.a027029

Kumar, P., Sannigrahi, S., & Tzeng, Y. L. (2012). The *Neisseria meningitidis* ZnuD zinc receptor contributes to interactions with epithelial cells and supports heme utilization when expressed in *Escherichia coli*. *Infection and Immunity*, *80*(2), 657–667. https://doi.org/10.1128/IAI.05208-11

Küper, C., & Jung, K. (2006). CadC-mediated activation of the *cadBA* promoter in *Escherichia coli*. *Journal of Molecular Microbiology and Biotechnology*, *10*(1), 26–39. https://doi.org/10.1159/000090346

Kupz, A., Fischer, A., Nies, D. H., Grass, G., Göbel, U. B., Bereswill, S., & Heimesaat, M. M. (2013). Impact of metal ion homeostasis of genetically modified *Escherichia coli* Nissle 1917 and K12 (W3110) strains on colonization properties in the murine intestinal tract. *European Journal of Microbiology & Immunology*, *3*(3), 229. https://doi.org/10.1556/EUJMI.3.2013.3.12

Kusuma, C., Jadanova, A., Chanturiya, T., & Kokai-Kun, J. F. (2007). Lysostaphin-resistant variants of *Staphylococcus aureus* demonstrate reduced fitness in vitro and in vivo. *Antimicrobial Agents and Chemotherapy*, *51*(2), 475–482. https://doi.org/10.1128/AAC.00786-06

Lamas, G. A., & Ergui, I. (2016). Chelation therapy to treat atherosclerosis, particularly in diabetes: is it time to reconsider? *Expert Review of Cardiovascular Therapy*, *14*(8), 927–938. https://doi.org/10.1080/14779072.2016.1180977

Lamas, G. A., Goertz, C., Boineau, R., Mark, D. B., Rozema, T., Nahin, R. L., Lindblad, L., Lewis, E. F., Drisko, J., & Lee, K. L. (2013). Effect of disodium EDTA chelation regimen on cardiovascular events in patients with previous myocardial infarction: The TACT randomized trial. *JAMA - Journal of the American Medical Association*, *309*(12), 1241–1250. https://doi.org/10.1001/jama.2013.2107

Lambert, R. J. W., Hanlon, G. W., & Denyer, S. P. (2004). The synergistic effect of EDTA/antimicrobial combinations on *Pseudomonas aeruginosa*. *Journal of Applied Microbiology*, *96*(2), 244–253. https://doi.org/10.1046/j.1365-2672.2004.02135.x

Lambert, R. J. W., & Lambert, R. (2003). A model for the efficacy of combined inhibitors. *Journal of Applied Microbiology*, *95*(4), 734–743. https://doi.org/10.1046/j.1365-2672.2003.02039.x

Lanigan, R. S., Yamarik, T. A., & Andersen, F. A. (2002). Final report on the safety assessment of EDTA, calcium disodium EDTA, diammonium EDTA, dipotassium EDTA, disodium EDTA, TEA-EDTA, tetrasodium EDTA, tripotassium EDTA, trisodium EDTA, HEDTA, and trisodium HEDTA. *International Journal of Toxicology*, *21*(2_suppl), 95–142. https://doi.org/10.1080/10915810290096522

Lau, C. K. Y., Krewulak, K. D., & Vogel, H. J. (2016). Bacterial ferrous iron transport: the Feo system. *FEMS Microbiology Reviews*, *40*(2), 273–298. https://doi.org/10.1093/FEMSRE/fuv049

Leber, A. (2016). Synergism testing: broth microdilution checkerboard and broth macrodilution methods. In *Clinical Microbiology Procedures Handbook* (pp. 1–23). ASM Press. https://doi.org/10.1128/9781555818814.ch5.16

Leive, L. (1965a). Actinomycin sensitivity in *Escherichia coli* produced by EDTA. *Biochemical and Biophysical Research Communications*, *18*(1), 13–17. https://doi.org/10.1016/0006-291X(65)90874-0

Leive, L. (1965b). Release of lipopolysaccharide by EDTA treatment of *Escherichia coli*. *Biochemical and Biophysical Research Communications*, *21*(4), 290–296. https://doi.org/10.1016/0006-291X(65)90191-9

Leive, L. (1974). The barrier function of the Gram-negative envelope. *Annals of the New York Academy of Sciences*, *235*(1), 109–129. https://doi.org/10.1111/j.1749-6632.1974.tb43261.x

Leon-Sicairos, N., Reyes-Cortes, R., Guadrón-Llanos, A. M., Madueña-Molina, J., Leon-Sicairos, C., & Canizalez-Román, A. (2015). Strategies of intracellular pathogens for obtaining iron from the environment. *BioMed Research International*, *2015*, 2–4. https://doi.org/10.1155/2015/476534

Lewis, K. (2007). Persister cells, dormancy and infectious disease. *Nature Reviews Microbiology*, *5*(1), 48–56. https://doi.org/10.1038/nrmicro1557

Leyn, S. A., Zlamal, J. E., Kurnasov, O. V., Li, X., Elane, M., Myjak, L., Godzik, M., Crecy, A. de, Garcia-Alcalde, F., Ebeling, M., & Osterman, A. L. (2021). Experimental evolution in morbidostat reveals converging genomic trajectories on the path to triclosan resistance. *Microbial Genomics*, *7*(5). https://doi.org/10.1099/MGEN.0.000553

Li, L.-H., Wu, P., Lee, J.-Y., Li, P.-R., Hsieh, W.-Y., Ho, C.-C., Ho, C.-L., Chen, W.-J., Wang, C.-C., Yen, M.-Y., Yang, S.-M., & Chen, H.-W. (2014). Hinokitiol induces DNA damage and autophagy followed by cell cycle arrest and senescence in gefitinib-resistant lung adenocarcinoma cells. *PLoS ONE*, *9*(8), e104203. https://doi.org/10.1371/journal.pone.0104203

Li, M., Cha, D. J., Lai, Y., Villaruz, A. E., Sturdevant, D. E., & Otto, M. (2007). The antimicrobial

peptide-sensing system *aps* of *Staphylococcus aureus*. *Molecular Microbiology*, *66*(5), 1136–1147. https://doi.org/10.1111/J.1365-2958.2007.05986.X

Lisher, J. P., & Giedroc, D. P. (2013). Manganese acquisition and homeostasis at the host-pathogen interface. *Frontiers in Cellular and Infection Microbiology*, *3*(DEC). https://doi.org/10.3389/fcimb.2013.00091

Liu, N., Song, W., Schienebeck, C. M., Zhang, M., & Tang, W. (2014). Synthesis of naturally occurring tropones and tropolones. *Tetrahedron*, *70*(49), 9281–9305. https://doi.org/10.1016/j.tet.2014.07.065

Liu, Z., Lin, Y., Lu, Q., Li, F., Yu, J., Wang, Z., He, Y., & Song, C. (2017). *In vitro* and *in vivo* activity of EDTA and antibacterial agents against the biofilm of mucoid *Pseudomonas aeruginosa*. *Infection*, *45*(1), 23–31. https://doi.org/10.1007/s15010-016-0905-z

Livermore, D. M. (1987). Mechanisms of resistance to cephalosporin antibiotics. *Drugs*, *34*(2), 64–88. https://doi.org/10.2165/00003495-198700342-00007

Lobanovska, M., & Pilla, G. (2017). Penicillin's discovery and antibiotic resistance: lessons for the future? *Yale Journal of Biology and Medicine*, *90*(1), 135–145. /pmc/articles/PMC5369031/

Lonergan, Z. R., & Skaar, E. P. (2019). Nutrient Zinc at the Host–Pathogen Interface. *Trends in Biochemical Sciences*, *44*(12), 1041–1056. https://doi.org/10.1016/j.tibs.2019.06.010

Loskill, P., Pereira, P. M., Jung, P., Bischoff, M., Herrmann, M., Pinho, M. G., & Jacobs, K. (2014). Reduction of the peptidoglycan crosslinking causes a decrease in stiffness of the *Staphylococcus aureus* cell envelope. *Biophysical Journal*, *107*(5), 1082–1089. https://doi.org/10.1016/j.bpj.2014.07.029

Lovering, A. L., De Castro, L. H., Lim, D., & Strynadka, N. C. J. (2007). Structural insight into the transglycosylation step of bacterial cell-wall biosynthesis. *Science*, *315*(5817), 1402–1405. https://doi.org/10.1126/SCIENCE.1136611

Lovering, A. L., De Castro, L., & Strynadka, N. C. J. (2008). Identification of dynamic structural motifs involved in peptidoglycan glycosyltransfer. *Journal of Molecular Biology*, *383*(1), 167–177. https://doi.org/10.1016/J.JMB.2008.08.020

Macomber, L., & Imlay, J. A. (2009). The iron-sulfur clusters of dehydratases are primary intracellular targets of copper toxicity. *Proceedings of the National Academy of Sciences of the United States of America*, *106*(20), 8344–8349. https://doi.org/10.1073/pnas.0812808106

MAK Value Documentation. (2015). Diethylenetriaminepentakis-(methylenephosphonic acid) and its sodium salts. In *The MAK-Collection for Occupational Health and Safety* (pp. 1–16). Wiley-VCH Verlag GmbH & Co. KGaA. https://doi.org/10.1002/3527600418.mb1582760kske4515

Mani, N., Tobin, P., & Jayaswal, R. (1993). Isolation and characterization of autolysis-defective mutants of *Staphylococcus aureus* created by Tn917-lacZ mutagenesis. *Journal of Bacteriology*, *175*(5), 1493–1499. https://doi.org/10.1128/JB.175.5.1493-1499.1993

McCall, K. A., Huang, C. C., & Fierke, C. A. (2000). Function and mechanism of zinc metalloenzymes. *Journal of Nutrition*, *130*(5 SUPPL.), 1437–1446. https://doi.org/10.1093/jn/130.5.1437s

McMurry, L. M., Oethinger, M., & Levy, S. B. (1998). Triclosan targets lipid synthesis. *Nature 1998 394:6693*, *394*(6693), 531–532. https://doi.org/10.1038/28970

Meehl, M., Herbert, S., Götz, F., & Cheung, A. (2007). Interaction of the GraRS two-component system with the VraFG ABC transporter to support vancomycin-intermediate resistance in *Staphylococcus aureus*. *Antimicrobial Agents and Chemotherapy*, *51*(8), 2679–2689. https://doi.org/10.1128/AAC.00209-07

Miethke, M. (2013). Molecular strategies of microbial iron assimilation: from high-affinity

complexes to cofactor assembly systems. *Metallomics*, *5*(1), 15–28. https://doi.org/10.1039/c2mt20193c

Miethke, M., & Marahiel, M. A. (2007). Siderophore-based iron acquisition and pathogen control. *Microbiology and Molecular Biology Reviews*, *71*(3), 413–451. https://doi.org/10.1128/mmbr.00012-07

Mikhaylina, A., Ksibe, A. Z., Scanlan, D. J., & Blindauer, C. A. (2018). Bacterial zinc uptake regulator proteins and their regulons. *Biochemical Society Transactions*, *46*(4), 983–1001. https://doi.org/10.1042/BST20170228

Miller, A. F. (2012). Superoxide dismutases: Ancient enzymes and new insights. *FEBS Letters*, *586*(5), 585–595. https://doi.org/10.1016/j.febslet.2011.10.048

Miller, S. I. (2016). Antibiotic resistance and regulation of the Gram-negative bacterial outer membrane barrier by host innate immune molecules. *MBio*, *7*(5). https://doi.org/10.1128/mBio.01541-16

Milne, J., & Zhitomirsky, I. (2018). Application of octanohydroxamic acid for liquid-liquid extraction of manganese oxides and fabrication of supercapacitor electrodes. *Journal of Colloid and Interface Science*, *515*, 50–57. https://doi.org/10.1016/j.jcis.2018.01.021

Mok, W. W. K., & Brynildsen, M. P. (2018). Timing of DNA damage responses impacts persistence to fluoroquinolones. *Proceedings of the National Academy of Sciences of the United States of America*, *115*(27), E6301–E6309. https://doi.org/10.1073/pnas.1804218115

Morita, Y., Sakagami, Y., Okabe, T., Ohe, T., Inamori, Y., & Ishida, N. (2007). The mechanism of the bactericidal activity of hinokitiol. *Biocontrol Science*, *12*(3), 101–110. https://www.jstage.jst.go.jp/article/bio1996/12/3/12_3_101/_pdf

Müller, S. I., Valdebenito, M., & Hantke, K. (2009). Salmochelin, the long-overlooked catecholate siderophore of *Salmonella*. *BioMetals 2009 22:4*, *22*(4), 691–695. https://doi.org/10.1007/S10534-009-9217-4

Nabil A. Amro, Lakshmi P. Kotra, Kapila Wadu-Mesthrige, Alexy Bulychev, Shahriar Mobashery, * and, & Liu*, G. (2000). High-resolution atomic force microscopy studies of the *Escherichia coli* outer membrane: structural basis for permeability. *Langmuir*, *16*(6), 2789–2796. https://doi.org/10.1021/LA991013X

Nagy, T. A., Moreland, S. M., Andrews-Polymenis, H., & Detweiler, C. S. (2013). The ferric enterobactin transporter Fep is required for persistent *Salmonella enterica* serovar Typhimurium infection. *Infection and Immunity*, *81*(11), 4063. https://doi.org/10.1128/IAI.00412-13

Nakano, K., Chigira, T., Miyafusa, T., Nagatoishi, S., Caaveiro, J. M. M., & Tsumoto, K. (2015). Discovery and characterization of natural tropolones as inhibitors of the antibacterial target CapF from *Staphylococcus aureus*. *Scientific Reports*, *5*(1), 1–10. https://doi.org/10.1038/srep15337

Navratna, V., Nadig, S., Sood, V., Prasad, K., Arakere, G., & Gopal, B. (2010). Molecular basis for the role of *Staphylococcus aureus* penicillin binding protein 4 in antimicrobial resistance. *Journal of Bacteriology*, *192*(1), 134–144. https://doi.org/10.1128/JB.00822-09

Ng, W. (2020). ICP-MS analysis of metal and metalloid concentrations of common microbiological growth media reveals presence of heavy metals. *BioRxiv Preprint Server*. https://doi.org/10.1101/2020.09.25.313221

Ng, W., & Ting, Y.-P. (2017). Zeta potential of bacterial cells: effect of wash buffers. *PeerJ Preprints*. https://doi.org/10.7287/PEERJ.PREPRINTS.110V7

Nicas, T. I., & Hancock, R. E. W. (1980). Outer membrane protein H1 of *Pseudomonas aeruginosa*: involvement in adaptive and mutational resistance to ethylenediaminetetraacetate, polymyxin B, and gentamicin. *Journal of Bacteriology*,

143(2), 872–878. https://doi.org/10.1128/jb.143.2.872-878.1980

Nichols, R. J., Sen, S., Choo, Y. J., Beltrao, P., Zietek, M., Chaba, R., Lee, S., Kazmierczak, K. M., Lee, K. J., Wong, A., Shales, M., Lovett, S., Winkler, M. E., Krogan, N. J., Typas, A., & Gross, C. A. (2011). Phenotypic landscape of a bacterial cell. *Cell*, *144*(1), 143–156. https://doi.org/10.1016/j.cell.2010.11.052

Nishi, H., Komatsuzawa, H., Fujiwara, T., McCallum, N., & Sugai, M. (2004). Reduced content of lysyl-phosphatidylglycerol in the cytoplasmic membrane affects susceptibility to moenomycin, as well as vancomycin, gentamicin, and antimicrobial peptides, in *Staphylococcus aureus*. *Antimicrobial Agents and Chemotherapy*, *48*(12), 4800. https://doi.org/10.1128/AAC.48.12.4800-4807.2004

Nishi, H., Komatsuzawa, H., Yamada, S., Fujiwara, T., Ohara, M., Ohta, K., Sugiyama, M., Ishikawa, T., & Sugai, M. (2003). Moenomycin-Resistance Is Associated with Vancomycin-Intermediate Susceptibility in *Staphylococcus aureus*. *Microbiology and Immunology*, *47*(12), 927–935. https://doi.org/10.1111/J.1348-0421.2003.TB03466.X

Nodwell, M. B., Koch, M. F., Alte, F., Schneider, S., & Sieber, S. A. (2014). A subfamily of bacterial ribokinases utilizes a hemithioacetal for pyridoxal phosphate salvage. *Journal of the American Chemical Society*, *136*(13), 4992–4999. https://doi.org/10.1021/JA411785R

Noinaj, N., Buchanan, S. K., & Cornelissen, C. N. (2012). The transferrin–iron import system from pathogenic *Neisseria* species. *Molecular Microbiology*, *86*(2), 246–257. https://doi.org/10.1111/MMI.12002

Nörtemann, B. (1999). Biodegradation of EDTA. *Applied Microbiology and Biotechnology*, *51*(6), 751–759. https://doi.org/10.1007/s002530051458

Osman, D., Martini, M. A., Foster, A. W., Chen, J., Scott, A. J. P., Morton, R. J., Steed, J. W., Lurie-Luke, E., Huggins, T. G., Lawrence, A. D., Deery, E., Warren, M. J., Chivers, P. T., & Robinson, N. J. (2019). Bacterial sensors define intracellular free energies for correct enzyme metalation. *Nature Chemical Biology*, *15*(3), 241–249. https://doi.org/10.1038/s41589-018-0211-4

Oviedo, C., & Rodríguez, J. (2003). EDTA: The chelating agent under environmental scrutiny. *Quimica Nova*, *26*(6), 901–905. https://doi.org/10.1590/S0100-40422003000600020

Pagnout, C., Sohm, B., Razafitianamaharavo, A., Caillet, C., Offroy, M., Leduc, M., Gendre, H., Jomini, S., Beaussart, A., Bauda, P., & Duval, J. F. L. (2019). Pleiotropic effects of *rfa*-gene mutations on *Escherichia coli* envelope properties. *Scientific Reports*, *9*(1). https://doi.org/10.1038/s41598-019-46100-3

Palmer, L. D., & Skaar, E. P. (2016). Transition metals and virulence in bacteria. *Annual Review of Genetics*, *50*(1), 67–91. https://doi.org/10.1146/annurev-genet-120215-035146

Pandey, R. S., Sreenivas, K. N., Patil, N. M., & Swamy, H. S. (1981). Dopamine β-hydroxylase inhibition in a patient with Wilson's disease and manic symptoms. *American Journal of Psychiatry*, *138*(12), 1628–1629. https://doi.org/10.1176/ajp.138.12.1628

Parquet, M. del C., Savage, K. A., Allan, D. S., Davidson, R. J., & Holbein, B. E. (2018). Novel iron-chelator DIBI inhibits *Staphylococcus aureus* growth, suppresses experimental MRSA infection in mice and enhances the activities of diverse antibiotics *in vitro*. *Frontiers in Microbiology*, *9*(AUG), 1811. https://doi.org/10.3389/fmicb.2018.01811

Parrow, N. L., Fleming, R. E., & Minnick, M. F. (2013). Sequestration and scavenging of iron in infection. *Infection and Immunity*, *81*(10), 3503–3514. https://doi.org/10.1128/IAI.00602-13

Paterson, J. R., Beecroft, M. S., Mulla, R. S., Osman, D., Reeder, N. L., Caserta, J. A., Young, T. R., Pettigrew, C. A., Davies, G. E., Williams, J. A. G., & Sharples, G. J. (2022). Insights into the antibacterial mechanism of action of chelating agents by selective deprivation of

iron, manganese, and zinc. *Applied and Environmental Microbiology*, *88*(2), 1–38. https://doi.org/10.1128/AEM.01641-21

Patzer, S. I., & Hantke, K. (1998). The ZnuABC high-affinity zinc uptake system and its regulator Zur in *Escherichia coli*. *Molecular Microbiology*, *28*(6), 1199–1210. https://doi.org/10.1046/j.1365-2958.1998.00883.x

Patzer, S. I., & Hantke, K. (2001). Dual repression by Fe2+-Fur and Mn2+-MntR of the *mntH* gene, encoding an NRAMP-like Mn2+ transporter in *Escherichia coli*. *Journal of Bacteriology*, *183*(16), 4806. https://doi.org/10.1128/JB.183.16.4806-4813.2001

Percy, M. G., & Gründling, A. (2014). Lipoteichoic acid synthesis and function in Gram-positive bacteria. *Annual Review of Microbiology*, *68*(1), 81–100. https://doi.org/10.1146/annurev-micro-091213-112949

Peschel, A., Jack, R. W., Otto, M., Collins, L. V., Staubitz, P., Nicholson, G., Kalbacher, H., Nieuwenhuizen, W. F., Jung, G., Tarkowski, A., Van Kessel, K. P. M., & Van Strijp, J. A. G. (2001). *Staphylococcus aureus* resistance to human defensins and evasion of neutrophil killing via the novel virulence factor MprF is based on modification of membrane lipids with L-lysine. *Journal of Experimental Medicine*, *193*(9), 1067–1076. https://doi.org/10.1084/jem.193.9.1067

Peschel, A., Otto, M., Jack, R. W., Kalbacher, H., Jung, G., & Götz, F. (1999). Inactivation of the *dlt* operon in *Staphylococcus aureus* confers sensitivity to defensins, protegrins, and other antimicrobial peptides. *Journal of Biological Chemistry*, *274*(13), 8405–8410. https://doi.org/10.1074/jbc.274.13.8405

Pettit, L. (2009). The IUPAC stability constants database. *Chemistry International -- Newsmagazine for IUPAC*, *28*(5), 14–15. https://doi.org/10.1515/ci.2006.28.5.14

Pfaller, M. A., Sheehan, D. J., & Rex, J. H. (2004). Determination of fungicidal activities against yeasts and molds: lessons learned from bactericidal testing and the need for standardization. *Clinical Microbiology Reviews*, *17*(2), 268–280. https://doi.org/10.1128/CMR.17.2.268-280.2004

Pinto, I. S. S., Neto, I. F. F., & Soares, H. M. V. M. (2014). Biodegradable chelating agents for industrial, domestic, and agricultural applications—a review. *Environmental Science and Pollution Research*, *21*(20), 11893–11906. https://doi.org/10.1007/s11356-014-2592-6

Pirkanniemi, K., Sillanpää, M., & Sorokin, A. (2003). Degradative hydrogen peroxide oxidation of chelates catalysed by metallophthalocyanines. *Science of the Total Environment*, *307*(1–3), 11–18. https://doi.org/10.1016/S0048-9697(02)00499-0

Porru, S., & Alessio, L. (1996). The use of chelating agents in occupational lead poisoning. *Occupational Medicine (Oxford, England)*, *46*(1), 41–48. https://doi.org/10.1093/occmed

Prachayasittikul, V., Isarankura-Na-Ayudhya, C., Tantimongcolwat, T., Nantasenamat, C., & Galla, H.-J. (2007). EDTA-induced membrane fluidization and destabilization: biophysical studies on artificial lipid membranes. *Acta Biochimica et Biophysica Sinica*, *39*(11), 901–913. https://doi.org/10.1111/J.1745-7270.2007.00350.X

Qamar, A., & Golemi-Kotra, D. (2012). Dual roles of FmtA in *Staphylococcus aureus* cell wall biosynthesis and autolysis. *Antimicrobial Agents and Chemotherapy*, *56*(7), 3797–3805. https://doi.org/10.1128/AAC.00187-12

Quan, G., Xia, P., Lian, S., Wu, Y., & Zhu, G. (2020). Zinc uptake system ZnuACB is essential for maintaining pathogenic phenotype of F4ac+ enterotoxigenic *E. coli* (ETEC) under a zinc restricted environment. *Veterinary Research 2020 51:1*, *51*(1), 1–10. https://doi.org/10.1186/S13567-020-00854-1

Ragland, S. A., & Criss, A. K. (2017). From bacterial killing to immune modulation: Recent insights into the functions of lysozyme. *PLoS Pathogens*, *13*(9), e1006512. https://doi.org/10.1371/journal.ppat.1006512

Rahman, M. M., Hunter, H. N., Prova, S., Verma, V., Qamar, A., & Golemi-Kotra, D. (2016).

The *Staphylococcus aureus* methicillin resistance factor FmtA is a D-amino esterase that acts on teichoic acids. *MBio*, *7*(1). https://doi.org/10.1128/mBio.02070-15

Rajagopal, M., Martin, M. J., Santiago, M., Lee, W., Kos, V. N., Meredith, T., Gilmore, M. S., & Walker, S. (2016). Multidrug intrinsic resistance factors in *Staphylococcus aureus* identified by profiling fitness within high-diversity transposon libraries. *MBio*, *7*(4). https://doi.org/10.1128/MBIO.00950-16

Ramirez, M. S., & Tolmasky, M. E. (2010). Aminoglycoside modifying enzymes. *Drug Resistance Updates*, *13*(6), 151–171. https://doi.org/10.1016/j.drup.2010.08.003

Rapisarda, V. A., Volentini, S. I., Farías, R. N., & Massa, E. M. (2002). Quenching of bathocuproine disulfonate fluorescence by Cu(I) as a basis for copper quantification. *Analytical Biochemistry*, *307*(1), 105–109. https://doi.org/10.1016/S0003-2697(02)00031-3

Rawlinson, L. A. B., O'Gara, J. P., Jones, D. S., & Brayden, D. J. (2011). Resistance of *Staphylococcus aureus* to the cationic antimicrobial agent poly(2-(dimethylamino ethyl)methacrylate) (pDMAEMA) is influenced by cell-surface charge and hydrophobicity. *Journal of Medical Microbiology*, *60*(7), 968–976. https://doi.org/10.1099/jmm.0.025619-0

Raymond, K. N., Dertz, E. A., & Kim, S. S. (2003). Enterobactin: An archetype for microbial iron transport. *Proceedings of the National Academy of Sciences of the United States of America*, *100*(7), 3584–3588. https://doi.org/10.1073/pnas.0630018100

Rebets, Y., Lupoli, T., Qiao, Y., Schirner, K., Villet, R., Hooper, D., Kahne, D., & Walker, S. (2014). Moenomycin resistance mutations in *Staphylococcus aureus* reduce peptidoglycan chain length and cause aberrant cell division. *ACS Chemical Biology*, *9*(2), 459–467. https://doi.org/10.1021/cb4006744

Reed, P., Atilano, M. L., Alves, R., Hoiczyk, E., Sher, X., Reichmann, N. T., Pereira, P. M., Roemer, T., Filipe, S. R., Pereira-Leal, J. B., Ligoxygakis, P., & Pinho, M. G. (2015). *Staphylococcus aureus* survives with a minimal peptidoglycan synthesis machine but sacrifices virulence and antibiotic resistance. *PLOS Pathogens*, *11*(5), e1004891. https://doi.org/10.1371/JOURNAL.PPAT.1004891

Remy, L., Carrière, M., Derré-Bobillot, A., Martini, C., Sanguinetti, M., & Borezée-Durant, E. (2013). The *Staphylococcus aureus* Opp1 ABC transporter imports nickel and cobalt in zinc-depleted conditions and contributes to virulence. *Molecular Microbiology*, *87*(4), 730–743. https://doi.org/10.1111/mmi.12126

Ren, L., Qiu, H., Qin, W., Zhang, M., Li, Y., & Wei, P. (2018). Inhibition mechanism of Ca2þ, Mg2þ and Fe3þ in fine cassiterite flotation using octanohydroxamic acid. *Royal Society Open Science*, *5*(8). https://doi.org/10.1098/rsos.180158

Ricerca, B. M., Di Girolamo, A., & Rund, D. (2009). Infections in thalassaemia and hemoglobinopathies. *Mediterranean Journal of Hematology and Infectious Diseases*, *1*(1). https://doi.org/10.4084/mjhid.2009.028

Robertson, E. J., Wolf, J. M., & Casadevall, A. (2012). EDTA inhibits biofilm formation, extracellular vesicular secretion, and shedding of the capsular polysaccharide glucuronoxylomannan by *Cryptococcus neoformans*. *Applied and Environmental Microbiology*, *78*(22), 7977–7984. https://doi.org/10.1128/AEM.01953-12

Rodionov, D. A., Hebbeln, P., Gelfand, M. S., & Eitinger, T. (2006). Comparative and functional genomic analysis of prokaryotic nickel and cobalt uptake transporters: evidence for a novel group of ATP-binding cassette transporters. *Journal of Bacteriology*, *188*(1), 317–327. https://doi.org/10.1128/JB.188.1.317-327.2006

Rolfe, M. D., Rice, C. J., Lucchini, S., Pin, C., Thompson, A., Cameron, A. D. S., Alston, M., Stringer, M. F., Betts, R. P., Baranyi, J., Peck, M. W., & Hinton, J. C. D. (2012). Lag phase is a distinct growth phase that prepares bacteria for exponential growth and involves transient metal accumulation. *Journal of Bacteriology*, *194*(3), 686–701.

https://doi.org/10.1128/JB.06112-11

Rosch, J. W., Gao, G., Ridout, G., Wang, Y.-D., & Tuomanen, E. I. (2009). Role of the manganese efflux system *mntE* for signalling and pathogenesis in *Streptococcus pneumoniae*. *Molecular Microbiology*, *72*(1), 12. https://doi.org/10.1111/J.1365-2958.2009.06638.X

Rott, E., Steinmetz, H., & Metzger, J. W. (2018). Organophosphonates: a review on environmental relevance, biodegradability and removal in wastewater treatment plants. *Science of the Total Environment*, *615*, 1176–1191. https://doi.org/10.1016/j.scitotenv.2017.09.223

Sachla, A. J., Luo, Y., & Helmann, J. D. (2021). Manganese impairs the QoxABCD terminal oxidase leading to respiration-associated toxicity. *Molecular Microbiology*, *116*(3), 729–742. https://doi.org/10.1111/MMI.14767

Samanovic, M. I., Ding, C., Thiele, D. J., & Darwin, K. H. (2012). Copper in microbial pathogenesis: meddling with the metal. *Cell Host and Microbe*, *11*(2), 106–115. https://doi.org/10.1016/j.chom.2012.01.009

Sánchez, P., Gálvez, N., Colacio, E., Mirñones, E., & Domínguez-Vera, J. M. (2005). Catechol releases iron(III) from ferritin by direct chelation without iron(II) production. *Dalton Transactions*, *4*, 811–813. https://doi.org/10.1039/b416669h

Santoscoy, M. C., & Jarboe, L. R. (2019). Streamlined assessment of membrane permeability and its application to membrane engineering of *Escherichia coli* for octanoic acid tolerance. *Journal of Industrial Microbiology and Biotechnology*, *46*(6), 843–853. https://doi.org/10.1007/s10295-019-02158-6

Sarvan, S., Butcher, J., Stintzi, A., & Couture, J. F. (2018). Variation on a theme: investigating the structural repertoires used by ferric uptake regulators to control gene expression. *BioMetals*, *31*(5), 681–704. https://doi.org/10.1007/s10534-018-0120-8

Sauvage, E., Kerff, F., Terrak, M., Ayala, J. A., & Charlier, P. (2008). The penicillin-binding proteins: structure and role in peptidoglycan biosynthesis. *FEMS Microbiology Reviews*, *32*(2), 234–258. https://doi.org/10.1111/j.1574-6976.2008.00105.x

Schindler, C. A., & Schuhardt, V. T. (1964). Lysostaphin: a new bacteriolytic agent for the *Staphylococcus*. *Proceedings of the National Academy of Sciences of the United States Of*, *51*(3), 414–421. https://doi.org/10.1073/pnas.51.3.414

Schlünzen, F., Zarivach, R., Harms, J., Bashan, A., Tocilj, A., Albrecht, R., Yonath, A., & Franceschi, F. (2001). Structural basis for the interaction of antibiotics with the peptidyl transferase centre in eubacteria. *Nature*, *413*(6858), 814–821. https://doi.org/10.1038/35101544

Schmidt-Rose, T., Braren, S., Fölster, H., Hillemann, T., Oltrogge, B., Philipp, P., Weets, G., & Fey, S. (2011). Efficacy of a piroctone olamine/climbazol shampoo in comparison with a zinc pyrithione shampoo in subjects with moderate to severe dandruff. *International Journal of Cosmetic Science*, *33*(3), 276–282. https://doi.org/10.1111/j.1468-2494.2010.00623.x

Schuster, C. F., Wiedemann, D. M., Kirsebom, F. C. M., Santiago, M., Walker, S., & Gründling, A. (2020). High-throughput transposon sequencing highlights the cell wall as an important barrier for osmotic stress in methicillin resistant *Staphylococcus aureus* and underlines a tailored response to different osmotic stressors. *Molecular Microbiology*, *113*(4), 699–717. https://doi.org/10.1111/mmi.14433

Scudamore, R. A., Beveridge, T. J., & Goldner, M. (1979). Outer-membrane penetration barriers as components of intrinsic resistance to beta-lactam and other antibiotics in *Escherichia coli* K-12. *Antimicrobial Agents and Chemotherapy*, *15*(2), 182. https://doi.org/10.1128/AAC.15.2.182

Sears, M. E. (2013). Chelation: harnessing and enhancing heavy metal detoxification—a

review. *The Scientific World Journal*, *219840*, 1–2. https://doi.org/10.1155/2013/219840

Seo, S. W., Kim, D., Latif, H., O'Brien, E. J., Szubin, R., & Palsson, B. O. (2014). Deciphering fur transcriptional regulatory network highlights its complex role beyond iron metabolism in *Escherichia coli*. *Nature Communications*, *5*(1), 1–10. https://doi.org/10.1038/ncomms5910

Sezonov, G., Joseleau-Petit, D., & D'Ari, R. (2007). *Escherichia coli* physiology in Luria-Bertani broth. *Journal of Bacteriology*, *189*(23), 8746–8749. https://doi.org/10.1128/JB.01368-07

Shahabadi, N., Zendehcheshm, S., Khademi, F., Rashidi, K., Chehri, K., & Fatahi Dehpahni, M. (2021). Green synthesis of chloroxine-conjugated silver nanoflowers: promising antimicrobial activity and *in vivo* cutaneous wound healing effects. *Journal of Environmental Chemical Engineering*, *9*(3), 105215. https://doi.org/10.1016/j.jece.2021.105215

Shahmirzadi, S. V., Nguyen, M.-T., & Götz, F. (2016). Evaluation of *Staphylococcus aureus* lipoproteins: role in nutritional acquisition and pathogenicity. *Frontiers in Microbiology*, *7*(SEP), 1404. https://doi.org/10.3389/FMICB.2016.01404

Sheldon, J. R., & Heinrichs, D. E. (2012). The iron-regulated *Staphylococcal* lipoproteins. *Frontiers in Cellular and Infection Microbiology*, *2*, 41. https://doi.org/10.3389/FCIMB.2012.00041

Shen, X., Zhang, H., He, X., Shi, H., Stephan, C., Jiang, H., Wan, C., & Eichholz, T. (2019). Evaluating the treatment effectiveness of copper-based algaecides on toxic algae *Microcystis aeruginosa* using single cell-inductively coupled plasma-mass spectrometry. *Analytical and Bioanalytical Chemistry*, *411*(21), 5531–5543. https://doi.org/10.1007/s00216-019-01933-9

Shih, Y. H., Chang, K. W., Hsia, S. M., Yu, C. C., Fuh, L. J., Chi, T. Y., & Shieh, T. M. (2013). *In vitro* antimicrobial and anticancer potential of hinokitiol against oral pathogens and oral cancer cell lines. *Microbiological Research*, *168*(5), 254–262. https://doi.org/10.1016/j.micres.2012.12.007

Sidarovich, V., Adami, V., Gatto, P., Greco, V., Tebaldi, T., Tonini, G. P., & Quattrone, A. (2015). Translational downregulation of HSP90 expression by iron chelators in neuroblastoma cells. *Molecular Pharmacology*, *87*(3), 513–524. https://doi.org/10.1124/mol.114.095729

Sigdel, T. K., Easton, J. A., & Crowder, M. W. (2006). Transcriptional response of *Escherichia coli* to TPEN. *Journal of Bacteriology*, *188*(18), 6709–6713. https://doi.org/10.1128/JB.00680-06

Siibak, T., Peil, L., Xiong, L., Mankin, A., Remme, J., & Tenson, T. (2009). Erythromycin- and chloramphenicol-induced ribosomal assembly defects are secondary effects of protein synthesis inhibition. *Antimicrobial Agents and Chemotherapy*, *53*(2), 563–571. https://doi.org/10.1128/AAC.00870-08

Simpson, W., Olczak, T., & Genco, C. A. (2000). Characterization and expression of HmuR, a TonB-dependent hemoglobin receptor of *Porphyromonas gingivalis*. *Journal of Bacteriology*, *182*(20), 5737–5748. https://doi.org/10.1128/JB.182.20.5737-5748.2000

Singh, M., Sasaki, T., Matsuo, M., Morimoto, Y., Aiba, Y., & Hiramatsu, K. (2015). Complete genome sequence of the drug-naive classical *Staphylococcus aureus* strain FDA209P. *Genome Announcements*, *3*(6), e01343-15. https://doi.org/10.1128/genomeA.01343-15

Smith, D. R., & Chapman, M. R. (2010). Economical evolution: microbes reduce the synthetic cost of extracellular proteins. *MBio*, *1*(3). https://doi.org/10.1128/mBio.00131-10

Spicer, A. B., & Spooner, D. F. (1974). The inhibition of growth of *Escherichia coli* spheroplasts by antibacterial agents. *Journal of General Microbiology*, *80*, 37–50.

Stapleton, P. D., & Taylor, P. W. (2002). Methicillin resistance in *Staphylococcus aureus*:

mechanisms and modulation. *Science Progress*, *85*(Pt 1), 57–72. https://doi.org/10.3184/003685002783238870

Stewart, C. M., Cole, M. B., Legan, J. D., Slade, L., & Schaffner, D. W. (2005). Solute-specific effects of osmotic stress on *Staphylococcus aureus*. *Journal of Applied Microbiology*, *98*(1), 193–202. https://doi.org/10.1111/j.1365-2672.2004.02445.x

Sun, X., Ge, R., Chiu, J. F., Sun, H., & He, Q. Y. (2008). Lipoprotein MtsA of MtsABC in *Streptococcus pyogenes* primarily binds ferrous ion with bicarbonate as a synergistic anion. *FEBS Letters*, *582*(9), 1351–1354. https://doi.org/10.1016/J.FEBSLET.2008.03.020

Sutton, J. A. F., Carnell, O. T., Lafage, L., Gray, J., Biboy, J., Gibson, J. F., Pollitt, E. J. G., Tazoll, S. C., Turnbull, W., Hajdamowicz, N. H., Salamaga, B., Pidwill, G. R., Condliffe, A. M., Renshaw, S. A., Vollmer, W., & Foster, S. J. (2021). *Staphylococcus aureus* cell wall structure and dynamics during host-pathogen interaction. *PLoS Pathogens*, *17*(3), e1009468. https://doi.org/10.1371/JOURNAL.PPAT.1009468

Szczepanik, W., Czarny, A., Zaczyńska, E., & Jezowska-Bojczuk, M. (2004). Preferences of kanamycin A towards copper(II). Effect of the resulting complexes on immunological mediators production by human leukocytes. *Journal of Inorganic Biochemistry*, *98*(2), 245–253. https://doi.org/10.1016/j.jinorgbio.2003.10.013

Tipper, D. J., & Strominger, J. L. (1965). Mechanism of action of penicillins: a proposal based on their structural similarity to acyl-D-alanyl-D-alanine. *Proceedings of the National Academy of Sciences of the United States of America*, *54*(4), 1133–1141. https://doi.org/10.1073/pnas.54.4.1133

Tooke, C. L., Hinchliffe, P., Bragginton, E. C., Colenso, C. K., Hirvonen, V. H. A., Takebayashi, Y., & Spencer, J. (2019). β-Lactamases and β-Lactamase Inhibitors in the 21st Century. *Journal of Molecular Biology*, *431*(18), 3472–3500. https://doi.org/10.1016/j.jmb.2019.04.002

Trust, T. J. (1975). Antibacterial activity of tropolone. *Antimicrobial Agents and Chemotherapy*, *7*(5), 500–506. http://aac.asm.org/

Tuchscherr, L., Kreis, C. A., Hoerr, V., Flint, L., Hachmeister, M., Geraci, J., Bremer-Streck, S., Kiehntopf, M., Medina, E., Kribus, M., Raschke, M., Pletz, M., Peters, G., & Lö ffler, B. (2016). *Staphylococcus aureus* develops increased resistance to antibiotics by forming dynamic small colony variants during chronic osteomyelitis. *Journal of Antimicrobial Chemotherapy*, *71*(2), 438–448. https://doi.org/10.1093/jac/dkv371

Turner, R. D., Vollmer, W., & Foster, S. J. (2014). Different walls for rods and balls: The diversity of peptidoglycan. *Molecular Microbiology*, *91*(5), 862–874. https://doi.org/10.1111/mmi.12513

Umerska, A., Strandh, M., Cassisa, V., Matougui, N., Eveillard, M., & Saulnier, P. (2018). Synergistic effect of combinations containing EDTA and the antimicrobial peptide AA230, an arenicin-3 derivative, on gram-negative bacteria. *Biomolecules*, *8*(4). https://doi.org/10.3390/biom8040122

Vaara, M. (1992). Agents that increase the permeability of the outer membrane. *Microbiological Reviews*, *56*(3), 395–411. https://doi.org/10.1128/mmbr.56.3.395-411.1992

Vestergaard, M., Nøhr-Meldgaard, K., Bojer, M. S., Krogsgård Nielsen, C., Meyer, R. L., Slavetinsky, C., Peschel, A., & Ingmer, H. (2017). Inhibition of the ATP synthase eliminates the intrinsic resistance of *Staphylococcus aureus* towards polymyxins. *MBio*, *8*(5). https://doi.org/10.1128/mBio.01114-17

Vinuesa, V., & McConnell, M. J. (2021). Recent advances in iron chelation and gallium-based therapies for antibiotic resistant bacterial infections. *International Journal of Molecular Sciences*, *22*(6), 1–19. https://doi.org/10.3390/ijms22062876

Voss, J. G. (1967). Effects of organic cations on the Gram-negative cell wall and their bactericidal activity with ethylenediaminetetra-acetate and surface active agents. *Microbiology*, *48*(3), 391–400. https://doi.org/10.1099/00221287-48-3-391

Waldron, K. J., & Robinson, N. J. (2009). How do bacterial cells ensure that metalloproteins get the correct metal? *Nature Reviews Microbiology*, *7*(1), 25–35. https://doi.org/10.1038/nrmicro2057

Waldron, K. J., Rutherford, J. C., Ford, D., & Robinson, N. J. (2009). Metalloproteins and metal sensing. *Nature*, *460*(7257), 823–830. https://doi.org/10.1038/nature08300

Walsh, S. E., Maillard, J.-Y., Russell, A. D., Catrenich, C. E., Charbonneau, D. L., & Bartolo, R. G. (2003). Activity and mechanisms of action of selected biocidal agents on Gram-positive and -negative bacteria. *Journal of Applied Microbiology*, *94*(2), 240–247. https://doi.org/10.1046/j.1365-2672.2003.01825.x

Wecke, J., Madela, K., & Fischer, W. (1997). The absence of D-alanine from lipoteichoic acid and wall teichoic acid alters surface charge, enhances autolysis and increases susceptibility to methicillin in *Bacillus subtilis*. *Microbiology*, *143*(9), 2953–2960. https://doi.org/10.1099/00221287-143-9-2953

Weinberg, E. D. (1957). The mutual effects of antimicrobial compounds and metallic cations. *Department of Bacteriology, Indiana University*. http://mmbr.asm.org/

Weiser, R., Asscher, A. W., & Wimpenny, J. (1968). In vitro reversal of antibiotic resistance by ethylenediamine tetraacetic acid. *Nature*, *219*(5161), 1365–1366. https://doi.org/10.1038/2191365a0

Weiss, G., & Carver, P. L. (2018). Role of divalent metals in infectious disease susceptibility and outcome. *Clinical Microbiology and Infection*, *24*(1), 16–23. https://doi.org/10.1016/j.cmi.2017.01.018

Wiegand, I., Hilpert, K., & Hancock, R. E. W. (2008). Agar and broth dilution methods to determine the minimal inhibitory concentration (MIC) of antimicrobial substances. *Nature Protocols*, *3*(2), 163–175. https://doi.org/10.1038/nprot.2007.521

Wilson, B. R., Bogdan, A. R., Miyazawa, M., Hashimoto, K., & Tsuji, Y. (2016). Siderophores in iron metabolism: from mechanism to therapy potential. *Trends in Molecular Medicine*, *22*(12), 1077–1090. https://doi.org/10.1016/j.molmed.2016.10.005

Wilson, W. W., Wade, M. M., Holman, S. C., & Champlin, F. R. (2001). Status of methods for assessing bacterial cell surface charge properties based on zeta potential measurements. *Journal of Microbiological Methods*, *43*(3), 153–164. https://doi.org/10.1016/S0167-7012(00)00224-4

Wood, Z. A., Poole, L. B., & Karplus, A. P. (2001). Structure of intact AhpF reveals a mirrored thioredoxin-like active site and implies large domain rotations during catalysis. *Biochemistry*, *40*(13), 3900–3911. https://doi.org/10.1021/BI002765P

Yannone, S. M., Hartung, S., Menon, A. L., Adams, M. W. W., & Tainer, J. A. (2012). Metals in biology: defining metalloproteomes. *Current Opinion in Biotechnology*, *23*(1), 89–95. https://doi.org/10.1016/j.copbio.2011.11.005

Ye, J., Kandegedara, A., Martin, P., & Rosen, B. P. (2005). Crystal Structure of the *Staphylococcus aureus* pI258 CadC Cd(II)/Pb(II)/Zn(II)-Responsive Repressor. *Journal of Bacteriology*, *187*(12), 4214. https://doi.org/10.1128/JB.187.12.4214-4221.2005

Yin, E. S., Rakhmankulova, M., Kucera, K., De Sena Filho, J. G., Portero, C. E., Narváez-Trujillo, A., Holley, S. A., & Strobel, S. A. (2015). Fusaric acid induces a notochord malformation in zebrafish *via* copper chelation. *BioMetals*, *28*(4), 783–789. https://doi.org/10.1007/s10534-015-9855-7

Young, T. R., Martini, M. A., Foster, A. W., Glasfeld, A., Osman, D., Morton, R. J., Deery, E., Warren, M. J., & Robinson, N. J. (2021). Calculating metalation in cells reveals CobW acquires Co II for vitamin B 12 biosynthesis while related proteins prefer Zn II. *Nature*

Communications 2021 12:1, *12*(1), 1–15. https://doi.org/10.1038/s41467-021-21479-8

Zhao, J., & Sakai, K. (2003). Peroxidases are involved in biosynthesis and biodegradation of β-thujaplicin in fungal elicitor-treated *Cupressus lusitanica* cell cultures. *New Phytologist*, *159*(3), 719–731. https://doi.org/10.1046/j.1469-8137.2003.00841.x

Zhu, Y., Weiss, E. C., Otto, M., Fey, P. D., Smeltzer, M. S., & Somerville, G. A. (2007). *Staphylococcus aureus* biofilm metabolism and the influence of arginine on polysaccharide intercellular adhesin synthesis, biofilm formation, and pathogenesis. *Infection and Immunity*, *75*(9), 4219–4226. https://doi.org/10.1128/IAI.00509-07

Zuegg, J., Muldoon, C., Adamson, G., McKeveney, D., Le Thanh, G., Premraj, R., Becker, B., Cheng, M., Elliott, A. G., Huang, J. X., Butler, M. S., Bajaj, M., Seifert, J., Singh, L., Galley, N. F., Roper, D. I., Lloyd, A. J., Dowson, C. G., Cheng, T. J., … Cooper, M. A. (2015). Carbohydrate scaffolds as glycosyltransferase inhibitors with in vivo antibacterial activity. *Nature Communications*, *6*. https://doi.org/10.1038/ncomms8719